A multi-omics approach to understand mesenchymal stem cell ageing



Chao Jiang

Kellogg College

Nuffield Department of Orthopaedics,

Rheumatology and Musculoskeletal Sciences

University of Oxford

Thesis submitted for the degree of

Doctor of Philosophy

Trinity term 2019

A multi-omics approach to understand mesenchymal stem cell ageing

Chao Jiang

Kellogg College

Doctor of Philosophy, Trinity term 2019

Abstract

Mesenchymal stem cell (MSC) ageing is characterised by impaired proliferation and osteoblast differentiation, leading to a reduction in bone mass and bone strength. Recent evidence indicates that transcriptional and epigenetic changes may underlie the impaired MSC functions with age. This thesis aims to systematically characterise the transcriptional and epigenetic changes associated with MSC ageing and to identify candidates for restoring MSC functions.

RNA-seq, DNA methylation-array and ATAC-seq were carried out on undifferentiated bone marrow-derived MSCs from young (20 - 29 years) and old (62 – 87 years) donors. The RNA-seq data showed that an increased donor age was associated with significant changes in the expression of lineage determining genes. Moreover, the DNA methylation array and ATAC-seq analysis revealed a less permissible epigenetic state for osteogenesis in the old donors, indicating that a shift in lineage preference was already evident in MSCs prior to differentiation.

In order to compare transcriptional changes during osteogenesis between MSCs from young and old donors, RNA-seq time-course experiments consisting of 16 time points were carried out. The expression profiles of a panel of tri-lineage differentiation markers indicated that the old donor MSCs were unable to fully commit towards osteoblast differentiation upon osteogenic induction and were diverted towards an adipogenic fate. The top 3 enriched gene networks amongst the 91 differentially expressed genes were associated with the canonical WNT, JAK/STAT and PPARG pathways. Canonical WNT activation via GSK3B inhibition significantly increased the ALP activity and matrix mineralisation of the old donors. Interestingly, WNT activation shifted the transcriptomic profiles of the old donors towards the young donors, thus further supporting the thesis that the canonical WNT pathway could be a potential target for restoring the osteogenic potential of ageing MSCs. More importantly, this study demonstrates the validity of the concept that a multi-omics approach has a promising potential for identifying therapeutic candidates to restore MSC functions in the elderly.

Acknowledgements

I would like to express my gratitude to Professor Udo Oppermann, Dr Martin Philpott, Dr James Dunford and Dr Scott Roberts. Udo, for this fantastic opportunity, and everything I have learned and achieved in this DPhil would not be possible without his support and guidance. Being able to ask questions to Martin and Jim was the cornerstone for me to survive the last four years. They both have generously given me so much of their time. I am grateful to Scott for believing in my research and becoming my supervisor in my second year, and despite the distance of travel, has given me a great deal of continuing guidance over the three years. I would also like to thank the amazing group of researchers at the Oppermann group who have helped me, including Dr Adam Cribbs, Graham Wells, Dr Chen Yi, Dr Manman Guo.

I would like to thank Professor Afsie Sabokbar for her support from my DPhil application to submission. Many thanks to Professor Mandy Peffers and Dr Dimitris Karamitros for kindly providing the MSCs, Professor John Loughlin and Dr Kat Cheung for the guidance on DNA methylation array analysis. Many thanks to Dr Pavlo Lutski and Professor Christoph Plass for the opportunity to collaborate. Special thanks to Professor James Edward, Dr Gillian Farnie, Dr Sarah Gooding and Dr Edward Hookway for all the advice on research and beyond.

The last four years have been an especially enjoyable experience thanks to the many great friends in the DPhil gang including Anna James-Bott, Johnny Chan, Laura Diment, Aneka Sowman, Na Wu, Ruby Chen and Zuzana Kalivodova. I'm especially thankful to have met the other member of our dynamic duo Henry Lee, the kind Veronika Hartleb, my gym buddy Frank Penkava, my pillar of emotional support Ju Han, and the greatest flatmate and friend Johnny Chan.

Most of all, I am so fortunate to have the love and support of my amazing family. I would like to dedicate this thesis to my loving mother Dr JingFeng Wang, father ZhengYu Jiang, grandmothers YanLin Mei and JianPing Cao and grandfather NaYan Jiang.

The work in this thesis has been generously supported by UCB Celltech, the Royal Commission for the Exhibition 1851 and China Oxford Scholarship Fund.

Contents

1 General introduction 1
1.1 Overview 1
1.2 Mesenchymal stem cells 2
1.2.1 Stem cells 2
1.2.2 Mesenchymal stem cells 3
1.2.3 Lineage potential of MSCs 4
1.2.4 Application of MSCs 5
1.3 Bone biology 7
1.3.1 Osteoblasts, osteocytes and osteoclasts 9
1.3.2 Bone formation and resorption 10
1.3.3 Signalling pathways 11
1.4 Ageing 19
1.4.1 Osteoblast and osteoclast balance 19
1.4.2 Age-associated bone diseases 20
1.4.3 Hallmarks of MSC ageing 22
1.5 Epigenomics, transcriptomics, and proteomics 30
1.5.1 RNA-seq 31
1.5.2 ATAC-seq 33
1.5.3 DNA methylation array 35
1.5.4 CyTOF 37
1.5.5 Statistics in –omics data 37
1.6 Summary 40
1.7 Aims 40
2 Methods 42
2.1 Cell culture 42
2.1.1 Mesenchymal stem cells 42

2.1.2 Osteoblast differentiation 42
2.2 Proliferation assays 43
2.2.1 PrestoBlue assay 43
2.2.2 Cumulative population doubling 43
2.3 Differentiation assays 43
2.3.1 ALP assay 43
2.3.2 Alizarin Red staining 44
2.3.3 Oil Red O staining 44
2.4 Lentiviral packaging 45
2.5 RNA-seq 46
2.5.1 RNA extraction 46
2.5.2 RNA library preparation 46
2.6 ATAC-seq 47
2.7 DNA methylation array 49
2.8 Sequencing 49
2.9 Data processing 50
2.9.1 RNA-seq 50
2.9.2 ATAC-seq 51
2.9.3 DNA methylation array 51
2.10 CyTOF 52
2.11 Chapter specific methods 53
2.11.1 Chapter 3 - Luciferase reporter assay 53
2.11.2 Chapter 5 shRNA-seq 54
2.11.3 Chapter 6 RNA-seq timecourse 55
2.11.4 Chapter 7 BIO treatment 55
3 Phenotypic changes during MSC ageing 56
3.1 Introduction 56

3.1.1 Models of MSC ageing 56
3.1.2 Donor age model 56
3.1.3 Cell passage model 60
3.1.4 Other models of human BM-MSC ageing 61
3.2 Aims 62
3.3 Results 62
3.3.1 MSC quality validation 62
3.3.2 Phenotypic changes with increased donor age 65
3.3.3 Phenotypic changes with increasing cell passage 68
3.4 Discussion 70
4 Multi-omics characterisation of MSC ageing in the donor age model 71
4.1 Introduction 71
4.1.1 DNA methylation and gene expression 71
4.1.2 Histone modifications and gene expression 75
4.1.3 Proteomic changes 77
4.2 Aims 77
4.3 Results 78
4.3.1 Transcriptomic characterisation of MSC ageing with RNAseq 78
4.3.2 Epigenomic characterisation of MSC ageing with DNAme profiling 86
4.3.3 Epigenomic characterisation of MSC ageing with ATAC-seq 88
4.3.4 Protein-level characterisation of MSC senescence and apoptosis with CyTOF 90
4.3.5 Common mechanisms amongst –omics data 92
4.4 Discussion 95
4.4.1 Role of canonical WNT pathway in MSC ageing 95
4.4.2 Epigenetic changes of MSC ageing 97
4.4.3 Additional targets from multi-omics data 99
5 Multi-omics characterisation of MSC ageing in the cell passage model 101

5.1 Introduction 101
5.1.1 RNA interference 101
5.1.2 Lentiviral vectors 101
5.1.3 shRNA-seq 102
5.2 Aims 103
5.3 Results: 105
5.3.1 Transcriptomic characterisation of MSC long term culture with RNAseq 105
5.3.2 Identification of epigenetic regulators of MSC proliferation 109
5.3.3 Protein-level characterisation of MSC proliferation, senescence and apoptosis with CyTOF in the passage model 111
5.4 Discussion: 112
5.4.1 Comparing gene expression changes in donor age and cell culture models of ageing 112
5.4.2 shRNA screen and PYGO1 113
6 High-resolution RNA-seq time-course identifies differential gene expression in response to osteogenic induction with age 116
6.1 Introduction 116
6.1.1 Gene expression change during osteogenesis 116
6.1.2 Lineage fate decision between osteoblast and chondrocyte differentiation 118
6.1.3 Lineage fate decision between osteoblast and adipocyte differentiation 119
6.2 Aims 120
6.3 Results 121
6.3.1 High-resolution RNA-seq time-course for osteogenesis 121
6.3.2 Change in lineage commitment of MSCs with age 124
6.3.3 Differentially expressed genes and gene networks 126
6.3.4 Phases of change in gene expression during osteogenesis 129
6.3.5 Differentially expressed canonical WNT pathway genes during osteogenesis 132
6.4 Discussion 135

6.4.1 WNT misregulation resulted in the decline of osteoblast differentiation 135
6.4.2 Early phase DEGs during osteoblast differentiation 137
7 WNT activation restores the osteogenic potential of old donor MSCs 139
7.1 Introduction 139
7.1.1 Canonical WNT signalling pathway 139
7.1.2 WNT agonist for rescuing osteogenic potential of aged MSCs 143
7.2 Aims 144
7.3 Results 145
7.3.1 GSK3B inhibition rescues osteoblast differentiation 145
7.3.2 Transcriptomic changes after BIO treatment 147
7.3.3 Differentially expressed genes after BIO treatment 153
7.4 Discussion 156
8 Discussion 159
References 164
Appendix 195

List of Figures

Figure 1-1 MSC lineages. 5

Figure 1-2 Major parts of the bone. 7

Figure 1-3 The periosteum layers. 7

Figure 1-4 Cortical bone structure. 8

Figure 1-5 Major signalling pathways regulating osteogenesis. 18

Figure 1-6 RNA-seq principle. 33

Figure 1-7 ATAC-seq principle. 34

Figure 1-8 Bisulfite conversion based DNAme-array. 36

Figure 2-1 CyTOF gating. 53

Figure 3-1 MSC quality validation. 64

Figure 3-2 Proliferation and osteogenesis assays of MSCs from young and old donors. 66

Figure 3-3 Senescence assay of MSCs from young and old donors. 67

Figure 3-4 Characterisation of MSCs with increasing passage number. 69

Figure 4-1 Venn diagram overlapping the differentially methylated genes associated with MSC ageing in three studies. 74

Figure 4-2 Transcriptomic changes in old vs young donor undifferentiated MSCs. 81

Figure 4-3 Changes in the canonical WNT signalling pathway with age. 82

Figure 4-4 Normalised counts of β-catenin target gene expression. 83

Figure 4-5 The DEGs mapped to the KEGG WNT signalling pathways. 84

Figure 4-6 The DEGs mapped to the KEGG Hedgehog (HH) signalling pathway 85

Figure 4-7 DNA methylation changes in young and old donor undifferentiated MSCs. 87

Figure 4-8 Changes in chromatin accessibility in old vs young donor MSCs. 90

Figure 4-9 Quantification of the CyTOF data of young and old donor MSCs. 91

Figure 4-10 Common mechanisms amongst multi-omic data of MSC ageing. 93

Figure 4-11 Pathway analysis of the multi-omics data. 94
Figure 5-1 Transcriptomic changes during MSC passaging. 106
Figure 5-2 DEGs during MSC passaging. 108
Figure 5-3 Identification of epigenetic regulators of MSC proliferation. 110
Figure 5-4 Quantification of the CyTOF data of early and late passage MSCs. 111
Figure 6-1 Overview of RNA-seq time course during osteogenesis. 122
Figure 6-2 Transcriptomic changes in old vs young donor MSCs during osteogenesis. 123
Figure 6-3 Lineage commitment of MSCs differ with age. 125
Figure 6-4 Differentially expressed genes in response to osteogenic condition with age. 127
Figure 6-5 Enriched gene networks amongst the DEGs. 128
Figure 6-6 Phases of change in gene expression during osteogenesis. 130
Figure 6-7 Different profiles of DEGs during osteogenesis. 131
Figure 6-8 Differentially expressed Canonical WNT pathway genes during osteogenesis 133
Figure 6-9 Important canonical WNT pathway genes during osteogenesis. 135
Figure 7-1 Canonical WNT signalling pathway. 140
Figure 7-2 GSK3B Inhibition rescues osteoblast differentiation in old donors 146
Figure 7-3 Transcriptomic changes in old vs young donor MSCs during osteogenesis with BIO treatment. 150
Figure 7-4 Lineage commitment of MSCs was altered by BIO treatment 152
Figure 7-5 Differentially expressed lineage panel genes. 154
Figure 7-6 Overlapped differentially expressed genes in response to osteogenic conditions (+/- BIO) with age. 156

Supplementary Figure S1. CyTOF analysis of the expression of senescence and apoptosis regulators in young and old donor MSCs. 195
Supplementary Figure S2. CyTOF analysis of the expression of senescence and apoptosis regulators in early and late passage MSCs. 196
Supplementary Figure S3. STRING protein interaction network of the 22 candidate genes from shRNA-seq screening.....197
Supplementary Figure S4. Phases of change in gene expression during osteogenesis at an individual donor level. 198
Supplementary Figure S5. Transiently upregulated DEGs between 1 – 24 hrs during osteogenesis. 200
Supplementary Figure S6. BIO treatment dosage response and validations. 201
Supplementary Figure S7. Transcriptomic changes in old vs young donor MSCs during osteogenesis and in DMEM control.....202
Supplementary Figure S8. Transcriptomic changes in old vs young donor MSCs during osteogenesis with BIO treatment. 203

List of Tables

Table 3-1 Changes in proliferation, differentiation and senescence with increased donor age. 59

Table 3-2 Changes in proliferation, differentiation and senescence with increased passage number. 61

Table 4-1 Summary of DNA methylation changes associated with MSC ageing from previous literature. 73

Table 4-2 Summary of histone modifications associated with MSC ageing from previous literature. 76

Table 6-1 Transiently upregulated DEGs between 1 – 24 hrs during osteogenesis. 131

Table 7-1 Small molecule activators of the canonical WNT signalling pathway.....142

Supplementary table S1. Donor details.....204

Supplementary table S2. Lentiviral shRNA library gene targets.....209

Supplementary table S3. shRNA-seq library prep custom primers. 209

Abbreviations

ADIPOQ	Adiponectin
ADRA2C	Alpha-2-adrenergic receptor
AGO	Argonaut
ALP	Alkaline phosphatase
APC	adenomatosis polyposis coli
AREG	Amphiregulin
ASCT	Autologous Stem Cell Transplant
ATAC	Assay for Transposase-Accessible Chromatin using sequencing
ATF4	Activating Transcription Factor 4
ATP	Adenosine Triphosphate
AZR	Alizarin Red
BGLAP	Bone Gamma-Carboxyglutamate Protein
BMD	Bone mineral density
BMP	Bone morphogenetic protein
CASP-3	Caspase 3
CD105	Endoglin
CD146	Melanoma cell adhesion molecule
CD151	Aggrecan
CD45	Protein Tyrosine Phosphatase Receptor Type C
CD73	Ecto-5′-nucleotidase
CD90	Thy-1
CFU	Colony forming units

ChIP-seq	Chromatin Immunoprecipitation followed by Sequencing
CK1α	casein kinase
COL1	Collagen 1
CTNNB1	β-catenin
cumPD	Cumulative population doubling
CyTOF	cytometry by time-of-flight mass spectrometry
DAP	Differentially accessible peak
DEG	Differentially expressed gene
DEX	Dexamethasone
DLX5	Distal-Less Homeobox 5
DMEM	Dulbecco's modified Eagle's medium
DMP	Differentially methylated position
DMSO	Dimethylsulfoxide
DNA	Deoxyribose Nucleic Acid
DNAme	DNA methylation
DNMT	DNA methyltransferase
DVL	Dishevelled
EBF1	EBF family transcription factor 1
ECM	Extracellular Matrix
ESC	Embryonic stem cell
EZH1/2	Enhancer of Zeste 1/2
FABP4	Fatty acid-binding protein
FASN	Fatty acid synthase

FGF	Fibroblast growth factor
FGFR	Fibroblast Growth Factor Receptor
FPKM	Fragments Per Kilobase of transcript per Million mapped
FRP4	Frizzled related protein 4
FZD	Frizzled
GO	gene ontology
GSK3	Glycogen Synthase Kinase 3
HDAC	Histone deacetylase
HH	Hedgehog
HLA-DR	Major Histocompatibility Complex DR isotype
HOX	Homeobox
HSC	Haematopoietic Stem Cells
IL-6	Interleukin-6
JAK	Janus kinase
JAK/STAT	Janus kinase/Signal transducer and activator of transcription
KDM	Lysine Demethylase
LRP5/6	lipoprotein receptor-related protein 5/6
MBD	Methyl-CpG Binding Domain
MEOX2	Mesenchyme homeobox 2
MGUS	Monoclonal Gammopathy of Undetermined Significance
miRNA	microRNA
MLL	Mixed Lineage Leukaemia
MMP	Matrix metalloprotease

MOI	Multiplicity of infection
mRNA	Messenger ribose nucleic acid
MSC	Mesenchymal stem cells (hMSCs, human mesenchymal stem cells)
MTF2	Metal Response Element Binding Transcription Factor 2
MYC	MYC Proto-Oncogene
ncRNA	non-coding RNA
NF-κβ	Nuclear factor kappa-β
OA	Osteoarthritis
OI	Osteogenesis imperfecta
OPG	Osteoprotegerin
OSM	Oncostatin M
P	Passage
P16	Cyclin-dependent kinase inhibitor 2A
P21	Cyclin-dependent kinase inhibitor 1
P53	Tumour Protein P53
PBS	Phosphate buffered saline
PCA	Principal component analysis
PcG	Polycomb Group
PFA	Paraformaldehyde
PPARG	Peroxisome proliferator-activated receptor gamma
pri-miRNA	Primary miRNA
PRMT8	Arginine methyltransferase 8
PTH	Parathyroid hormone

PYGO	Pygopus
RA	Rheumatoid arthritis
RANK	Receptor activator of nuclear factor kappa-β
RANKL	Receptor activator of nuclear factor kappa-β ligand
RASL11B	RAS-Like Family 11 Member B
RISC	RNA Induced Silencing Complex
RNA	Ribonucleic acid
RNAi	RNA interference
RNA-seq	RNA sequencing
RUNX2	Runt-related transcription factor 2 (also CBFA1)
SA-β-Gal	Senescence-associated β-galactosidase
SHOX2	Short stature homeobox 2
shRNA	small hairpin RNA
SLC7A8	LAT2 amino acid transporter
SND1	Staphylococcal nuclease domain-containing protein 1
SOST	Sclerostin
SOX9	Sex-determining region Y-box 9
SP7	Osterix
SPIN1	Spindlin 1
SPRI	Soild phase reversible immobilisation
STAT	Signal transducer and activator of transcription protein
SVA	Surrogate Variable Analysis
TGF-β	Transforming growth factor-β

TMM	Trimmed mean of M-values
TNF-α	Tumour necrosis factor-α
TPM	Transcripts Per Million
TRAP	Tartrate resistant acid phosphatase
tRNA	Transfer RNA
β-TrCP	β-transducin repeats-containing protein

1 General introduction

1.1 Overview

The global population is ageing at a rate that the UN describes as "unprecedented, without parallel in human history" [6]. Consequently, age-associated conditions, such as musculoskeletal degenerative diseases, are rapidly rising in prevalence [7]. A major clinical implication of diseases affecting bones lies in the fragility fractures that arise. Such fractures cause severe pain and disability to individuals, and the cost to the National Health Service has been predicted to increase from £2.3 billion in 2011 to £6 billion in 2036 [8].

The risk of fragility fractures significantly increases with age, especially in women, from 2% at 50 years to more than 25% at 80 years, due to an imbalance in bone homeostasis [9]. With increasing age, there is an increase in the number and activity of bone reabsorbing cells (osteoclasts) and a decline in the number and activity of bone-forming cells (osteoblasts) [10]. This results in the decline of bone mass, leading to age-related bone pathologies such as osteopenia and osteoporosis. Current treatments for patients with a high risk of fracture primarily aim to inhibit further bone erosions, but the repair of existing bone lesions, while feasible, rarely occurs [11]. Therefore, replenishment of osteoblasts to restore bone mass remains an important challenge within this field. Osteoblasts are derived by osteogenic differentiation from mesenchymal stem cells (MSCs), which lose their proliferative and osteogenic potential with age [12]. This introduction will review mesenchymal stem cells, bone biology, and ageing. The current understanding of the mechanisms of MSC ageing that lead to the loss of bone homeostasis will be discussed. Finally, recent technological advancements that will enable a greater understanding of the molecular mechanisms of MSC ageing and osteogenesis will be highlighted.

1.2 Mesenchymal stem cells

1.2.1 Stem cells

The concept of stem cells was proposed more than 100 years ago to address two of the major embryological questions at the time [13]. Stem cells were used to describe the origin of the hematopoietic system and the continuity of the germline. This original concept of stem cells still captures the important aspects of stem cell biology today. Stem cells are defined as precursor cells that are capable of indefinite self-renewal and have the ability to give rise to at least one type of mature (differentiated) cell [14].

The potency of stem cells specifies their potential to differentiate into different cell types. Totipotent stem cells can give rise to all necessary cells for a viable multicellular organism. In humans, this includes the fetus and the placenta. Zygotes formed at fertilisation and the embryonic cells within the first few divisions are shown to be totipotent in plants and mammals [15]. However, the time window of totipotency in humans is unclear. After the zygote undergoes several cell divisions, a blastocyst is formed. Pluripotent stem cells can be derived from the inner cell mass of the blastocyst. These embryonic stem cells (ESCs) can give rise to all somatic cells in an organism, but not the extra-embryonic cells. Additionally, the breakthrough in cellular reprogramming by Gurdon et al. and the generation of induced pluripotent stem cells (iPSCs) by Yamanaka et al. enabled direct reprogramming of differentiated cells back into pluripotent stem cells [16, 17]. Reprograming was shown to be possible with four transcription factors OCT3/4, SOX2, KLF4 and C-MYC. Alternative combinations of transcription factors have been studied to improve reprogramming efficiency and reduce the tumorigenic risk of the iPSCs generated [18].

Multipotent stem cells are more limited in their self-renewal capacity and the number of cell types they can differentiate into [19]. Adult or somatic stem cells are multipotent stem cells. They have important roles in tissue maintenance and repair. Adult stem cells are thought to be present in all types of organs and tissues, including the hematopoietic, epithelial, muscular and neural compartments [20].

Stem cells hold promising potential in the area of regenerative medicine to replace or repair damaged organs and tissues [20]. However, there are also limitations including safety and ethical concerns. Pluripotent ESCs can be obtained through *in vitro* fertilisation, but their usage is controversial as it requires the destruction of the embryos. iPSCs are a more ethical alternative to ESCs, but reports of genomic instability and increased tumorigenic potential have raised concerns about clinical translation [21]. Multipotent adult stem cells with a lower self-renewal capacity have a lower tumorigenic risk, but they can be difficult to expand in culture. Many types of adult stem cells can be easily isolated from the human body enabling autologous therapy, but *ex vivo* treatments are often required to overcome the effect of ageing and disease from the donor [22].

1.2.2 Mesenchymal stem cells

Fibroblast-like cells were first isolated from the bone marrow by Friedenstein [23]. They were clonogenic and were capable of bone and cartilage formation. As the mesoderm lineage is responsible for generating skeletal elements, the term “mesenchymal stem cells” was proposed by Caplan to describe this population of multipotent cells [24]. They are also referred to as mesenchymal stromal cells or skeletal stem cells. The International Stem Cell Therapy Committee proposed three minimum criteria for defining MSCs [25].

1. MSCs must be plastic-adherent in culture conditions.

2. MSCs must express CD105, CD73 and CD90, and not express CD45, CD34, CD14 and HLA-DR.
3. *In vitro*, MSCs must be able to differentiate into osteoblasts, adipocytes and chondrocytes.

As these criteria highlight, there is no single marker that is specific for MSCs [26]. Using these criteria, MSCs were also identified from other tissues, including adipose, synovium, dermis, periodontal ligament, dental pulp, bursa and the umbilical cord. However, MSC from different tissues can exhibit differences in their cellular markers and differentiation potential, typically characteristic of their tissue of origin [27, 28]. In this thesis, unless stated otherwise, the term MSC refers solely to those of bone marrow origin.

1.2.3 Lineage potential of MSCs

MSCs have tri-lineage potential to differentiate into osteoblasts, adipocytes and chondrocytes (Figure 1-1). *In vitro*, the differentiation of MSCs requires particular factors in the culture conditions. The most commonly used osteogenic factors are a combination of dexamethasone, β-glycerolphosphate and ascorbic acid [29]. Other common osteogenic inducers include vitamin D, BMP and oncostatin M [30-32]. Additionally, physical stimuli and mechanical stress have also been shown to induce osteoblast differentiation [33]. However, it remains an on-going challenge to identify all the factors that contribute to MSC osteogenesis.

In addition to the tri-lineage, MSCs have been shown to differentiate into tenocytes, myocytes and endothelial cells. *In vitro*, trans-differentiation of MSCs into neuronal cell types of ectoderm lineage has also been demonstrated [34]. However, while the differentiated cells demonstrated a neuron-like morphology and the firing of a single-action potential, their ability to fully function as neuron remains unclear [35].

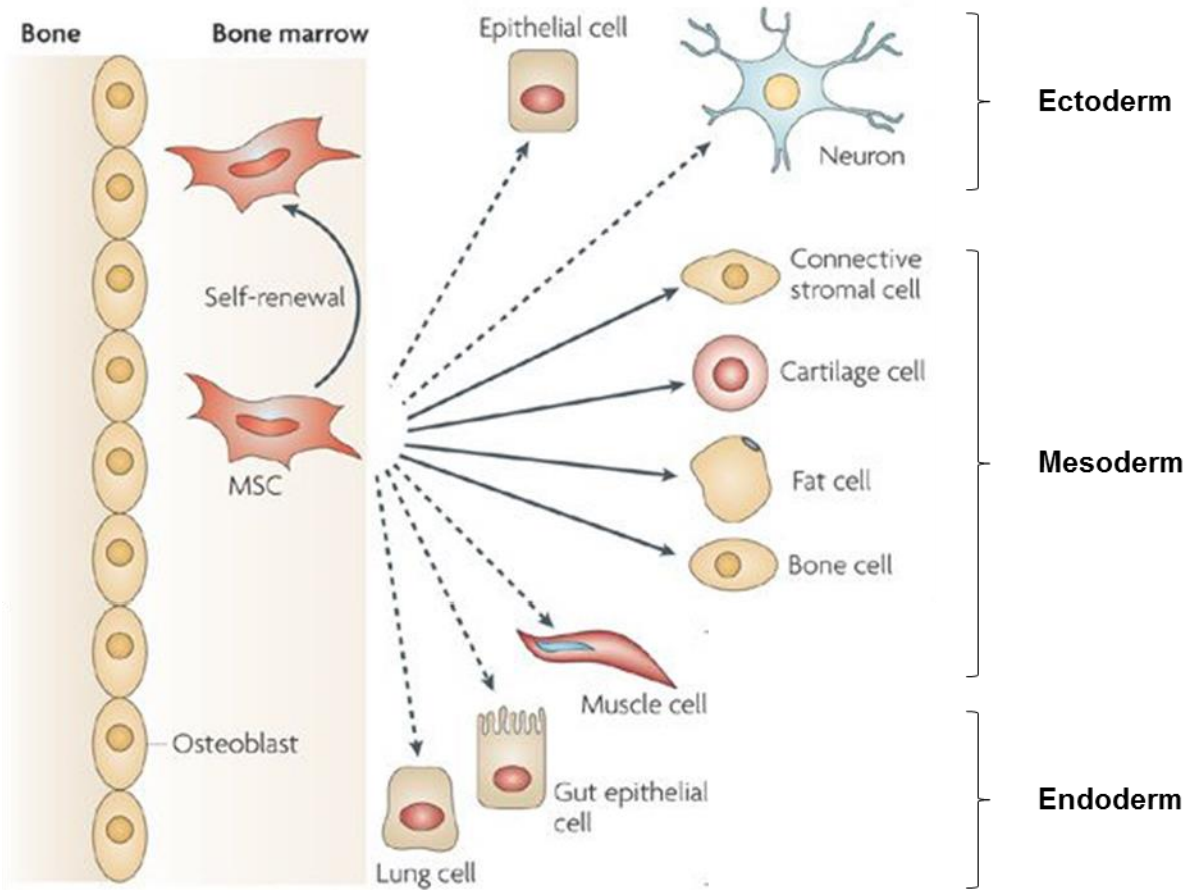


Figure 1-1 ***MSC lineages****. MSC can differentiate into lineages in the mesoderm (solid line), and trans-differentiate into lineages within the ectoderm and endoderm (dashed line). Adapted from [4]*

1.2.4 Application of MSCs

In addition to their ability to differentiate into various cell lineages, MSCs have shown properties such as secreting pro-proliferative and pro-survival factors, migrating to the site of injury and modulating the immune response. Therefore, diverse sources of MSCs and their properties have made them an attractive option for treating various diseases. In 2016, more than 400 clinical trials using MSCs were reported to be completed or on-going [36]. The largest percentage (19 %) of the MSc based clinical trials were for treating bone and cartilage diseases. Three methods of stem cells treatments were typically used:

1. Allogenic transplantation, where MSCs were isolated from a healthy donor and transplanted into a patient.
2. Autologous transplantation, where MSCs were isolated from the same patient that they are transplanted into, typically after modification *ex vivo*.
3. Systematic administration of drugs that target MSCs.

Allogenic transplantation of MSCs was used for the treatment of osteogenesis imperfecta (OI), which is caused by dominant mutations in collagen type 1 alpha 1 chain (*COL1A1*), resulting in reduced bone formation and multiple fractures. Allogenic MSCs transplanted into children with OI was able to migrate to bones, differentiate into osteoblasts and improve bone density [37]. However, allogeneic stem cell transplantation is limited by the availability of bone marrow donors and the concern for immunogenicity [26]. Autologous stem cell transplantation has been used for the treatment of osteoarthritis, and systemic administration of romosozumab has been used to promote osteoblast differentiation in post-menopause women with osteoporosis [38] (Age-related bone diseases are reviewed in greater detail in section 1.4). Despite these promising results, in order to deliver more effective and safe MSC-based therapies for bone diseases, a better understanding of the regulation of MSC differentiation in normal physiology and disease is required.

1.3 Bone biology

Bone is a metabolically active organ and serves three main physiological functions [1]:

1) To provide structural support, facilitate movement and to protect internal organs.
2) To regulate metabolism, including the storage of calcium and phosphate. The yellow marrow also stores fatty acids and regulates blood glucose through the release of osteocalcin [39].
3) To produce haematopoietic lineage cells.

Major parts of the bone consist of the periosteum, cartilaginous joints, the mineralised cortical and trabecular bone, and the bone marrow (Figure 1-2) [1].

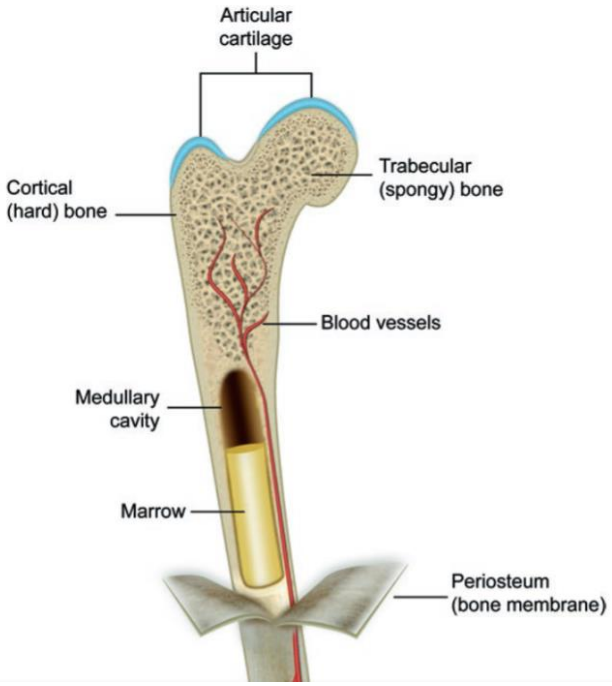


Figure 1-2 ***Major parts of the bone****. Bone consists of the cortical (hard) bone, trabecular (spongy) bone, periosteum and the bone marrow. adapted from [1]*

The periosteum is a thin fibro-cellular membrane on the surface of the bone (Figure 1-3) [3]. It is vascularised and innervated, and consists of two layers: an outer fibrous layer populated mainly by fibroblasts, and an inner layer (cambium) that contains periosteum derived progenitor cells (PDPCs), which have MSC-like properties [40]. The PDPCs can differentiate into osteoblasts and chondrocytes

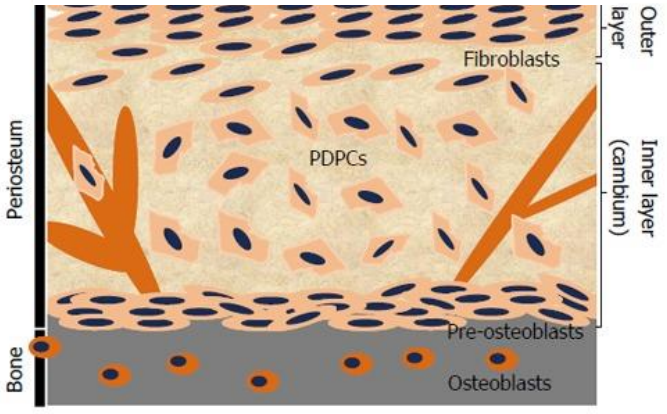


Figure 1-3 ***The periosteum layers****. The outer layer is populated by fibroblasts, whereas the inner layer (cambium) contains periosteum-derived progenitor cells (PDPCs). Adapted from [3]*

to increase bone width during development and contribute towards fracture repair.

The cortical bone or compact bone is the hard layer between the periosteum and the cancellous bone (Figure 1-4) [5]. As the name suggests, it is highly dense and rigid, which functions to carry mechanical loads and store the majority of calcium and phosphate in the human body. The cortical bone is intricately packed with columns called osteon. Each osteon consists of multiple layers of osteoblasts and osteocytes embedded in the bone matrix surrounding a central canal, which connects to other osteons. The canals allow the vasculature and neurons to connect between the periosteum and the cancellous bone, which is important for exchanging nutrients and signalling factors to regulate bone turnover. In a developed bone, the osteon is highly organised (laminar bone), whereas a disorganised osteon (woven bone) can be found during development or in diseases with high bone turnovers [41].

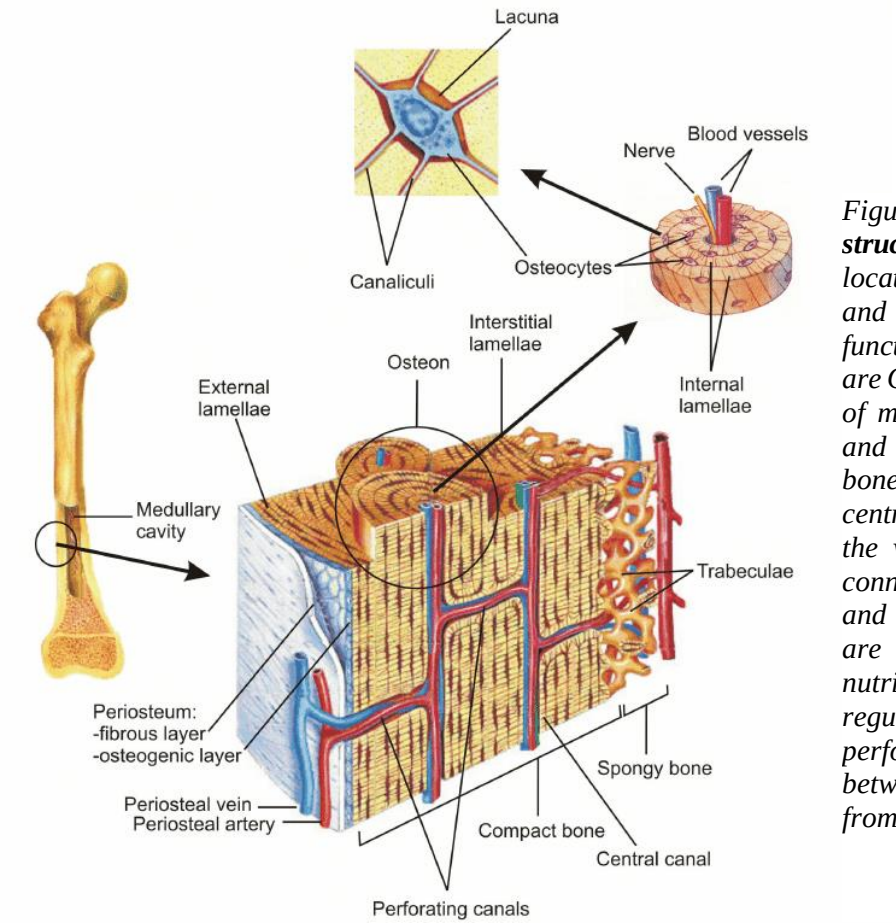


Figure 1-4 ***Cortical bone structure****. Cortical bone is located between the periosteum and the trabecular bone. The functional units in a cortical bone are Osteons. Each osteon consists of multiple layers of osteoblasts and osteocytes embedded in the bone matrix surrounding a central canal. The canals allows the vasculature and neurons to connect between the periosteum and the cancellous bone, which are important for exchanging nutrients and signalling factors to regulate bone turnover. The perforating canal connects between osteons. Figure adapted from [5]*

The trabecular, cancellous or spongy bone is the inner layer of the bone. It has a porous network (mesh), giving it more surface area to exchange calcium ions and to absorb mechanical impact [1]. The porous network is made up of trabeculae, which are structurally and functionally similar to the osteon. However, a blood supply is not needed due to the large surface area, eliminating the need for a central canal. Cancellous bone also contains bone marrow, in which HSCs and MSCs reside.

Bone marrow is found in the trabecular bone or the bone marrow cavity (medullary cavity) [42]. Bone marrow contains HSCs for haematopoiesis and MSCs, which are important for bone development and maintenance. The Bone marrow also contains adipocytes which may serve as an energy store and regulate lipid metabolism. In adults, the bone marrow adipocyte number has been shown to increase with age [43].

1.3.1 Osteoblasts, osteocytes and osteoclasts

During bone formation, osteoblasts secrete osteoid consisting of collagen (around 90%) and non-collagen proteins (NCPs), including Alkaline Phosphatase (ALP), Integrin Binding Sialoprotein (IBSP), secreted Phosphoprotein 1 (SPP1), and Bone Gamma-Carboxyglutamate Protein (BGLAP) [44]. The osteoid makes up the un-mineralised extracellular matrix (ECM). Subsequently, the ECM is mineralised through the formation and propagation of hydroxyapatite crystals (the osteoid and ECM are reviewed in greater detail in chapter 6.1). After active bone formation, osteoblast can undergo apoptosis, terminally differentiate into osteocytes or become quiescent bone lining cells. However, quiescent bone lining cells can be reactivated in response to parathyroid hormone (PTH) in order to contribute to local bone formation [45, 46].

Osteocytes make up over 90% of the bone cells, compared to 4-6% osteoblasts and 1 -2 % osteoclasts [47]. They are embedded within the matrix but are able to exchange nutrients and signal other cells via the canaliculi. Upon detecting stress in the skeletal environment, such as mechanical load or micro-damage, they can initiate bone remodelling through secreted factors [48, 49].

Osteoclasts are multinucleated cells responsible for bone resorption. Osteoclasts are differentiated from monocytes in the haematopoietic lineage. Ligands such as receptor activator of nuclear factor-κB ligand (RANKL) and macrophage-colony stimulating factor (M-CSF or CSF-1) are secreted by the osteoblasts, osteocytes and activated T cells [50, 51], and they are critical for driving osteoclast differentiation and maturation. Osteoprotegerin (OPG), also known as tumour necrosis factor receptor superfamily member 11B (TNFRSF11B), is an osteoblast- and osteocyte-secreted decoy receptor that inhibits osteoclastogenesis [52]. The OPG and RANKL/M-CSF balance is important to protect the bone from excess resorption.

1.3.2 Bone formation and resorption

Two types of bones are most frequently discussed in the literature, long bones, such as the femur, and flat bones, such as the skull. Developmentally, long bones are formed by endochondral ossification, whereas flat bones are formed through intramembranous ossification. Intramembranous ossification occurs through the condensation of MSCs followed by osteoblast differentiation. The osteoblasts deposit osteoid and minerals, and they become embedded within the mineralised bone matrix [53]. In contrast, during endochondral ossification, MSCs condense to form chondrocytes and osteoprogenitors called perichondrial cells [54, 55]. The chondrocytes form a hyaline cartilage template, and subsequently, undergo hypertrophy due to the limited vasculature. The perichondrial cells in the perichondrium

surrounding the hyaline cartilage differentiate into osteoblasts and replace the cartilage template with mineralised bone tissue. Simultaneously, blood vessels invade the cartilage to facilitate osteoblast differentiation and form a nascent bone marrow cavity. Lastly, bone remodelling occurs to reorganise the woven bone into the laminar bone.

Bone remodelling is not only important during development, but it is also needed for the replacement of apoptotic osteocytes and repair of bone damage. Activated mature osteoclasts adhere to the bone matrix to form an enclosed Howship's lacuna [56]. Acidification of the enclosed lacuna by carbonic anhydrase leads to decalcification of bone matrix, leaving the exposed osteoid, consisting largely of type I collagen. Degradation of the collagen occurs through the secretion of proteolytic enzymes such as Cathepsin K (Cat K), matrix metalloproteinases (MMPs), and tartrate-resistant acid phosphatase (TRAP). In a balanced system, bone marrow MSCs would migrate to the site of bone resorption, and differentiate into osteoblasts to refill the lacuna. In healthy individuals, the balance between bone formation and bone resorption during remodelling is mildly negative [57]. During ageing, bone homeostasis becomes more negative [58]. In women, the bone resorption rate doubles at menopause, and triples 13 years later [59].

1.3.3 Signalling pathways

Osteoblast differentiation is a complex molecular process regulated by numerous signalling pathways. The interaction between these pathways is important for MSC fate decision and bone turnover. Some of the major pathways involved are described below and depicted in Figure 1-5.

1.3.3.1 WNT

Wingless types MMTV integration site (WNT) signalling was identified to play an essential role in cell fate determination, proliferation and differentiation [60]. WNT signalling pathways consist of the canonical β-catenin dependent pathway and the non-canonical β-catenin independent pathways. Both canonical and non-canonical WNT pathways have been shown to regulate osteoblast differentiation. The canonical WNT pathway is mediated through the regulation of β-catenin. Upon WNT activating ligands binding to the receptor frizzled (FZD) and co-receptor lipoprotein receptor-related protein 5/6 (LRP5/6), the resulting signalling cascade releases β-catenin from the destruction complex consisting of glycogen synthase kinase 3 (GSK3), axin and adenomatous polyposis coli protein (APC) (Figure 1-5B). Subsequently, β-catenin translocates into the nucleus, where it forms a complex with LEF/TCF to regulate gene expression. Activation of the canonical WNT pathway via WTN3a treatment of MSCs directly induced *RUNX2* expression and promoted osteoblast differentiation [61, 62]. Simultaneously, canonical WNT activation down-regulated *PPARG* expression and adipocyte formation. Additionally, activation of the canonical WNT signalling with a stabilised β-catenin mutant, i.e. it cannot be degraded by the destruction complex, upregulated *OPG* expression and downregulated *RANKL* expression in osteoblast cell-lines [63]. When treated with WNT3a, osteoblasts co-cultured with osteoclast progenitors inhibited osteoclast formation. [64].

The non-canonical WNT pathways include the planar cell polarity pathway (PCP) and the Ca^{2+} pathway. The PCP and Ca^{2+} pathways are similarly activated by the interaction between WNT ligands and FZD, but they differ in the downstream mediators involved [65]. The PCP pathway is primarily mediated through the activation of Rho family GTPases member A (RhoA) and its effector Rho-associated kinase (ROCK), or through the activation of c-Jun N-terminal kinase (JNK). The PCP pathway is important for cytoskeletal reorganisation during cell differentiation [65]. RhoA/ROCK was shown to mediate *RUNX2* expression under mechanical strain [66].

Similarly, overexpressing a constitutively active RhoA promoted osteoblast differentiation, whereas, overexpressing a constitutively repressed RhoA promoted adipocyte differentiation [67]. The Ca^{2+} signalling pathway is mediated through the activation of phosphodiesterase (PDE) and phospholipase C (PKC), which can subsequently promote or inhibit calcium release from the endoplasmic reticulum. Increased calcium level directly activates calcineurin and overexpression of calcineurin in MSCs increased *RUNX2*, *ALP*, *IBSP* and *BGLAP* expression [68], whereas knockout of calcineurin in mice resulted in severe osteoporosis [69]. WNT5a treatment in osteoblast progenitors induced both PCP and Ca^{2+} signalling and enhanced osteogenesis. Interestingly, WNT5a treatment also induced JNK and PKC mediated *RANKL* expression in osteoblasts and enhanced osteoclastogenesis of co-cultured osteoclast precursors [70, 71]. Therefore, the non-canonical WNT pathway may promote bone turn over by regulating both osteoblast and osteoclast differentiation.

1.3.3.2 BMP

Bone morphogenetic proteins are members of the transforming growth factor β (TGFβ) superfamily that play an important role in bone and cartilage formation. Over 20 BMPs have been identified, with BMP2, 4, 6, 7 and 9 shown to promote osteogenesis and BMP3 shown to inhibit osteogenesis [72]. BMP binding results in the dimerization, phosphorylation and activation of serine-threonine kinase BMP receptors (type I and II). This subsequently initiates the SMAD1/4/5/8, mitogen-activated protein kinase (MAPK) or JNK pathways. BMP2 is the most extensively characterised. BMP2 treatment promotes osteoblast differentiation through the activation of SMAD and MAPK pathways, subsequently promoting *RUNX2* expression. In contrast, *BMP2* knockout in mice limbs resulted in frequent fractures that failed to heal [73]. However, while murine derived MSCs generally show a robust pro-osteogenic response to BMP2 signalling, its effect on human-derived MSCs has been variable [74]. BMP2 have also

been shown to promote *PPARG* expression and adipocyte differentiation through the SMAD and MAPK pathways [75]. Several studies have suggested that different BMP receptors (BMPR) regulate the osteogenic or adipogenic aspect of BMP signalling [76, 77].

1.3.3.3 HH

The hedgehog (HH) proteins family consist of Sonic hedgehog (SHH), Indian hedgehog (IHH) and Desert hedgehog (DHH). IHH and SHH are particularly critical in osteogenesis as disruption of their expression during development resulted in severe skeletal abnormalities [78]. HH ligands bind to their receptor patched (PTCH), which releases the inhibition of smoothened (SMO) from PTCH. Activated SMO inhibits the generation of proteolytically cleaved transcriptional repressor GLI3 and promotes the generation of full-length transcriptional activator Gli2 [2]. $IHH^{-/-}$ mouse embryos showed an absence of *RUNX2* expression in osteoprogenitor cells [79]. However, overexpression of *RUNX2* did not rescue osteoblast formation in the $IHH^{-/-}$ embryos, suggesting that IHH regulates other critical osteogenic factors in addition to *RUNX2*. The transcriptional activator Gli2 was also shown to upregulate *BMP2* expression in murine MSCs and BMP signalling was demonstrated to be required for HH induced osteogenesis [80]. Interestingly, HH may mediate as the switch between the pro-adipogenic and the pro-osteogenic effect of BMPs, as treatment with SHH suppressed the pro-adipogenic effects of BMP2 in murine MSCs [81]. Similarly, purmorphamine induced HH signalling significantly decreased the expression of adipogenic genes including *PPARG* [82].

1.3.3.4 TGFβ

TGFβs (1, 2 and 3) are members of the TGFβ superfamily. These multifunctional cytokines play important roles in bone development and post-natal bone remodelling. Similar to BMPs signalling, TGFβs interact with the serine-threonine kinase TGFβ receptors and regulate gene expression through SMAD2/3, MAPK and JNK signalling cascades [83]. In mice, *TGFβ1* knockout resulted in a significant decrease in osteoblast number and trabecular bone density [84]. In humans, a gain-of-function TGFβ1 mutation causes Camurati–Engelmann disease (CED), characterised by cortical bone thickening and fluctuating bone volume [85]. The bone volume fluctuation is thought to be due to TGFβ1 having an effect on bone formation and resorption that is differentiation stage-dependent and dosage-dependent. *In vitro,* MSCs treated with TGFβ1 showed increased proliferation and RUNX2+ pre-osteoblast commitment, but reduced osteoblast maturation and mineralisation [83, 84]. The concentration of TGFβ1 also regulates the ratio of RANKL/OPG secreted by osteoblasts, where low dosage promoted osteoclastogenesis but high dosage inhibited osteoclast differentiation in co-culture experiments [86, 87].

1.3.3.5 Notch

The Notch pathway mediates cell contact-dependent (juxtacrine) signalling. The binding of a Notch ligand to a Notch receptor (1-4) mediates the proteolytic cleavage of the receptor by γ-secretase. This releases the intracellular domain of the Notch receptor (NICD). NICD translates into the nucleus, where it forms a transcriptional regulation complex with the CSL family transcription factor (RBPJ). Notch is commonly regarded as a negative regulator of osteoblast formation. Notch1 and Notch2 knockout in the murine embryonic limb mesenchyme resulted in an increased osteoblast number and bone mass [88]. Mechanistically, Notch signalling has been shown to inhibit *RUNX2* expression through the upregulation of Hes-related family

BHLH transcription factor with YRPW motif 1 (*HEY1*) and HEY-like protein (*HEYL*). However, in the presence of BMP2, inhibition of Notch was shown to repress BMP target gene expression and delayed ossification, which suggests that Notch signalling may also synergise with BMP signalling to promote osteoblast differentiation [89].

1.3.3.6 FGF

The role of fibroblast growth factors (FGFs) on osteoblast differentiation has been reported to be highly variable, depending on numerous factors such as the stage of osteoblast differentiation and the stage of embryonic development [90, 91]. In general, FGF2, 8, 9 and 10 have been shown to be essential for skeletal development. FGF binding to the FGF receptor (FGFR) results in the phosphorylation and activation of the intracellular domain of FGFRs, which recruits and activate members of the MAPK, phosphoinositide 3-kinase (PI3K), signal transducer and activator of transcription 1 (STAT1) and PKC pathways. In murine MSCs, FGF2 treatment was shown to upregulate *RUNX2* expression and promote pro-osteoblast proliferation and differentiation [92]. The pro-osteogenic effect of FGF2 treatment is in part mediated through the activation of BMP2 and canonical WNT signalling [93, 94].

1.3.3.7 JAK/STAT

The Janus kinase (JAK) and signal transducer and activator of transcription (STAT) pathway was first identified to be important in bone formation in response to interleukin-6 family proteins, which includes interleukin-6 (IL-6), oncostatin M, leukaemia inhibitory factor (LIF) and cardiotrophin-1 (CT-1) [95]. The binding of IL-6 family cytokines to their receptors leads to the activation of JAK/STATs. Activated STATs dimerise and translocate into the nucleus to regulate gene expression. STAT3 is frequently implicated in the regulation of bone

development and remodelling. A heterozygous loss of function mutation in STAT3 results in Job syndrome, which is an immunodeficiency disorder with skeletal defects, including reduced bone mineral density, scoliosis and frequent fractures, indicating that STAT3 is required for correct bone development. Similarly, the loss of osteoblast formation was observed in *STAT3* knockout mice. However, in the presence of BMP2, the inhibition of the STAT3 signalling pathway accelerated BMP induced osteoblast differentiation in MSCs [96].

Other pathways that may be important in osteoblast differentiation includes the neural EGFL like 1 (NELL-1) and the insulin growth factor-1 (IGF-1) signalling pathways. NELL-1 upregulation was identified in patients with sporadic coronal craniosynostosis, characterised with premature bone formation [97]. Similarly, NELL-1 overexpression in mice resulted in bone overgrowth. NELL1 is thought to promote osteogenesis through the canonical WNT and JNK pathways [98, 99]. IGF signalling is mediated through IGF-1 receptor and the regulation of AKT and MAPK pathways [100]. In mouse studies, IGF-1 treatment was shown to promote both osteoblast and adipocyte differentiation [101, 102].

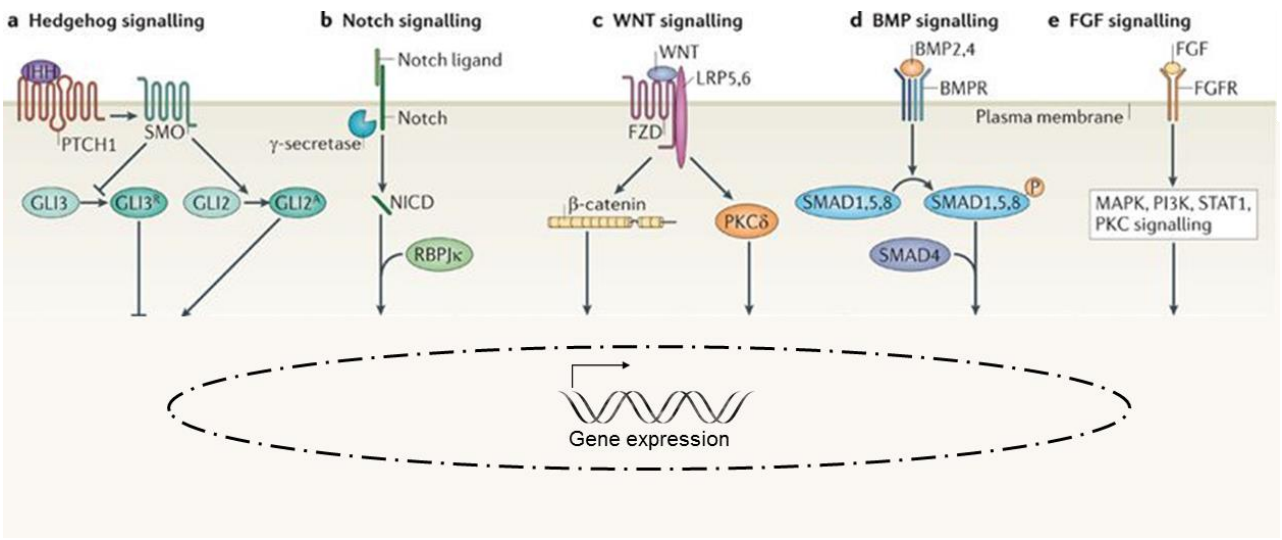


Figure 1-5 ***Major signalling pathways regulating osteogenesis. A)*** *Hedgehog (HH) binds to the receptor patched (PTCH), which activates HH signalling through smoothened (SMO). SMO inhibits the formation of transcriptional repressor GLI3, and promotes the formation of transcriptional activator GLI2.* ***B)*** *Notch binds to the Notch receptor (1-4), which mediates the proteolytic cleavage of the receptor by γ-secretase. This releases the Notch intracellular domain (NICD), which forms a transcriptional regulatory complex with the CSL family transcription factor (RBPJ).* ***C)*** *Canonical WNT binds to the WNT receptor Frizzled and co-receptor lipoprotein receptor-related protein 5/6 (LRP5/6), which stabilises β-catenin from degradation and promotes its nuclear translocation and formation of a transcriptional regulatory complex with LEF/TCF. The non-canonical WNT pathway mediates signalling through a similar mechanism but diverges at protein kinase Cδ (PKCδ).* ***d)*** *BMP binding results in the dimerization, phosphorylation and activation of serine-theronine kinase BMP receptors (type I and II), which subsequently phosphorylate SMAD1/5/8. SMAD1/5/8 forms a complex with SMAD4 to regulate gene expression.* ***e)*** *FGF binding to the FGF receptor (FGFR) results in the phosphorylation and activation of the intracellular domain of FGFRs, which recruits and activates members of the mitogen-activated protein kinase (MAPK), phosphoinositide 3-kinase (PI3K), signal transducer and activator of transcription 1 (STAT1) and PKC pathways. Figure adapted from [2].*

1.4 Ageing

1.4.1 Osteoblast and osteoclast balance

Around 10% of total bone volume is replaced by bone remodelling within a year [103]. As described in chapter 1.2.3, a balanced system involves the osteogenic differentiation of MSCs at the site of bone resorption to replace the skeletal cells and replenish the bone matrix. However, multiple studies reported a net loss in bone volume and density with increasing age, including a significant reduction in trabecular and cortical bone density, accompanied by a decreased cortical thickness and increased porosity [58, 104, 105]. At the age of 30, trabecular bone density begins to decline, and at the age of 50, cortical bone density also begins to decline. In women, the rate of bone loss accelerates after menopause. This significantly increases the risk of fracture and age-related bone diseases.

Multiple pieces of evidence point to an age-related decline in the proliferative and osteogenic capability of MSCs. In mice, rhesus monkeys and humans, a significant decline in the clonogenic potential and population doubling rate of MSCs were reported in old donors compared to young donors. Similarly, studies have found that MSCs derived from old donors showed a significant decrease in osteoblast formation and bone matrix mineralisation. Immunostaining of homogenised cells obtained from the cancellous bone of old human donors showed significantly decreased expression of *RUNX2*, *OPN*, and *OCN* [106]. Moreover, a decline in osteoblast number in bones has been observed with age [107]. Ageing MSCs also contribute to increased bone resorption since the expression of *RANKL* and *M-CSF* in MSCs significantly increased with age and the expression of *OPG* significantly decreased with age. Co-culturing of old donor MSCs with osteoclast progenitors significantly increased number of active osteoblasts by TRAP staining compared to co-culturing with young donor MSCs [108]. A contrary result was also found, where immunohistochemical staining of trabecular bone showed significantly more active osteoclasts in young human donors compared to the old

[106]. However, the same study also reported a significant decline in the trabecular bone mineral density with increased donor age, indicating that there may be a stronger decline in bone formation compared to the decreased bone resorption.

1.4.2 Age-associated bone diseases

The balance between bone formation and bone resorption can be further disrupted in age-associated bone diseases. "Bone ageing" can be accelerated by inflammation and cancer. While transient inflammation is essential for bone healing, chronic systemic inflammation in conditions such as osteoporosis, rheumatoid arthritis (RA), osteoarthritis (OA), chronic obstructive pulmonary disease, and diabetes mellitus is detrimental to bone homeostasis [6]. Haematological malignancies such as multiple myeloma are also characterised with bone loss, mediated by a variety of biological modifiers including osteoclast-activating factors and osteoblast inhibitory factors produced either directly by malignant plasma cells (MPCs) or through their interaction with the bone marrow microenvironment [109].

Osteoporosis affects 1 in 5 people over the age of 50. It is characterised by reduced bone mass and bone strength, leading to an increased risk of fracture in the spine, hip and wrist. It is caused by the imbalance in bone turnover. However, much of the environmental and genetic contribution to the disease remains unknown [110]. The decline of oestrogen has been implicated as an important contributor as osteoporosis is most prevalent in post-menopausal women. Similarly, the conditional knockout of ERα in osteoprogenitors of female mice resulted in low cortical bone mass [111]. Oestrogen binding to the nuclear oestrogen receptors (ERα or ERβ) can either directly mediate gene expression or indirectly regulate gene expression through interaction with other transcription factors. For example, ERα functions synergistically with the canonical WNT signalling. WNT3a treatment upregulated ERα expression [112], and

activation of ER by estradiol (E2) enhanced WNT3a mediated osteogenesis [112]. In contrast, deletion of ERα reduced WNT3a mediated osteogenesis [111]. The canonical WNT signalling pathway has also been implicated in osteoporosis. High serum level of sclerostin (SOST), a canonical WNT inhibitor, has been shown to be strongly associated with increased risk of osteoporosis-related fractures [113]. SOST treatment has been shown to significantly impair osteoblast differentiation and bone formation, whereas anti-SOST antibody (Romosozumab) treatment has been shown to significantly increase bone mineral density and reduce fracture risk in postmenopausal women with osteoporosis.

Rheumatoid arthritis (RA) is a painful, potentially debilitating autoimmune condition that affects around 2-3% of the population over the age of 60 [114]. It is characterised by chronic inflammation of the joint, which promotes osteoclast-mediated bone resorption, and suppresses osteoblast mediated bone formation. As a result, patients experience bone erosion over time. This age-associated increase in inflammation is thought to be caused, at least in part, by immunosenescence, which is characterised by a more active innate immunity and a less active adaptive immunity. The cause of immunosenescence is unclear, but it is marked by serval physiological changes:

- A decline in the production of naïve T-cells and an increase in the number of senescent T cells.
- Chronic low-grade inflammation due to increased serum inflammatory cytokines, including TNFα, IL1 and IL6.

Tumour necrosis factor-alpha (TNFα) has been shown to upregulate the expression of *RANKL* and *M-CSF* in stromal cells and promote osteoclastogenesis [115]. Similarly, IL1 and IL6 were found to upregulate the expression of *RANKL* on the surface of osteoblasts and promote the differentiation of co-cultured osteoclast progenitors [116]. However, direct interaction between

IL6 and osteoclast-progenitors has been shown to inhibit osteoclast differentiation. Therefore, the overall effect of IL6 on osteoclast differentiation likely depends on the microenvironment [117]. Systematic administration of anti-TNFα antibody (infliximab) and anti-IL6R antibody (Tocilizumab) have been used to reduce inflammation and bone resorption in RA patients [118, 119].

Current therapies for osteoporosis and RA can effectively inhibit bone resorption, but promoting bone formation remains a clinical challenge. In order to develop effective bone anabolics, a better understanding of the mechanism of the age-related decline in MSC self-renewal and osteogenic potential is required.

1.4.3 Hallmarks of MSC ageing

Ageing is characterised as a time-dependent progressive decline in function and increased vulnerability to death [120]. Over the last two decades, there has been an accelerated progression in the understanding of molecular and cellular causes of ageing, through which, the hallmarks of ageing were proposed:

1.4.3.1 Genomic instability

There is a random accumulation of DNA damage with age, which can lead to the loss of genomic stability [121]. This may be caused by endogenous risks, such as DNA replication error, or reactive oxygen species (ROS) generated by cell metabolism. DNA damage can also accumulate from environmental factors, such as ultraviolet (UV) radiation, viral infections, or chemical agents. DNA damage can lead to point mutations, which, in turn, can lead to the loss or gain of gene functions. In addition, DNA damage reduces genomic stability, which can lead to chromosomal translocations, gains or losses. Reduced genomic stability can result in a

number of diseases, such as Werner syndrome (progeria), which exhibits symptoms of premature ageing. Progeria syndrome is a rare monogenic disease, commonly caused by a mutation in Lamin A. Normal lamins (type A and B) are filament proteins integral to the nuclear lamina, which is important for nuclear stability, chromatin structure regulation and gene expression regulation [122]. Mutations in progeria result in the production and pathological accumulation of a truncated protein called progerin, which disrupts the nuclear lamina structure. iPSC-derived MSCs from progeria patients showed increased DNA damage and reduced osteogenic potential [123]. Interestingly, low amounts of progerin have been detected in vascular smooth muscles cells (VSMCs) during normal ageing *in vivo* and *in vitro,* suggesting a possible role of progerin accumulation in ageing [124].

1.4.3.2 Telomere attrition

The phenomena of a finite replicative capacity in somatic cells is known as the Hayflick limit. To address the Hayflick limit in somatic cells, Olonikov proposed that there is an attrition of DNA after each cell replication until cell division ends [125]. This has been shown to be true with the discovery of telomeres by Blackburn and colleagues. Telomeres are regions of repeating "TTAGG" nucleotide sequences at both ends of a chromosome. During DNA replication, polymerases are unable to completely replicate the telomere, resulting in telomere shortening. Telomerase is an enzyme that functions to maintain the telomere length by adding the missing nucleotides. In murine models, shortened telomeres were associated with decreased life span [126]. Similarly, a progressive telomere shortening is frequently reported in human MSCs with age and is strongly associated with an increase in mortality. MSCs derived from telomerase knockout mice showed a significant decrease in their proliferative and osteogenic potential [127]. Telomere shortening also resulted in the upregulation of *P21* and *P53*, which are proteins that mediate cell cycle arrest, senescence or apoptosis. However, in humans,

MSCs isolated from young and old donors showed no significant difference in telomere length [128, 129]. This suggests that telomere shortening may not be the primary cause for the decline of human MSC function with age.

1.4.3.3 Epigenetic alterations

Epigenetic changes are heritable changes of gene expression without alterations in DNA sequences. Epigenetic changes that occur at the chromatin level include DNA methylation, histone modification, and chromatin remodelling. Early studies observed a global hypomethylation with age in MSCs [130, 131]. Subsequent results varied, with many studies reporting no global changes in DNA methylation in MSCs with age [132, 133]. However, these studies agreed that there are significant changes in DNA methylation at specific CpG sites with increased age, including that of tumour suppressor genes, polycomb target genes and senescence-associated genes. Recently, it has been shown that specific DNA methylation biomarkers can be predictive of cellular age, this is referred to as the epigenetic clock [134].

Age-related changes in DNA methylation at specific genes can affect the osteogenic potential of MSCs. For example, Homeobox (*HOX)* family genes were found to be differentially methylated in aged MSCs. *HOX* genes encode a family of 39 homeodomain-containing transcription factors that are critical for embryonic patterning. Recent studies found *HOX* genes may have important roles beyond embryonic development in fracture repair [135]. In aged MSCs, studies found increases in methylation of *HOXA3*, *HOXA5*, *HOXA6*, *HOXB2*-B5, *HOXB7* and *HOXC4*, and corresponding decreases in gene expression [136, 137]. In contrast, MSCs overexpressing *HOXB7* showed increased proliferation, reduced senescence and enhanced osteogenic differentiation [138]. Subsequent studies showed that FGF and IHH signalling are required for *HOX* mediated proliferation and osteoblast differentiation [139].

MSC ageing is also associated with changes in histones marks, such as a decreased H3K9 and H3K14 acetylation at stemness genes - OCT4, SOX2 and Tert [140]. There is also a correlated decline in the expression of these stemness genes. A number of histone modifiers are also found to be dysregulated during MSC ageing. For example, the sirtuin family of ADP-ribosyltransferases and NAD-dependent protein deacetylases (SIRT) was one of the first epigenetic regulators of ageing to be discovered. Overexpression of *SIRT2* (or *SIRT1* in mammals) significantly extended the lifespan of invertebrates [141] but varied between studies in mammals [142, 143]. In addition to longevity, *SIRT1* overexpression in old mice resulted in decreased cellular DNA damage and a reduced incidence of carcinomas and sarcomas [143]. *SIRT1* overexpression also increased osteoblast number and bone mass. Mechanistically, SIRT1 was found to regulate the expression of a number of genes involved in the WNT, IGF, FOXO3 and P53 pathways [142, 144-146]. For example, *SIRT1* heterozygous deletion resulted in an increased *SOST* expression in murine MSCs. Chromatin immunoprecipitation (ChIP) showed that SIRT1 deacetylates histone H3K9 to repress SOST expression [147]. Additionally, SIRT1 directly deacetylates β-catenin to promote its nuclear accumulation. Homozygous *SIRT1* deletion significantly reduced the osteogenic and chondrogenic potential of murine MSCs [145]. Interestingly, *SIRT1* knockout resulted in more severe bone loss in old mice than young mice, indicating there may be an age-related increase in *SIRT1* dependent osteogenesis. In addition, SIRT3, SIRT6 and SIRT7 have also been found to regulate skeletal development and turnover in ageing and age-related bone diseases [148].

In addition to DNA methylation and histone modifications, non-coding RNAs also play an important role in MSC ageing. For example, microRNA (miRNA) 218, 196, 188 and 141 were found to be upregulated in MSCs with age [149-151]. Interestingly, miRNA196 has been shown to downregulate *HOXB7* expression, suggesting that an age-related change in gene expression can be caused by multiple epigenetic mechanisms.

1.4.3.4 Protein homeostasis

Autophagy, chaperone-mediated protein folding, and ubiquitination are important regulatory mechanisms of protein homeostasis. In MSCs, inhibition of autophagy significantly impaired proliferation and osteogenesis, and it significantly enhanced adipogenesis [152]. mTOR is a serine/threonine protein kinase that plays an important role in autophagy. mTOR participate in two distinct protein complexes: mTOR complex 1 (mTORC1) and mTOR complex 2 (mTORC2) [153]. mTORC1 and mTORC2 share common subunits such as mLST8, DEPTOR and PRAS40. However, the regulatory-associated protein of mTORC1 (Raptor) is exclusive to mTORC1 and the rapamycin-insensitive companion of mammalian target of rapamycin (Rictor) is exclusive to mTORC2, as knockout of Raptor and Rictor impaired only mTORC1 and mTORC2 signalling, respectively. mTORC1 inhibits autophagy through the inhibition of ULK1 (an autophagy activating kinase), and TFEB (a transcription factor that mediates the expression of autophagy and lysosomal genes). mTORC2 regulates a distinct group of target genes instead. Due to their differences, acute rapamycin treatment only inhibits mTORC1. In MSCs derived from aged mice, rapamycin treatment stimulated autophagy and restored both osteogenic and differentiation potential [154]. Similarly, *in vivo* administration of rapamycin increased the bone mineral density of old mice [155]. However, studies have also shown that mTORC1 is required for osteogenesis as Raptor knockout impaired osteogenesis, suggesting that mTORC1 may regulate osteogenesis in a dose-dependent manner [156].

Heat shock proteins are stress-induced chaperone proteins important for stabilising nascent proteins and refolding misfolded proteins. Early studies showed that overexpressing HSP-16, HSP-22 and HSP-70 in C.elegans increased their life-span and resistance to oxidative stress [157, 158]. In mice, increased expression of HSPs was observed in long-lived dwarf mice. Interestingly, SIRT1 induces HSP-70 expression, so the increase in longevity by SIRT

overexpression may be partly mediated through the HSP. In human MSCs, knockdown of HSP-70 significantly impaired osteogenesis during thermal stress condition [159]. However, the role of HSP in normal MSC ageing is unclear.

1.4.3.5 Nutrient sensing

Dietary restriction (DR), defined as 50 to 70% of *ad libitum* feeding, has been shown to increases the lifespan of invertebrates and non-primates. While DR-mediated increase in longevity in primates has been controversial, DR-mediated increase in healthspan was more often agreed upon. One of the key nutrient-sensing pathways implicated in DR is the insulin/insulin-like growth factor (IIS) signalling pathway. Inhibition of the IIS pathway has been shown to extend the lifespan of worms, flies and mice [160]. In MSCs, inhibition of IIS signalling occurs via the overexpression of insulin-like growth factor binding protein 7 (IGFBP7) – a secreted protein that binds IGF receptors to inhibit IIS signalling [161], significantly increased osteogenic potential *in vitro* and enhanced bone healing in rats *in vivo* [162]. The pro-osteogenic effect of IIS inhibition is thought to be mediated in part through increased canonical β-catenin signalling activity [163]. Insulin/IGF inhibition has also inhibited mTORC1 [164]. In addition to promoting autophagy, mTORC1 inhibition has also impaired adipogenesis [165]. Therefore, IIS signalling may regulate the balance between osteogenesis and adipogenesis with age.

1.4.3.6 Mitochondria and ROS

The free radical theory of ageing proposes that the cumulative exposure to reactive oxygen species (ROS) during ageing results in mitochondrial and cellular damage. ROS, including hydrogen peroxide, hydroxyl radicals and superoxide anions, are by-products of aerobic

metabolism. ROS exposure can result in DNA, protein and lipids damages, leading to genomic instability, telomere attrition and the loss of protein homeostasis. ROS can induce cellular apoptosis throughout the activation of P53/BCL-2 and caspase-dependent pathways [166]. ROS has also been also shown to promote mTORC1 activation and to repress mTORC2 activation [107]. Hydrogen peroxide treatment has been shown to upregulate miR-218 expression, which then inhibits Rictor expression and reduces osteoblast number and accelerates bone loss in aged mice. In contrast, there is also evidence that ROS can stimulate cellular stress responses that increases longevity [167]. Thus, the role and mechanism of ROS in health and ageing remain yet to be fully elucidated.

1.4.3.7 Senescence

Cellular senescence can be defined as an arrest of cell division coupled to an increase in the senescence-related phenotype. The most commonly used phenotypical marker is senescence-associated β-galactosidase (SA-β-Gal). SA-β-Gal is a pH-dependent lysosomal β-galactosidase that accumulates in senescent cells through an unclear mechanism [168]. Molecular markers of senescence include cell cycle regulator genes *P16, P21* and *P53* [169]. These cell cycles regulators have been shown to accumulate with age and prolonged exposure to cellular stress. Cellular senescence is important in healthy tissue turnover and in preventing tumour formation, as loss-of-function mutations of P16 are frequently observed in cancers. However, the age-related decline in senescent cell clearance and the exhaustion of progenitor capacity to replace senescent cells can contribute to the decline of tissue function. A recent proteomic study has shown that the profile of secreted cytokines, growth factors and matrix metalloproteinases of senescent MSCs differs significantly to that of non-senescent MSCs. This is referred to as the senescence-associated secretory phenotype (SASP), which may contribute towards the senescence of neighbouring cells [170].

1.4.3.8 Stem cell exhaustion

The age-related decline in the proliferative potential of somatic stem cells has been observed in almost all adult stem cells, including the haemopoietic, neuronal, mesenchymal, and muscle progenitors [171-174]. Although it is difficult to determine whether *in vivo* depletion of MSCs occurs with age, the decline in proliferative potential of MSCs *in vitro* with age has been extensively characterised (more details in chapter 3.1). Transplantation of MSCs from young mice to old mice was shown to increase bone density [175]. However, it is unclear whether the therapeutic effect is due to the replenishment of MSCs or is mediated through the secreted factors of the transplanted cells [176].

1.4.3.9 Intercellular communications

An age-associated increase in the cellular production of pro-inflammatory cytokine is referred to as inflammageing. Old donor MSCs have been shown to express more RANKL and IL-6. Co-culturing osteoclast progenitors with old donor MSCs have significantly increased the number of active osteoclasts compared to co-culturing with young donor MSCs [106, 108]. Conversely, blood transfusion from young mice improved fracture repair in old mice.

In summary, MSCs ageing is regulated through a number of inter-related factors. The underlying molecular pathways that are altered during MSC ageing have begun to emerge. However, the mechanism of MSC ageing remains poorly understood. The next section describes some of the recent development in -omics approaches that will enable the identification of regulators and mechanisms that mediates changes in MSC proliferation and osteogenic potential with age.

1.5 Epigenomics, transcriptomics, and proteomics

A multi-omics approach presents the opportunity to understand the multi-layered information that underlies human ageing. These layers include the epigenome, the genome, the transcriptome and the proteome.

Epigenetic changes are heritable changes of gene expression without alterations in DNA sequences. These changes occur at the chromatin level and include DNA methylation, histone modification, and chromatin remodelling. These epigenetic changes are described in more detail below:

DNA methylation is the covalent addition of a methyl group to cytosine, mediated by DNA methyltransferases (DNMT). In eukaryotes, this preferentially occurs at a CpG site – a cytosine followed by a guanine. CpG islands are short stretches of DNA <500bp with a GC content of >55% [177]. CpG islands are typically located at the promoter region of genes, and the increased DNA methylation at CpG islands is typically associated with transcriptional silencing of those genes. DNA methylation-seq or DNA methylation microarray are commonly used methods to examine genome-wide methylation profiles (detailed in section 1.5.3).

Histones are proteins which DNA is wrapped around, facilitating condensation of the chromatin structure. Histone modifications such as methylation, acetylation, phosphorylation, ubiquitination and sumoylation alter the transcriptional activity by either having a direct impact on the accessibility of DNA within the chromatin or through recruiting ‘readers’ of histone marks to mediate downstream biological effects [178].

Chromatin remodelling is a protein-mediated process to regulate the accessibility of DNA by rearranging chromatin. For example, the well-characterised switch/sucrose nonfermenting

(SWI/SNF) complex carries out adenosine triphosphate (ATP)-dependent remodeling of DNA within the chromatin, allowing certain gene regions to gain better access to the transcriptional machineries [179]. Methods such as ATAC-seq and DNase-seq can be used to identify accessible regions of DNA within chromatin (detailed in section 1.5.2). ChIP-seq can be used to examine regions of DNA associated with a particular histone mark.

RNA expression is the transcription of DNA to RNA, partially regulated by DNA methylation, DNA accessibility and histone marks. RNAs have an array of functions: Messenger RNAs (mRNAs) carry protein-coding information. tRNAs and rRNAs are important parts of the ribosomal protein translation complex. miRNA and anti-sense RNA mediate post-transcriptional silencing of mRNAs [180]. RNA-seq is commonly used to examine the transcriptome (detailed in section 1.5.1).

Proteins are translated from mRNAs. Protein translation is partially regulated by the availability of mRNAs, but it also depends on factors such as the post-transcriptional modifications of mRNAs and RNA silencing. Proteins have an array of functions including catalysing chemical reactions, intercellular signalling, structural support and transport of small molecules. CyTOF is an emerging method that has the potential to carry out high-throughput protein detection at a single-cell resolution (detailed in section 1.5.4).

1.5.1 RNA-seq

RNA-seq enables relative quantification of gene expression across the transcriptome. The most commonly used RNA-seq method today uses the whole transcriptome shotgun next-generation sequencing (NGS) method. This involves the fragmentation of the transcripts, reverse transcription of the fragmented transcript to generate a cDNA library, and the PCR of the cDNA

library to generate a sequencing library (*Figure 1-6*). Depending on the sequencing chemistry used, the sequencing library can be non-strand specific (non-directional) or strand-specific (directional). Retaining the strandedness of the sequencing library captures the sense and anti-sense complexity of the genome [181]. After the sequencing library is made, single-end or paired-end sequencing can be performed. Single-end sequencing is when each fragment is only "read" from one end, whereas paired-end sequencing is when each fragment is "read" from both ends. Paired-end sequencing can effectively improve the coverage of the transcript. This is because the distance between the paired reads is known, so the alignment algorithms can use this information to improve mapping quality. Mapping is the alignment of the reads (typically between 50 to 300 bp) to a reference genome, which is required for the quantification of gene expression. However, mapping of these short reads can often be ambiguous or to multiple genomic loci, leading to a source of bias in RNA-seq data. Other sources of bias and computational methods to overcome these biases are discussed in section 1.5.5.

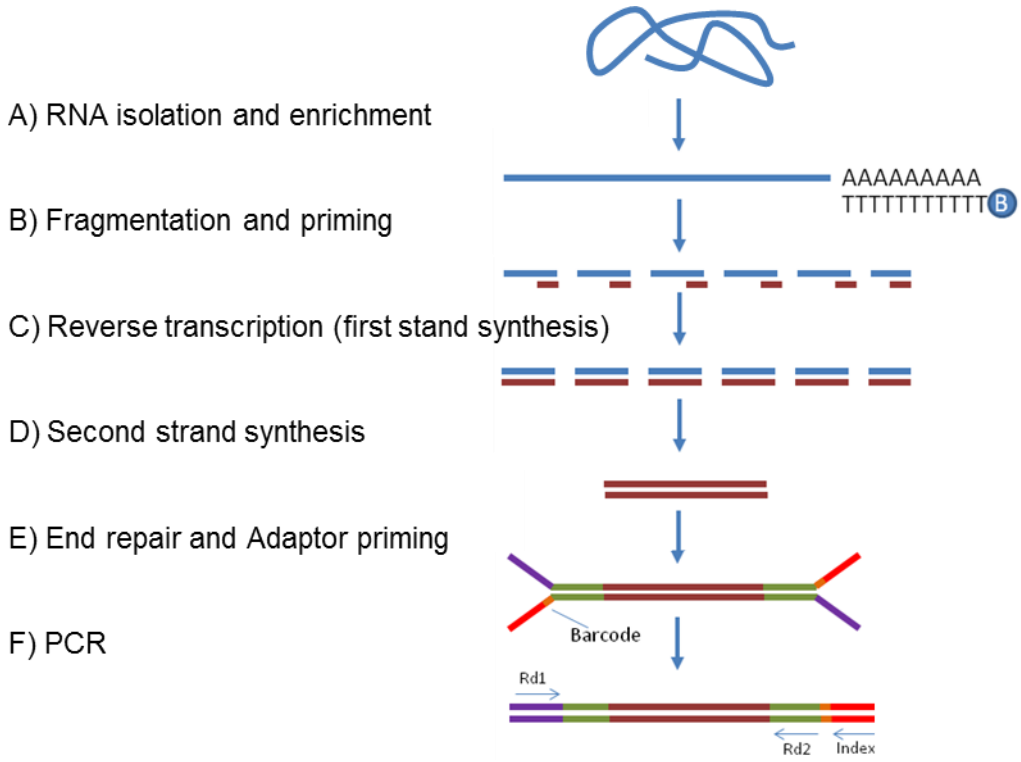


Figure 1-6 ***RNA-seq principle.*** *A) RNA is isolated from cells. Polyadenylated RNA and ribosomal RNA can be enriched or reduced to sequence subtypes of the transcriptome. B) Enriched RNA is fragmented and in C&D) reverse transcription is carried out. E&F) Adaptor index/barcode can be altered for multiplexing samples. During sequencing, DNA can be read from only one end (Rd1) or both ends (Rd1&Rd2), referred to as single-end or paired-end sequencing, respectively.*

1.5.2 ATAC-seq

Assay for transposase accessible chromatin with high-throughput sequencing (ATAC-seq) is a recently developed method used to assess genome-wide chromatin accessibility [182]. ATAC-seq uses hyperactive Tn5 transposase to cut DNA at regions of open chromatin. Simultaneously, the transposase ligates adapters onto the fragmented DNA for subsequent PCR amplification and sequencing (*Figure 1-7*). The PCR and sequencing steps are identical in principle to the RNA-seq library preparation methods. ATAC-seq has been used to identify genome-wide chromatin accessibility changes in cancer and in blood cell differentiation studies [183, 184]. Similar methods such as DNase-seq and FAIRE-seq were previously developed.

However, ATAC-seq is a far more rapid protocol, requiring fewer cells while still delivering a comparable sensitivity to the other methods [182].

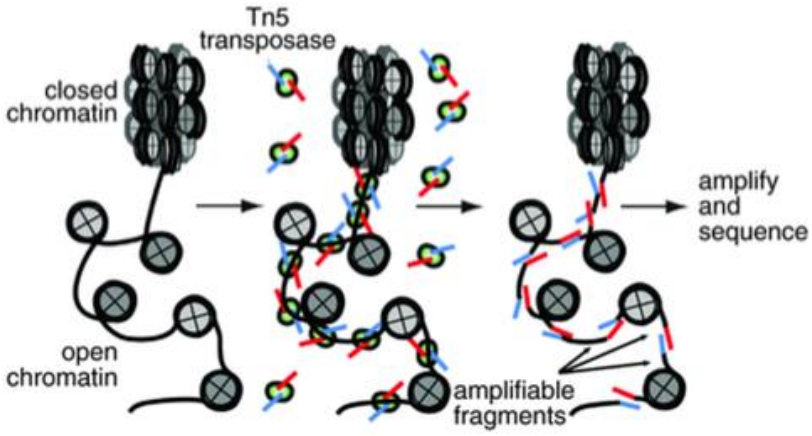


Figure 1-7 ***ATAC-seq principle****. In a permeabilised cell or nuclei extract, hyperactive Tn5 transposase is introduced to cut accessible chromatin DNA, and simultaneously ligate adapters onto the fragmented DNA for subsequent PCR and sequencing. Figure adapted from [182]*

1.5.3 DNA methylation array

A DNA methylation array (DNAme-array) is used to examine genome-wide DNA methylation profiles. The most commonly used approach is bisulfite conversion based DNAme-array (*Figure 1-8*), which consists of two major steps: 1) Bisulfite conversion deaminates unmethylated cytosine to uracil, whereas methylated cytosine is unaffected. Subsequently, the uracil is converted to thymidine when the bisulfite-treated DNA is amplified and fragmented. 2) The fragmented DNA library anneals to the oligonucleotide probes on the array. A single-base extension will then occur to incorporate a fluorescently labelled nucleotide. The Illumina Infinium methylation array uses two types of chemistry. Type I contains two oligonucleotide probe types complimentary to either methylated or unmethylated CpGs, thus the probe type can distinguish the methylation state. Type II uses only one probe type, but the 3' end of the probe is always one nucleotide upstream of the CpG query site [185]. Therefore, the methylation state is determined by the single base extension of the differentially labelled nucleotide. In both cases, the relative fluorescent intensity of the methylated vs unmethylated CpG loci is measured and quantified as β-values (ratio of methylated probe intensity vs unmethylated probe intensity). However, type I and type II chemistries have different biases in β-value at low and high-value ranges. Therefore, when using an array containing both type I and type II chemistries, intra-sample comparison is subjected to bias, making inter-sample comparison recommended. An additional consideration of a microarray is the coverage of CpG sites. The Infinium 450K array (type I and type II chemistries) queries 485,577 CpG sites including multiple CpG sites at 99% of human reference genes and 96% of CpG islands [186]. The Infinium 850K array (type I and type II chemistries) detects an additional 333,265 CpG sites located at enhancer regions identified by the ENCODE and FANTOM5 projects [187]. The 450K and 850K microarrays have been used extensively for profiling DNA methylation changes in cancer, ageing and inter-individual variability [188-192].

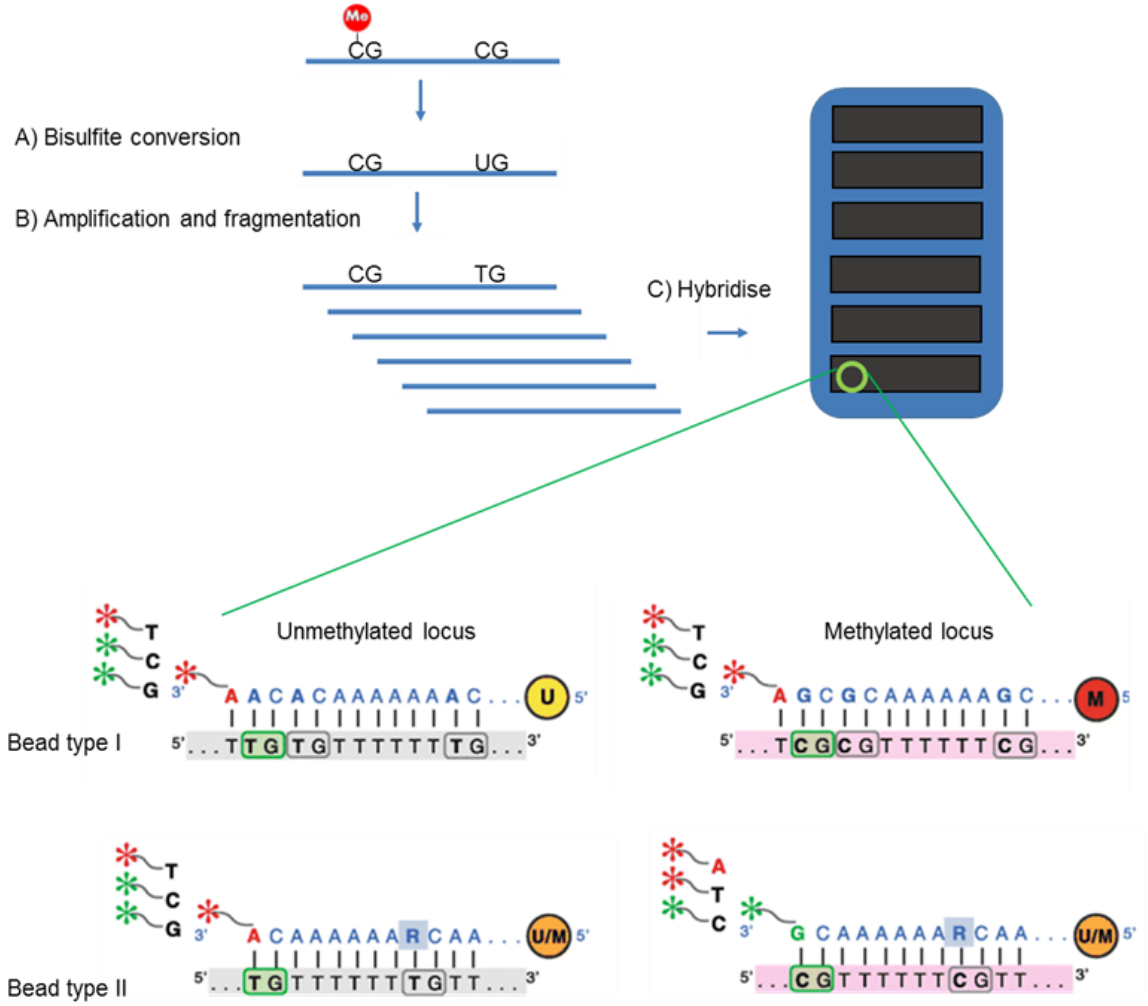


Figure 1-8 ***Bisulfite conversion based DNAme-array****. A) Bisulfite conversion deaminates unmethylated cytosine to uracil, whereas methylated cytosine is unaffected. B) The uracil is converted to thymidine when the bisulfite-treated DNA is amplified and fragmented. C) The fragmented DNA library anneals to the oligonucleotide probes on the array. A single-base extension will occur to incorporate a fluorescently labelled nucleotide. The Illumina Infinium methylation array uses two types of probe chemistry. Type I uses two probe types (U and M) to determine the methylation state. The oligonucleotide probe is complementary to either methylated or unmethylated CpGs, so single base extension can only occur with the complementary probe. Type II uses only 1 bead type (U/M). The 3' end of the probe is always one nucleotide upstream of the CpG query site, so the methylation state is determined by the fluorescent colour of the incorporated nucleotide. Figure adapted from [193].*

1.5.4 CyTOF

Cytometry by time-of-flight (CyTOF) or mass cytometry is an emerging technology that can simultaneously profile >40 protein (and RNA) markers in a single cell [194, 195]. This technology overcomes the limitation of spectral overlap of fluorescent tags in flow cytometry to increase the number of markers that can be measured. Rather than fluorescent tags, antibodies are labelled using rare heavy-metal isotopes that are not normally present in cells. The labelled cells are introduced sequentially to a mass cytometer, which detects and quantifies the metal labels. Cell surface, cytoplasmic and intracellular markers can all be quantified depending on the cell staining protocol. CyTOF enables detection of entire signalling networks, and it has been used to create a single-cell atlas of tumours and the immune system [196].

1.5.5 Statistics in –omics data

The principle reason for statistical analysis in NGS data is to detect significant differences between two or more samples while accounting for technical and biological variability. The major aspects of the statistical analysis of NGS data are normalisation, dispersion, distribution modelling, and hypothesis testing [197].

Normalisation is the process of scaling raw count values to account for some of the intra-library and inter-library variation. There are three important factors to consider:

- Sequencing depth i.e. the total number of reads for each sample. It is unlikely that all the samples are sequenced to the exact same depth. Normalisation methods such as fragments per kilobase million (FPKM), transcripts per kilobase million (TPM), and median of ratio account for the sequencing depth [198].
- Transcript length: a longer transcript will have more fragments than a shorter transcript, hence more reads. This is less of a concern when the same genes are compared between

two samples in differential gene expression (DE). However, it is more important when different genes are compared within a sample. Methods such as FPKM and TPM account for the transcript length [198].

- Library composition: empirical data suggests that a few highly and differentially expressed genes can influence the total read counts for a sample, which skews the ratio of counts per genes in the sample compared to other samples. This is important for DE between samples. Methods such as median of ratio used in DESeq2 account for the library composition [199].
- Batch effect and confounding factors: unwanted variation due to experimental design can lead to batch effects. Known or unknown biases in samples can lead to confounding factors. Removing these effects are often difficult. Supervised normalisation tools – defined here as methods that are aware of the experimental design, have been developed to aggressively remove these unwanted variations. Tools such as surrogate variable analysis (SVA) and remove unwanted variation (RUV) estimate and remove large-scale unmodeled factors (i.e. factors not in the experimental design) from the expression data [200, 201]. However, the usage of these supervised normalisation tools can introduce spurious signal to many genes, thus their usage has been controversial.

Dispersion is the variability in normalised counts between replicates. Traditional methods calculate the variance of the normalised count values for each gene between replicates. However, NGS experiments are frequently performed with a small number of replicates, resulting in high uncertainty in variance estimates. RNA-seq statistical packages employ various methods to overcome this. For example, the DESeq2 method assumes the variance is similar across genes with similar expression strength, so genes of a similar expression strength are pooled to estimate the expected variance. The variance of each gene is then shifted towards

the expected variance value for its expression strength in a process called empirical bays shrinkage [199].

Normalised counts and dispersion values are used to fit a distribution model. The negative binomial (NB) distribution is one of the most commonly used models for RNA-seq, ChIP and ATAC-seq data, used by packages such as DESeq2 and edgeR. The NB distribution is a probability distribution for discrete data such as read counts in NGS. It is a combination of Poisson and gamma distribution. The Poisson distribution best captures the within-sample (technical) variability of the sequencing data, whereas gamma distribution best captures the between-sample (biological) variability of the sequencing data [202].

Lastly, hypothesis testing is performed to examine whether any difference in the distributions between two or more sample groups occurred by random chance. In DESeq2, a Wald test is used for comparison between two sample groups and a LRT test is used for comparison between multiple sample groups. Multiple test correction is carried out to reduce the number of false positives [197]. This is important as a pvalue at 0.05 indicates there is a 5% chance that the observed difference occurred by random chance i.e. a false positive. Therefore, 1000 false positives are expected when 20,000 comparisons are made across the transcriptome. The Benjamini-Hochberg test is the standard method employed in DESeq2 to correct for multiple testing and to control the false discovery rate (FDR) [199].

Many different statistical packages are available for NGS data analysis using a wide array of statistical methods. A comparison of the eight most common statistical methods showed that different statistical packages can significantly affect analysis outcome [203]. Therefore, choosing a statistical package most suited for the data is essential for detecting true biological change. Comparisons of the different packages using human transcriptomic data have found that DESeq2 and Limma have produced the lowest rates of false positives in sample sizes

between 4 – 14. In addition, DESeq2 has been widely used with ChIP-seq and ATAC-seq data, allowing the same package to be used when comparing results from different -omics datasets. While the discussion on the statistics has been focused on NGS data, the principle of statistics in microarray data is highly similar. For example, Limma was originally developed for microarray data but is now widely used in RNA-seq data analysis.

1.6 Summary

Ageing is associated with decreased bone mass and bone strength, leading to an increased risk of fragility fractures. This is caused by an imbalance between bone formation and bone resorption with age. The loss of bone homeostasis is further accelerated in conditions such as osteoporosis and RA. The current treatments for patients with a high risk of fracture primarily aim to inhibit further bone erosion, but the repair of existing bone lesions remains challenging. Therefore, the replenishment of osteoblasts to regenerate bone mass is an area of strong clinical interest. Osteoblasts are derived by osteogenic differentiation from mesenchymal stem cells (MSCs), which lose their proliferative and osteogenic potential with age. However, the mechanism of MSC ageing remains poorly understood. Recent developments in -omics approaches will enable the systematic identification of regulators and mechanisms that mediates the changes in MSC proliferation and osteogenic potential with age, potentially leading to therapeutic candidates to replenish osteoblast numbers and restore bone mass in patients with age-associated bone diseases.

1.7 Aims

This thesis aims to characterise the molecular changes during MSC ageing and identify candidates to restore the proliferative and osteogenic potential of aged MSCs.

Chapter 3 aims to validate the MSC ageing models that will be used in this thesis by comparing the phenotypes of those MSCs with the existing literature.

Chapter 4 aims to characterise the epigenetic, transcriptional and protein changes between MSCs derived from young and old donors.

Chapter 5 aims to characterise the epigenetic, transcriptional and protein changes between MSCs at early and late passages.

Chapter 6 aims to identify differences in gene expression between young and old MSCs in response to osteogenic induction.

Chapter 7 aims to examine whether canonical WNT signalling activation could restore the osteogenic potential of old donor MSCs, and then understand the mechanism by which canonical WNT signalling activation promoted osteogenesis.

2 Methods

2.1 Cell culture

2.1.1 Mesenchymal stem cells

Human bone marrow MSCs from young donors were purchased from Lonza (Lonza, Switzerland) or were kindly gifted by Dimitris Karamitros (University of Oxford, UK). Young donors were at ages between 20 - 29 years. Human bone marrow MSCs from old donors were purchased from PromoCell (PromoCell, Germany) or Millipore (MerckMillipore, USA) or were kindly gifted by Dr Mandy Peffers (University of Liverpool, UK). Old donors were at ages between 62 – 87 years. The individual age, gender, ethnicity and sources of the donors are detailed in supplementary table S1.

MSCs were maintained in MesenPRO-RS™ medium (Life Technologies, UK), supplemented with 100 U/ml penicillin and 100 µg/ml streptomycin (P/S) and 2mM L-glutamine (both from Invitrogen, UK). At 70 - 80% confluency, MSCs were passaged with TrypLE (Thermo Fisher Scientific, USA) and were seeded at a density of 5000 cells/cm^2.

2.1.2 Osteoblast differentiation

MSCs were seeded at a density of 5000 cells/cm^2 in the maintenance medium (MesenPRO-RS™ medium + supplements) and were incubated for 3 days to achieve higher confluency. To induce osteogenesis, medium was replaced with Dulbecco's Modified Eagle Medium (DMEM) supplemented with 15% fetal bovine serum (FBS), P/S, 1x non-essential amino acids (NEAA), 2mM L-glutamine, 50 µg/ml ascorbic acid, 10 mM β-glycerophosphate, and 10 nM dexamethasone (Sigma-Aldrich, USA). The osteogenic medium was changed every 2 days. All cell culture was carried out at atmospheric oxygen conditions.

2.2 Proliferation assays

2.2.1 PrestoBlue assay

The cell culture medium was aspirated from cells and replaced with fresh medium of the same type (maintenance or osteogenic medium) supplemented with 10% Presto Blue® reagent (Life Technologies). The cells were incubated at 37°C for 120 minutes. Subsequently, the fluorescence activity was measured using a FLUOStar OPTIMA fluorescence plate reader (BMG, Germany) with wavelengths of 360 nm for excitation and 460 nm for emission.

2.2.2 Cumulative population doubling

Cells were passaged as described in section 2.1.1. At each passage, cell numbers were counted using a haemocytometer. Subsequently, cells were seeded at a density of 5000 cells/cm^2. This process was repeated for several passages until no increase in the cell number was observed. Cumulative population doubling (cumPD) was calculated as:

cumPD = $\Sigma\,{}^{Ps}_{Pe}$ [(number of cells seeded/number of cells counted at passage)/2]

Ps = starting passage and Pe = end passage.

2.3 Differentiation assays

2.3.1 ALP assay

In a 96 well plate, cells were washed twice with Phosphate-buffered saline (PBS) and lysed using CelLytic M™ (Sigma-Aldrich, USA) supplemented with x1 Complete™ protease inhibitor cocktail tablet (Roche, Switzerland). After a 15-minute incubation period, the plate was sealed and placed on a plate shaker at 500 RPM for 30 seconds. A solution with 3:1 ratio of 4-Methylumbelliferyl phosphate (4-MUP; Sigma-Aldrich, USA) and TRIS (50mM at pH 8)

was added to the lysate. The fluorescence activity was measured at 0 minutes and 120 minutes after substrate addition using a FLUOStar OPTIMA fluorescence plate reader (BMG, Germany) with wavelengths of 360 nm for excitation and 460 nm for emission.

2.3.2 Alizarin Red staining

Alizarin Red (AZR) staining was carried out at day 28 of osteogenesis. For preparing the AZR staining solution, Alizarin Red S (Sigma-Aldrich, USA) was dissolved in distilled water at a concentration of 20 g/L. The pH of the solution was adjusted to 4.1 - 4.3 using HCl, and the solution was filtered with a 0.22 µm syringe filter. For AZR staining, cells were fixed with 1% (v/v) formaldehyde for 20 mins. After fixation, cells were washed once with 50% (v/v) ethanol. The AZR staining solution was added at a volume of 100 µL/cm^2, then cells were incubated with the solution at RT for 45 mins. After staining, cells were washed three times with PBS and were visualised by photo scanning and light microscopy.

2.3.3 Oil Red O staining

Oil Red O staining was carried out at day 15 of adipogenesis. For preparing an Oil Red O stock solution, Oil Red O (Sigma-Aldrich, USA) was dissolved in isopropanol at a concentration of 5 g/L. Oil Red O working solution was made fresh before each use by 1:1 dilution with distilled water. The working solution was filtered using a 0.22 µm syringe filter. For Oil Red O staining, cells were fixed with 1% (v/v) formaldehyde for 20 mins. After fixation, cells were washed once with 60% (v/v) isopropanol. The Oil Red O working solution was added at a volume of 100 µL/cm^2, and the cells were incubated with the solution for 15 minutes at RT. After staining, cells were washed three times with 60% (v/v) isopropanol and visualised by light microscopy.

2.4 Lentiviral packaging

Lentivirus production was carried out based on a protocol by Wang et al [25]. In brief, HEK293T cells were seeded in 6 well plates at a density of 75,000 cell/cm^2 in DMEM supplemented with 10% FBS, P/S, and 2mM L-glutamine. The next day, a transfection mix was prepared for each well consisting of 1.29 μg of pGIPZ, 0.5 μg of psPAX2 and 0.21 μg of pMD2.G plasmids, 6 μL of JetPrime transfection reagent and 200 μL of JetPrime transfection buffer (Polyplus transfection, France). The transfection mix was vortexed, incubated at RT for 10 minutes and then added dropwise to each well. 24 hours post-transfection, the medium was replaced with fresh DMEM to remove the plasmids and transfection reagents. At 48 and 72 hours post-transfection, viruses were collected from the media. The collected media was centrifuged at 1600g for 15minutes to pellet and remove cell debris. The supernatant containing the virus was aliquoted and stored at -80 °C.

To titer the virus, MSCs were seeded in 96 well plates at a density of 5,000 cell/cm^2 in maintenance medium. The next day, the medium was aspirated from each well and 200 μL of transduction solution containing 1:4 serial dilutions of the virus, 5μg/mL of polybrene (Sigma-Aldrich USA) and MSC maintenance medium was added. The transduction solution was replaced with the maintenance medium 24 hours post-transduction. After 72 hours, the maintenance medium was replaced by a DNA staining solution containing 10 ng/mL Hoechst 33342 (Thermo Fisher Scientific, USA) in PBS, and was incubated for 30 minutes in the dark. The number of cells positive for GFP and Hoechst counterstain was determined by fluorescence-microscopy and image analysis with ImageJ (ImageJ script deposited at https://github.com/cjbio/imageJ).

2.5 RNA-seq

2.5.1 RNA extraction

RNA was isolated using the Direct-zol RNA miniPrep kit (Zymo Research, USA) according to the manufacturer's instructions. In brief, for each sample, around 50,000 cells were lysed in 350µL of TRIzol (Invitrogen, USA) and the lysate was transferred to a microcentrifuge tube. An equal volume of ethanol was added to the lysed cells. The solution was vortexed, added to a miniPrep column and centrifuged (16,000 g). The column was washed once with wash buffer, before 30 units of DNAse I was added to the column, and the column incubated at RT for 15 minutes. Columns were washed once with pre-wash buffer and twice with wash buffer, then the RNA was eluted in 30 - 50 µL of nuclease-free water. The RNA concentration was quantified using a NanoDrop 1000 spectrophotometer (Thermo Fisher Scientific, USA) and stored at -80 °C.

2.5.2 RNA library preparation

RNA library preparation was carried out using the NEBNext Ultra II direction RNA library prep kit (NEB, USA) according to the manufacturer's instructions. In brief, RNA concentration for all samples was standardised to 100 ng in 50 µL. Poly-adenylated RNA was enriched using the NEBNext polyA mRNA magnetic isolation module (NEB, USA) with the following modifications: 1) volume of oligo dT Beads used per sample was reduced to 10 µL. 2) Incubation of the RNA with the oligo dT beads was changed to 10 minutes at room temperature (RT) with gentle shaking at 200 RPM. After polyA selection, the fragmentation of the polyA enriched RNA was carried out in a thermal cycler at 94°C for 15 minutes. First-strand synthesis and second-strand synthesis were carried out to generate the double-stranded cDNA library. Subsequently, the cDNA was purified using solid-phase reversible immobilisation (SPRI) beads. 1.8X SPRI beads were added to the cDNA (v/v). The mixture was incubated at RT for

5 minutes and washed twice with 80% (v/v) ethanol. The cDNA-bound SPRI beads were air-dried for 5 – 10 minutes until they were 1) not shiny, 2) changed colour from black to brown, and 3) started to crack. The cDNA was eluted in 50 µL of 0.1X TE Buffer. Subsequently, end prep and adaptor ligation steps were carried out. For Adaptor ligation, the NEBNext adaptor concentration was adjusted depending on the starting RNA concentration. For library preps using 100 ng of starting RNA, the adaptor was diluted 1:30 in nuclease-free water. The product after adaptor ligation was purified again using 0.9x SPRI beads. The PCR step was carried out with the following modifications: 1) In order to minimise PCR duplicates, the number of PCR cycles was reduced to 11 for library preps using 100 ng of starting RNA. 2) Single indexing or dual indexing was carried out depending on the number of samples. The PCR product, i.e. a sequencing library, was purified using 0.9x SPRI beads. The concentration and quality of the sequencing library were assessed using a high sensitive D1000 ScreenTape and Agilent 22000 TapeStation (Agilent, USA) according to the manufacturer's instructions.

2.6 ATAC-seq

100,000 cells were harvested using TrypLE (Thermo Fisher Scientific, USA). Cell pellets were collected by centrifugation at 500 g for 3 mins at 4 °C. Each pellet was washed once with fresh maintenance medium or osteogenic medium. For transposition, 97.5 µl the transposition mix was added to the cells. The transposition mix consists of:

TRANSPOSITION MIX	**VOL (µL)**
2X TD BUFFER	50
1% DIGITONIN (FINAL 0.05% V/V)	5
TN5	2.5

NUCLEASE-FREE H2O	40
TOTAL	**95**

The reaction mix was incubated at 37°C for 30 minutes with gentle agitation on a plate shaker (300 RPM). After transposition, the DNA was purified using a MinElute Reaction Cleanup Kit (Qiagen, USA) according to the manufacturer's instructions. The DNA was eluted in 20 µl of 10 mM Tris-Cl at pH 8. A PCR reaction was carried out using the following conditions:

PCR MIX	**VOL (µL)**
TRANSPOSED DNA	10
Q5 HOT START HIGH FIDELITY 2X MASTER MIX	25
NUCLEASE FREE WATER	10
ATAC-SEQ UNIVERSAL PRIMER (25 µM STOCK)	2.5
2.5 UL ATAC-SEQ INDEX PRIMER (25 µM STOCK)	2.5
TOTAL	50

Thermal cycles:

I. 72 C, 5 min
II. 98 C, 30 sec
III. 98 C, 10 sec
IV. 63 C, 30 sec
V. 72 C, 1 min

VI. Repeat steps 3-5, 11X
VII. Hold at 4 C

The PCR products, i.e. ATAC sequencing libraries, were purified using 0.9x SPRI beads. The concentration and quality of the sequencing libraries were assessed using high sensitive D1000 ScreenTapes and the Agilent 2200 TapeStation.

2.7 DNA methylation array

1,000,000 cells were harvested using TrypLE (Thermo Fisher Scientific, USA). Genomic DNA was isolated using the PureLink genomic DNA mini kit (Thermo Fisher Scientific, USA). The DNA concentration was quantified using a NanoDrop 1000 spectrophotometer (Thermo Fisher Scientific, USA). DNA methylation profiling was performed using the Infinium 850K MethylationEPIC Kit (Illumina, USA), which was carried out by the clinical research facility at the University of Edinburgh, UK.

2.8 Sequencing

Typically, libraries were pooled based on their TapeStation quantitation such that they were equimolar in the final pool (although this could be altered depending on the depth of sequencing required for each sample), with 16-24 libraries per pool. If residual primer or adapter peaks were present in any individual libraries, the pooled library was purified again using 0.9x SPRI beads. The final concentration of the pooled library was confirmed using the TapeStation. Sequencing was performed on a NextSeq 500 (Illumina, USA) according to the manufacturer's instructions. Briefly, 20 fmoles of the pooled DNA library was denatured with an equal volume of 0.2 M NaOH for 5 minutes at RT, followed by addition of an equal volume of 0.2 M Tris-

HCl at pH 7. The denatured library was topped up to 1 ml using HT1 buffer (Illumina, USA) to give a 20 pM library. This was then further diluted by transferring 117 uL of the 20 pM library to 1183 uL of HT1 buffer to give the final 1.8 pM library, which was loaded into a NextSeq 500/550 High Output Reagent Cartridge (75 Cycles) and sequenced on a NextSeq 500 according to the manufacturer's instructions. For RNA-seq and ATAC-seq paired-end sequencing was carried out with read lengths of 42 or 37 for single-indexed or dual-indexed libraries, respectively.

2.9 Data processing

2.9.1 RNA-seq

The bioinformatics workflow has been deposited in GitHub (https://github.com/cjbio/NGS_RNA). In brief, FASTQ files containing raw reads were generated by the Illumina software CASAVA v1.8. The quality of the reads was assessed with FASTQC, and quality trimming was carried out with a base quality threshold of 30. Raw reads were mapped to the GRCh38 reference genome using HiSat2 (v2.0.5). The mapped reads were visualised using IGV (v2.3.74). Duplicate reads were annotated using Picard MarkDuplicates (v2.3.0). The quantification of the mapped reads against the GRCh38 reference genome annotation was carried out using FeatureCount (v1.5.0), and differential gene expression was determined using DESeq2 (v1.16.1). Unpaired Wald tests were used for hypotheses testing in chapter 4. Paired Wald tests were used for hypothesis testing in chapter 5 and 7. LRT test was used for hypothesis testing in the time course data in chapter 6. Significance was set at padj<0.05 post Benjamini-Hochberg correction.

2.9.2 ATAC-seq

The bioinformatics workflow has been deposited in GitHub (https://github.com/cjbio/NGS_ATAC). In brief, read quality control (QC) was the same as for RNA-seq data processing (detailed in section 2.9.1). Raw ATAC reads were mapped to the GRCh38 reference genome using Bowtie2 (v2.2.6). Mapped read visualisation was carried out using Deeptools (3.1.3) and IGV (v2.3.74), and duplicate removal was identical to RNA-seq data processing (detailed in section 2.9.1). Non-chromatin related mitochondria reads were removed using samtools idxstats (0.1.19). Peak calling was carried out using macs2 (v2.1.0). The identification of consensus peaks and the quantification of the identified peaks were carried out using DiffBind (v2.4.8). Differential peak expression was determined using DESeq2 (v1.16.1). Significance was set at padj<0.05 using unpaired Wald test post Benjamini-Hochberg correction.

2.9.3 DNA methylation array

The bioinformatics workflow was deposited in GitHub (https://github.com/cjbio/NGS_DNAme). In brief, probe QC was carried out with Lumi (v2.28.2). Probes with p>0.05 were removed. Probes were annotated with the Illumina human methylation EPIC manifest. The filtering of the probes was carried out using Minfi (v1.22.1). The filtering steps were carried out to remove sources of bias, including the removal of probes at genomic loci of natural C/T single nucleotide polymorphisms (SNPs), on the sex chromosome and probes that cross-react with multiple genomic loci [204]. Co-variant removal was carried out using SVA (v3.24.4). Differential methylation analysis was determined using Limma (v3.32.10). Significance was set at padj<0.05 using unpaired t-test post Benjamini-Hochberg correction.

2.10 CyTOF

For CyTOF, 1 – 3 million MSCs were gently detached from the T175 culture flask using Accutase (Thermo Fisher Scientific, USA) according to the manufacturer's instructions. Cells were washed twice with PBS. All centrifugation steps were carried out at 500 g. The subsequent staining procedure was adapted from the Maxpar Nuclear antigen staining protocol [205]. In brief, 1 – 3 million cells were suspended in 1 mL of MaxPar staining buffer (Fluidigm, USA). For dead cell staining, 2 µL of 5 µM MaxPar intercalator Rh 103 (Fluidigm, USA) was added to 1 mL of resuspended cells. Samples were incubated at 37 °C for 15 minutes. Cells were then washed twice with the MaxPar staining buffer. Barcoding of the samples was carried out to allow multiple samples to be pooled in the subsequent staining procedure and CyTOF run. Barcoding was carried out using the Cell ID 20 Plex Pd barcoding kit (Fluidigm, USA) according to the manufacturer's instructions. After barcoding, samples were pooled into one 5 mL round bottom polystyrene tube. To minimise false-positive staining, human Fc receptor blocking was carried out by adding 5 uL of TruStain FcX (BioLegend, USA) into 45 µL of cells resuspended in the MaxPar staining buffer. The mixture was incubated at RT for 10 minutes. For surface antigen staining, metal conjugated CyTOF surface staining antibody mixture was prepared and topped up to a total volume of 50 µL with the MaxPar staining buffer. The 50 µL of antibody mixture was added to the 50 µL of cells, mixed gently by flicking and incubated at 4 °C for 30 minutes. Subsequently, cells were washed twice with the MaxPar staining buffer. For fixing and permeabilising the cells, FOXP3 fix and perm kit (BioLegend, USA) was used according to the manufacturer's instructions. For intracellular antigen staining, CyTOF intracellular staining antibody mixture was prepared and topped up to a total volume of 100 µL with the MaxPar staining buffer. The 100 µL of antibody mixture was added to the cell pellet, gently mixed by flicking and incubated at 4 °C for 30 minutes. Cells were then

washed twice with the perm buffer (BioLegend, USA). For all-cells staining, 1 µL of 125 µM cell-ID intercalator Ir (Fluidigm, USA) was added to a mixture of 1 mL of Fix and perm buffer containing 1.6% paraformaldehyde (Thermo Fisher Scientific, USA). The all-cell staining solution was added to the cell pellet and incubated at 4 °C overnight. The next day, the cells were washed twice with MaxPar Staining buffer, followed by two washes with MaxPar water (Fluidigm, USA). Cells were resuspended to a concentration of 0.5 million cells per mL in MaxPar water. Cells were vortexed and filtered through a 35 µm mesh cell strainer to achieve a single-cell suspension. Calibration beads were added at 1:10 (v/v) ratio to the resuspended cells. Finally, data were acquired on the mass cytometer. CyTOF data was debarcoded using Fluidigm debarcoder v1.7.0. The gating in CyTOF was carried out using CytoBank v7.2.0. The gating protocol was adapted from Lai et al. [206]. First, calibration beads were excluded. Second, live cells were selected using the Rh103 and Ir191 ratio. Third, singlets were selected using the Ir191 and Ir193 ratio (Figure 2-1).

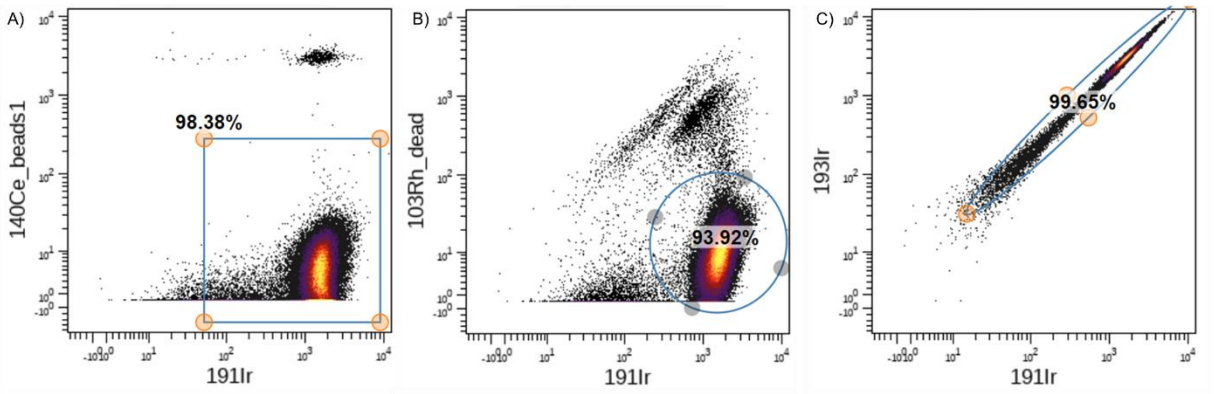


Figure 2-1 ***CyTOF gating****. **A)** non-bead cells were selected, **B)** Ir191+ and Rh103- cells were selected and **C)** singlets were selected using the Ir191 and Ir193 ratio.*

2.11 Chapter specific methods

2.11.1 Chapter 3 - Luciferase reporter assay

MSCs were seeded at a density of 5000 cells/cm^2 in a 6 well plate (Corning, USA) in maintenance medium (MesenPRO-RS™ medium + supplements). The next day, MSCs were

transduced at a MOI of 1 with the Cignal Lenti LEF/TCF luciferase reporter (Qiagen, USA) using the protocol described in chapter 2.11.2. 3 days post transduction, a luciferase reporter assay was carried out using the ONE-Glo luciferase assay system (Promega, USA) according to the manufacturer's instructions. The luminescence intensity was measured on a FLUOStar OPTIMA plate reader at default luminescence settings.

2.11.2 Chapter 5 - shRNA-seq

One million MSCs were seeded in a T175 cell culture flask in the maintenance medium (MesenPRO-RS™ medium + supplements). The next day, transduction of the pooled lentiviral-shRNA library were carried out at MOI of 0.1. A 25 mL transduction solution containing 100,000 infection units of lentivirus, 5 µg/mL of polybrene and MSC maintenance medium was added to the cells. 24 hrs post transduction, the transduction solution was removed and replaced with fresh MSC maintenance medium. 72 hrs post transduction, the treated cells were harvested with TrypLE. Half of the harvested cells were re-seeded at a density of 5000 cells/cm^2 in a T175 flask, and the other half was used for shRNA-seq. This process was repeated for subsequent passages. The cells harvested at 72 hrs post transduction were used as the baseline, and the subsequent passages were treatment time points.

Genomic DNA was extracted from the harvested cells using the PureLink Genomic DNA mini kit (Thermo Fisher Scientific, USA) according to the manufacturer's instructions. shRNA-seq library prep was adapted from a protocol by Sim et al. [207]. In brief, 200ng of genomic DNA was PCR amplified using the AccuPrime™ Pfx SuperMix (Thermo Fisher Scientific, USA) according to the manufacturer's instruction using custom primers (Supplementary table 3). The PCR products were visualised on a 1.5% (w/v) TBE agarose gel, and subsequently purified using the GeneJET gel extraction kit (Thermo Fisher Scientific, USA) according to the

manufacturer's instructions. After sequencing, the quantification of shRNA hairpins was carried out using edgeR based on a protocol by Dai et al. [208]. The full script of the shRNA analysis workflow has been deposited in GitHub (https://github.com/cjbio/shRNA_seq). In brief, each raw read was mapped to the sequences in the reference shRNA library. The number of reads mapped to each shRNA was quantified and normalised to the library size of the sample. The enrichment of shRNAs between baseline and each passage was tested using the Fisher's exact test with significance threshold at padj<0.05 post Bonferroni correction.

2.11.3 Chapter 6 - RNA-seq timecourse

At day minus 3, MSCs were seeded at a density of 5000 cells/cm^2 in 6 well plates (Corning, USA) in maintenance medium (MesenPRO-RS™ medium + supplements). At day 0, the MSCs were treated with the osteogenic medium described in chapter 2.1.2. RNA samples were collected at 0, 0.5, 1, 2, 4, 6, 8, 12, 16, 24, 48, 72, 96, 120, 168, 336 and 504 hrs post-initiation of osteoblast differentiation. RNA-seq was carried out according to the protocol described in section 2.5.

2.11.4 Chapter 7 - BIO treatment

At day minus 3, MSCs were seeded at a density of 5000 cells/cm^2 in a 6 well plate (Corning, USA) in maintenance medium. 1 – 2 µM BIO working solutions were diluted from a 10 mM BIO stock solution (Selleckchem, USA) with the osteogenic medium (chapter 2.1.2). At day 0, the maintenance medium was aspirated and 3 mL of the working BIO solution was added. Subsequent differentiation assays and RNA-seq were carried out as described in chapter 2.3 and 2.5, respectively.

3 Phenotypic changes during MSC ageing

3.1 Introduction

3.1.1 Models of MSC ageing

As previously defined in chapter 1.3, ageing is a progressive decline in function and increased vulnerability to death. Proliferation and differentiation are important functions of MSCs, so changes in the proliferative and differentiation potentials serve as phenotypic markers for characterising MSC ageing models.

3.1.2 Donor age model

One of the most commonly studied models of MSC ageing is MSCs derived from donors of different age groups. A systematic review has examined the changes in the number of population doublings (PD) of MSCs with increased donor age [209]. For example, Stenderup et al. passaged MSCs from young (aged 18 - 29, n = 6) and old donors (aged 68 - 81, n = 5) to their proliferative limit. The young donor MSCs achieved 41 ± 10 PD, whereas the old donor MSCs reached their proliferative limit at around 24 ± 11 PD [210]. Amongst the seven studies selected in the review, all have concluded that there has been a significant decrease in population doubling (per unit time) of ageing hMSCs, strongly indicating a decline in proliferative potential with increased donor age [209].

Proliferative potential can also be estimated by colony forming units (CFU) - MSCs that can clonogenically expand *in vitro*. Six studies have observed a significant decrease in colony-forming units (CFU) with increased donor age, whereas four studies have found no significant change (

Table 3-1). This inconsistency in findings may be attributed to the differences in the threshold of CFU, as studies that defined CFU as more than 50 cells found a significant decline in CFU, whereas, studies that defined CFU as less than 8 or 16 cells did not [211].

Proliferation is also closely linked with metabolism as an increased anabolic metabolism is necessary to generate the biomass required for cell division. Mammalian cells rely primarily on mitochondrial oxidative phosphorylation, which generates reducing agents such as NADPH. Assays such as MTT (colourimetric) or PrestoBlue (fluorescent) could be used to quantify this change in metabolic activity, and by proxy, proliferating cells. Aksoy et al. showed that the increase in each age group (infants 0 – 3 years of age, n = 6), children (ages 4– 12, n = 6), adolescents (ages >12 – 19, n = 6) young adults (19–35, $n = 6$) and old adults (36 – 50, $n = 5$) was accompanied by a significant reduction in metabolic activity [212].

MSCs must also function to differentiate into various lineages, such as adipocytes, chondrocytes and osteoblasts/osteocytes. Numerous studies have examined the changes in this tri-lineage differentiation potential of MSCs with age (Table 2.1). Changes in the osteogenic potential of bone marrow MSCs have been the most frequently reported. Early evidence has suggested a decline in osteoblast number with age, which have led to speculations that the rate of osteoblast formation may have declined with age [107]. Therefore, several studies then examined the osteogenic potential of MSCs from young and old donors using *in vitro* assays such as ALP activity assays and Ca2+ matrix mineralisation staining [12, 130, 210, 212-215]. The majority of the studies have found a significant decline in osteogenic potential with age (

Table 3-1).

A recent theory of MSC ageing suggests that there may be a shift of lineage commitment towards adipogenesis and away from osteogenesis [216]. An increased number of adipocytes have been found in the bone marrow of the elderly [43] and patients with osteoporosis [217].

In vitro, several studies reported that MSCs from young and old donors showed no significant differences in adipocyte formation with Oil Red O staining [218]. With an impaired osteogenic potential while retaining their adipogenic capacity, MSCs may thus exhibit a shift in lineage commitment.

Amongst the tri-lineages, changes in the chondrogenic potential with age have been the least studied. This may be partially due to the experimental difficulties associated with chondrogenic differentiation, e.g. requiring a large number of cells (around $1x10^7$). As the proliferative decline is associated with increased donor age, the cell number requirement for chondrogenesis may have been a limiting factor. Stolzing et al. have examined the chondrogenic potential of children (7 - 18 years, n=3) and young adults (19 - 40 years, n=3), and have found no significant differences between the two age groups. However, the differences between young adults and older donors (>40 years) have not been investigated.

Cellular senescence is also an important hallmark of ageing. It can be caused by DNA damage or telomere shortening, leading to an increased susceptibility to cell death. Cellular senescence can be detected by an increased expression of growth regulatory genes such as *P16*, *P21*, and *P53*, or an accumulation of SA-βGal. Stenderup et al. have found that there have been no significant changes in the number of SA-βGal positive cells or telomere length with increasing donor age of MSCs. However, MSCs from the old donors have exhibited signs of senescence (SA-βGal and telomere shortening) more rapidly in culture [210]. Therefore, MSCs from old donors may be more susceptible to senescence when subjected to cell culture stress, but no conclusive evidence has suggested that these cells became more senescent *in vivo*.

Ageing model	Passage	Proliferation	Differentiation	Senescence	Ref
Young (19-35, n=6); Old 36-50, n=5)	P3	Decrease * (MTT)	Decreased osteogenesis (Alizarin Red) No change in adipogenesis (Oil Red O)	N/A	[212]
Continuous (3- 70, n=41)	Not specified	Decrease * (CFU)	Decreased osteogenesis* (ALP)	N/A	[213]
Young (25-50 years, n = 6); Old (>60 years, n = 6)	P4	Decrease (cumPD) *	N/A	N/A	[214]
Children (7-18, n=3); Young (19-40, n=3); Old (>40, n=3)	Not specified	Decrease *	Decreased osteogenesis* (ALP) No change in adipogenesis (Oil Red O) No change in chondrogenesis (Alcian Blue)	N/A	[12]
Young (37-50, n=11); Old (50-86, n=19)	Not specified	N/A	Decreased osteogenesis* (ALP histology, qPCR)	N/A	[219]
Young (18–29, n=5); Old (68–81, n=3)	Not specified	decrease * (cumPD)	No change in osteogenesis (ALP, MSC graft in mice) No change in adipogenesis (Oil Red O)	No change in senescence (SA-β-Gal, telomere length)	[210]
Young (<45, n=11); Old (>65, n=11)	P3	decrease* (CFU)	No change in osteogenesis (Alizarin Red), adipogenesis (Oil Red O) or chondrogenesis (Alcian blue)	N/A	[215]

Table 3-1 ***Changes in proliferation, differentiation and senescence with increased donor age.*** ** indicates statistical significance. N/A indicates the experiment was not carried out.*

3.1.3 Cell passage model

An increasing passage number in cell culture is also a commonly used model for MSC ageing. As MSCs are multipotent cells, they are expected to be capable of indefinite self-renewal. On the contrary, as MSCs expand in culture, they show signs of age-associated functional decline (Table 3-2). Using similar assays to those described above, studies have consistently observed a significant decrease in the proliferative, osteogenic, adipogenic and chondrogenic potential with increased passage number. In contrast to the donor age model, numerous studies have found significant increases in MSCs senescence with cell passaging, including increased SA-β-Gal positive cells, telomere shortening, and increased expression of *P16* and *P21*.

Ageing model	Proliferation	Differentiation	Senescence	Ref
Early (P4); Late (P8, n= 5)	Decrease* (PD)	Decreased osteogenesis* (Alizarin Red) Decreased adipogenesis* (Oil Red O)	NA	[220]
P1 to P10 (n=11)	Decrease* (PD)	Decreased osteogenesis* (Van Kossas) Decreased adipogenesis* (Oil Red O)	Increased senescence* (telomere length)	[221]
Early (<30% total PD); Late (>80% total PD, n=4	Decrease* (PD)	Decreased osteogenesis* (Alizarin Red) Decreased adipogenesis* (Oil Red O)	Increased senescence* (SA-β-Gal)	[210]
Early (P3); Late (P8-11, n=3)	Decrease* (CFU, PD)	Decreased osteogenesis* (Alizarin Red) Increased adipogenesis* (Oil Red O) Decreased chrondrogenesis* (Alcian Blue)	Increased senescence* (SA-β-Gal, telomere length)	[222]

Table 3-2 ***Changes in proliferation, differentiation and senescence with increased passage number****. * indicates statistical significance. N/A indicates the experiment was not carried out.*

3.1.4 Other models of human BM-MSC ageing

Hutchinson-Gilford progeria syndrome is a rare monogenic disease caused by a mutation in Lamin A, resulting in the production of a truncated protein (progerin). The symptoms include premature ageing of mesenchymal lineage-derived cells, leading to progressive atherosclerosis and loss of subcutaneous fat. Zhang et al. has recruited progeria patients to generate MSCs from fibroblast-derived iPSCs. The iPSC-MSCs have shown a moderate decline in osteogenesis and adipogenesis compared to young adult BM-MSCs. In addition, the accumulation of progerin was associated with a significant increase in DNA damage with

culture expansion [123]. However, due to the rarity and high childhood mortality of the condition, a characterisation of bone-marrow-derived MSCs from progeria patients has not been reported so far.

Overall, the donor age and passage models have been extensively characterised. Other human ageing models such as progeria could provide additional insight, but have shown limited feasibility. While a significant decline in proliferative and osteogenic potential is the consensus in different ageing models, evidence suggesting the contrary has also been found. Therefore, this chapter will first confirm the functional phenotypes of the ageing models, before preceding to investigating the underlying mechanisms.

3.2 Aims

Two models of ageing to be validated:

a. Donor age – young vs old donors
b. Cell culture – early vs late passages

This chapter aims to validate the two MSC ageing models by comparing the functional changes of these MSCs with the existing literature.

3.3 Results

3.3.1 MSC quality validation

To ensure a valid cell model is used for subsequent studies, MSC quality assessments have been carried out. A CyTOF panel was used to examine cells for MSC positive (CD146, CD105, CD90, CD73, CD44) and negative (CD14, CD34, CD45, HLA-DR) selection markers. Cells

assessed were indeed positive and negative for their respective positive and negative selection markers (Figure 3-1.A).

To assess the lineage multi-potency of these cells, they were treated with adipogenic and osteogenic media. After 15 days in adipogenic condition, the formation of lipid droplets (LDs) was observed, and the differentiated cells were stained with Oil Red O (Figure 3-1.B.d,e). After 28 days in osteogenic condition, the formation of bone nodules was observed, and the differentiated cells were stained with Alizarin Red (Figure 3-1.B.b,c).

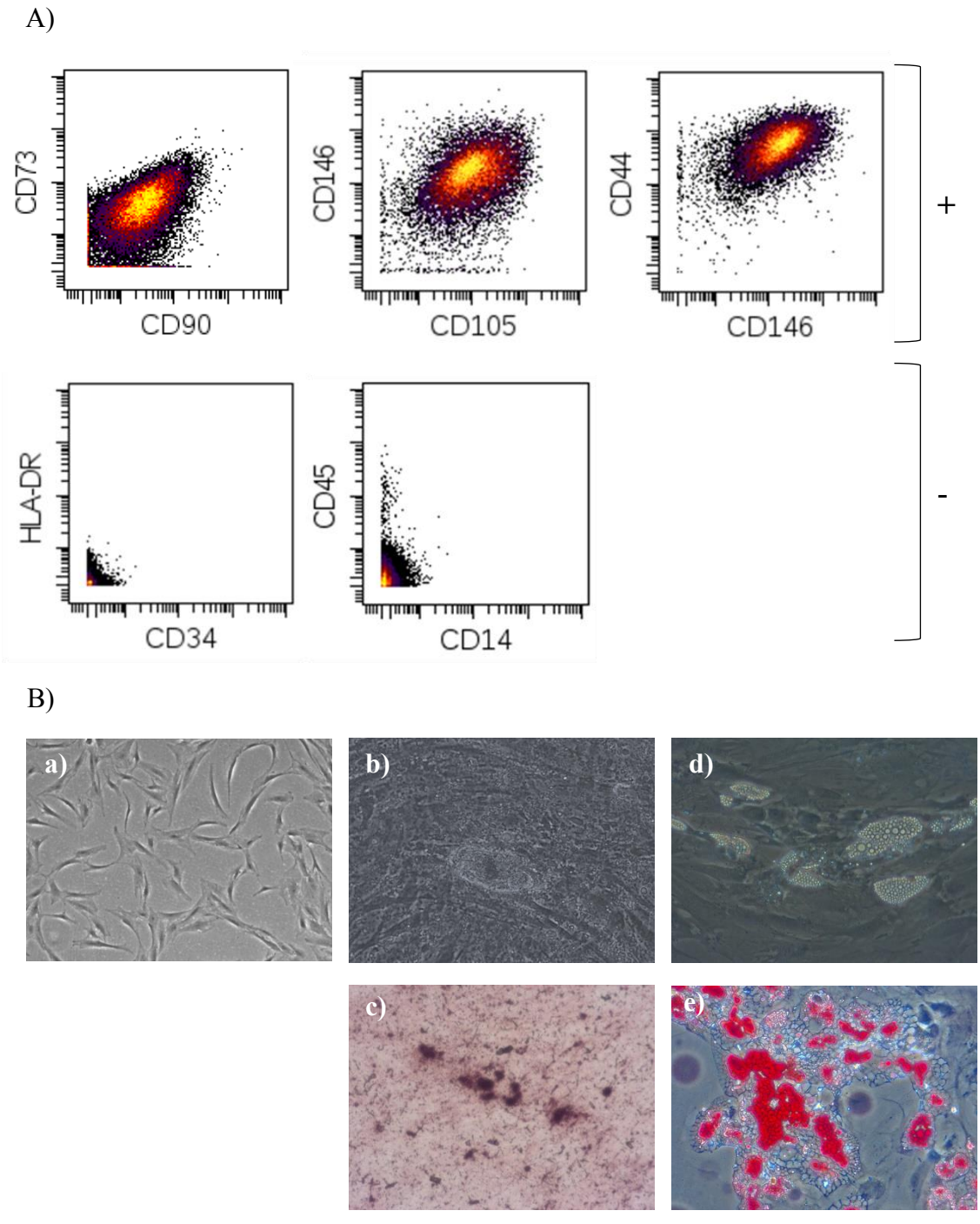


Figure 3-1 ***MSC quality validation. A)*** *CyTOF analysis of MSCs with MSC selection markers. Positive selection markers (+): CD146, CD105, CD90, CD73, CD44; Negative selection markers (-): CD14, CD34, CD45, HLA-DR.* ***B)*** *phase contrast microscopy showing a) undifferentiated MSCs, b) bone nodule formation at day 28 post osteogenic induction c) matrix mineralisation stained with Alizarin Red, d) adipocyte formation at day 15 during adipogenesis, and e) lipid vacuoles stained with Oil Red O. Figure a, b & d was at 10X magnification and figure c & d was at 4X magnification.*

3.3.2 Phenotypic changes with increased donor age

In the donor age model, the phenotypic changes were compared between two donor age groups: 20 – 29 years (young), 62 – 87 years (old). To characterise changes in proliferative potential with increased donor age, prestoBlue activity and PDs were measured. After allowing the MSCs to proliferate for 4 days after seeding, the change in metabolic activity was measured by prestoBlue assay. A significantly lower metabolic activity was observed in old donor MSCs compared to the young donor MSCs (Figure 3-2.A; young donors (n = 6) and old donors (n = 5), all at P5; unpaired t-test, sig at $P<0.05$). The number of cumulative population doublings (cumPD) from P5 until quiescence was recorded for each donor (Figure 3-2.B). The old donors showed on average a decrease in the cumPD compared to the young donors. However, as the inter-donor variability was large, the decrease in cumPD was not statistically significant.

To characterise the changes in osteogenic potential with increased donor age, ALP activity assay and Alizarin Red staining were carried out. At day 7 of osteogenesis, a lower ALP activity was observed in the old donors compared to the young donors. The difference in ALP activity was greater at day 10, showing significantly lower ALP activity in the old donors (Figure 3-2.C; young donors (n=5) and old donors (n=5), unpaired t-test, sig at $P<0.05$). Alizarin Red staining was carried out at day 28. Young donors stained mostly positive for calcium-phosphate mineralisation, while the staining was mostly negative in the old donors (Figure 3-2.D).

To examine whether the decline in MSC proliferation and osteogenesis is associated with cellular senescence, SA-β-Gal staining was carried out (Figure 3-3.A). No significant differences in the percentage of cells positive for senescence was observed comparing the young and old donors (Figure 3-3.B, young donors n = 4 and old donors n = 4).

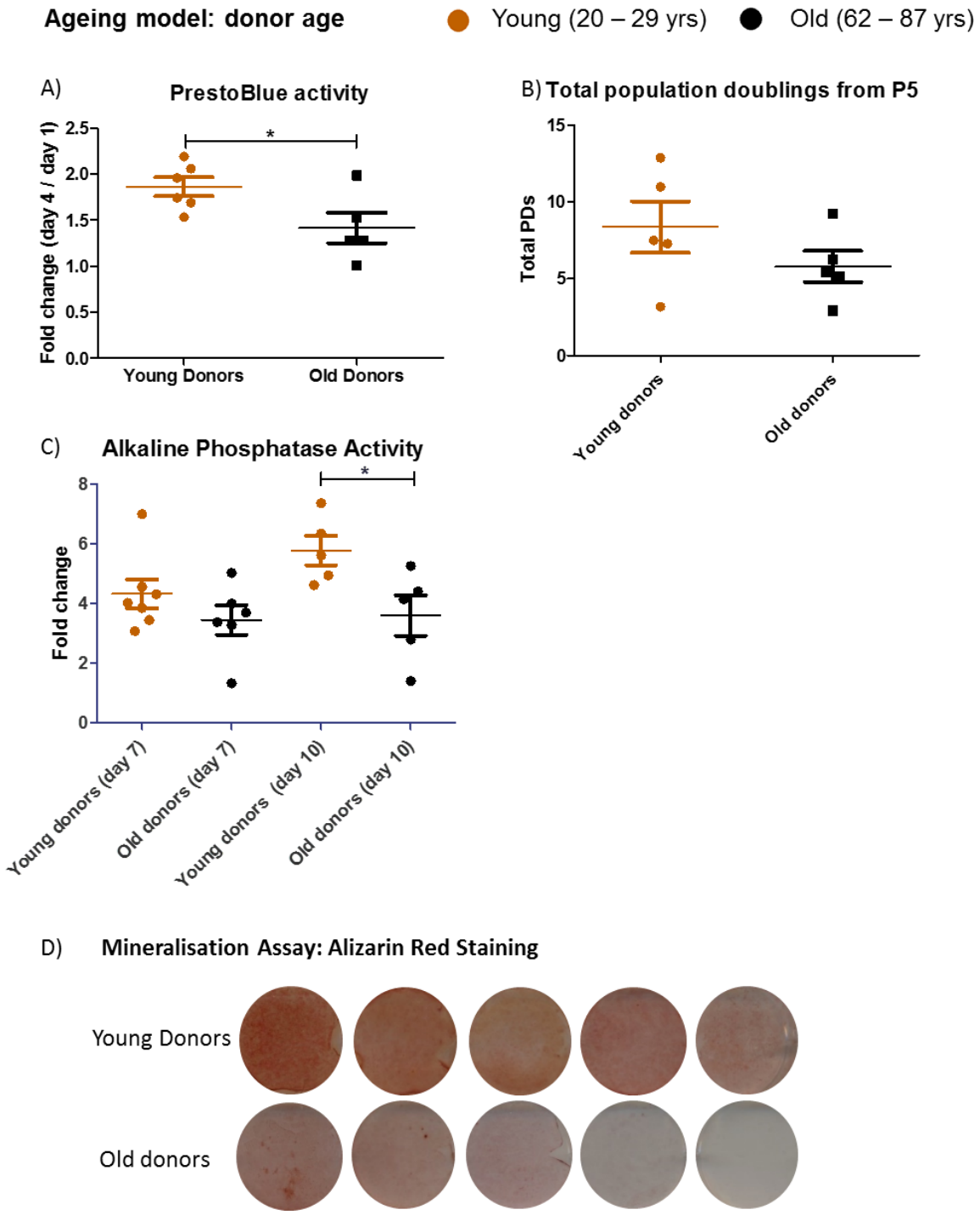


Figure 3-2 ***Proliferation and osteogenesis assays of MSCs from young and old donors. A)*** *prestoBlue activity of MSCs 4 days after seeding, normalised to prestoBlue activity at day 1 (young donors n=6 and old donors n=5, unpaired t-test, significant at p<0.05),* ***B)*** *total number of population doublings from each donor (n=10).* ***C)*** *ALP activity of MSCs treated with osteogenic media for 7 or 10 days, normalised to control MSCs in MensenPro maintenance media (young donors n=5 and old donors n=5, unpaired t-test, sig at p<0.05).* ***D)*** *Alizarin Red staining of MSCs treated with osteogenic media for 28 days (young donors n=5 and old donors n=5).*

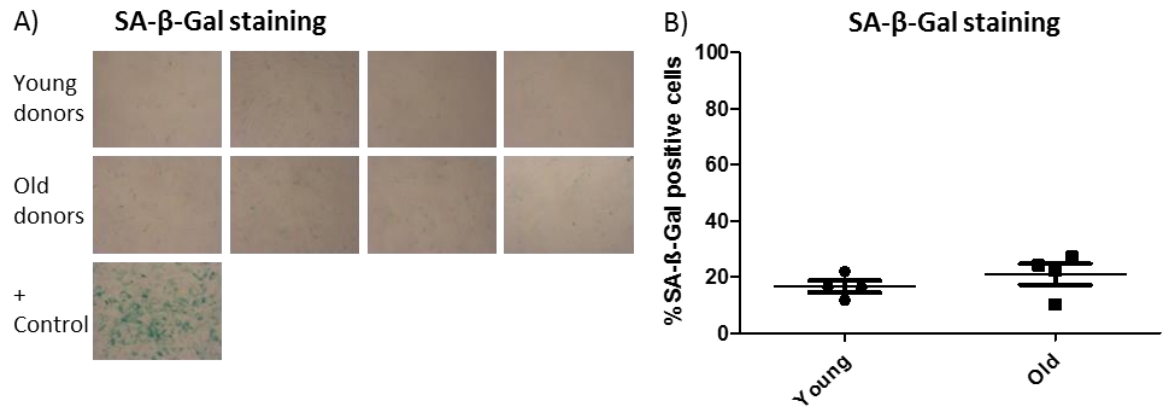


Figure 3-3 ***Senescence assay of MSCs from young and old donors. A)*** *Bright field microscopy at x10 magnification of MSCs stained for SA-βgal, and* ***B)*** *percentage of MSCs positive for SA-βGal staining (young donors n=4 and old donors n=4).*

3.3.3 Phenotypic changes with increasing cell passage

In the cell culture model, the phenotypic changes over several passages were examined. Population doubling rate was shown to decrease with increasing passage number (Figure 3-4.A). Similarly, a 40% decrease in ALP activity was observed from P9 to P16 (Figure 3-4.B). Additionally, Alizarin Red staining showed a decline in calcium-phosphate mineralisation at P16 compared to P9 MSCs (Figure 3-1.C). These results suggest a loss of proliferative and osteogenic potential of these MSCs at later passages.

From early to late passage, a distinct change in cell morphology was observed - from thin and spindly towards a larger and a more rounded phenotype (Figure 3-4.D). SA-β-Gal assay indicated a gradual increase in the percentage of senescent cells with increasing passage number. Between P9 to P16, the percentage of senescent cells increased two-fold from 39% to 80% (Figure 3-4.E).

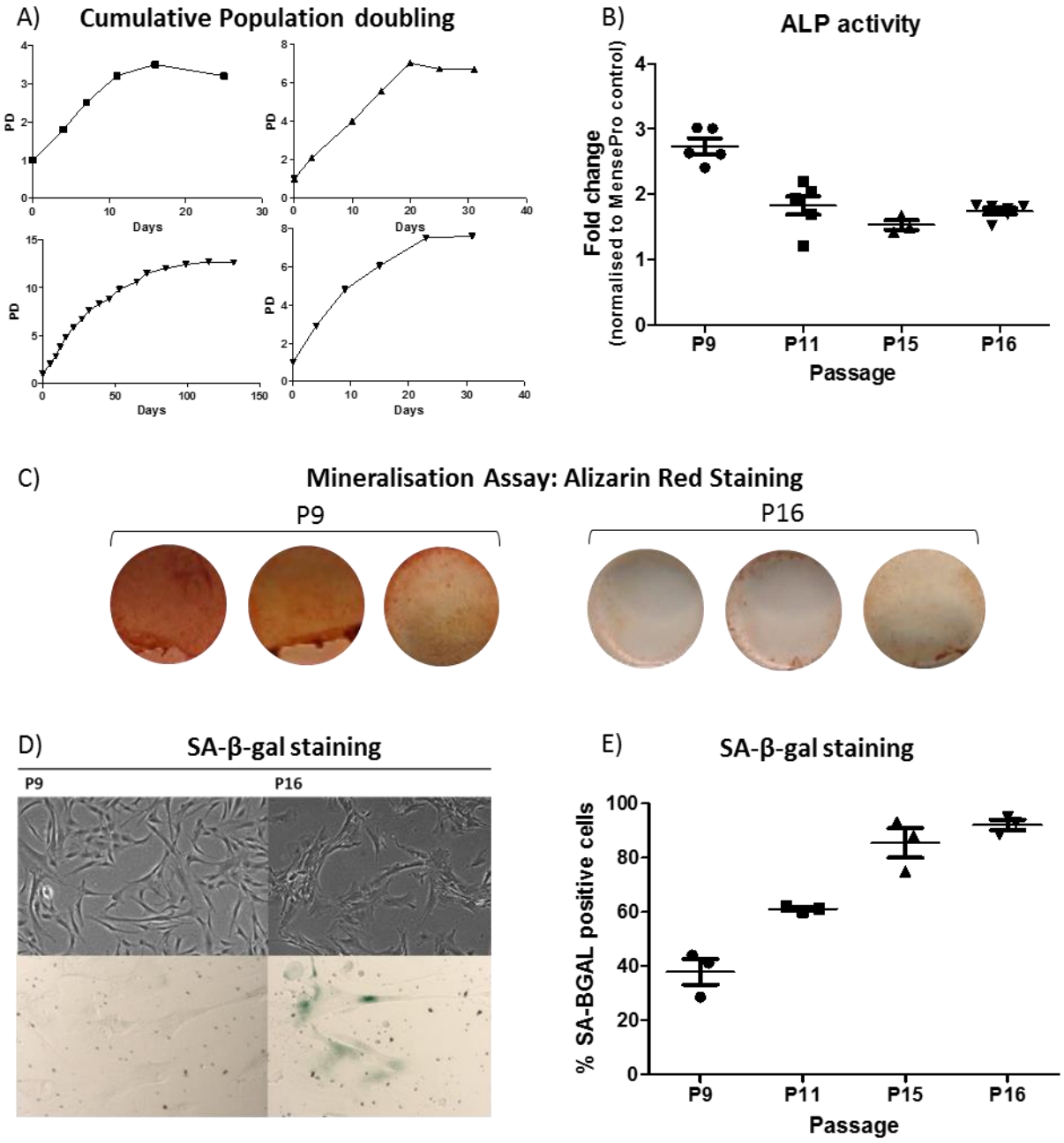


Figure 3-4 ***Characterisation of MSCs with increasing passage number. A)*** *Cumulative population doubling with culture expansion starting at P5, showing four representative young donors.* ***B)*** *ALP activity of MSCs from different passages treated with osteogenic media for 7 days, normalised to control MSC in MensenPro maintenance media,* ***C)****Alizarin Red staining of P9 and P16 MSCs after treatment with osteogenic media for 28 days.* ***D)*** *Morphology and SA-β-Gal staining of MSCs at P9 and P16.* ***E)*** *Percentage of MSCs positive for SA-β-Gal staining from P9 to P16.*

3.4 Discussion

In both ageing models, a significant decline in proliferation and osteogenic potential was observed. These results are consistent with the findings in the literature described in section 3.1. Therefore, both ageing models will be used to examine the mechanisms leading to the proliferative and osteogenic decline of MSCs with human ageing.

There was also a difference between the two models. A continuous increase in the percentage of senescent cells was found with increasing passage number, whereas, no significant increase in senescence was observed with increased donor age. This may indicate that:

1. Senescence was caused by stress related to cell culture, which is contributing more towards the functional decline of MSCs. Indeed, while the increase in MSC senescence after culture expansion is extensively reported, the evidence for changes in senescence with donor age is inconsistent.
2. Senescence cells are rapidly eliminated *in vivo* [223, 224]
3. Senescent MSCs become non-adherent in culture following isolation, leading to observational bias [170].

Taken together, the influence of senescence towards MSC ageing *in vivo* remains unclear and will be investigated further in the next chapter.

While using the passage model to study the mechanisms of ageing may be confounded by the stresses and stochastic changes during cell culture, the donor age model has been shown to have large inter-donor variability. This could be compensated by overlapping the changes observed in both models, and thus, eliminating the false positives due to stress in cell culture or inter-donor viability. This approach will be adopted in this thesis.

4 Multi-omics characterisation of MSC ageing in the donor age model

4.1 Introduction

As described in chapter 3, MSC ageing is associated with altered cellular phenotypes, such as a decline in proliferation and osteogenic potential. Such changes are coupled with a variety of transcriptional, epigenetic and proteomic changes described below.

4.1.1 DNA methylation and gene expression

During the last decade, many studies have examined the changes in DNA methylation with hMSC ageing [130-133, 140, 225, 226] (Table 4-1). Interestingly, these studies have observed no global changes in methylation levels but have found significant alternations in the patterns of methylation marks i.e. hyper- and hypomethylation have been observed at specific CpG sites. These CpG sites include the promoters of senescence-associated genes (Cdkn2b), "stemness" maintenance genes (Sox2), and lineage-determining genes (RUNX2, Dlx5, Hox family) [132, 133, 140].

Changes in gene expression have also been examined in a number of these studies [131-133, 140, 226]. Largely, no significant association between the changes in DNA methylation and gene expression has been found. This may reflect the dynamic nature of epigenetic regulation, where the transcription silencing effect of DNA methylation is balanced with other regulatory mechanisms such as histone modifications, chromatin remodelling and miRNA regulation [227]. Interestingly, the gene expression of the senescence-associated genes, "stemness" maintenance genes and lineage-determining gene has indeed correlated with changes in their DNA methylation pattern. Therefore, while its independent biological effect may be limited, DNA methylation seems to play a more important role with respect to regulating MSC function with age.

To determine the important genes regulated by DNA methylation, differentially methylated CpG sites from three studies were overlapped (Figure 4-1). Interestingly, only a small number of genes were differentially methylated in all three studies. This could reflect the lack of statistical power in some of these studies. More importantly, this suggests that the individual variability of MSC donors or cell culture conditions may represent the majority of changes in DNA methylation in these studies. Thus, a method for eliminating these confounding factors will be required for future studies.

MSC source	ageing model (n-number)	method	DNA methylation change (old vs young)	Gene expression change	Ref
BM-MSC	P5 (4) P10 (4)	Bisulfite microarray	No sig global change, 517 differential methylated SA-CpG sites	N/A	[132]
BM-MSC	2- 22 yr 61 -92 yr (total n=34)	Bisulfite microarray	(18,735) 29% hyper-Me, (45,407) 71% hypo-Me	N/A	[130]
BM-MSC	P3 (6) P13 (6)	Bisulfite sequencing	No sig global change 1,702 hyper-Me 2,116 hypo-Me	No overall correlation 648 up, 499 down	[226]
BM-MSCs	21-50 yr (4) 53-85 yr (4)	Bisulfite microarray	No sig global change, 295 hyper-Me 249 hypo-Me	No overall correlation, But *DLX5*, *HOXA5*, *CDKN2B*, *S100A4*, *RUNX3*, and *C10orf27* expression coincided with methylation pattern	[133]
BM-MSCs	P2 (8) P8 – 15 (8)	Bisulfite sequencing	No sig global change, 29 hyper-Me 55 hypo-Me	N/A	[133]
PC-MSC	P1 (?) P6 (?)	Bisulfite sequencing	↓*SOX2* No change *RUNX2*, *OCT4*, *TERT*	↓*TERT*, ↓*SOX2* ↓*OCT4*	[140]
BM-MSCs	P3 (3) P11 (3)	Bisulfite sequencing	Hyper – *GRM7*, *CASR* Hypo – *PRAMEF2*, *SELP*, *CASP14*, *KRTAP13*-3	Not expressed in hMSCs Predict cumulative population doubling	[225]
BM-MSC	21.8 yr (4) 65.5 yr (4)	Bisulfite microarray	70 hyper-Me 117 hypo-Me	No overall correlation, *HOXB7*, *HAND2* and *MKRN3* expression coincided with methylation pattern	[131]

Table 4-1 ***Summary of DNA methylation changes associated with MSC ageing from previous literature.*** *MSC sources include bone marrow (BM) and placenta (PC). Two models of ageing were studied – donor age and passage number. Both changes in DNA methylation and gene expression are shown in the table.*

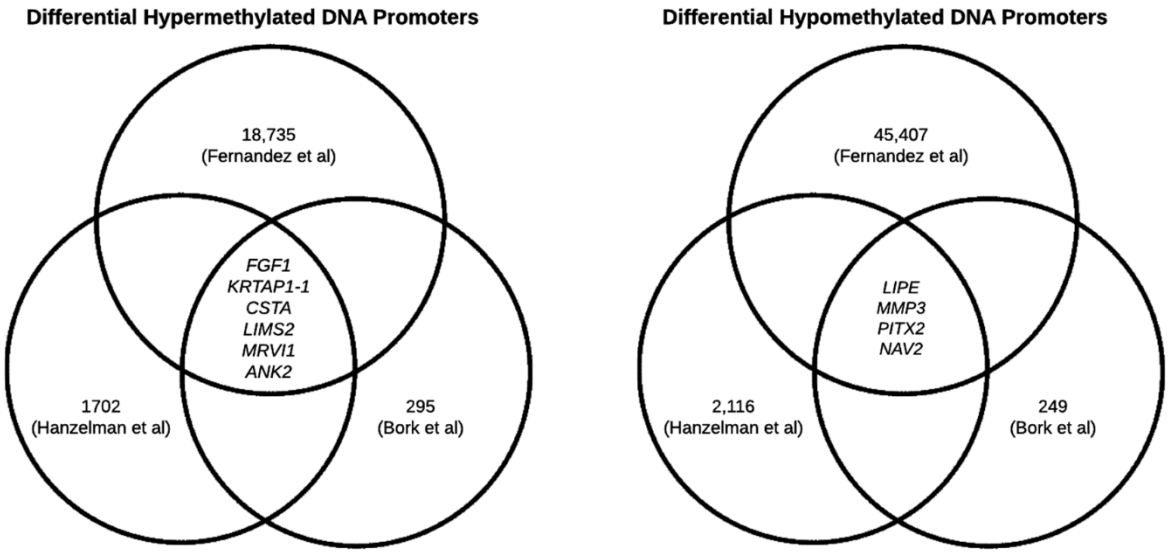


Figure 4-1 ***Venn diagram overlapping the differentially methylated genes associated with MSC ageing in three studies.*** *The DNA promoters of six genes were concordantly hyper-methylated, and the DNA promoters of four genes were concordantly hypo-methylated. The three studies have been conducted by Fernandez et al., [130], Hanzelman et al., [226] and Bork et al., [133].*

4.1.2 Histone modifications and gene expression

Using enzymatic assays, global histone deacetylase (HDAC) activity was found to increase in later passages of placenta-derived hMSCs [228]. To determine whether this increased HDAC activity led to decreased histone acetylation, total histone H3/4 acetylation assays were carried out in early and late passage MSCs. Acetylation levels of histone H3/4 were significantly reduced in the late passage MSCs, supporting the global increase in HDAC activity observed. Most importantly, chromatin immuno-precipitation PCR (ChIP-PCR) showed that at promoter regions, where a reduction of histone acetylation marks was observed, the expression of the corresponding gene was significantly reduced.

Five studies have used ChIP-PCR to examine the changes in histone modification at specific genomic regions with increased passage number (

Table 4-2) [140, 149, 228-230]. In two studies, a decrease in histone acetylation and gene expression has been observed at the promoter of stemness maintenance genes (Sox2 and oct4) [140, 228]. At the promoter of the adipocyte lineage gene PPAR-y2, a significant increase in the binding of EZH2 (H3K27 methyl-transferase) has been shown. This resulted in an increase in the ratio of the transcriptional repressive mark K27me3 to the transcriptional activating mark K4me3. Consequently, a decrease in the gene expression of PPAR-y2 has been observed. This evidence highlights that histone modifications regulate some of the key genes determining MSC proliferation and differentiation with age. However, histone modifications have been characterised at a very limited number of gene regions using ChIP-PCR, thus genome-wide approaches such as ChIP-seq, and ATAC-seq are needed to systematically examine chromatin changes at the genomic level. Additionally, as a result of the limited number of studies, very few epigenetic regulators have been identified as candidates for therapeutic intervention of age-related MSC dysfunction.

MSC source	ageing model	method	Histone modification change	Gene expression change	Ref
AD-MSC,	P5 (3) P30 (3)	CHIP-PCR	EZH2: ↑PPAR-y2, ↑FABP4, ↑MYOG, ↑GAPDH, ↓LPL Bmi1: no sig change	N/A	[229]
BM-MSCs	P3 (5) P5 (5) P7 (5)	CHIP-PCR	K4me3/k27me3 ratio: ↓PPARG,	↓PPARG	[230]
PC-MSC	P1 (?) P6 (?)	CHIP-PCR	H3K9ac and H3K14ac: ↓TERT, ↓Sox2 ↓Oct4	↓TERT, ↓Sox2 ↓Oct4	[140]
PC-MSC	P3 (5) P8 (5)	CHIP-PCR	Total histone H3/H4 acetylation: ↓Oct4 No change - TERT, Sox2	↓TERT, ↓Sox2 ↓Oct4	[228]
UCB-MSC	P6 (4) P16 (4)	CHIP-PCR	H4ac: ↑ miR-141-3p H3K9me3: ↓ miR-141-3p H3K27me3: ↓ miR-141-3p H3ac: same	↑miR-141-3p	[149]

Table 4-2 ***Summary of histone modifications associated with MSC ageing from previous literature.*** *MSC sources include bone marrow (BM), adipose tissue (AD), placenta (PC) and umbilical cord blood (UCB). Two models of ageing were studied – donor age and passage number. The changes in histone modification and gene expression are shown in the table.*

4.1.3 Proteomic changes

A recent proteomic study has identified that 777 quantifiable proteins are expressed in human BM-derived MSCs, of which 118 are differentially expressed with increasing donor age [131]. Interestingly, 116 proteins have shown increased expression with age, whereas, only 2 proteins have shown decreased expression, indicating that there may be an overall increase in protein translation and/or a decline in protein degradation. Amongst the differentially expressed proteins with age, enriched biological processes included mitochondrial-related cellular metabolism and apoptosis. On the other hand, senescence-related proteins such as P53, P21 and P16 were not found to be differentially expressed. However, it is important to note that protein expression is highly heterogeneous between donors. A study, which has detected a total of 7,753 proteins shared between 6 donors, has found that only 1,024 proteins (13%) were present in all donors [231].

4.2 Aims

While characterisations of MSC ageing at epigenetic, transcriptomic and proteomic levels have been carried out, studies to simultaneously examine these changes at multi-omics levels have rarely been carried out. An extensive multi-omics characterisation would strongly facilitate the understanding of the mechanism of MSC ageing. Therefore, this chapter aims to characterise MSC ageing at the epigenetic, transcriptional and protein level.

In the chapter introduction, DNA methylation array results between different studies have shown little overlap. This may be partially due to the lack of standardisation of donor age and passage number, which are factors that have affected MSC phenotypes in chapter 3. Therefore, to increase comparability between different experiments, all experiments in this chapter were

carried out using MSCs at P5, from young donors at the age between 20 – 29 years and old donors at the age between 62 – 87 years.

4.3 Results

4.3.1 Transcriptomic characterisation of MSC ageing with RNAseq

To investigate the transcriptomic changes during MSC ageing, RNA-seq experiments of young and old donor MSCs were carried out (young donors n = 10, 20 – 29 years; old donors n = 8, 62 – 87 years). Principal component analysis (PCA) showed distinct clustering of young and old donors (Figure 4-2.A), and the top 100 genes contributed to this age-related separation were involved in extracellular structure organisation, cell proliferation and skeletal system morphogenesis (Figure 4-2.B), which is consistent with the loss of MSC proliferation and osteogenesis observed in functional assays (detailed in chapter 3).

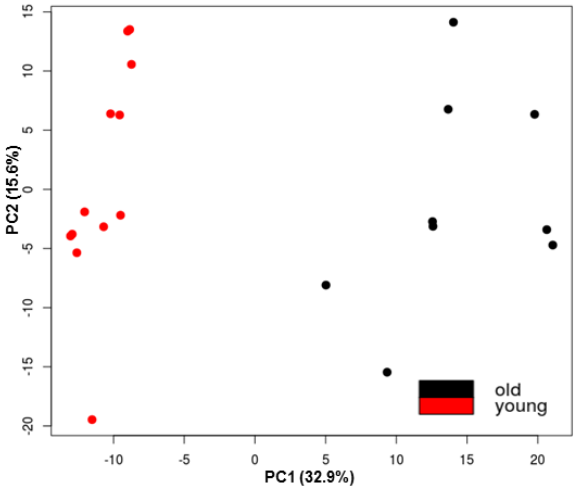
3,114 differential expressed genes (DEGs) were identified in old versus young donors (sig. at padj<0.05), of which 1,673 genes were upregulated, and 1,441 genes were downregulated. A Venn diagram shows the overlap of DEGs to databases containing known epigenetic regulators, and known ageing-associated genes. 309 DEGs in old versus young donors were epigenetic or transcriptional regulators. 61 DEGs were previously identified in ageing. Combining all three datasets, 17 genes were identified to be epigenetic regulators associated with ageing that were differentially expressed between old and young MSCs (Figure 4-2.E).

Gene Ontology (GO) analysis showed that mitochondria-related processes were most significantly altered amongst the DEGs upregulated with age (Figure 4-2.C), whereas, cell adhesion, WNT signalling pathway and axon guidance were most significantly altered amongst the down-regulated DEGs with age (Figure 4-2.D). As the WNT signalling pathway is one of

the most important pathways regulating MSC proliferation and osteogenesis [232], age-related changes in this pathway were further investigated. A heatmap of the fold gene expression changes of positive regulators of the canonical WNT pathway showed an overall decrease in the expression of those genes (Figure 4-3.A). This includes critical members of the canonical WNT pathway such as Frizzled, LRP5/6, DVL and TCF/LEF. Strikingly, 5 out of 10 members of the Frizzled receptor family were differentially expressed, all of which were significantly down-regulated (Figure 4-3.B).

To examine whether the decline in the canonical WNT pathway gene expression leads to an impaired WNT signalling activity, a LEF/TCF luciferase reporter assay has been carried out. The lentiviral reporter construct contains multimerised LEF/TCF binding motifs to detect canonical WNT signalling activity. Three days after the young and old donor MSCs were transduced with the lentiviral luciferase reporter, the luciferase activity was measured. A significantly lower luminescence intensity value was observed in the old donor MSCs compared to the young donor MSCs (Figure 4-3.C) (young donors ($n = 4$) and old donors ($n = 4$), unpaired t-test, sig at $p<0.05$).

A)



B) **PC1:**

GO Complete Biological process	FDR
Extracellular structure organization	3.53E-02
Cell proliferation	4.43E-02
Tissue development	4.62E-04
Skeletal system morphogenesis	5.71E-02

C) **Upregulated DEGs**

PANTHER GO-slim biological process	FDR
ATP synthesis coupled proton transport	8.64E-05
Ribosomal large subunit assembly	8.64E-04
Inner mitochondrial membrane organization	3.41E-03
Intracellular protein transmembrane transport	1.51E-02
Mitochondrial membrane organization	1.76E-02
Protein transmembrane import into intracellular organelle	1.89E-02
Protein transmembrane transport	1.90E-02
Pyrimidine nucleotide metabolic process	2.24E-02
Maturation of LSU-rRNA	2.82E-02
Mitochondrial electron transport, ubiquinol to cytochrome c	3.46E-02

Panther pathways	FDR
De novo purine biosynthesis	7.04E-03

D) **Downregulated DEGs**

PANTHER GO-slim biological process	FDR
Cell adhesion	3.31E-07
Canonical Wnt signalling pathway	1.51E-04
Axon guidance	6.30E-03
Animal organ morphogenesis	2.06E-02
Muscle contraction	2.26E-02
Regulation of axonogenesis	3.24E-02
Positive regulation of transcription by RNA polymerase II	3.36E-02
Extracellular matrix organization	3.38E-02
Actin filament organization	4.47E-02
Enzyme linked receptor protein signalling pathway	4.72E-02

Panther pathways	FDR
Alzheimer disease-presenilin pathway	3.76E-07
Wnt signaling pathway	4.15E-07
Cadherin signaling pathway	3.27E-06
Alzheimer disease-amyloid secretase pathway	4.02E-05
Circadian clock system	1.09E-03
Gonadotropin-releasing hormone receptor pathway	1.19E-03
Angiogenesis	1.21E-03
JAK/STAT signaling pathway	3.27E-02
Integrin signalling pathway	3.69E-02
PDGF signaling pathway	4.68E-02

E)

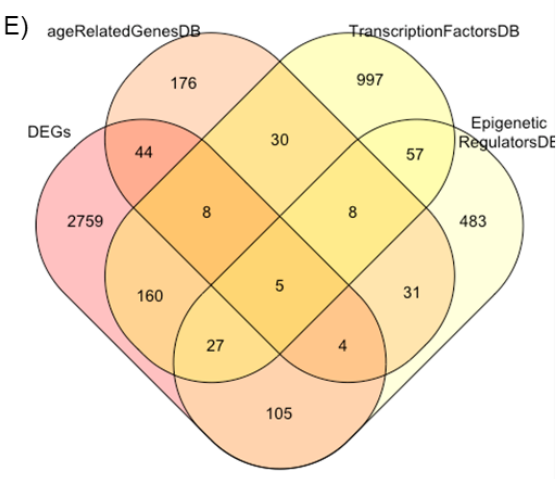


Figure 4-2 ***Transcriptomic changes in old vs young donor undifferentiated MSCs. A****) Principal component analysis (PCA) of RNA-seq data, showing the variability in gene expression between samples. Blue = young donors (n=10, 20 – 29 years), Red = old donors (n=8, 62 – 87 years).* ***B)*** *Gene Ontology (GO) terms of the enriched processes of the top 100 genes observed in PC1.* ***C)*** *Go terms of the enriched processes and pathways in the upregulated DEGs and* ***D)*** *the downregulated DEGs.* ***E)*** *Venn diagram of DEGs overlapping with databases of known age-related genes [233], transcription factors [234] and epigenetic regulators [235].*

As the canonical WNT signalling pathway directly interacts with a number of master regulators that can determine MSC fate (detailed in chapter1.3), it was examined whether the decline in the canonical WNT pathway activity is associated with changes in the gene expression of these regulators. In the old donor MSCs, there was a significant increase in *PPARG* expression with age (Wald test, sig at padj<0.05, post Benjamini Hochberg correction), whereas, *RUNX2* expression slightly declined (Figure 4-4). In addition, there was a significant decline in both *SOX9* and *OPG* (*TNFRSF11B*) expression in the old donor MSCs (Wald test, sig at padj<0.05, post Benjamini Hochberg correction). This indicates that there may be WNT-related changes to the predisposition of MSC fate, as well as changes to the regulation of osteoclastogenesis by MSCs.

To examine the changes in other pathways critical to MSC proliferation and osteogenesis, the DEGs were mapped to the Kegg pathways. A number of important pathways for MSC proliferation and osteogenesis were highly represented amongst the DEGs, including WNT, HH, mTOR, MAPK, IG, Notch, and BMP pathways. A global decrease in gene expression of members of the non-canonical WNT pathways and the hedgehog pathways was observed (Figure 4-5, Figure 4-6).

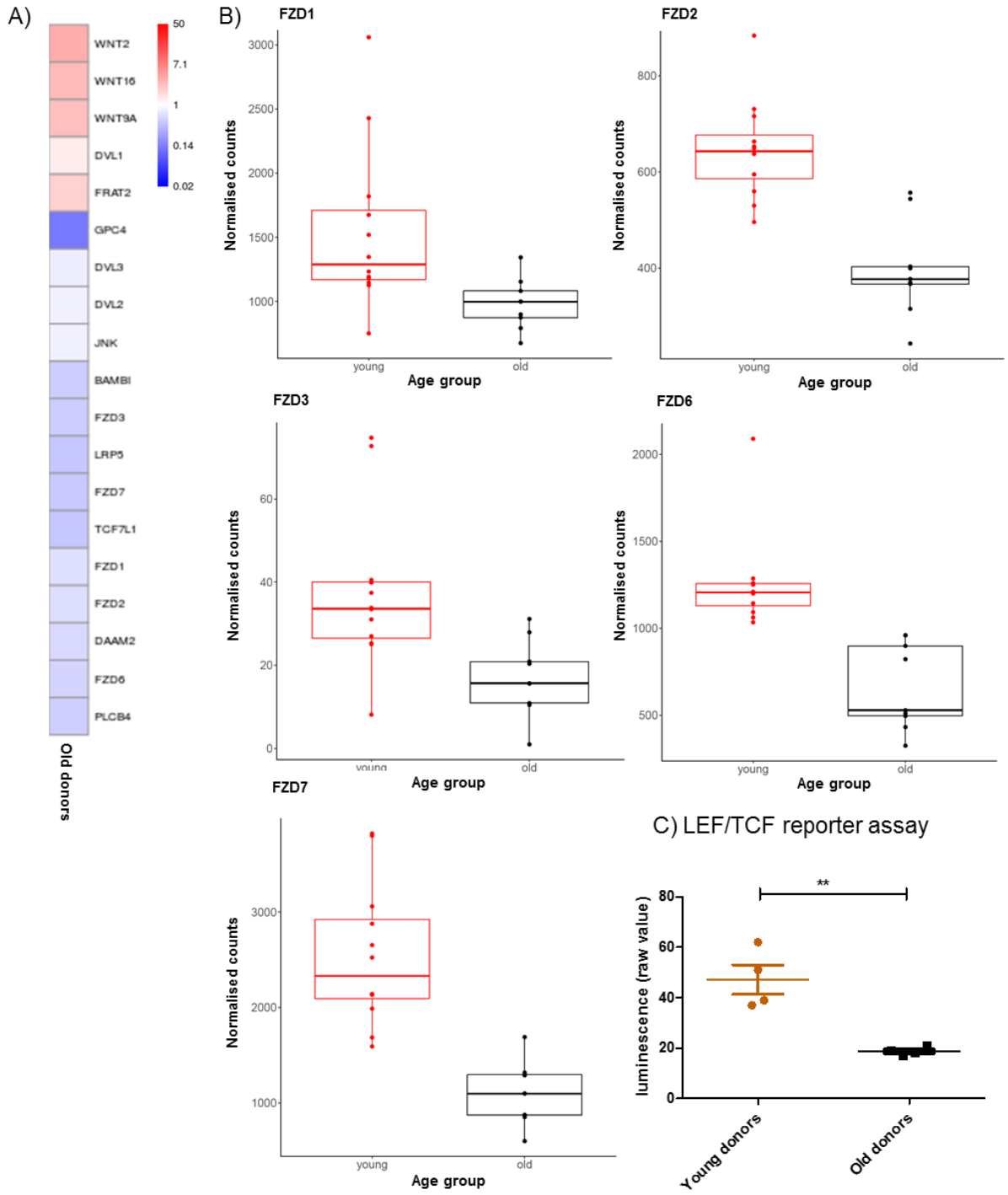


Figure 4-3 ***Changes in the canonical WNT signalling pathway with age. A)*** *Heatmap of fold change (old vs young donors) in gene expression, showing the positive regulators of the canonical WNT pathway amongst the DEGs (significant at padj<0.05, Deseq2 Walt test, post Benjamini-Hochberg correction).* ***B)*** *Normalised counts of the differentially expressed FZD family genes (significant at padj<0.05, Deseq2 Walt test, post Benjamini-Hochberg correction).* ***C)*** *LEF/TCF luciferase reporter assay for quantification of β-catenin signalling activity in vitro (unpaired t test, **sig at p<0.01).*

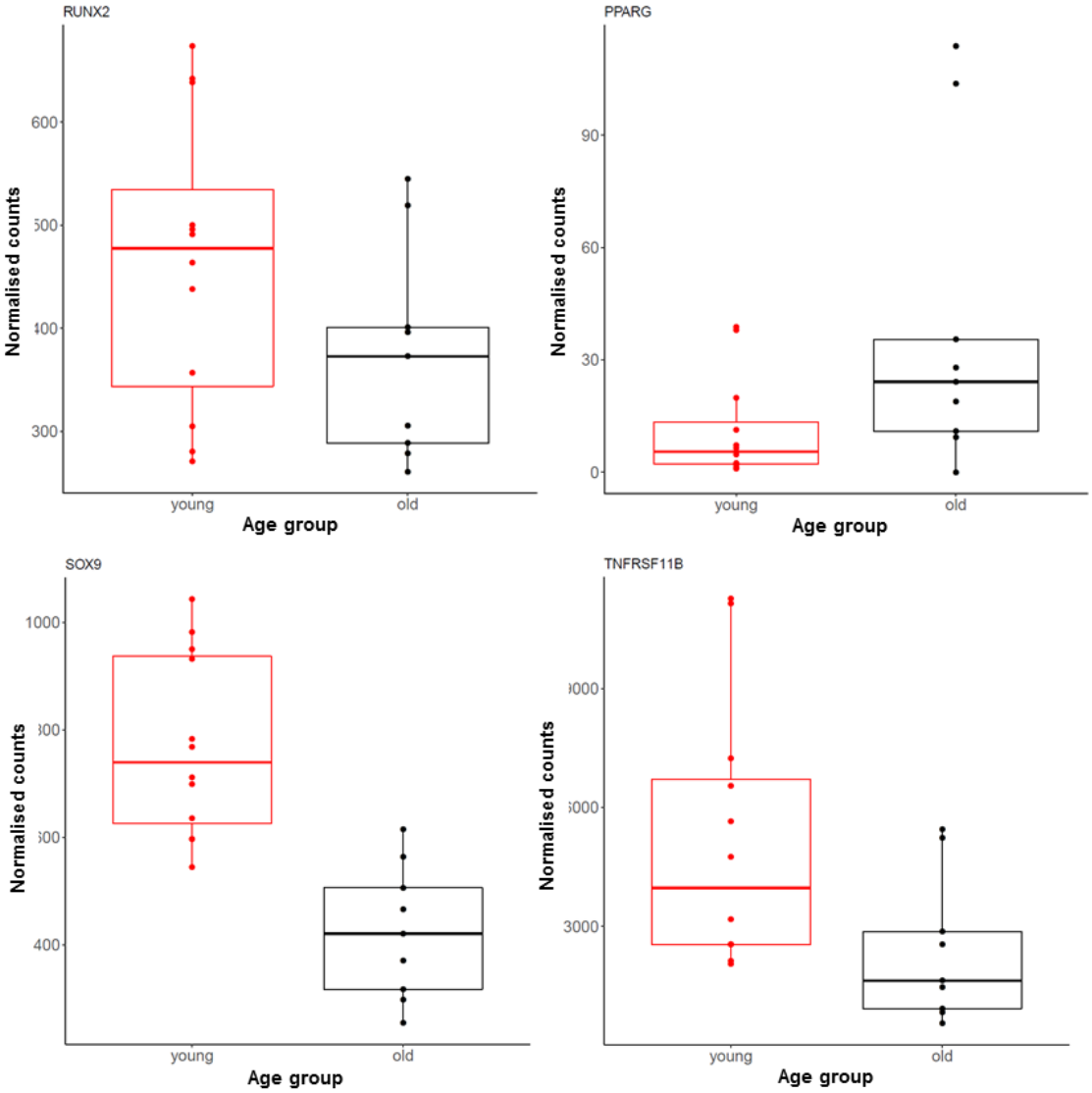


Figure 4-4 ***Normalised counts of β-catenin target gene expression.*** *PPARG, SOX9 and OPG (TNFSRF11B) were amongst the DEGs (significant at padj<0.05, Deseq2 Walt test, post Benjamini-Hochberg correction).*

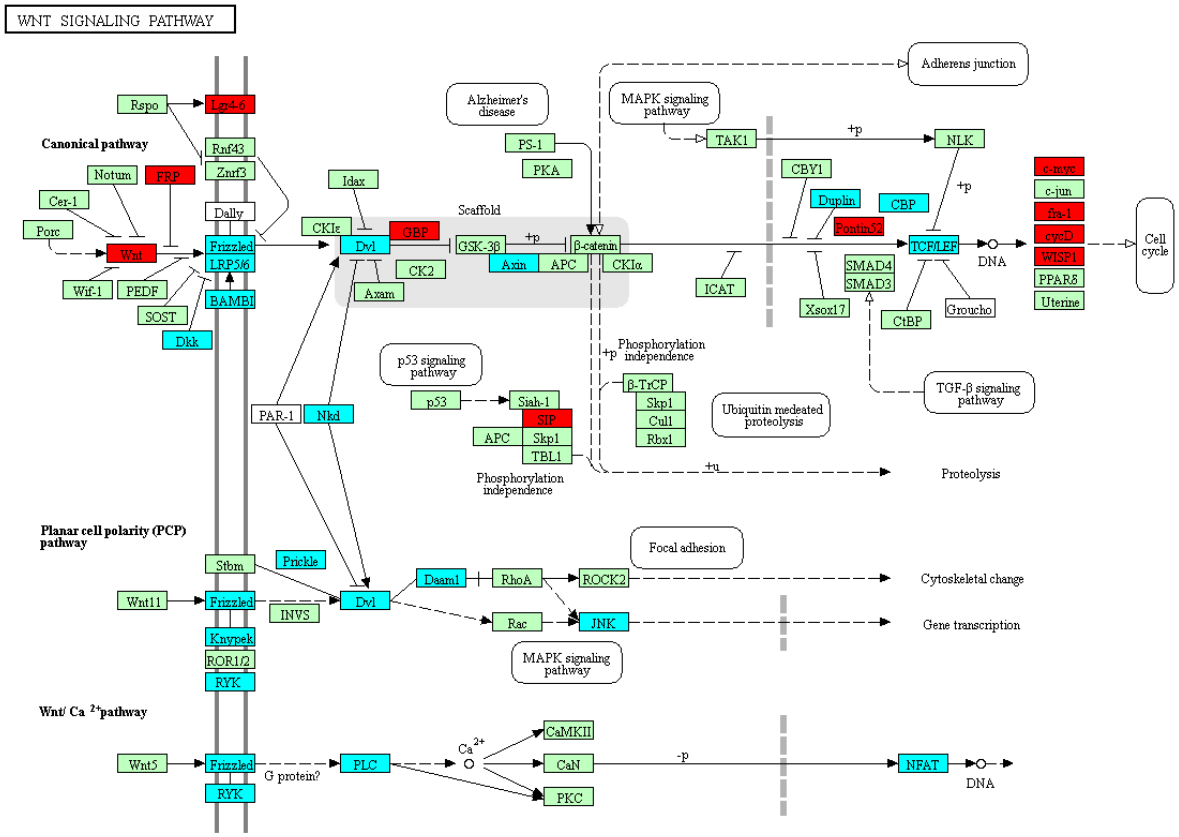


Figure 4-5 ***The DEGs mapped to the KEGG WNT signalling pathways.*** *Significantly downregulated genes are shown in cyan, significantly up regulated genes are shown in red. No significant changes in gene expression are shown in green.*

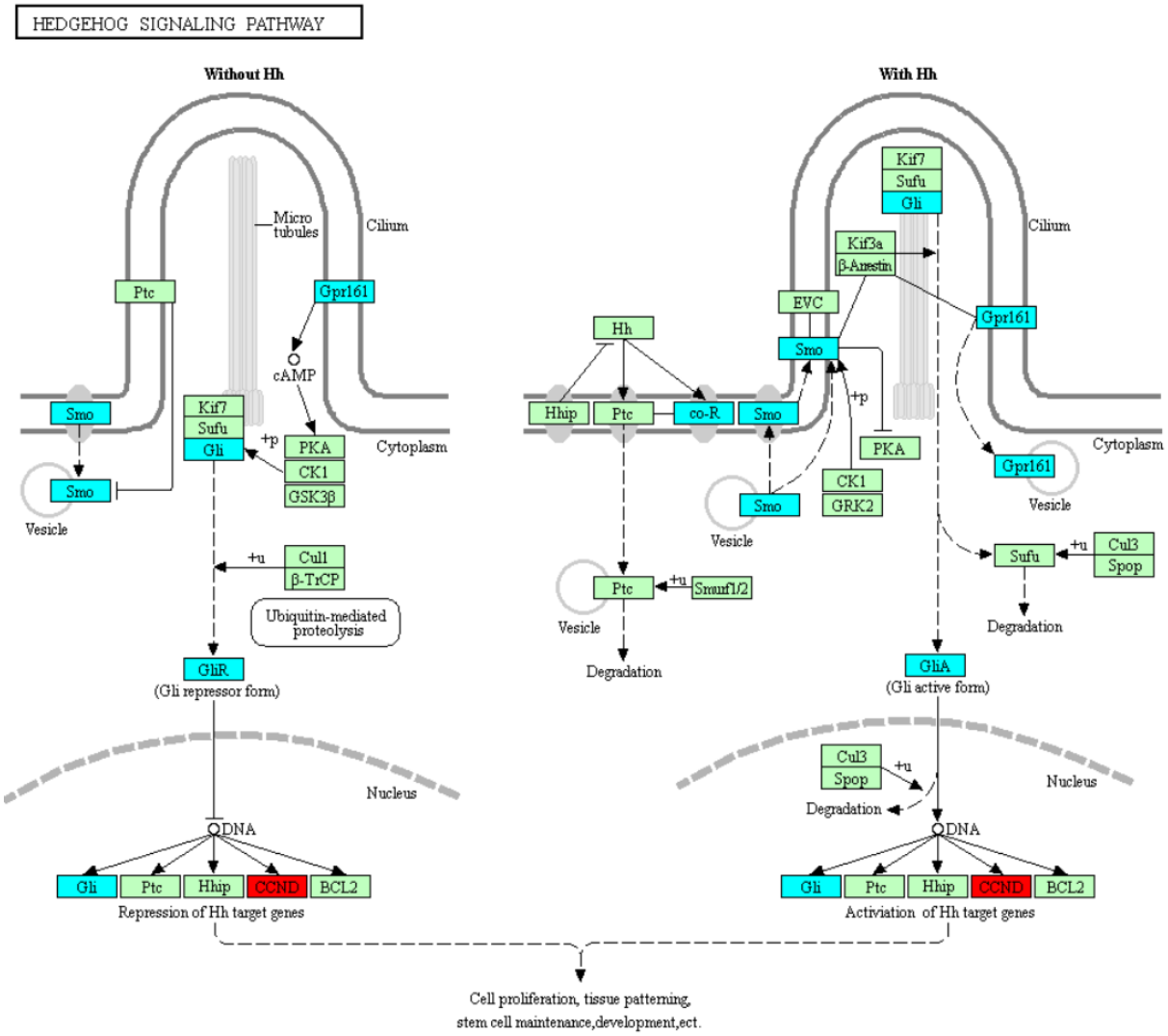


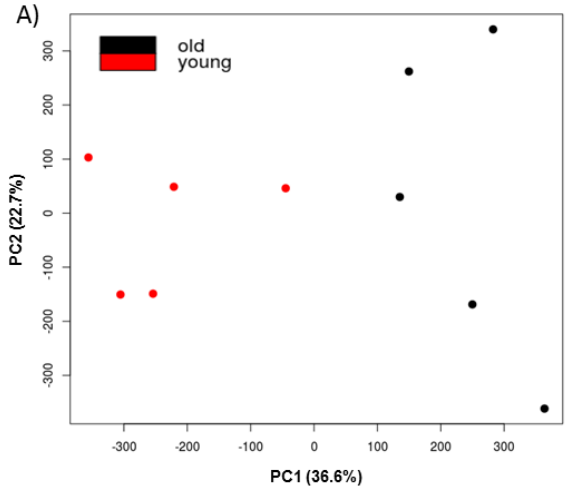
Figure 4-6 ***The DEGs mapped to the KEGG Hedgehog (HH) signalling pathway****. Significantly downregulated genes are shown in cyan, significantly up regulated genes are shown in red. No significant changes in gene expression are shown in green.*

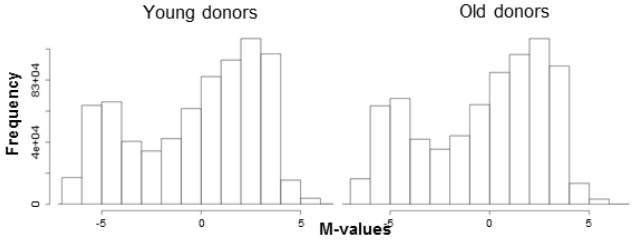
4.3.2 Epigenomic characterisation of MSC ageing with DNAme profiling

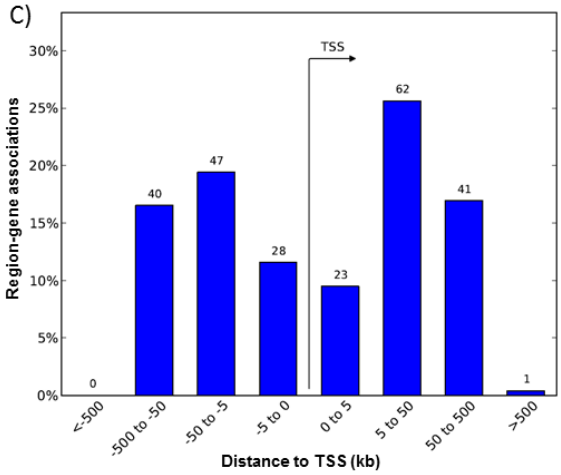
To examine the changes in DNA methylation with age, genome-wide DNA methylation profiling of young and old donor MSCs was carried out (young donors n = 5, 21 – 26 years; old donors n = 5, 62 – 81 years). Principal component analysis (PCA) showed an indistinct clustering of young and old donors. The clustering was improved post-SVA correction (Figure 4-7.A), possibly due to the removal of inter-donor variability. Histograms of M-values for young and old donor MSCs shows the distribution of DNA methylation with age (Figure 4-7.B), with mean M-values of -0.28 and -0.34 for young and old donors, respectively. The histogram and mean M-values indicate no global shift in DNA methylation level with age.

While global changes in DNA methylation were not observed, changes at specific CpG sites could occur. To identify these changes, differential methylation analysis was carried out on the 722,684 CpG sites post-filtering between the young and old donors. 243 differentially methylated positions (DMPs) were found, and the distance of these DMPs to transcriptional start sites (TSSs) is shown (Figure 4-7.C). The majority of DMPs were between 5 to 500kb, indicating that DNA methylation changes may have occurred more frequently at enhancer regions than TSSs.

The 243 DMPs corresponded to 92 genes, as several DMPs were located on the same genes. The top 10 significantly enriched processes associated with changes in DNA methylation included bone development, but other processes specific to proliferation, adipogenesis or chondrogenesis were not observed. Motif analysis of the DMPs showed a significant (FDR<0.05) enrichment of RUNX2 binding motif (Figure 4-7.D). The RUNX2 motif-containing differentially methylated genes include the transcription factors *HOXB4, HOXB5, TCF4 and TCF12.*







D)

MSigDB predicted promoter motifs	FDR
Motif NWNATCGATTANYNN matches CUTL1: cut-like 1, CCAAT displacement protein	2.29E-42
Motif NNCATCAATCAANNW matches PBX1: pre-B-cell leukemia transcription factor 1	5.60E-41
Motif ACCACANM matches RUNX2: runt-related transcription factor 2	8.25E-40
Motif NMGATANSG matches LMO2: LIM domain only 2	1.16E-37
Motif NANWGGAAAANN matches NFAT: Nuclear Factor of Activated T-Cells	1.34E-37
Motif NNCWGATARNNNN matches GATA1: GATA binding protein 1	4.12E-37
Motif NNNNNGATANKGNN matches GATA1: GATA binding protein 1	4.15E-36
Motif TGATTTRY matches GFI1: growth factor independent 1	2.76E-35
Motif STTTCRNTTT	1.37E-34
Motif GATAAGR	1.43E-34

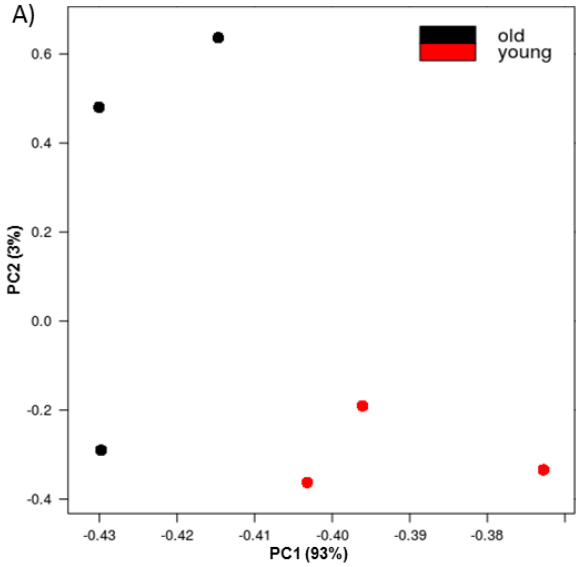
Figure 4-7 ***DNA methylation changes in young and old donor undifferentiated MSCs.*** ***A)*** *PCA of DNA methylation data (β-values) of young and old donor MSCs showing variance between samples post-SVA correction.* ***B)*** *Histogram of M-values of young and old donor MSCs. A M-value of –infinity indicates the CpG site is completely unmethylated, and a M-value of +infinity indicates the CpG site is completely methylated. Mean M-value for young donors = -0.28, Mean M-value for old donors = -0.34.* ***C)*** *The distance of the 243 differentially methylated positions (DMPs) to the transcription start sites (TSS).* ***D)*** *Top 10 differentially methylated transcription factor binding motifs.*

4.3.3 Epigenomic characterisation of MSC ageing with ATAC-seq

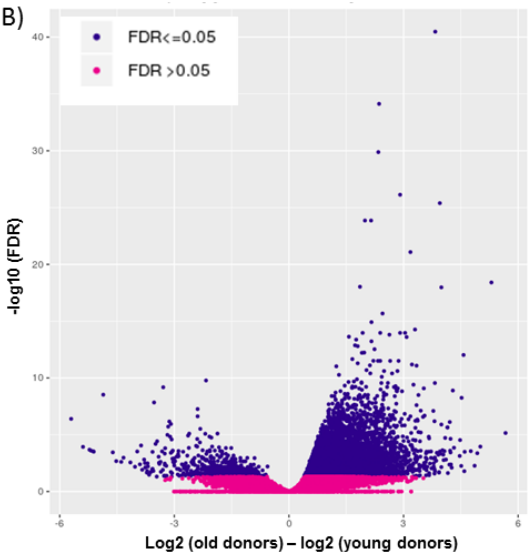
To examine changes in chromatin accessibility with age, ATAC-seq was carried out on young and old donor MSCs (young donors n = 3, 20 – 29 years; old donors n = 3, 62 – 87 years). PCA of the ATAC-seq data showed a non-overlapping separation of young and old donors in PC1, which accounts for 93% of the variance within the data (Figure 4-8.A). To identify specific differences in chromatin accessibility, differential peak analysis was carried out on 59,073 consensus peaks post peak calling and filtering. As a result, 6,790 differentially accessible peaks (DAPs) were found (FDR<0.05, log2(FC)>1). The majority of DAPs were <50kb from TSSs and were most abundant between 0 – 5kb from the TSSs (Figure 4-8.C).

To examine changes in the global pattern of chromatin accessibility with age, the FDR values versus FC was illustrated on a volcano plot, with the DAPs (FDR<0.05) highlighted in blue (Figure 4-8.B). The volcano plot demonstrated an overall increase in chromatin accessibility with age. The 6,790 DAPs were mapped to 4,519 genes, of which, 4,026 genes corresponded to increased peak accessibility (FDR<0.05, log2 > 1), and 493 genes corresponded to decreased peak accessibility (FDR<0.05, log2 < -1). The genes associated with significantly increased chromatin accessibility showed significant enrichment in processes such as collagen biosynthesis and epithelial cell-related processes (Figure 4-8.D). Conversely, genes associated with significantly decreased chromatin accessibility showed significant enrichment in processes involved in skeletal system morphogenesis and axonogenesis. (Figure 4-8.E).

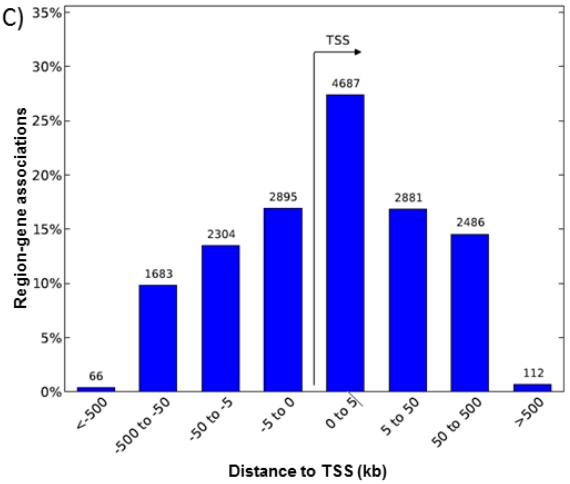
A)



B)



C)



D) Increased DAPs

GO biological process complete	FDR
Collagen fibril organization	1.46E-03
Chondrocyte development	3.22E-03
Regulation of vascular permeability	5.64E-03
Positive regulation of focal adhesion assembly	7.91E-03
Embryonic forelimb morphogenesis	9.69E-03
Response to thyroid hormone	1.03E-02
Neuron projection regeneration	1.13E-02
Collagen biosynthetic process	2.04E-02
ERK1 and ERK2 cascade	3.04E-02
Lung epithelial cell differentiation	3.25E-02

E) Decreased DAPs

GO biological process complete	FDR
Regulation of multicellular organismal development	6.69E-03
Negative regulation of transcription by RNA polymerase II	2.47E-02
Axonogenesis	2.94E-02
Skeletal system morphogenesis	3.05E-02
Locomotion	3.13E-02
Positive regulation of MAPK cascade	4.97E-02

Figure 4-8 ***Changes in chromatin accessibility in old vs young donor MSCs. A)*** *PCA of ATAC-seq expression of young and old donor MSCs showing variance between samples post peak calling and counting (young donors n = 3, 20 - 29 years, old donors n = 3, 62 – 87 years).* ***B)*** *Volcano plot of ATAC-seq expression fold change (FC) vs false discovery rate (FDR) in old vs young MSCs. The differentially accessible peaks (DAPs) are highlighted in blue.* ***C)*** *The distance of the DAPs to the transcription start sites (TSS).* ***D)*** *Top 5 enriched GO terms for increased DAPs with age, indicating that these processes are associated with a more open chromatin structure with age.* ***D)*** *Top 5 enriched GO terms for decreased DAPs with age, indicating that these processes are associated with a more closed chromatin structure with age.*

4.3.4 Protein-level characterisation of MSC senescence and apoptosis with CyTOF

CyTOF was carried out to examine the donor age-related changes of MSCs at the protein level. The antibody panel included the following senescence markers: P16, P53 and MYC, and the following apoptosis markers: BCL2-XL, CASP-3, CASP-8 and MCL-1. Dot plots showing the intensities of the marker expression are provided in supplementary figure S1. The relative percentage of the positive cells for each marker was quantified and compared between the two age groups (Figure 4-9) (young donors n = 3, 20 – 29; old donors n = 4, 62 – 87 years. No significant changes in the expression of the senescence and apoptosis markers were observed between the two donor age groups (sig at $p<0.05$, post-Bonferroni correction).

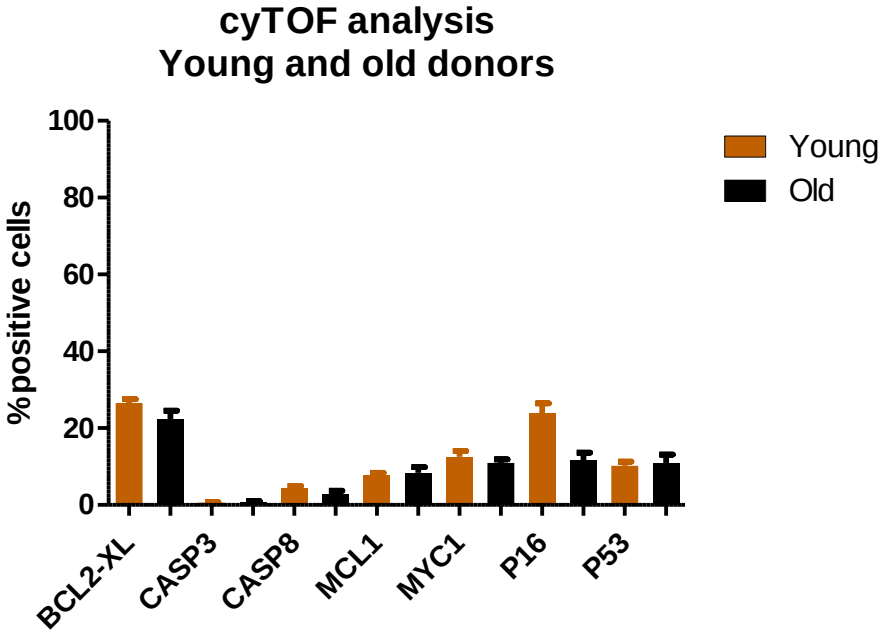


Figure 4-9 ***Quantification of the CyTOF data of young and old donor MSCs.*** *The percentages of MSCs positive for each of the senescence (P16, P53 and MYC) and apoptosis (BCL2-XL, CASP-3, CASP-8 and MCL-1) markers. Young donors n = 3, age 20 – 29 years; old donors n=4, age 62 – 87 years.*

4.3.5 Common mechanisms amongst –omics data

To further understand the mechanisms of MSC ageing, common changes between the various -omics approaches were compared. A Venn diagram shows the overlap between the significant genes from the three -omics datasets (Figure 4-10.A). 24 differentially methylated genes (26%) were differentially expressed, and 607 genes with differential chromatin accessibility (13%) were differentially expressed. 6 genes were significantly altered with age in all three datasets, amongst which, *ADD3*, *BMP6* and *EBF1* showed decreased DNA methylation and increased chromatin accessibility and gene expression with age, and *NLRP3* showed increased DNA methylation and decreased chromatin accessibility and gene expression with age (Figure 4-10.B.i).

To examine the coherence between the epigenetic and transcriptional changes, the Log2FC values of the DEGs were plotted against the Log2FC values of the DMPs and DAPs (Figure 4-10.C). Linear regression found no significant correlation between the changes in DNA methylation and gene expression ($R = -0.1$, $p = 0.2$). On the other hand, a significant positive correlation was observed between the changes in chromatin accessibility and gene expression ($R = 0.5$, $p < 0.01$). A similar trend can be visualised with a heatmap of the log2 FC comparing the –omics datasets (Figure 4-10.B.ii,iii).

To examine the significantly altered pathways common amongst the three –omics data sets, MetaCore pathway analysis was carried out. Amongst the top 10 enriched processes, the processes related to the canonical WNT signalling pathway was the most frequently altered (Figure 4-11.A). Amongst the gene targets regulated by β-catenin, *FGF18*, *FST*, *MYC* showed a significant increase in chromatin accessibility and gene expression with age, whereas, *TNFSF11b*/*OPG* and *FZD7* showed a significant decrease in chromatin accessibility and gene expression with age (Figure 4-11.B).

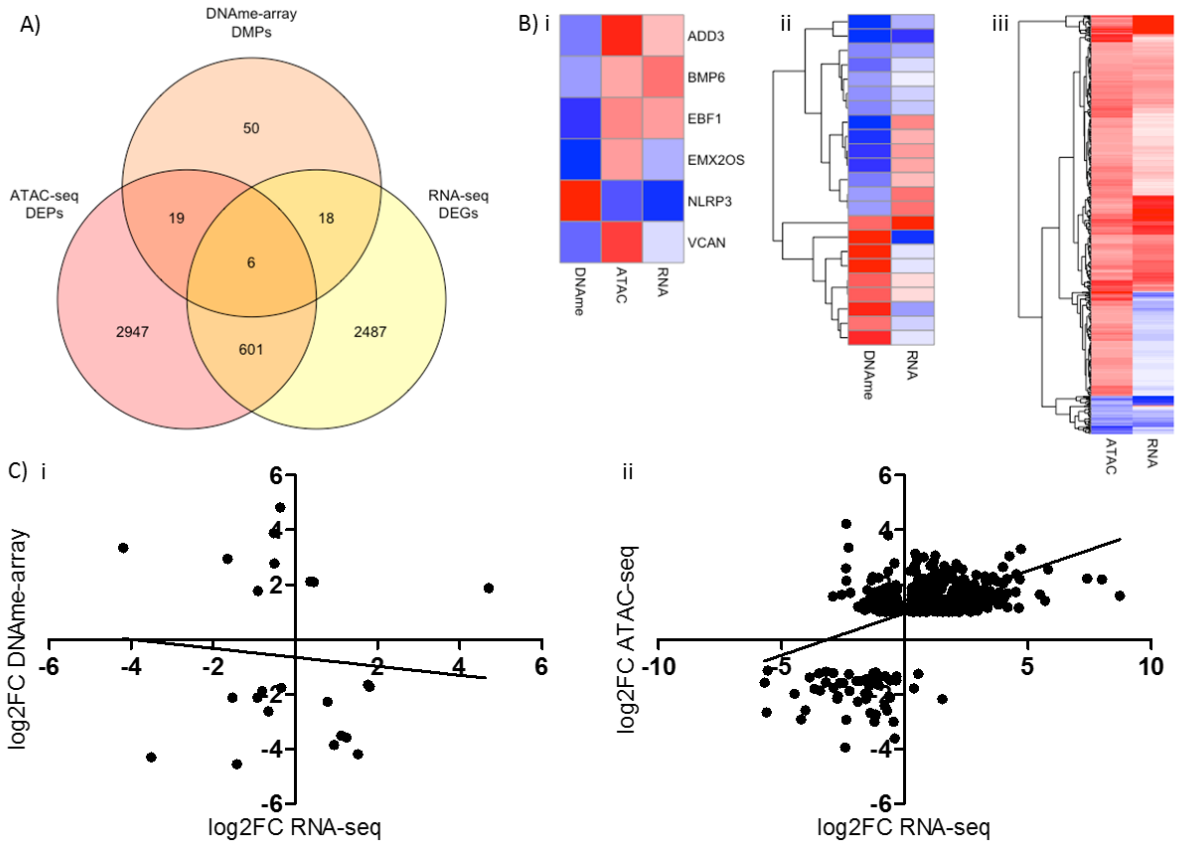


Figure 4-10 ***Common mechanisms amongst multi-omic data of MSC ageing. A)*** *Venn diagram showing the overlap of significant genes associated with ATAC-seq, DNAme-array and RNA-seq.* ***B)*** *Heatmap of the Log2FC (old vs young) of the genes common between i) all three -omics datasets, ii) between RNA-seq and DNAme-array, and iii) between RNA-seq and ATAC-seq.* ***C)*** *i) Scatterplot of Log2FC of the DEGs (RNA-seq) against DMPs (DNAme-array). Linear regression shows no significance at R=-0.1, p=0.2. ii) Scatterplot of Log2FC of the DEGs (RNA-seq) against DAPs (ATAC-seq). Linear regression shows significance at R= 0.5, p<0.01.*

A)

MetaCore enriched biological process	-log(pValue) 0 1 2 3 4 5 6 7 8	FDR	Ratio
Cytokeleton remodelling regulation of actin cytoskeleton organization by the kinase effectors of Rho GTPase		2.464e-6 2.785e-1 4.139e-6	23/58 2/58 23/58
Growth factors in regulation of oligodendrocyte precursor cells survival in multiple sclerosis		4.127e-1 2.785e-1 4.616e-6	6/42 1/42 19/42
Canonical WNT signalling pathway in colorectal cancer		7.715e-4 2.822e-1 7.705e-6	20/66 1/66 24/66
DKK1 signalling in multiple myeloma		2.515e-3 2.785e-1 8.260e-6	9/19 1/19 12/19
Development WNT/Beta-catenin signalling in the nucleus		1.195e-1 2.785e-1 8.887e-6	11/59 2/59 22/59
Chemotaxis Lysophosphatidic acid signalling via GPCRs		2.046e-3 2.785e-1 1.312e-5	29/129 2/129 35/129
Signal transduction Leptin signalling via JAK/STAT and MAPK cascade		7.163e-2 2.785e-1 1.326e-5	9/39 1/39 17/39
WNT signalling in HCC		1.537e-3 2.785e-1 1.887e-5	14/40 1/40 17/40
Stem cell Schema: Histone H3 demethylase in stem cells		7.937e-1 2.785e-1 1.887e-5	3/32 1/32 15/32
NRF2 regulation of oxidative stress reponse		2.993e-3 2.785e-1 2.087e-5	16/54 1/54 20/54

ATAC DNA RNA

B)

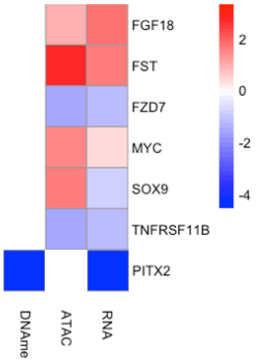


Figure 4-11 ***Pathway analysis of the multi-omics data. A)*** *The top 10 combined pathway over-representation for ATAC DAPs, DNA DMPs and RNA DEGs.* ***B)*** *Heatmap of the FC (old vs young) of β-catenin target genes that were significantly altered in two or more datasets (RNA-seq, ATAC--seq and DNAme-array).*

4.4 Discussion

4.4.1 Role of canonical WNT pathway in MSC ageing

In the RNA-seq data, the top 100 genes that separated the two age groups were enriched in processes involved in cell proliferation and skeletal system morphogenesis, suggesting that the phenotypic changes characterised with MSC ageing (detailed in chapter 3) can be captured by the differences in gene expression. Therefore, this chapter sought to use the transcriptomic data to identify mechanisms that underline MSC ageing.

The canonical WNT signalling pathway is well known for its important role during development, driving cell proliferation and determining cell fate [236]. However, the role of the canonical WNT pathway during the ageing process in human MSCs is less well characterised. The RNA-seq data revealed a global decline in the expression of the canonical WNT pathway activator genes. In particular, several members of *FZD* (1,2,3,6,7) and its co-receptor *LRP5* were significantly downregulated. *FZD* and *LRP5* are important genes governing MSC fate [237, 238]. For example, competitive inhibition of FZD significantly reduced ALP activity and matrix mineralisation in human MSCs [237], whereas knockout of a *FZD* antagonist *FRZB* significantly increased cortical bone mass in mice [239]. Similarly, *LRP5* loss-of-function mutation causes osteoporosis pseudo-glioma, characterised by a significant decline in bone mass [240], and *in vitro* inhibition of LRP5 by DKK1 promoted adipogenesis [241].

Ultimately, the repression in canonical WNT pathway gene expression resulted in the decline of WNT signalling activity. Multiple studies have found that the activation of canonical WNT signalling or the accumulation of β-catenin resulted in the priming of MSCs in favour of osteogenic fate and away from adipogenic fate [242-244]. This is mediated by the interaction of β-catenin-LEF/TCF complex with the osteogenic master regulator - RUNX2 and adipogenic master regulator PPARG [245]. In this chapter, there was a significant increase in *PPARG*

expression and a non-significant decline in *RUNX2* expression with increasing donor age of MSCs. Interestingly, the upregulation of *PPARG* can further inhibit β-catenin signalling and suppresses RUNX2 activity [240, 246, 247]. This is likely associated with the increased DNA methylation at genes containing RUNX2 binding motifs, and the significantly decreased chromatin accessibility of genes involved in skeletal system development. This suggests that the changes in the gene expression and the activity of the canonical WNT pathway may be a mechanism that alters the lineage preference of MSCs with age.

In chapter 1.4, the literature review describes that the age-associated bone loss is not only caused by an altered MSC fate away from osteogenesis, but also by excess bone resorption. Interestingly, the age-related decline in the canonical WNT signalling may be associated with increased bone resorption. *OPG*, an important osteoclastogenesis inhibitor secreted by MSCs and osteoblasts/osteocytes [248], its expression is regulated by β-catenin [249]. Coincidently, there was a significant decrease in the chromatin accessibility and gene expression of *OPG* with increasing donor age. Furthermore, the RNA-seq and ATAC-seq data showed that the gene expression and chromatin accessibility of *IL-6* were significantly increased. Numerous age-associated bone diseases are tied to *IL-6* overexpression, including RA and osteoporosis [250]. In a murine model, increased secretion of IL-6 by bone marrow cells induced higher osteoclastogenesis [251]. The age-related changes in *OPG* and *IL-6* chromatin accessibility and gene expression may further drive the imbalance between the osteoblast/osteoclast number and activity. Therefore, rescuing WNT signalling activity may be a strong candidate in restoring the lineage preference of MSC with age and homeostasis in bone remodelling.

4.4.2 Epigenetic changes of MSC ageing

Previous reports have found no global shift in DNA methylation levels with increasing donor age [132, 133, 140, 226], which is consistent with the findings in this chapter. However, there were significant changes in the methylation of genes involved in bone development and genes containing RUNX2 binding motifs, suggesting that DNA methylation does play a role in RUNX2 related changes in osteogenic potential of MSCs with age. Differentially methylated RUNX2 motif-containing genes include *HOXA11, PITX2* and *MAP3K13*, which are involved in HOX, TGF-β and JNK signalling pathways, respectively. In particular, members of HOX family genes were previously reported to be strongly associated with age-related DNA methylation changes in MSCs [132, 133, 140].

Genome-wide changes in chromatin accessibility in MSCs with age has not been previously reported. The ATAC-seq data suggests that there was a global increase in chromatin accessibility with age. Given that pluripotent cells such as ESCs are typically associated with higher chromatin accessibility, the global increase in chromatin accessibility with age was surprising. However, hematopoietic cells also exhibited an increased chromatin accessibility with age by DNase 1 cleavage [252]. Interestingly, in that study by Cakouros and Gronthos, a global hypomethylation in aged HSCs has been found, which was not observed here in MSCs with age. This implies that changes in chromatin accessibility may play a more important role than DNA methylation during MSC ageing.

Alternatively, the variability in chromatin accessibility could also arise during the cell cycle or DNA repair: Firstly, global chromatin restructuring occurs during the S- and M- phases of the cell cycle [253]. Given the low number of biological replicates, it is possible that more cells in the old donors happened to be in S- or M- phase when sequenced. Secondly, the chromatin opens during DNA repair [254]. As MSCs accumulate DNA damage with age, they may

undergo more frequent DNA repairs [255, 256]. However, increased expression of genes involved in the double-stranded break (DSB) repair pathway was not observed.

While the cause of the increased chromatin accessibility in the old donors is unclear, there are important implications. For example, condensed chromatin protects DNA from damage. The dysregulation of chromatin accessibility may increase genomic instability, which is a hallmark of many diseases [257]. In addition, increased chromatin accessibility may also result in transcription factors (TFs) being less responsive to changes at a specific gene. TFs for non-housekeeping genes, such as *RUNX2*, are typically expressed at low levels and can bind to a large number of genomic loci (80,000 *RUNX2* binding sites was identified with ChIP) [258]. Therefore, upon osteogenic induction, *RUNX2* may be less responsive in binding to the *RUNX2* motif-containing osteogenic genes in the old donor MSCs, as the transcription factor is diverted to other regions of open chromatin.

The genomic locations of the DAPs and DMPs were different in the ATAC and DNA methylation data. DAPs most frequently occurred at genomic regions less than 5kb from the TSS. The proximity of the changes in chromatin accessibility to the sites of gene expression indicates that these age-related changes may directly influence gene expression. Indeed, a significant association was observed between the changes in chromatin accessibility and the expression of the nearest gene. In contrast, DMPs were generally at genomic loci more than 5kb from the TSS, suggesting that the age-associated changes in DNA methylation may preferentially occur at distal enhancer regions. Another study has similarly reported that MSCs from osteoarthritis patients exhibited accelerated ageing phenotypes and showed a significant increase in DNA methylation situated at distal enhancer regions [259]. As only 27% of the distal elements were found to interact with the nearest TSS [260], this may explain the lack of association found between DNA methylation and the expression of its nearest gene in section 4.3.5.

4.4.3 Additional targets from multi-omics data

Apart from the WNT pathway, there are additional targets that may be of interest for follow-up studies. *EBF1* showed a significant decrease in DNA methylation and a significant increase in chromatin accessibility and gene expression with age. The EBF family transcription factor 1 (*EBF1*) is essential for adipogenesis. A ChIP experiment showed that EBF1 binds directly to the promoter of *PPARG* to activate its transcription [261]. Knockdown of *EBF1* inhibited adipocyte formation [262] and its overexpression promoted adipogenesis [261]. The consequence of the age-related changes in *EBF1* in MSC fate decisions may be further investigated.

Recent studies found that the *Homeobox* (*HOX*) genes have important roles beyond embryonic development in fracture repair [135, 137]. The gene family includes 13 paralogues: *HOX 1 - 13*. With increasing donor age, *HOX 1 – 5* and *7 - 10* were significantly downregulated, whereas, *HOX 11 - 13* were significantly upregulated. Previous literature has also reported a decreased expression of *HOX7B* in old murine MSCs [138]. In addition, *HOX7B* overexpression improved the proliferative and osteogenic potential of old murine MSCs. Therefore, rescuing *HOX 1 - 10* expression in old donor human MSCs may result in a similar effect. In contrast, *HOX11-13* were previously shown to promote chondrocyte differentiation, as their knockout significantly impaired chondrocyte maturation [139]. This indicates that the age-related increase in *HOX1 – 10* expression and decrease in *HOX11 – 13* expression may have influenced MSC fate towards chondrogenesis and away from osteogenesis. In support of this, *HOX 11-13* showed decreased DNA methylation and increased chromatin accessibility. However, the DNA methylation and chromatin accessibility of *HOX 1 - 10* did not show an inhibitory change with age. Instead, the *HOX 1 - 11* genes may be regulated via other epigenetic mechanisms, such as miR-196a, which downregulates *HOXB7* expression in MSCs [138].

Other members of the *HOX* family include short stature homeobox 2 (SHOX2), which inhibits *RUNX2* expression in idiopathic short stature syndrome, and mesenchyme homeobox 2 (MEOX2), which is upregulated in progeria syndrome. Both *SHOX2* and *MEOX2* were significantly upregulated in old donor MSCs. Overall, the evidence suggests that the *HOX* family genes may play an important role in the age-related changes in MSC functions.

5 Multi-omics characterisation of MSC ageing in the cell passage model

5.1 Introduction

5.1.1 RNA interference

RNA interference (RNAi) enables the characterisation of gene function by specifically silencing target gene expression. RNAi is a process that occurs in normal cell physiology, mediated by small non-coding RNAs such as miRNAs [263]. The miRNA is transcribed as a longer polyadenylated primary miRNA (pri-miRNA). While inside the nucleus, the pri-miRNA is cleaved into a shorter hairpin shaped pre-miRNA by the Drosha complex. Subsequently, the pre-miRNA is transported to the cytoplasm, where it is further cleaved by Dicer into a 22-bp double-stranded mature miRNA. A single strand of the miRNA is incorporated into the miRNA-induced silencing complex (RISC), which include Dicer and Argonaut (AGO). The incorporated miRNA strand guides the RISC complex to target mRNAs using sequence complementarity. A miRNA can silence gene expression through multiple mechanisms. Most commonly, when there is a perfect sequence complementarity, the miRNA-RISC complex mediates the degradation of the target mRNAs. RNAi can be exploited experimentally to target a specific gene. Commonly, synthetic small interfering RNAs (siRNAs), which are similar to the mature miRNAs, are directly transfected into the cytoplasm, and small hairpin RNAs (shRNAs) that are similar to the pre-miRNAs are transduced into the nucleus through a viral vector.

5.1.2 Lentiviral vectors

Viruses are useful tools to deliver genetic material into cells, such as the DNA encoding shRNAs. The use of different viral vectors allows the DNA to be integrated into the genome

or to be expressed as an episomal vector. Lentiviruses are one of the most commonly used integrating vectors. The advantage of genomic integration is that the delivered genetic material can replicate together with the genomic DNA during cell division, so it is not diluted out in proliferating cells e.g. MSCs. Modified first, second or third generation lentiviruses are not replication competent due to the design of self-inactivating (SIN) vectors [264]. Therefore, after the lentivirus is removed, no further transduction can occur. This is important for safety and controlling the multiplicity of infection (MOI) – the ratio of viruses to cells. The pGIPZ transfer plasmid used in this chapter is a second-generation SIN-vector. Within the 5' and 3' long terminal repeats (LTRs) of the transfer plasmids contain the DNA that will be integrated into the genome, which consists of a CMV promoter, a GFP reporter, an internal ribosomal entry site, a puromycin selection marker and a shRNA hairpin. The other elements required for viral packaging and replication are removed from the pGIPZ transfer plasmid into separate envelope and packaging plasmids to achieve the SIN design. The transduction occurs through endocytosis, reverse transcription, nuclear import and integration. The GFP reporter expression indicates the successful integration of the DNA and the expression of the hairpin, which typically occurs around 24 - 48 hrs post transduction. The disadvantage of lentiviruses is that the insertion of DNA occurs at "random" genomic loci. Insertion into an exon or regulatory element can alter gene expression or function, which is referred to as insertional mutagenesis [265].

5.1.3 shRNA-seq

Lentivirus-shRNA knockdown assays have been a powerful tool in molecular biology, but individual shRNA screenings have limited throughput. To overcome this, a pooled approached was recently reported, in which libraries of lentivirus-shRNAs are pooled in a competitive screening approach [207]. After a certain treatment, the perturbation in the shRNA hairpin

population can be identified using NGS. In this chapter, the shRNA-seq method was modified to identify epigenetic regulators of MSC proliferation. A pooled lentiviral shRNA library targeting 398 epigenetic regulators were used to transduce a population of slow proliferating MSCs. If the knockdown by a shRNA in an individual MSC induced proliferation, then the MSC together with the integrated hairpin DNA would be over-represented in the cell population over several passages. The genomic DNA was isolated, PCR amplified and sequenced to identify the enriched shRNA hairpins. The data processing is similar in principle to RNA-seq (described in chapter 1.5). However, instead of the human genome, the reads were aligned to the sequences of the shRNA library to identify enriched shRNAs. In this chapter, the lentiviral-shRNA library contains the combined shRNA collection of the epigenetic targets from the Broad Institute (Cambridge, MA, USA) and the Target Discovery Institute (Oxford, UK). There are 2,471 unique shRNAs targeting 398 epigenetic regulators. Each epigenetic regulator is targeted by an average of 6 shRNA hairpins to improve knockdown success rate and gene coverage.

5.2 Aims

The previous chapter examined the epigenetic, transcriptional and protein changes in MSCs with increasing donor age. This chapter aims to characterise some of these changes in MSCs with long term cell culture and to compare the data between the two ageing models to identify common mechanisms. This chapter also aims to screen directly for epigenetic regulators important for MSC proliferation in the cell culture ageing model using shRNA-seq.

Chapter 3 has shown that there is variability in the number of passages achieved by MSCs from different donors. In order to compare early and late passage MSCs from different donors, in this chapter, an early passage is defined as a passage number that is less than or equals to 50% of the total number of passages achieved by the donor, and a late passage is defined as a passage

number that is more than or equals to 70% of the total number of passages achieved for the donor.

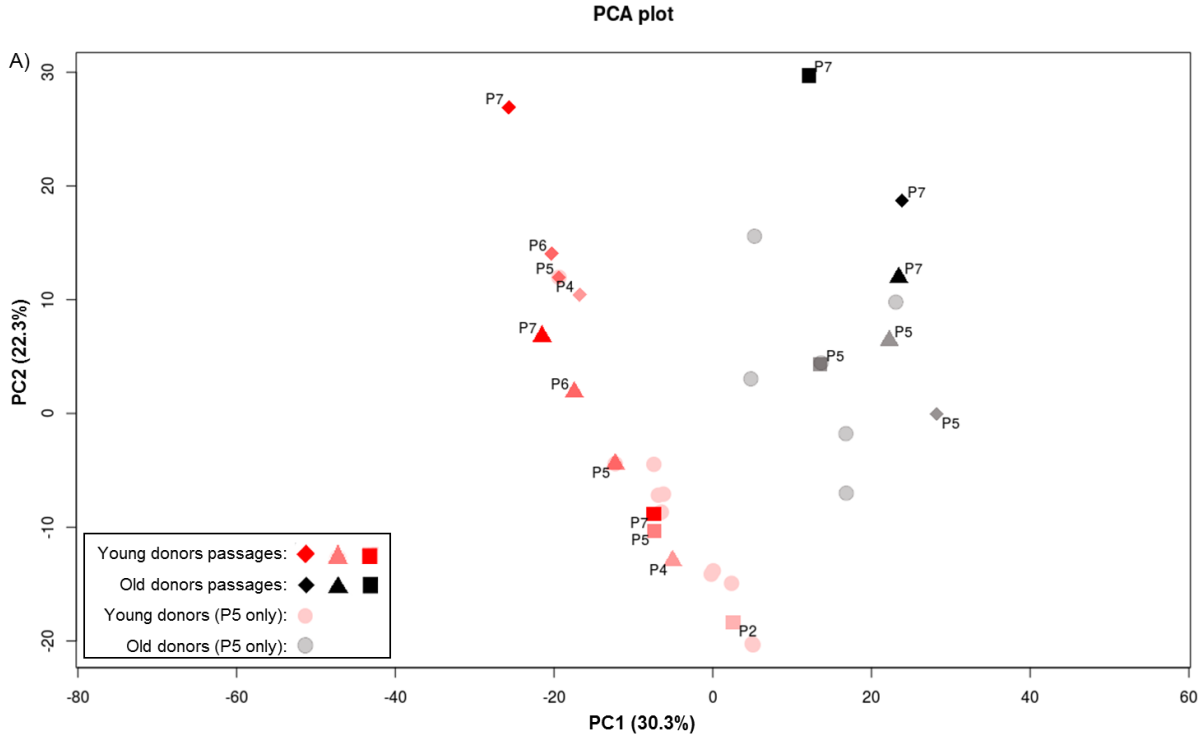
5.3 Results:

5.3.1 Transcriptomic characterisation of MSC long term culture with RNAseq

To investigate transcriptomic changes of MSCs over long term cell culture, RNA-seq of MSCs from early (P2 – P5) to late (P7) passages were carried out (young donors n = 3, 20 - 29 years, old donors n = 3, 62 – 87 years). In a PCA plot, PC1 appears to differentiate between young and old donors, whereas, PC2 appears to differentiate between passage numbers. Samples from early to late passages consistently shifted from negative to positive values in PC2 (Figure 5-1.A). The young and old donor MSCs at P5 (data from chapter 4) were also plotted in the PCA. The majority of the young donors at P5 clustered below 0 on PC2, whereas the majority of the old donors at P5 clustered above 0. GO analysis showed that the top 100 genes contributing to the variability in PC2 were significantly enriched in processes involved in mitosis (Figure 5-1.B). This suggests that increased donor age may be partially transcriptionally equivalent to a higher passage number in terms of proliferation.

There was also inter-donor variabilities across PC2. To examine whether the PC2 variability is associated with the variability in proliferative potential between donors, linear regression analysis of PC2 values against PD was carried out (Figure 5-1.C). There was a significant association ($R = -0.99$, $P < 0.05$) between PC2 values and PD in the young donors, while no association ($R = 0.24$, $P>0.05$) between PC2 value and PD was found in the old donors. This indicates the set of genes in PC2 may be predictive of proliferative potential of MSCs, at least amongst the young donors.

A)



B) **PC2:**

GO biological process	FDR
Mitotic spindle assembly checkpoint	5.86E-06
Mitotic spindle assembly	3.75E-04
Mitotic cytokinesis	4.26E-04
Mitotic anaphase	2.31E-03
Mitotic prometaphase	3.69E-03
Positive regulation of mitotic cell cycle phase transition	7.98E-03
Protein localization to kinetochore	1.04E-02
Meiotic chromosome segregation	1.38E-02
Mitotic chromosome condensation	1.83E-02
Positive regulation of mitotic nuclear division	2.63E-02

C)

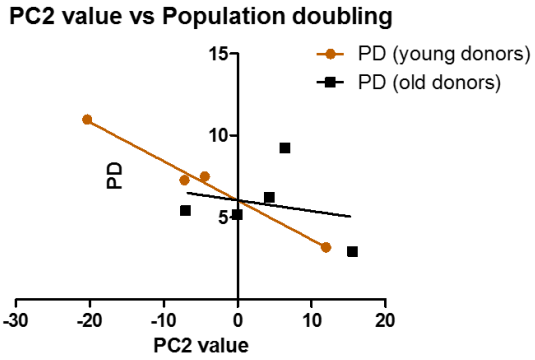
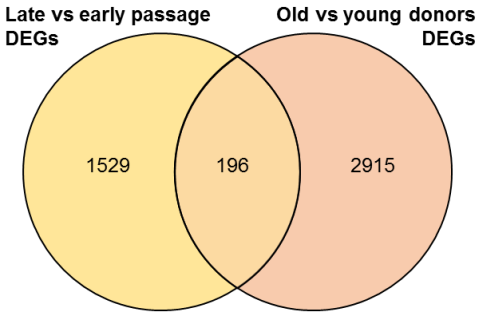
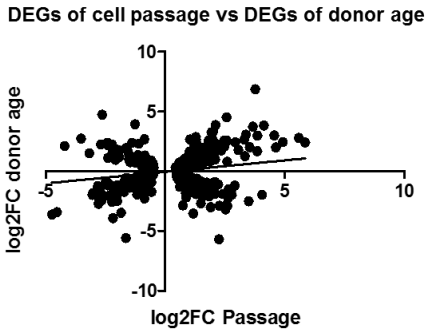


Figure 5-1 ***Transcriptomic changes during MSC passaging. A)*** *PCA of RNA-seq data showing the variability in gene expression between samples. Passage number is indicated as P[#]. Red = Young donors (aged 20 – 29; n=3,), Black = Old donors (aged 62 – 87; n=3). Diamonds, triangles and squares indicate different donors at several passages. Circles indicate young and old donors from the RNA-seq data in chapter 4.* ***B)*** *GO terms of the significantly enriched processes in the top 100 genes that represent the variability between samples in PC2.* ***C)*** *Scatter plot of PC2 values against total population doubling (PD) of young donors (aged 20 – 29 years; n=4) and old donors (aged 62 – 87 years; n=5) (data from chapter 1). Linear regression line fitted. Red = young donors, R = -0.99, P < 0.05; black = old donors, R = 0.24, P>0.05.*

1,725 genes were differentially expressed during long term culture (All vs baseline passage at P2 or P4, paired Walt test, sig. at padj<0.05), of which, only 196 DEGs showed concordant change with the DEGs in old vs young donors (Figure 5-2.A). Similarly, linear regression analysis of the DEGs from the two datasets (donor age and passage) showed a weak positive significant correlation (R=0.2, p<0.05). Go analysis identified the significantly enriched biological processes in the upregulated and downregulated concordant DEGs (Figure 5-2.B&C). There were 18 bone development-related genes amongst the concordant DEGs (Figure 5-2.D&E).

A)





B) **Concordant upregulated DEGs:**

GO Biological process	FDR
Positive regulation of endothelial cell proliferation	8.83E-03
Anatomical structure formation involved in morphogenesis	2.54E-02
Chemotaxis	2.57E-02
System development	2.65E-02
Tube development	2.84E-02
Regulation of multicellular organismal process	2.95E-02
Positive regulation of cell migration	4.68E-02

C) **Concordant downregulated DEGs:**

GO Biological process	FDR
Bone morphogenesis	3.31E-03
Epithelial tube morphogenesis	1.19E-02
Axonogenesis	3.16E-02
Developmental growth	3.40E-02
Roof of mouth development	3.68E-02
Embryonic organ morphogenesis	3.82E-02
Negative regulation of cell differentiation	3.87E-02
Morphogenesis of embryonic epithelium	3.88E-02
Regeneration	4.09E-02

D) **Concordant upregulated bone development DEGs:**

Gene symbol	Gene name	Late vs early passage (log2FC)	Old vs young donor (log2FC)
BMP6	Bone morphogenetic protein 6	3.1	1.8
CSGALNACT1	Chondroitin sulfate N-acetylgalactosaminyltransferase 1	1.9	3.3
FGF2	Fibroblast growth factor 2	1.0	0.6
RBP4	Retinol-binding protein 4	1.3	2.3
SFRP4	Secreted frizzled-related protein 4	2.5	2.5
TEK	Angiopoietin-1 receptor	1.7	1.3
TIMP1	Metalloproteinase inhibitor 1	1.5	1.3

E) **Concordant downregulated bone development DEGs:**

Gene symbol	Gene name	Late vs early passage (log2FC)	Old vs young donor (log2FC)
ALX1	ALX homeobox protein 1	-1.6	-5.6
DLX5	Homeobox protein DLX-5	-1.0	-0.9
FGFR2	Fibroblast growth factor receptor 2	-2.2	-3.9
GLI3	Transcriptional activator GLI3	-1.1	-0.9
HAS2	Hyaluronan synthase 2	-1.0	-1.1
MATN2	Matrilin-2	-0.8	-1.0
SOX11	Transcription factor SOX-11	-4.5	-3.4
TMEM119	Transmembrane protein 119	-2.8	-1.2
TRIM45	Tripartite motif-containing protein 45	-1.2	-0.5
VWA1	von Willebrand factor A domain-containing protein 1	-1.1	-1.7
ZNF385A	Zinc finger protein 385A	-1.0	-1.0

Figure 5-2 ***DEGs during MSC passaging. A)*** *Venn diagram of DEGs during passaging overlapped with DEGs between old vs young donors (data from chapter 4).* ***Linear regression*** *of the DEGs from the two datasets showed a weak positive significant correlation (R=0.2, and p<0.05).* ***B & C)*** *Go terms of the enriched biological processes in the 196 concordant DEGs.* ***D & E)*** *Go terms of the 18 bone development-related genes amongst the concordant DEGs.*

5.3.2 Identification of epigenetic regulators of MSC proliferation

In order to identify epigenetic regulators of MSC proliferation, shRNA-seq screens were carried out. Slow to non-proliferating MSCs at late passages (P10 – 12) were transduced with a pooled lentiviral shRNA library targeting 398 epigenetic regulators (supplementary table S2). If the knockdown by a shRNA in an individual MSC induced proliferation, then the MSC together with the shRNA would be over-represented in the cell population over several passages (Figure 5-3.A). 72 hours after transduction, around 10% of MSCs were transduced, indicated by GFP reporter expression. After 2 passages, the percentage of GFP positive cells increased (Figure 5-3.B), which may indicate a gain of proliferative advantage by some of the transduced cells.

To identify the over-represented shRNAs, the transduced MSCs were sequenced at 72 hours (baseline) and at each subsequent passage (5 replicates using late passage MSCs of 2 young donors aged 20 – 29 years). 52 significantly over-represented shRNAs were identified (Fisher's exact test, sig at padj<0.05, post Bonferroni correction), corresponding to 21 gene targets (fig.4.3.C). 8 out of the 21 gene targets were followed up (*PRMT8*, *TCF20*, *SND1*, *PYGO1*, *EZH1*, *MTF2*, *SPIN1*, *HDAC2*). Late passage (P12) MSCs were transduced with lentiviral-shRNAs that specifically knocked down each of the targets, or a sub-pool of the lentiviral-shRNAs targeting all 8 genes, or a non-targeting control. Amongst the 8 genes, only PYGO knockdown showed an increase (1.2 fold, unpaired t-test, sig at $p<0.05$) in MSC cell number 6 days post-transduction compared to the control MSCs (Figure 5-3.E). MSCs transduced with the sub-pool showed a 1.4 fold increase in cell number compared to the control (unpaired t-test, sig at $p<0.05$).

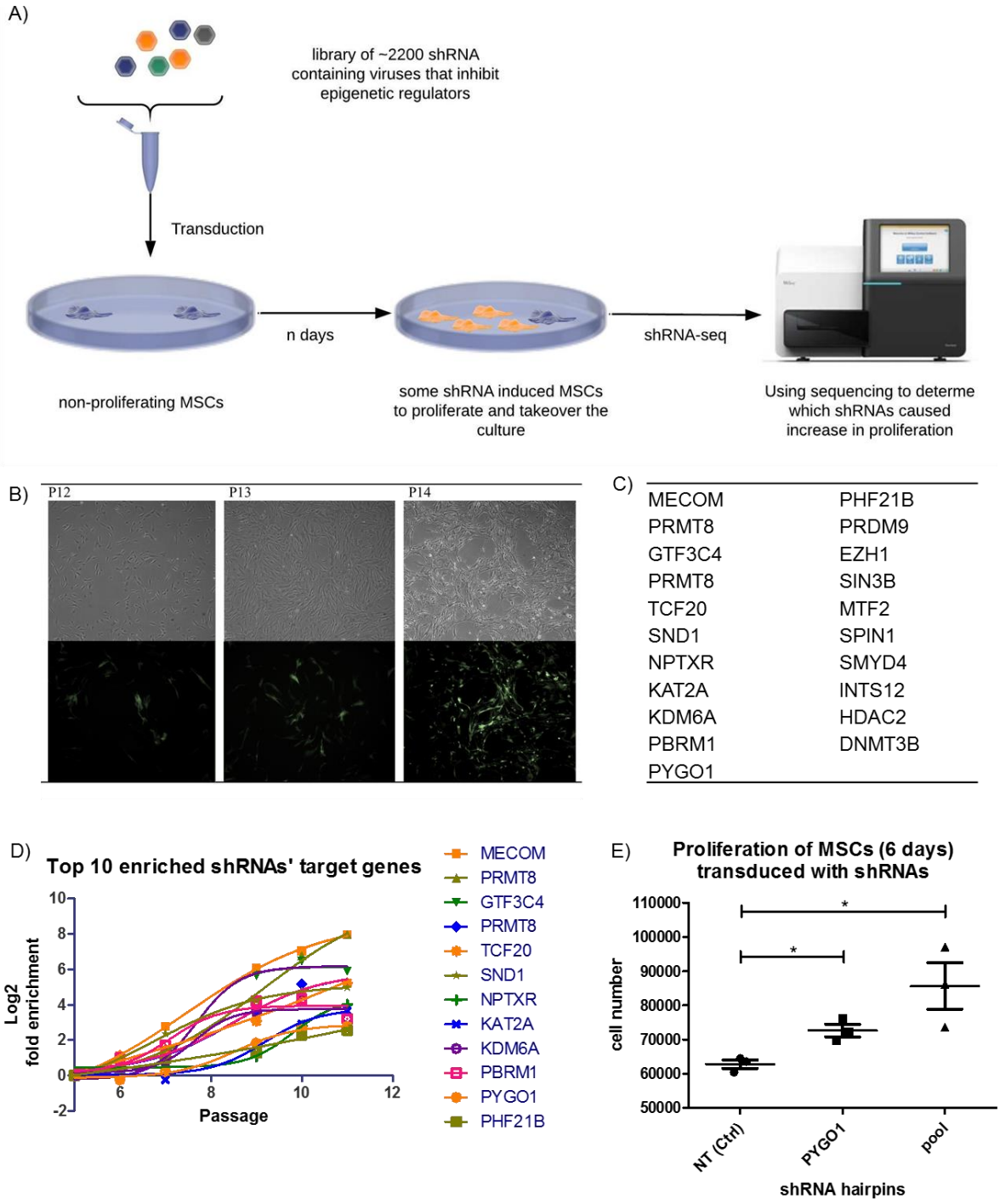


Figure 5-3 ***Identification of epigenetic regulators of MSC proliferation. A)*** *slow/non-proliferating MSCs at late passages were transduced with a pooled lentiviral shRNA library targeting ~400 epigenetic regulators. If the knockdown by a shRNA in an individual cell conferred a proliferative advantage, then this MSC, together with the shRNA, would be over-represented in the cell population over several passages. The shRNA can be identified with shRNA-sequencing (shRNA-seq). B) Phase contrast (top) and GFP (bottom) images of MSCs at P12 (72 hr post transduction), P13 and P14.* ***C & D)*** *significantly enriched shRNA target genes.* ***E)*** *Cell number of MSCs 6 days post-transduction of NT control, PYGO1 shRNA and a sub-pool of shRNAs targeting 8 gene targets (PRMT8, TCF20, SND1, PYGO1, EZH1, MTF2, SPIN1, HDAC2). Unpaired t-test, sig at $p<0.05$.*

5.3.3 Protein-level characterisation of MSC proliferation, senescence and apoptosis with CyTOF in the passage model

CyTOF was carried out to examine the cell passage-related changes of MSCs at the protein level. The antibody panel included the following senescence markers: P16, P53 and HDAC6, and the following apoptosis markers: BCL2-XL, BCL2, CASP-3 and CASP-8. Dot plots showing the intensities of the marker expression are provided in supplementary figure S2. The relative percentage of the positive cells for each marker was quantified and compared between the early and late passage groups (early passage = P5 – P9, late passage = P7 – P14; donors aged 20 – 29 years (n = 3)) (Figure 5-4). (Please note, early and late passages differ for each donor and are defined in section 5.2.) No significant changes were observed in the expression of these senescence and apoptosis markers (sig at padj<0.05, post-Bonferroni correction).

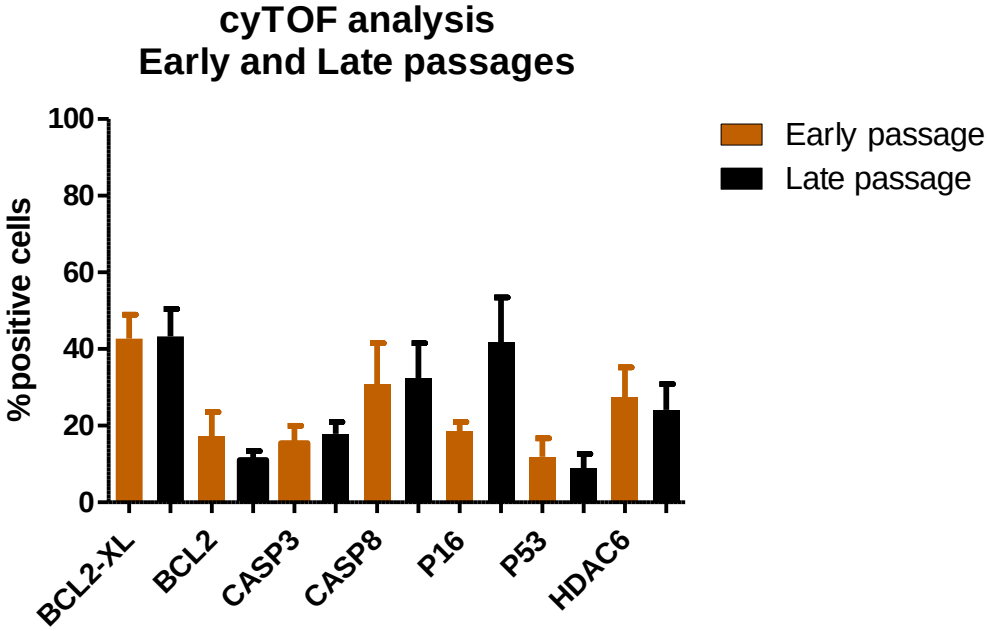


Figure 5-4 ***Quantification of the CyTOF data of early and late passage MSCs. S****howing the percentages of MSCs positive for each of the senescence (P16, P53 and HDAC6) and apoptosis (BCL2-XL, BCL2, CASP-3 and CASP-8) markers. Early passage = P5 – P9, Late passage = P7 – P14. Donors aged 20 – 29 years; n = 3.*

5.4 Discussion:

5.4.1 Comparing gene expression changes in donor age and cell culture models of ageing

While numerous studies demonstrated that the phenotypic changes between *in vivo* (donor age) and *in vitro* (passage number) ageing are similar [214, 256, 266-268], the transcriptomic changes between the two ageing models have not been extensively compared. A microarray study previously found that only 18 out of 184 (*in vivo ageing)* and 1257 (*in vitro* ageing) DEGs showed concordant changes between the two ageing models [136]. The RNA-seq data in this chapter showed that samples were primarily separated by donor age in PC1 and passage number in PC2. Additionally, the overlapping DEGs between the two datasets (old vs young donor and late vs early passage) showed only a weak positive correlation. Overall, this suggests that the transcriptional changes during donor ageing and long term culture may be largely different.

The discordance in gene expression may be caused by the different confounding factors in each of the ageing models, which is detailed in chapter 4. Thus, the small number of concordantly differentially expressed genes may provide insight towards the true biological mechanisms of MSC ageing. In chapter 4, the *HOX* gene family were highlighted as one of the key candidates for age-associated misregulation of MSC cell fate. Amongst the 18 bone development related concordant DEGs, *Distal-Less Homeobox 5 (DLX5)* was significantly downregulated. During development, *DLX5* knockout resulted in a significant reduction of *RUNX2*+ cells in the perichondrium and an absence or delay of endochondral ossification [269]. In addition, *DLX5* knockout mice showed an altered spatiotemporal expression pattern of *FGFR* and *IHH*. Key FGF and HH pathways genes *FGF2*, *FGFR* and *Gli3* were also amongst the concordant DEGs, suggesting a *HOX/DLX*-mediated dysregulation of FGF and HH pathways may be a mechanism in human MSC ageing. *Frizzled related protein 4 (FRP4)* was upregulated in both ageing models. FRP4 is a secreted protein that binds directly to WNT ligands, thus it can

compete with FZD receptors to act as an antagonist to WNT signalling [270]. The concordant upregulation of *FRP4* further supports the age-associated repression in the canonical WNT signalling pathway detailed in chapter 4.

PC2 values were found to be highly descriptive of MSCs with increased passage number. As proliferation was shown to decline with increasing passage number (detailed in chapter 3), it is unsurprising that PC2 genes were highly enriched in mitosis-related processes. Interestingly, PC2 values were also strongly correlated with the total PD of the young donors. This suggests that the proliferative potential of MSCs, at least from young donors, could be predicted by a set of genes within PC2. A similar concept was previously demonstrated with DNA methylation data [134, 271]. A panel of DNA methylation biomarkers was able to determine the epigenetic age of human tissues and cells. The epigenetic age was strongly correlated with the self-renewal and differentiation potential of cells. It was also highly correlative to passage number. However, in chapter 4, no significant correlation between DNA methylation and donor age was found.

Alternatively, the differences between donors in PC2 may represent the "true" passage number of the MSCs. This is because the passages of MSCs were difficult to standardise including the amount of time that cells were in culture and the number of population doublings at each passage. Therefore, to confirm whether PC2 is predictive for proliferative potential amongst donors or represent the "true passage" number, MSCs need to be sequenced directly after isolation with minimal passaging.

5.4.2 shRNA screen and PYGO1

Pygopus (PYGO) was identified in Drosophila to be an essential component of the canonical WNT signalling pathway. The C-terminal PHD domain of PYGO binds to Legless (LGS, or

BCL9 in mammals), which together form a complex with β-catenin [272]. The N-terminal domain of PYGO contains an N-terminal transactivation domain (NHD), which facilitates the transactivation of β-catenin target genes [273]. A nuclear localisation signal was also found in PYGO, indicating that it may also be important for the nuclear translocation of β-catenin [274, 275]. Given the facilitative role of PYGO in the canonical WNT signalling, it is unclear why *PYGO1* knockdown in the late passage MSCs resulted in a modest increase in proliferation. One possible explanation is that, in mammals, there are two orthologs of PYGO - PYGO1 and PYGO2 [274]. *PYGO2* homozygous knockout in mice was shown to significantly impair canonical WNT signalling and resulted in post-natal lethality. In contrast, $PYGO1^{-/-}$ mice showed no detectable developmental defects [276]. Interestingly, $PYGO1^{-/-}/PYGO2^{+/-}$ embryo showed more β-catenin reporter expression than the $PYGO1^{+/+}/PYGO2^{+/-}$ embryo in the heart, but less in the kidney, indicating the *PYGO1* may promote or repress canonical WNT activity in different cells or tissues [276].

The result suggests that shRNA-seq is a novel approach that could be useful in identifying important epigenetic regulators of proliferation in ageing models. However, only 1 out of 8 candidates tested showed increased proliferation when knocked down in isolation, which indicates a high number of false positives. This could arise due to a number of technical reasons, for example, the MOI was low in order to prevent the transduction of multiple types of shRNAs into a single cell, but the low MOI combined with a limited cell number resulted in an estimated 50 copies of each type of shRNA in the cell population. At a low copy number, intra-library differences in transduction efficiency, shRNA drop out or various cell culture-related changes could falsely inflate the enrichment of some shRNAs [277]. Scaling up the number of MSCs or developing a more robust statistical model may overcome this issue. Another potential cause of false positives is the lentiviral insertional mutagenesis, which can disrupt tumour suppressor genes and increase the proliferation of the host cells independent

from the functions of the shRNAs [278]. However, given that less than 2% of the human genome contains exons and far less of the genome contains proto-oncogene [279], the probability that a shRNA candidate was enriched due to insertional mutagenesis over 4 – 5 replicates is very low.

Alternatively, the 7 out of 8 candidates may not be false positives, rather, it may require the knockdown of a combination of epigenetic regulators to induce the proliferation of *in vitro* aged MSCs. The highest increase in proliferation was achieved via the treatment with the sub-pool that included all 8 candidates, indicating that there may be a synergy by targeting a combination of epigenetic regulators. A similar concept was established with the Yamanaka factors [16]. Furthermore, numerous interactions between the 22 identified epigenetic regulators were found (Supplementary figure S3). For example, EZH2 forms a corepressor complex with HDAC2 and MTF2 [280, 281]. In mice, MTF2 knockdown alone increased the self-renewal of ES cells by decreasing H3K27me3 at specific sites [282]. However, in humans, there may be additional regulators to limit proliferation. Indeed, HDAC2 was shown in human cell lines to also interact with SIN3 to inhibit cells growth [283]. Overall, the result suggests that shRNA-seq could be a novel method to identify epigenetic regulators of MSC ageing and proliferation, however, further validation is required. Potentially, a CRISPR/cas9 knock out library could be used to significantly reduce library complexity, and prevent possible random integration into tumour suppressor sites [284].

6 High-resolution RNA-seq time-course identifies differential gene expression in response to osteogenic induction with age

6.1 Introduction

6.1.1 Gene expression change during osteogenesis

Osteoblast differentiation consists of pre-osteoblast commitment, maturation and matrix mineralisation, marked by the expression of specific genes at different stages [285, 286]. The Runt-related transcription factor 2 (RUNX2) is an essential master regulator for osteoblast differentiation [287]. It is also known as core-binding factor subunit alpha-1 (CBFα1), as it is the α subunit of a heterodimeric transcription factor complex [288]. Two other α subunit genes have been identified – *RUNX1* and *RUNX3*, which were shown to regulate haematopoiesis and repress tumour formation in gastric cancer, respectively [289, 290]. Recently, RUNX3 was shown to have an emerging role in chondrocyte maturation [291]. The binding partner of RUNX proteins is core-binding factor subunit β (CBFβ). Together they form the basic transcription factor complex to regulate target gene expression [287]. Other co-factors CBFα1/ CBFβ interact with include c-Fos, C-Jun, HDAC3, and SMAD1/3 [292-296].

RUNX2 is crucial for osteoblast differentiation. In mice, *RUNX2* knockout completely arrests osteoblast differentiation and inhibits both endochondral and intra-membranous bone formation [297]. In humans, heterozygous mutations in *RUNX2* results in cleidocranial dysplasia, characterised by the poorly developed or absence of shoulder and cranial bones [298]. CBFβ is also needed for osteoblast differentiation, as post-natal knockout of *CBFβ* results in the retardation of osteoblast differentiation and bone formation [299, 300]. However, the loss of bone formation by *CBFβ* knockout is less severe than in *RUNX2* knockout mice, suggesting that *RUNX2* may be able to regulate bone formation independent of CBFβ, possibly through interacting with the other binding partners previously mentioned.

The upregulation of RUNX2 in MSCs is thought to signal the commitment towards osteoblast/chondrocyte fate [286]. These RUNX2+ cells are commonly referred to as osteoblast progenitors or pre-osteoblasts. One of the key inducers of *RUNX2* expression is the canonical WNT pathway. CTNNB1/TCF7 was shown to bind directly to the promoter of *RUNX2* gene [61], as well as forming an enhanceosome with DLX5/6, SP7, SOX5/6 and SMAD1 to promote the expression of *RUNX2* [301]. However, the expression of *RUNX2* is not completely dependent on WNT, as the conditional knockout of *CTNNB1* does not abolish *RUNX2* expression [232, 302]. Indeed, *RUNX2* expression is also regulated by IHH/SHH. In mice, *IHH* knockout results in the absence of *RUNX2* expression, and the complete loss of osteoblasts, indicating that IHH is needed for *RUNX2* expression and osteoblast differentiation [[303, 304]]. However, the dependency on IHH is transient, as conditional knockout of *IHH* after the presence of RUNX2+ osteoblast progenitors does not impair later *RUNX2* expression or the maturation of the progenitor cells into osteoblasts [305]. On the other hand, canonical WNT signalling is required after the stage of MSC to RUNX2+ preosteoblasts. With conditional knockout of *CTNNB1*, RUNX2+ osteoblast progenitors differentiate into chondrocytes instead. Later, it was found that canonical WNT signalling inhibits chondrocytes differentiation and direct MSCs towards osteoblast fate through direct the interaction and inhibition of *SOX9* gene expression [232, 303, 306].

RUNX2 promotes the expression of several key genes to facilitate the transition from RUNX2+ osteoblast progenitor to mature osteoblasts, including *SP7*, *COLA1*, *IBSP*, *OPN* (*SPP1*), *OCN* (*BGLAP*) and *ALP* (*ALPL*) [307]. SP7 is a transcription factor, and as previously stated, it can complex with TCF7/CTNNB1 to promote gene expression. Therefore, it is not surprising that *SP7* knockout results in chondrocyte formation instead of osteoblasts and suggests that *SP7* has a similar role as the canonical WNT pathway in inhibition of chondrocyte differentiation [308]. ALP, COLA1, IBSP, OPN (SPP1), and OCN (BGLAP) are secreted proteins required

for bone matrix mineralisation and mutations in any of these genes are often associated with osteogenesis imperfecta type I-IV [309-312]. Collagen Type I Alpha 1 Chain (COL1A1) is required for the formation of collagen fibrils in the extracellular matrix. Alkaline phosphatase (ALP) is also secreted to the extracellular matrix by binding to the membrane of the matrix vesicle, where it breaks down inorganic phosphate (ppi) to phosphate ions (pi) (at pH8 - 10). Pi is then incorporated into the hydroxyapatite crystal ($CaPO_4$) for its elongation and deposition into the collagen fibrils. Integrin Binding Sialoprotein (IBSP) or Bone Sialoprotein, binds tightly to the hydroxyapatite, and it appears to form an integral part of the mineralized matrix [313]. Similarly, Secreted Phosphoprotein 1 (SPP1), also known as Osteopontin, and Bone Gamma-Carboxyglutamate Protein (BGLAP) or Osteocalcin, binds to calcium and hydroxyapatite and also forms an integral part of the mineralised bone matrix [314]. Given their important roles in bone matrix mineralisation, and high bone tissue specificity, these proteins are most frequently used as markers for osteoblast differentiation [315]. However, it is unclear whether osteoblast maturation and matrix mineralisation occur simultaneously or sequentially, as mature osteoblast are functionally defined by the expression of these bone matrix mineralisation markers.

6.1.2 Lineage fate decision between osteoblast and chondrocyte differentiation

Sex-determining region Y-box 9 (SOX9) plays a pivotal role in the fate decision of MSCs towards chondrogenesis [316]. Loss of function mutation in *SOX9* causes campomelic dysplasia, characterised by impaired cartilage formation [317]. SOX9 regulates the expression of *SOX5* and *SOX6*, as *SOX9* knockout mice showed no expression of *SOX5/6* [318]. These two genes are also transcription factors important to cartilage formation, as *SOX5/6* double-knockout mice show severely impaired cartilage development [319]. SOX5/6/9 play an important role in regulating the expression of *collagen Type II Alpha 1 Chain* (*COL2A1*),

Collagen Type I Alpha 2 Chain (*COL1A2*) and *Aggrecan* (*CD151*), which code for important extracellular matrix proteins required for the formation and proper functions of the cartilage [320].

As mentioned previously, *SOX9* expression is inhibited by WNT during osteoblast differentiation [306]. Interestingly, SOX9 also inhibits canonical WNT signalling through direct interaction with β-catenin to promote its phosphorylation and its subsequent degradation [321]. Similarly, at the early stage of chondrocyte differentiation (pre-hypertrophic), RUNX2 inhibits chondrocyte maturation [322] by inhibiting the expression of *SOX9* [323]. However, RUNX2 is still weakly expressed during early chondrogenesis [324]. SOX9 prevents the accumulation of RUNX2 by directly binding to its Runt domain [325] and mediating its degradation [323]. Later during chondrogenesis (hypertrophic), *RUNX2* is highly upregulated to promote *COL10a1* expression and chondrocyte maturation [322].

6.1.3 Lineage fate decision between osteoblast and adipocyte differentiation

For directing MSCs towards adipogenic fate, Peroxisome proliferator-activated receptor gamma (PPARG) is amongst the most important and widely studied transcription factors [326]. *In vitro*, knockdown of *PPARG* in MSCs inhibits the formation of adipocytes. PPARG cooperates with another essential adipogenic transcription factor, C/EBPα. They mutually induce the expression of each other [327] and share a high degree of overlap in their target gene promoter binding sites [328]. The co-localisation of the two transcription factors were shown to be important in chromatin remodelling and synergistic activation or repression of the bound adipogenic genes. The transactivation of *PPARG* by a chemical agonist thiazolidinedione resulted in increased blood concentrations of adiponectin (ADIPOQ) – a hormone that regulates glucose and fatty acid metabolism during adipogenesis [329], and decreased blood

concentration of interleukin-6 (IL-6), which was linked to the reduction of subcutaneous adipogenesis in patients with type 2 diabetes [330]. PPARG also promotes the expression of fatty acid synthase (*FASN*) [331], lipoprotein lipase (*LPL*), and fatty acid-binding protein (*FABP4*) [332]. In addition to their role in promoting adipocyte differentiation, these proteins are specifically expressed in adipocytes and myeloid cells [333], therefore are used as markers for adipocyte formation.

During osteoblast differentiation, canonical WNT signalling inhibits *PPARG* expression and inhibit its post-translation activity through direct binding with β-catenin/TCF complex [245]. Conversely, transactivation of PPARG induced the proteasomal degradation of β-catenin in a GSK3B-dependent manner [243]. Therefore, similar to RUNX2 and SOX9, RUNX2 and PPARG also have a reciprocal control of the expression and activity of each other [334].

6.2 Aims

The competition between RUNX2, PPARG and SOX9 clearly plays a major role in lineage commitment and maturation of osteoblasts, but these regulators are not the only mediators of lineage decision. High-resolution time courses examining transcriptional differences between young and old MSCs during osteogenic differentiation may offer insight, and potential intervention targets, into impaired osteogenesis with age.

This chapter aims to identify differences in gene expression between young and old MSCs in response to osteogenic induction using high time resolution RNA-seq.

6.3 Results

6.3.1 High-resolution RNA-seq time-course for osteogenesis

To identify differences in gene expression in response to osteogenic induction between young and old donor MSCs, RNA-seq osteogenesis time-course experiments were carried out (young donors n=6, old donors n=6). The high resolution time-course consist of 17 time points, where RNA samples were collected at 0, 0.5, 1, 2, 4, 6, 8, 12, 16, 24, 48, 72, 96, 120, 168, 336 and 504 hrs post-initiation of osteoblast differentiation with dexamethasone (dex; Figure 6-1). In a PCA plot, young and old donors are shown in red and black, respectively (Figure 6-2-A). In PC1, dex treated samples showed a continuous and consistent shift from early (transparent) towards later (opaque) time points. This trend was not seen in DMEM control samples (supplementary figure S7), indicating that the gene expression change was induced by osteogenic treatment. PC2 showed a separation of young and old donors. The top 100 genes that represent the variability between samples in PC1 were enriched (FDR<0.05) in extracellular structure organisation, skeletal system development and bone growth processes, while the top 100 genes that represent the variability between samples in PC2 were enriched (FDR<0.05) in angiogenesis and cell proliferation-related processes (Figure 6-2-B). The transcriptomic data reflected both continuous changes in gene expression during osteogenesis, and a distinct difference between the two age groups.

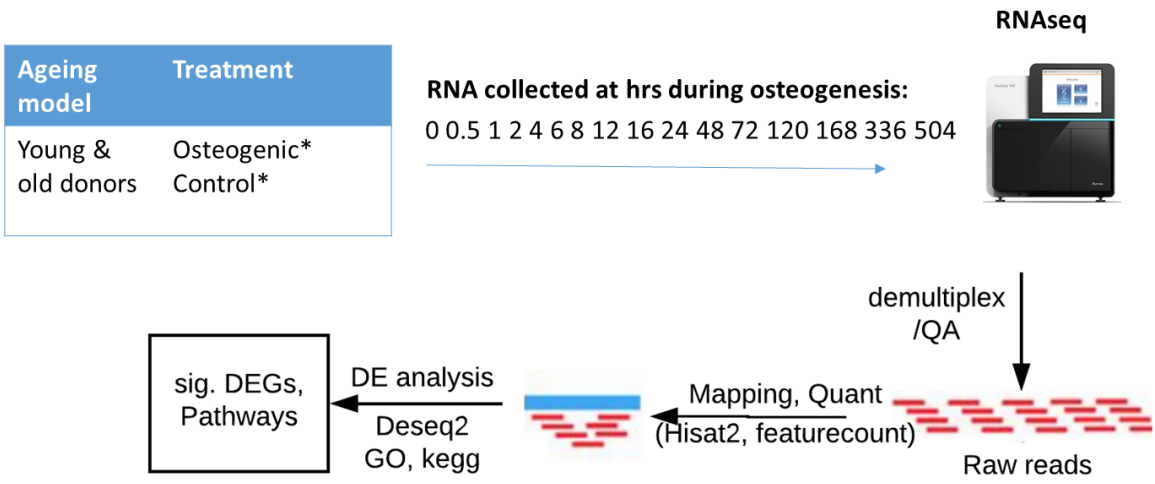
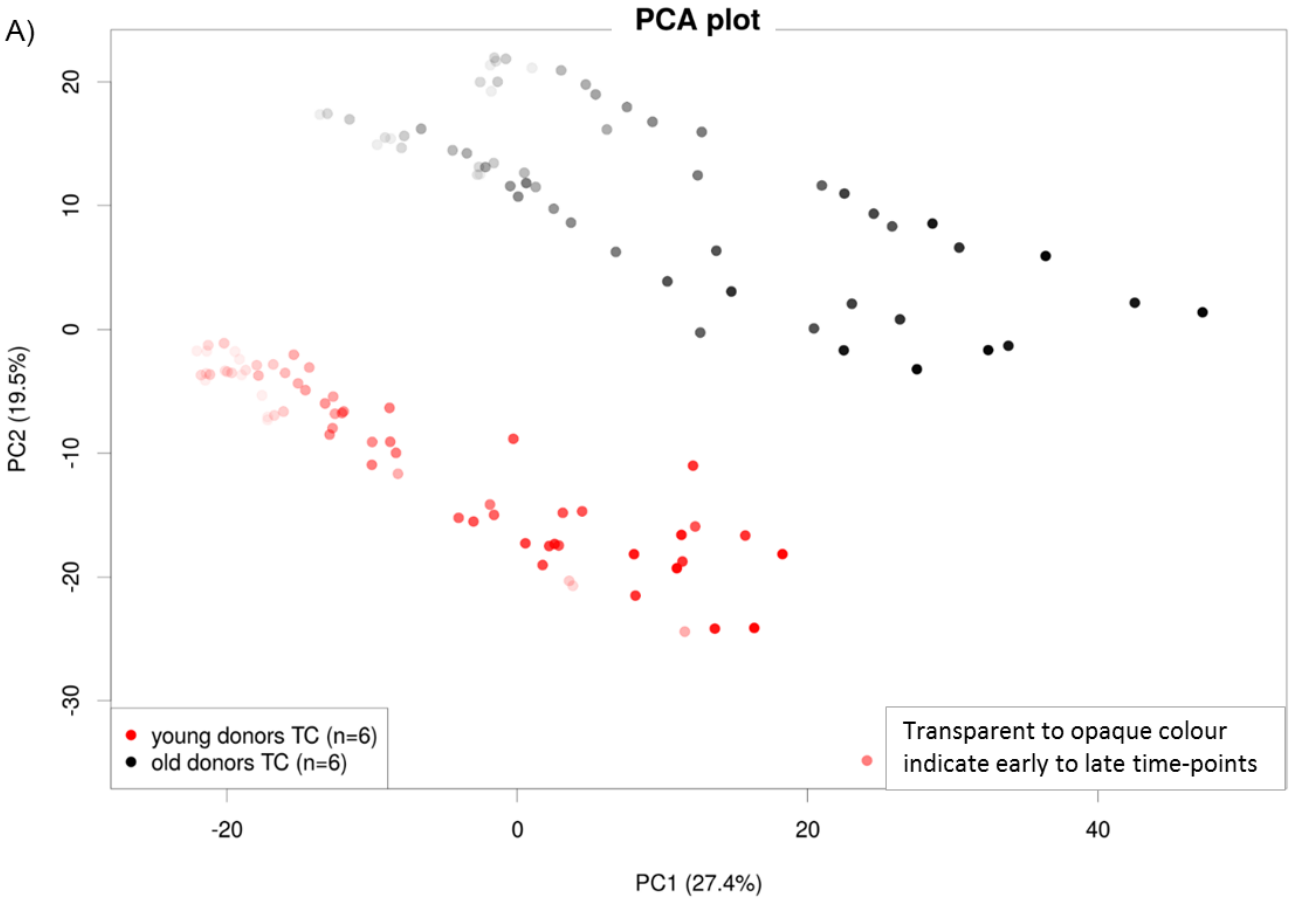


Figure 6-1 ***Overview of RNA-seq time course during osteogenesis.*** *MSCs from young donors (n=6, 20 – 29 years) and old donors (n=6, 62 – 87 years) were treated with osteogenic or control media. RNA samples were collected and sequenced at 0, 0.5, 1, 2, 4, 6, 8, 12, 16, 24, 48, 72, 96, 120, 168, 336 and 504 hrs during osteoblast differentiation. Mapping, quantification and differential gene expression analysis were carried out using HiSat2, featureCount and Deseq2. Control media: MesenPro and DMEM. Osteogenic media: 10nM Dex, 50ug/ml ascorbic acid, 10nM β-Glycerophosphate in DMEM.*

A)



B) PC1:

GO Biological process	FDR
Extracellular matrix organization	3.56E-13
Skeletal system development	5.02E-04
Bone growth	7.73E-04

PC2:

GO Biological process	FDR
Angiogenesis	1.27E-05
Cell proliferation	2.83E-04
Skeletal system development	3.00E-04

Figure 6-2 ***Transcriptomic changes in old vs young donor MSCs during osteogenesis. A)*** *PCA of RNA-seq time-course data showing the variability in gene expression between samples. Young donors (n = 6, 20 – 29 years) and old donors (n = 6, 62 – 87 years). Transparent to opaque indicate early (0 hr) to late (504 hr) time points.* ***B)*** *GO terms of the enriched processes in the top 100 genes that represent the variability between samples in PC1 and PC2 (Fisher's exact test, sig at FDR < 0.05).*

6.3.2 Change in lineage commitment of MSCs with age

To investigate whether MSC ageing has resulted in an altered expression profile of lineage commitment genes during osteogenesis, the expression of osteogenic, adipogenic and chondrogenic markers were examined (Figure 6-3-A). The heatmap shows the fold change (normalised to 0 hr) in gene expression of the two age groups. There was an increased expression of *ALP* between 168 – 504 hrs (14 – 21 days) in the young donors, but not in the old donors. *COL1A1*, *IBSP*, and *RUNX2* showed a similar pattern of expression in both age groups during the 21-day osteogenesis time course.

In the young donors, *PPARG* expression decreased 30 minutes after treatment with osteogenic media; whereas in the old donors, the expression of *PPARG* did not decrease until 8 hrs later. Additionally, there was less repression of *PPARG* expression in the old donor for the first 72 hrs. The expression of *CEBPA* coincided with the expression of *PPARG*. At the later time points (168 – 504 hrs), there was a higher increase in the expression of *ADIPOQ*, *FABP4* and *LPL* in the old donors.

SOX9 expression was repressed throughout the 21 days in the young donors. In the old donors, *SOX9* expression showed similar initial repression (0.5 – 24 hrs), however, its expression increased again between 48 – 504 hrs. The decrease in *SOX9* repression coincided with an elevated *SOX6* expression.

Adipocyte formation was examined in a sub-set of old (n = 3, 62 – 87 years) and young (n=3 20 – 29 years) donor MSCs at day 14 of osteogenic treatment. The formation of adipocytes was observed in 2 out of 3 old donor MSCs but was not seen in any of the young donors (Figure 6-3-B). This suggests that MSCs from old donors may be unable to fully commit towards osteoblast differentiation even upon osteogenic induction, and are diverted towards an adipogenic or chondrogenic fate.

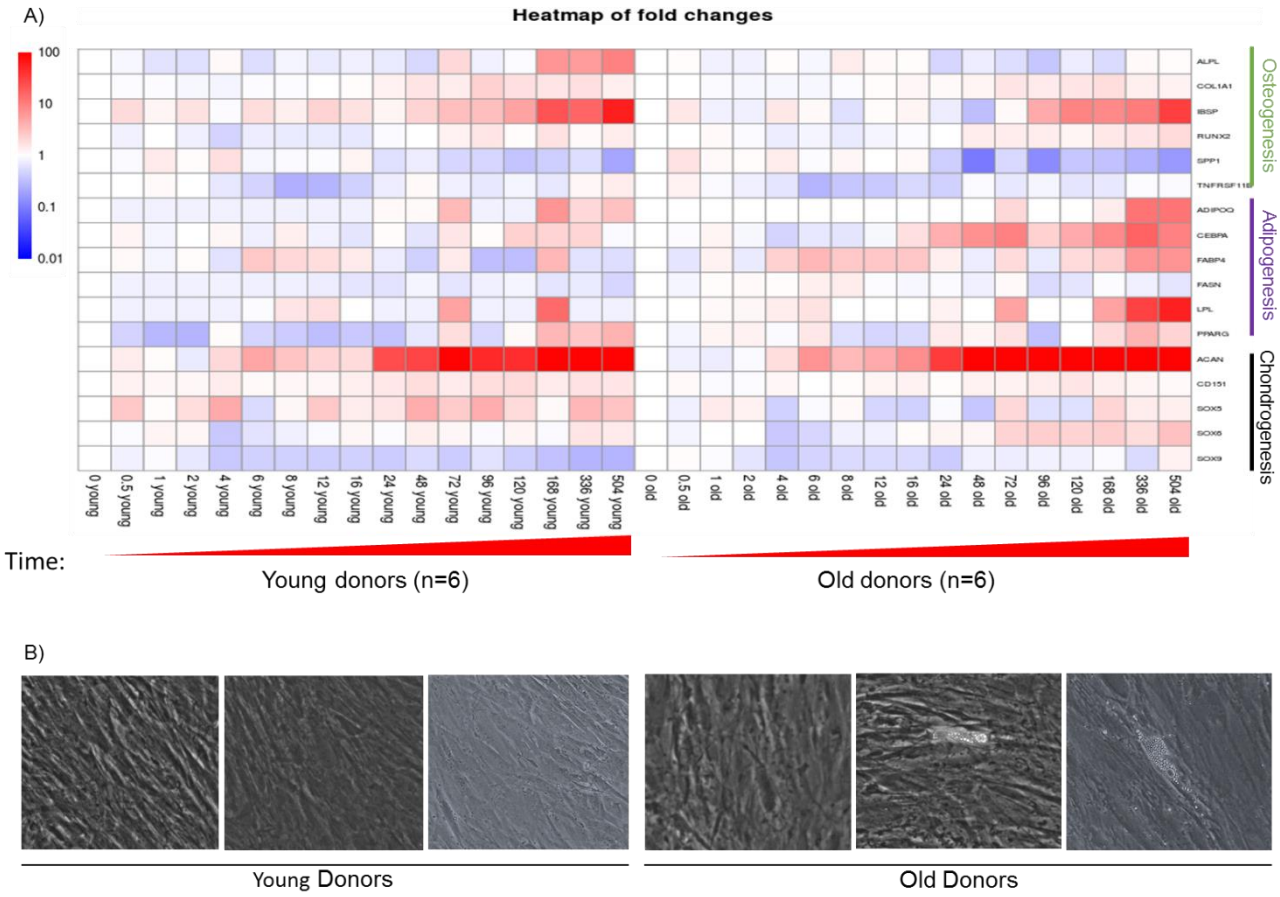


Figure 6-3 ***Lineage commitment of MSCs differ with age. A)*** *Heatmap of the FC (normalized to 0 hours) in gene expression of lineage markers of young donor (n=6, 20 – 29 years) and old donor (n=6, 62 – 87 years) MSCs during osteogenesis. Lineage panel consists of: osteogenesis (ALPL, COL1A1, IBSP, RUNX2, SPP1, TNFRSF1), adipogenesis (ADIPOQ, CEBPA, FABP4, FASN, LPL, PPARG) and chondrogenesis (ACAN, CD151, SOX5, SOX9) markers.* ***B)*** *50,000 young donor (n=3, 20 – 29 years) and old donor (n=3, 62 – 87 years) MSCs were seeded in 6 well plates and treated in osteogenic condition for 14 days, then visualised under a light microscope to identify the presence of adipocytes.*

6.3.3 Differentially expressed genes and gene networks

To identify novel genes that may contribute to the difference in osteogenic potential between young and old donor MSCs, differential gene expression analysis was carried out. 91 genes were found to respond significantly differently upon osteogenic induction comparing the two age groups (LRT test padj<0.05, post Benjamini-Hochberg correction) (Figure 6-4). Amongst the marker panel described previously, ALP expression was significantly decreased from day 7 onwards. To identify the relationship between the DEGs, gene network analysis was carried out with MetaCore. Top enriched gene networks amongst the DEGs were associated with β-catenin, JAK/STAT and PPARG pathways (Figure 6-5).

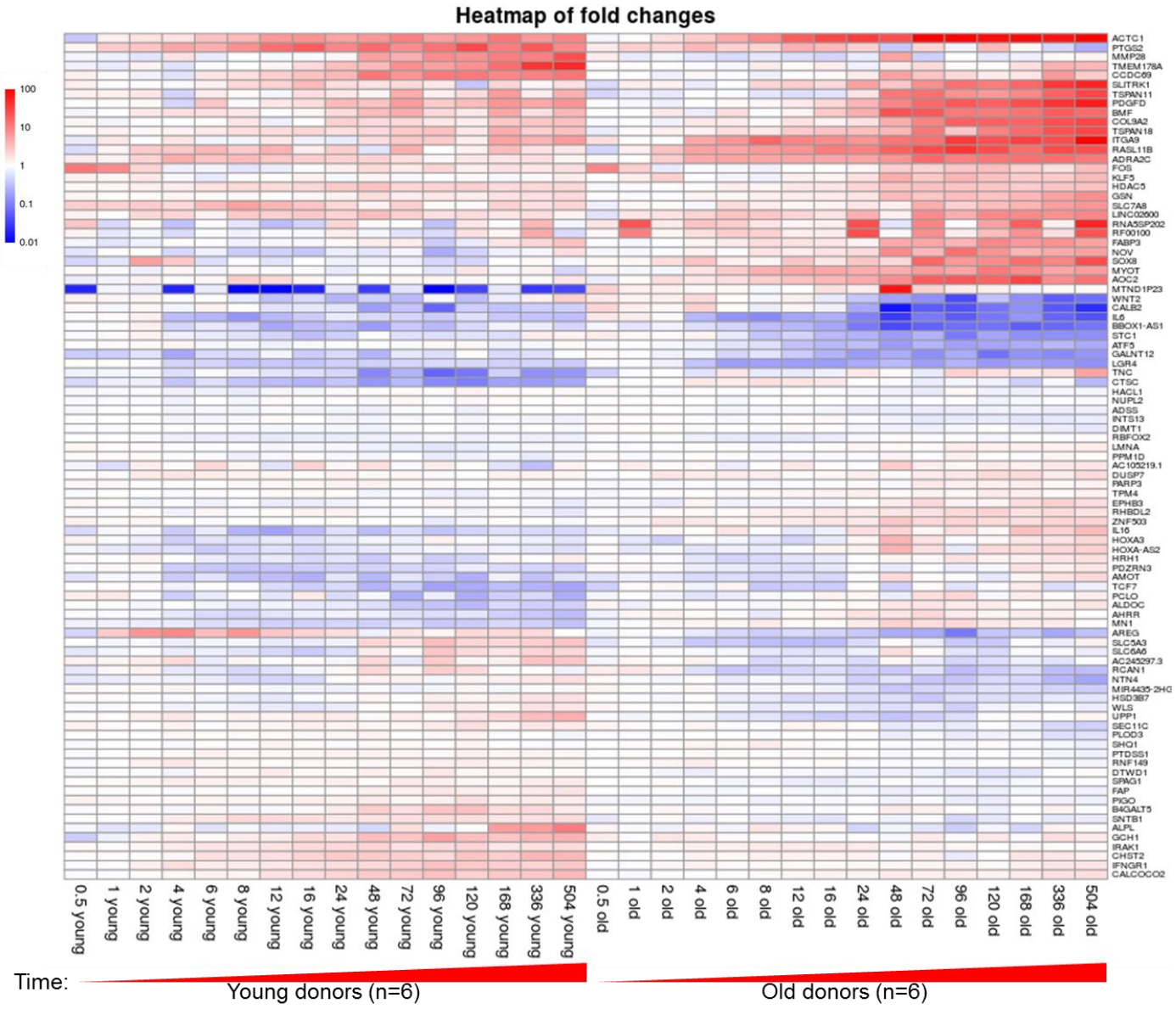
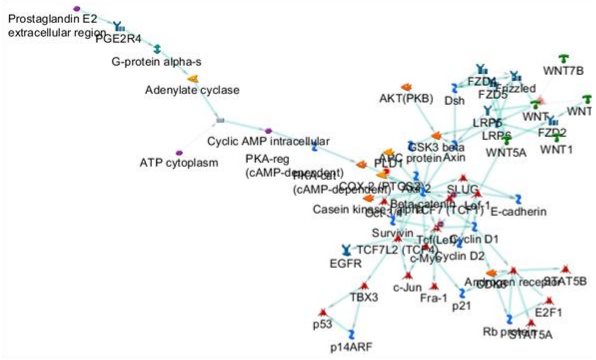
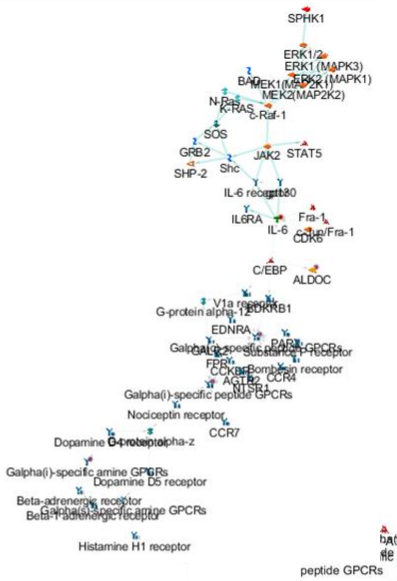


Figure 6-4 ***Differentially expressed genes in response to osteogenic condition with age.*** *Heatmap of the fold change (normalized to 0 hr) in gene expression (normalised counts) of DEGs (significant at padj < 0.05) of young and old donor MSCs during osteogenesis. The Deseq2 likelihood ratio test (LRT) was used to identify significant differences in gene expression between young and old age groups at any time point and to remove the difference between the two age groups at 0 hr. Therefore DEGs identified were genes that responded differentially to osteogenic condition due to donor age.*

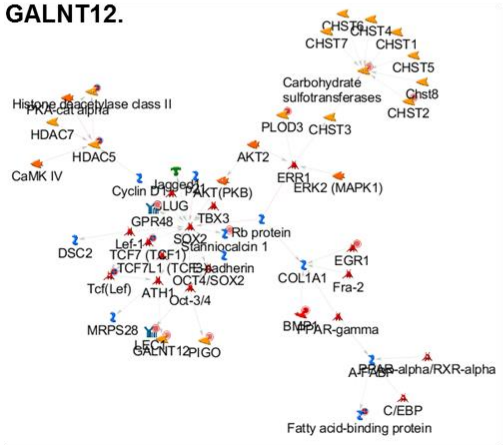
Tcf(Lef), WNT, TCF7 (TCF1), COX 2 (PTGS2), Beta catenin



IL 6, ALDOC, c Raf 1, Shc, JAK2.



HDAC5, Stanniocalcin 1, TCF7 (TCF1), GALNT12.



CPI 17, NOV, IFNGR1, MMP 28, ELOVL6.

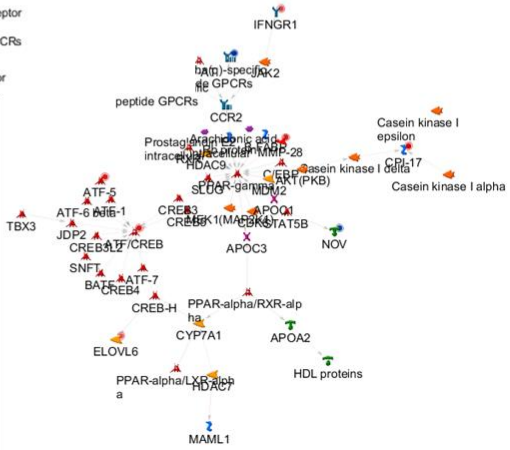


Figure 6-5 ***Enriched gene networks amongst the DEGs.*** *Gene network analysis was carried out with MetaCore using the 91 DEGs. Top 4 enriched gene networks are shown.*

6.3.4 Phases of change in gene expression during osteogenesis

Figure 6-6-A shows the correlation of gene expression (normalised counts) of all genes between different time points during osteogenesis. For both age groups, two major clusters of gene expression were observed, an "early" phase at 0 – 24 hrs, and a "late" phase at 48 – 504 hrs. This indicates that there was a major shift in genes expression at around 24hrs during osteogenesis. Additionally, at an individual donor level, a "very early" phase at 0 - 2 hrs was consistently observed (supplementary figure S4). However, this was not seen when the donors were grouped together by age.

Correlograms were also plotted for the DEGs (Figure 6-6-B). In the young donors, the DEGs followed the same two phases of change in gene expression at the "early" (0 – 24 hrs) and "late" (48 – 504 hrs) time points during osteogenesis. However, in the old donors, a shift between the two phases of gene expression was not observed amongst the DEGs.

To identify the genes that may be responsible for the lack of transition in gene expression between "early" and "late" phases during osteogenesis in the old donor MSCs, the different expression profiles of the DEGs were separated using unsupervised k-means clustering. 5 different expression profiles with respect to time were plotted, and the number of DEGs clustered into each profile is shown in Figure 6-7. In the young donors, cluster 1 showed a profile of "early rise and fall", where there was an upregulated gene expression between 1 - 24 hrs, followed by a downregulated gene expression from 48 hrs onwards. This profile of gene expression was not present in the old donor DEGs. There are five genes in cluster 1 of the young donors: *AREG, ADRA2C, LINC02600, RASL11B and SLC7A8.* In the old donors, *SLC7A8, RASL11B, ADRA2C* and *LINC02600* were upregulated at a later time point in cluster 1, 2 or 3, and *AREG* was downregulated during the osteogenesis time course in cluster 5 (Table 6-1, individual expression profiles of the five cluster 1 DEGs in both age groups are provided in supplementary figure S5).

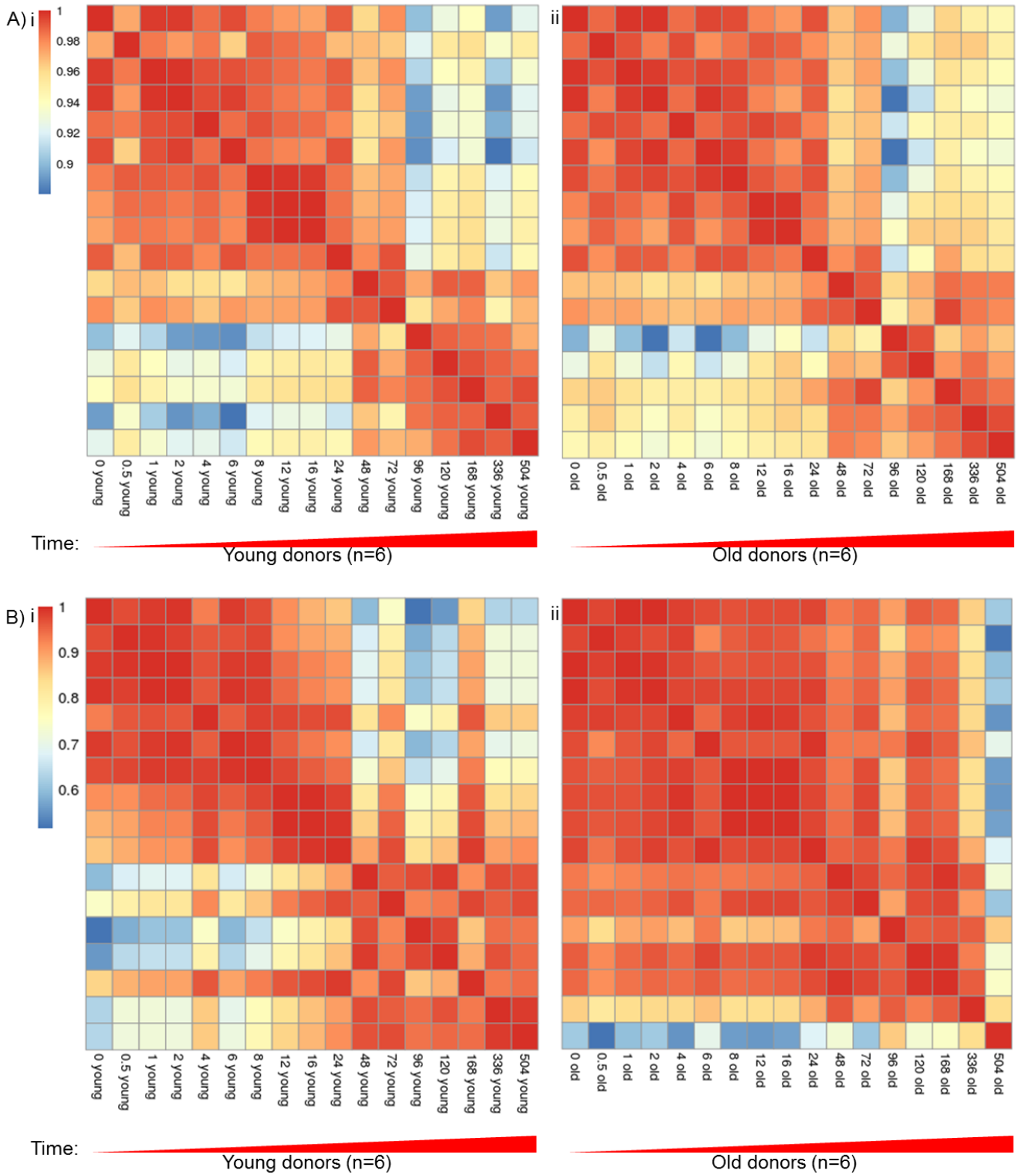


Figure 6-6 ***Phases of change in gene expression during osteogenesis. A)*** *Heatmap of the correlation of gene expression (normalised counts) between different time points during osteogenesis, in the i) young donors and ii) old donors. Red to blue indicate decreasing correlation.* ***B)*** *Heatmap of the correlation of the DEGs between different time points during osteogenesis, in the i) young donors, and ii) old donors. Red to blue indicate decreasing correlation.*

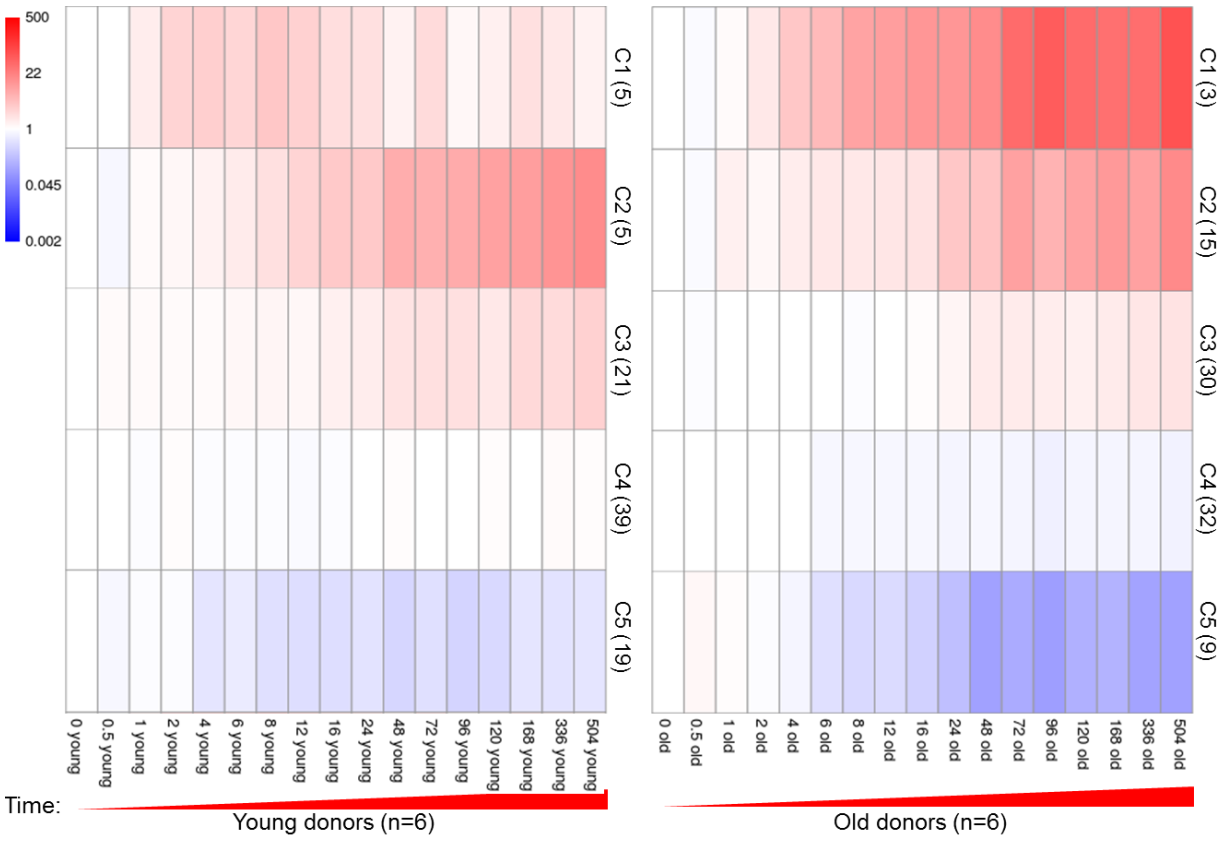


Figure 6-7 ***Different profiles of DEGs during osteogenesis.*** *DEGs were clustered into different expression profiles using unsupervised k-means clustering. Red indicates an increase in FC (vs 0 hr), and blue indicates a decrease in FC. C = cluster number, and the number of genes within a cluster is bracketed.*

Gene symbol	Gene name	Young donors	Old donors
ADRA2C	Alpha-2-adrenergic receptor	Cluster 1	Cluster 2
AREG	Amphiregulin	Cluster 1	Cluster 5
LINC02600	Long Intergenic Non-Protein Coding RNA 2600	Cluster 1	Cluster 2
RASL11B	RAS-Like Family 11 Member B	Cluster 1	Cluster 1
SLC7A8	Solute Carrier Family 7 Member 8	Cluster 1	Cluster 3

Table 6-1 ***Transiently upregulated DEGs between 1 – 24 hrs during osteogenesis.***

6.3.5 Differentially expressed canonical WNT pathway genes during osteogenesis

In both undifferentiated MSCs (detailed in chapter 4) and MSCs during osteoblast differentiation, the canonical WNT pathway was amongst the most significantly altered with donor ageing. Therefore, the differences in the canonical pathway gene expression between the two age groups were examined in more detail. During osteogenesis, 78 canonical WNT pathway genes were differentially expressed (All time points vs 0 irrespective of age, Wald test, sig at padj<0.05 post Benjamini-Hochberg correction). In the young donors, the correlogram of the 78 WNT pathway DEGs showed three phases of gene expression at 0 – 2 hrs, 4 – 24 hrs and 48 – 504 hrs (Figure 6-8), similar to the phases of transcriptomics changes during osteogenesis detailed in section 6.3.4. In the old donors, the transition in gene expression between 24 and 48 hrs was less distinct, only two phases of genes expression at 0 – 2 hrs and 4 – 504 hrs were observed.

Several key WNT pathway genes were differentially expressed during osteoblast differentiation (Figure 6-9-A), including *RUNX2*, *CTNNB1*, and *GSK3B*. *GSK3B* was significantly downregulated between 8 – 24 hrs during osteogenesis in the young donors. In the old donors, *GSK3B* expression was not significantly downregulated at any time point. *CTNNB1* was significantly upregulated between 6 – 501 hrs in both young and old donors, indicating the importance of β-catenin during osteogenesis. However, there was a 1.25 to 1.5 fold lower expression of *CTNNB1* between 0 – 48 hrs in the old donors compared to the young donors (Figure 6-9-B).

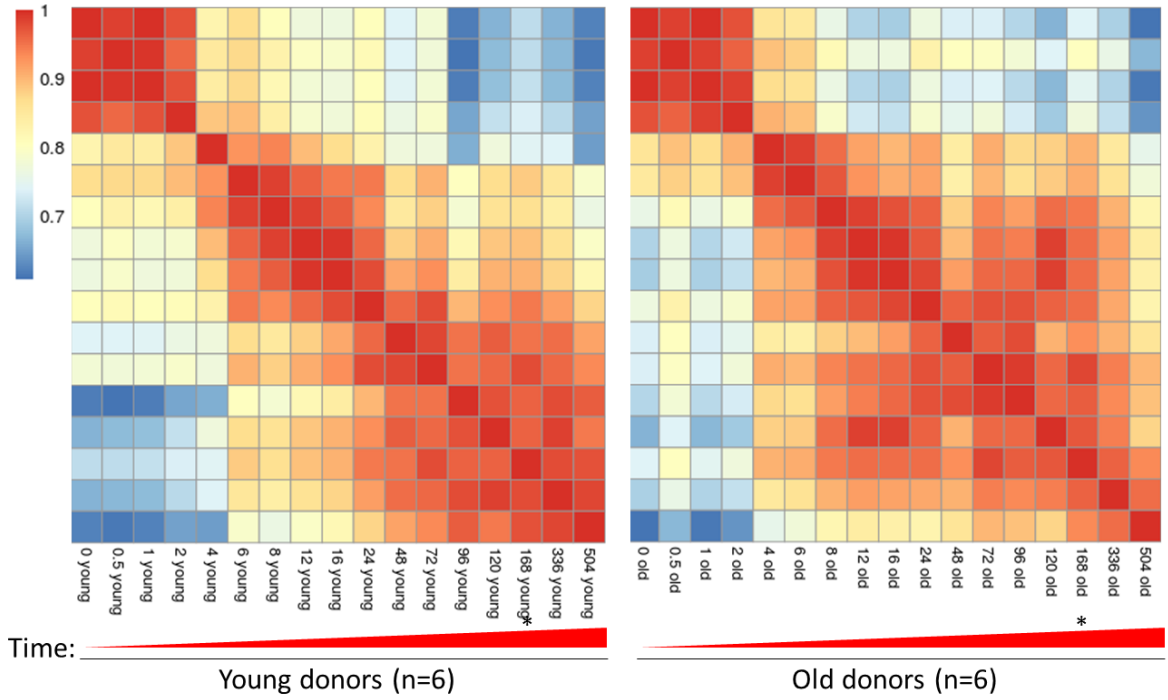
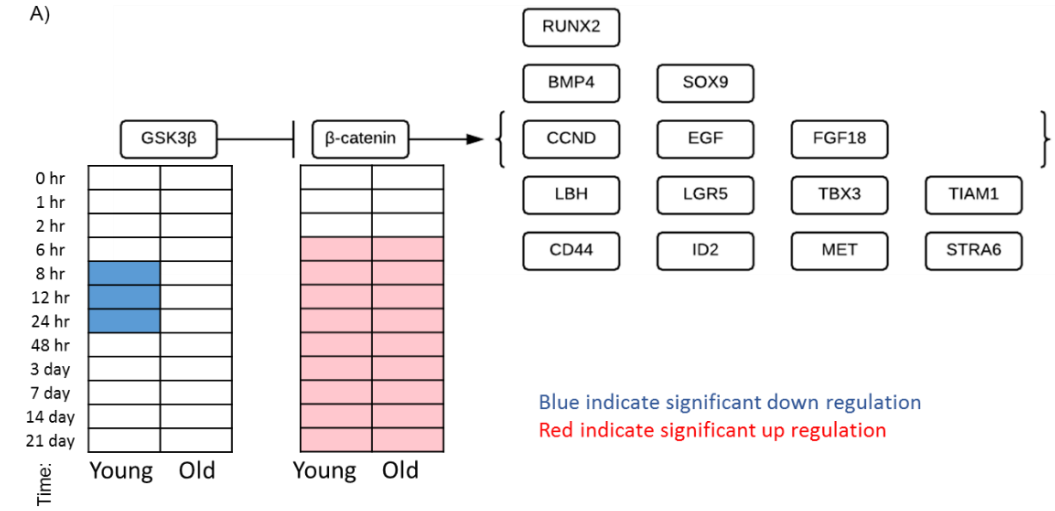
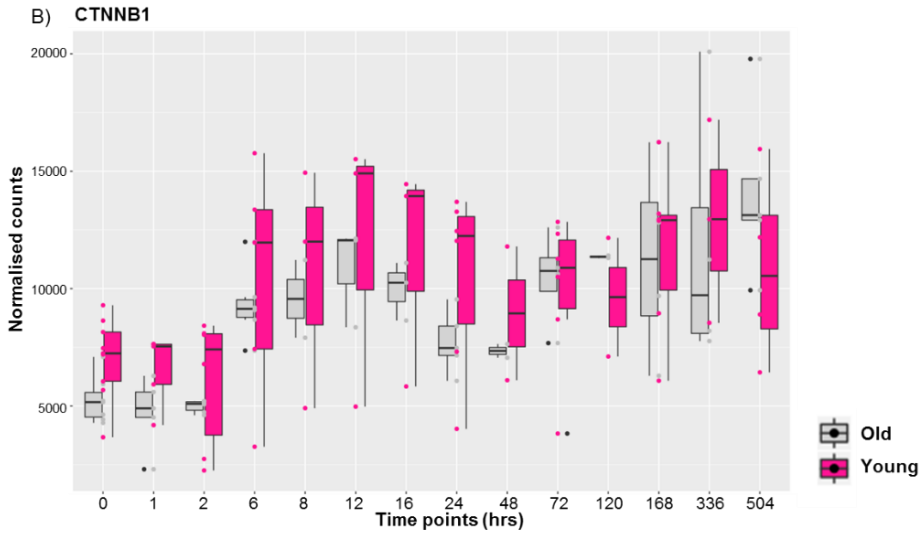


Figure 6-8 ***Differentially expressed Canonical WNT pathway genes during osteogenesis. A)*** *Heatmap of the correlation of the normalised counts of the Wnt pathway DEGs between different timepoints during osteogenesis, in the i) young donors and ii) old donors. Red to blue indicate decreasing correlation.*


A)
RUNX2
BMP4
SOX9
GSK3β
β-catenin
CCND
EGF
FGF18
LBH
LGR5
TBX3
TIAM1
CD44
ID2
MET
STRA6
0 hr
1 hr
2 hr
6 hr
8 hr
12 hr
24 hr
48 hr
3 day
7 day
14 day
21 day
Time:
Young
Old
Young
Old
Blue indicate significant down regulation
Red indicate significant up regulation


B)
CTNNB1
Normalised counts
20000
15000
10000
5000
0
1
2
6
8
12
16
24
48
72
120
168
336
504
Time points (hrs)
Old
Young

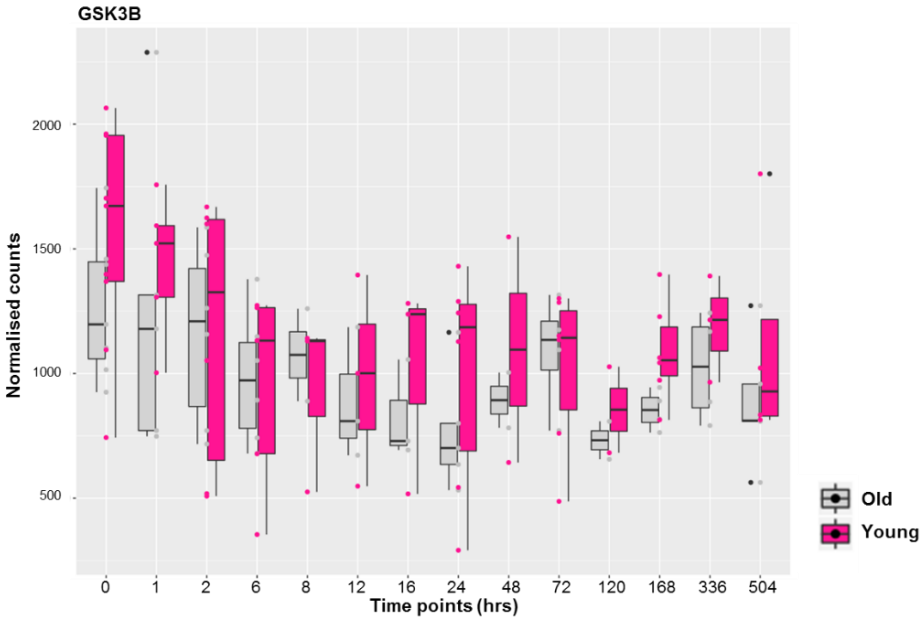

GSK3B
Normalised counts
2000
1500
1000
500
0
1
2
6
8
12
16
24
48
72
120
168
336
504
Time points (hrs)
Old
Young

Figure 6-9 ***Important canonical WNT pathway genes during osteogenesis. A)*** *Red indicates significantly upregulated expression (vs 0 hr), and blue indicates significantly downregulated expression (vs 0 hr) for important Wnt pathway DEGs during osteogenesis.* ***B)*** *Boxplot of the normalised counts of β-catenin (CTNNB1) and GSK3B expression during osteogenesis. Old donors are shown in grey, and young donors are shown in red.*

6.4 Discussion

6.4.1 WNT misregulation resulted in the decline of osteoblast differentiation

As outlined in the chapter introduction, lineage differentiation of MSCs is tightly regulated and fine-tuned by the antagonistic relationship between the lineage regulators and a large number of signalling pathways involved. Therefore, any changes to the expression and activity of the regulators and pathways can disrupt the balance between the competing lineage fates. This chapter demonstrates that misregulation of the canonical WNT pathway may be one example of that. The canonical WNT is an important pathway for osteoblast differentiation [61, 232, 286, 303, 305, 306, 315]. This was evident by the large number (78/204) of the canonical WNT pathway genes that were differentially expressed during osteogenesis. The WNT pathway was also the most significantly altered pathway between the young and old donors. More specifically, in the old donors, *CTNNB1* was lower expressed throughout the first 14 days of osteoblast differentiation and *GSK3B* was less downregulated at 8 – 24 hrs of osteogenesis. This dysregulation of the canonical WNT pathway may have led to the changes in the expression of the lineage regulators. As discussed in the chapter introduction, during osteoblast differentiation, the WNT pathway promotes the expression of *RUNX2* and inhibits the expression of *PPARG* and *SOX9*. Although the transcriptomic data showed that the *RUNX2* expression was similar between the two age groups, normalised counts for *RUNX2* was low (~200), so it may be difficult to reliably detect small changes. On the other hand, *PPARG* expression was increased in the old donors, which may divert MSCs away from the osteogenic

fate and towards an adipogenic fate. Evidence suggesting that adipocyte differentiation occurred in the old donor MSCs during osteogenesis include the increased *ADIPOQ*, *CEBPA*, *FABP3*, *FABP4* and *LPL* expression at multiple time points, and the presence of adipocytes at day 14. Osteoprogenitors may be further diverted toward the chondrocyte fate due to the loss of the repression of *SOX9*. Simultaneous upregulation of *SOX6* and *SOX8* was also found. The overexpression of *SOX8* was recently found to be able to drive chondrocyte differentiation in the absence of *SOX9* [335]. These results suggest that the misregulation of the canonical WNT pathway during MSC ageing may be associated with an altered expression of the lineage regulators, leading to a decline in osteogenesis. The next chapter will examine whether the activation of the canonical WNT pathway could rescue the osteogenic potential of the old donor MSCs.

The misregulation of the WNT signalling pathway is unlikely to be the only cause for the decline of osteogenic potential. Gene network analysis found that genes related to JAK/STAT and PPARG pathways may also be significantly altered with age during osteoblast differentiation. In addition, post-transcriptional regulation also plays an important role in controlling lineage fate. FGF2 via the ERK pathway and cAMP via the ubiquitin-proteasome pathway both regulate the post-translational activity of RUNX2 [336]. Therefore, the lack of difference in the expression of *RUNX2* between the two age groups does not mean that RUNX2 activity could not differ. Further analysis of the expression of genes that post-transcriptionally regulate the key mediators of lineage fate may help better understand the cause of the age-related osteogenic decline.

6.4.2 Early phase DEGs during osteoblast differentiation

There were two major phases of gene expression during osteogenesis – an "early" phase between 1 – 24 hrs and a "late" phase between 48 – 504 hrs. In the young donors, five DEGs were transiently upregulated during the "early" phase of osteoblast differentiation. In contrast, in the old donors, these genes were either upregulated at a later time point (*SLC7A8*, *RASL11B*, *ADRA2C* and *LINC02600*) or were not upregulated at all (*AREG*). The differences in the timing and the expression of these five genes between the two age groups suggest that they may be important for the early initiation of osteogenesis or for the transition between the two phases. Amphiregulin (AREG) is a member of the EGF family ligand, able to interact with both EGF and TGF-α receptors. Recently, it was found that in mice, an osteoblast-specific overexpression of *AREG* resulted in a transient increase in the trabecular bone mass [337]. Conversely, *AREG* knockout mice showed significantly less trabecular bone formation [338]. In addition, parathyroid hormone (PTH) was shown to highly upregulate *AREG* expression, which indicates that AREG may mediate the bone anabolic effect of PTH [339]. Interestingly, *in vitro* assay showed that short term treatment (4 days) of AREG strongly stimulated the growth of pre-osteoblasts, however, long term treatment (20 days) inhibited the maturation and mineralisation of osteoblasts at the later stages [338]. This supports the idea that the transient upregulation of *AREG* at 1 – 24 hrs promoted the osteoblast differentiation in the young donors. Therefore, transient overexpression of *AREG* in the old donor MSCs may promote their osteogenic potential. In addition to PTH, *AREG* expression was also shown to be stimulated by 1α,25-dihydroxyvitamin D3 and prostaglandin E2 [338]. Therefore, there are many ways to increase *AREG* expression pharmacologically.

SLC7A8 is an amino acid transporter, also known as LAT2. It was found to be expressed in bone tissues and osteoblasts [340]. The role of SLC7A8 in osteoblast differentiation is unclear. However, its function to regulate influx-efflux of amino acids may be an important metabolic

requirement during the early phase of osteoblast differentiation [341]. RAS-Like Family 11 Member B (RASL11B) is a member of the small GTPase protein family with a high degree of similarity to RAS. RASL11b was implicated in the regulation of developmental processes and its expression is induced by TGF-β1 during monocyte-macrophage maturation [342, 343]. Alpha-2-adrenergic receptor (ADRA2C) is a member of the G protein-coupled receptor, which was shown to directly interact with RUNX2/CBFβ transcription factor complex [294]. Another member of the adrenergic receptor family member - *ADRB2* was shown to be upregulated by glucocorticoids and is involved in bone catabolism after long term glucocorticoid treatment. *LINC02600* is a long intergenic non-coding RNA with unknown function. As gene expression or protein expression during osteoblast differentiation are typically studied after 3 or 7 days after osteogenic treatment [315], these gene identified at the early time points may have important undiscovered roles in osteoblast differentiation. Further studies are needed to examine whether age-related misregulation of these "very early rise and fall" genes have contributed towards the impaired osteogenic potential in the old donor MSCs.

7 WNT activation restores the osteogenic potential of old donor MSCs

7.1 Introduction

7.1.1 Canonical WNT signalling pathway

The canonical WNT signalling pathway was first identified in Drosophila, and it is a highly conserved pathway in mammalian cells [344, 345]. The pathway centres on the regulation of β-catenin, promoting its degradation or translocation into the nucleus in the absence or presence of WNT activating ligands (Figure 7-1).

In the absence of WNT activating ligands, cytoplasmic β-catenin is phosphorylated by a destruction complex, which includes adenomatosis polyposis coli (APC), Axin, casein kinase 1 α (CK1α) and glycogen synthase kinase 3 (GSK3). Subsequently, E3-ligase protein (β-TrCP) promotes the ubiquitination of phosphorylated β-catenin, leading to its degradation by a 26s proteasome [346-348].

In the presence of WNT activating ligands, the WNT receptors Frizzled (FZD) and lipoprotein receptor-related protein 5/6 (LRP5/6) dimerises upon binding to the ligands [349]. The conformational change of the transmembrane receptor dimer recruits Axin, localising it to the plasma membrane and reducing the cytoplasmic concentration of Axin for the destruction complex. The receptor dimer also recruits CKI and GSK3B to promote the phosphorylation of Dishevelled (DVL) [350, 351]. Subsequently, phosphorylated DVL inhibits GSK3 activity and stabilises the cytoplasmic β-catenin. While, the mechanism of β-catenin translocation is unclear, once inside the nucleus, β-catenin binds with TCF/LEF to form the transcription regulation complex [352].

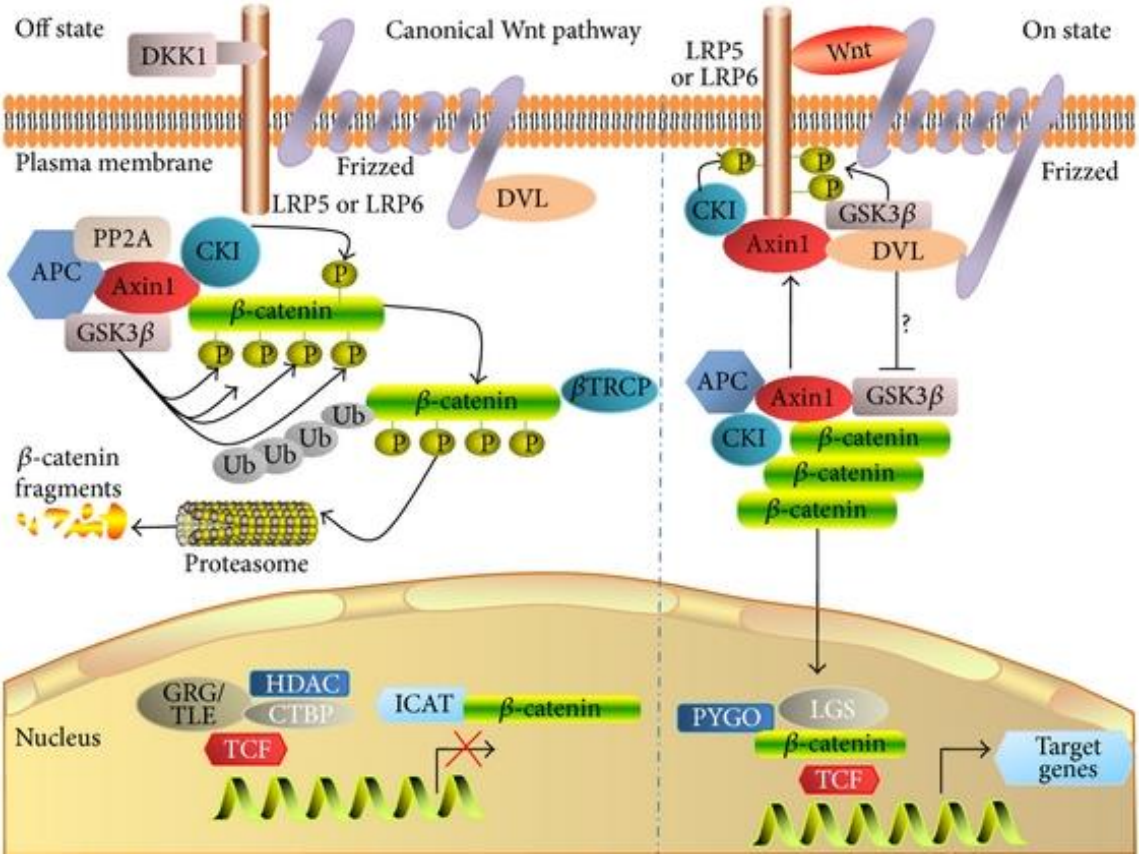


Figure 7-1 ***Canonical WNT signalling pathway****. Adapted from [353].*

WNTs are not the only ligands that bind to the FZD and LRP5/6 receptors. Other ligands can also inhibit WNT signalling through these receptors, most notably, DKK1 and SOST [354-356]. DKK1 is a secreted glycoprotein that directly competes with WNT ligands for the binding of LRP5/6 to inhibit its activity. *DKK1* knockout in mice is embryonic lethal, however, heterozygous mutants are viable and show increased bone formation [356]. Conversely, overexpression of *DKK1* results in a reduced number of osteoblasts and osteopenia. An anti-DKK1 antibody is currently under clinical trial for the treatment of RA and osteoporosis [355].

Sclerostin (SOST) is a secreted ligand that acts as a non-competitive inhibitor of LRP5/6 [356]. In humans, homozygous loss-of-function mutations in *SOST* result in sclerosteosis or Van Buchem disease. Both conditions share a similar phenotype that includes thickening of the

calvarium, leading to a potentially lethal increase of intracranial pressure. Carriers of heterozygous loss-of-function mutations in *SOST* have a 60% lower circulating SOST protein [357]. They also exhibit an increased bone mineral density but do not show any severe complications related to intracranial pressure.

Unlike *DKK1*, which is expressed in a number of tissues and cells, SOST is almost exclusively expressed in osteoclasts and osteocytes [354], making it an attractive candidate for therapeutic intervention. A recent phase III clinical trial showed that the inhibition of SOST by monoclonal antibodies (romosozumab) increased the bone mineral density and significantly decreased the risks of fractures in post-menopausal women with osteoporosis [358]. However, the treatment was also found to increase the risk of cardiovascular-related mortality, although the mechanism remains unclear.

GSK3 is a serine/threonine kinase that plays a critical role in the phosphorylation of β-catenin. GSK3 has two isoforms, GSK3A and GSK3B [359, 360]. They both have been found to be involved in the regulation of β-catenin and the WNT signalling pathway. However, *GSK3A* knockout mice are viable, whereas *GSK3B* knockout is embryonic lethal due to cardiac defects [361, 362], indicating the two isoforms may not have redundant roles. GSK3B is more often cited as the key player in the regulation of osteoblast differentiation. However, the differences between the two isoforms in regulating MSC fate have not been clearly examined.

GSK3 is one of the most targeted members of the pathway for activating WNT signalling. Currently, more than 30 small molecular inhibitors of GSK3 have been published [363]. These small molecules typically inhibit GSK3 activity through binding to the ATP-binding site of GSK3. For example, (2′Z,3′E)-6-Bromoindirubin-3′-oxime (BIO) inhibits both GSK3A and GSK3B through reversible competitive binding to the ATP-binding site. *In vitro*, BIO treatment in murine pre-osteoblasts was shown to increase osteoblast differentiation. Similar

results were found in human bone marrow MSCs of young donors, where increased ALP activity and matrix mineralisation was found in the BIO treated MSCs during osteoblast differentiation [360, 362]. However, a high dosage of BIO (>5uM) resulted in cell death. Additionally, there are small-molecule activators of WNT targeting other members of the pathway. Examples are shown in the table below (Table 7-1).

Compound	**IC50**	**Target**	**Effect on Target**	**Effect on signalling**
QS11	500 nM	ARFGAP1	Activates	Activates
DCA	63 nM	β -catenin	Activates	Activates
SB-216763	34 nM	GSK3	Inhibits	Activates
CHIR99021	10 nM	GSK3	Inhibits	Activates
BIO (6-bromoindirubin-3'-oxime)	5 nM	GSK3	Inhibits	Activates
meBIO (1-Methyl-6-bromo-indirubin-3'-oxime)	-	GSK3	Inactive control	Inactive control
LiCl	2000 nM	GSK3	Inhibits	Activates
IQ1	180 nM	PP2A	Activates	Activates
WAY-316606	500000 nM	SFRP	Inhibits	Activates
2-amino-4-[3,4-(methylenedioxy)benzyl-amino]-6-(3-methoxyphenyl)pyrimidine	-	unknown	Activates	Activates
(Hetero)arylpyrimidines	-	unknown	Activates	Activates

Table 7-1 ***Small molecule activators of the canonical WNT signalling pathway.***

7.1.2 WNT agonist for rescuing osteogenic potential of aged MSCs

Several studies demonstrated that WNT activation increased bone mineral density in age-related bone diseases, such as osteoporosis in post-menopausal women or patients with rheumatoid arthritis [354, 355, 357, 358, 360, 362, 364]. However, as shown in chapter 4 and chapter 6, with natural ageing, there is also a decline in the canonical WNT signalling activity and altered expression of genes involved in this pathway in non-differentiated MSCs and during osteogenesis. Several studies have been carried out in mice to examine whether canonical WNT signalling activation could restore the loss of osteogenic potential with age. Bone grafts from aged mice (>12 months) were treated with WNT3A *ex vivo* and transplanted into age match recipients. The treated old mice showed a significant increase in *RUNX2* and *SP7* expression compared to the control (PBS) treated old mice. In addition, the treated old mice showed a comparable *RUNX2* and *SP7* gene expression and bone mineral density to the young mice (3-4 months) [365-367]. Another study showed that transgenic mice overexpressing *WNT4* had significantly reduced trabecular bone loss at old age (12 – 24 month) compared to the WT. A significantly lower osteoclast number was found in the transgenic mice, but the osteoblast number was not reported. Furthermore, senescent osteopenic mice treated with a low dose (10 mg/kg per day) of parathyroid hormone (PTH) for 6 weeks showed increased axial bone volume and trabecular thickness [368]. This increase in bone formation is thought to be, at least partly, attributed to the canonical WNT pathway, as the MSCs and osteoblasts of the treated mice showed an increased expression of *WISP1*, which is primarily induced by the β-catenin dependent WNT pathway [368, 369]. Surprisingly, the effect of WNT activation on the osteogenic potential of MSCs from old donors has not been reported in humans.

7.2 Aims

This chapter aims to examine whether activation of the canonical WNT signalling could restore the osteogenic potential of old donor MSCs and to understand the mechanism by which canonical WNT signalling activation may have promoted osteogenesis.

7.3 Results

7.3.1 GSK3B inhibition rescues osteoblast differentiation

In chapter 6, it was hypothesised that the misregulation of the canonical WNT pathway during MSC ageing resulted in the decline of osteoblast differentiation, and that the activation of the canonical WNT pathway could rescue the osteogenic potential of the old donor MSCs. To investigate this, the GSK3 inhibitor compound BIO was used. The optimum concentration of BIO on MSCs (young donors n = 3) was determined to be between 1 – 2 µM based on ALP activity and cellular toxicity dosage response (supplementary figure S6). A LEF/TCF reporter assay confirmed a significant increase in the canonical WNT signalling activity 3 days post BIO treatment (1µM) (supplementary figure S5).

To investigate the effect of BIO treatment on the osteogenic potential of young and old donor MSCs, at day 0, 1 – 2 µM of BIO was added together with osteogenic media to the MSCs. At day 7, BIO was removed in the treated samples as prolonged treatment showed cellular toxicity. At day 10, the ALP assay showed that 1µM BIO treatment increased the ALP activity of the old donors to the level of the control young donors (young donors, n = 4, 20 – 29 years; old donors n = 4, 62 – 87 years) (Figure 7-2-A). Further increasing BIO concentration to 2µM significantly elevated the ALP activity of both young and old donors during osteogenesis (unpaired t-test, sig at $P<0.05$, young donors n = 5, 20 - 29 years, old donors n = 5, 62 – 87 years) (Figure 7-2-C). Additionally, at day 28, Alizarin Red staining showed that the old donors treated with BIO (2 µM) showed increased bone mineralisation compared to the control old donors without BIO (young donors n = 3, 20 - 29 years, old donors n = 3, 62 – 87 years) (Figure 7-2-C). However, BIO treatment (1 – 2µM) did not rescue the osteogenic potential of the late passage MSCs (supplementary figure S5).

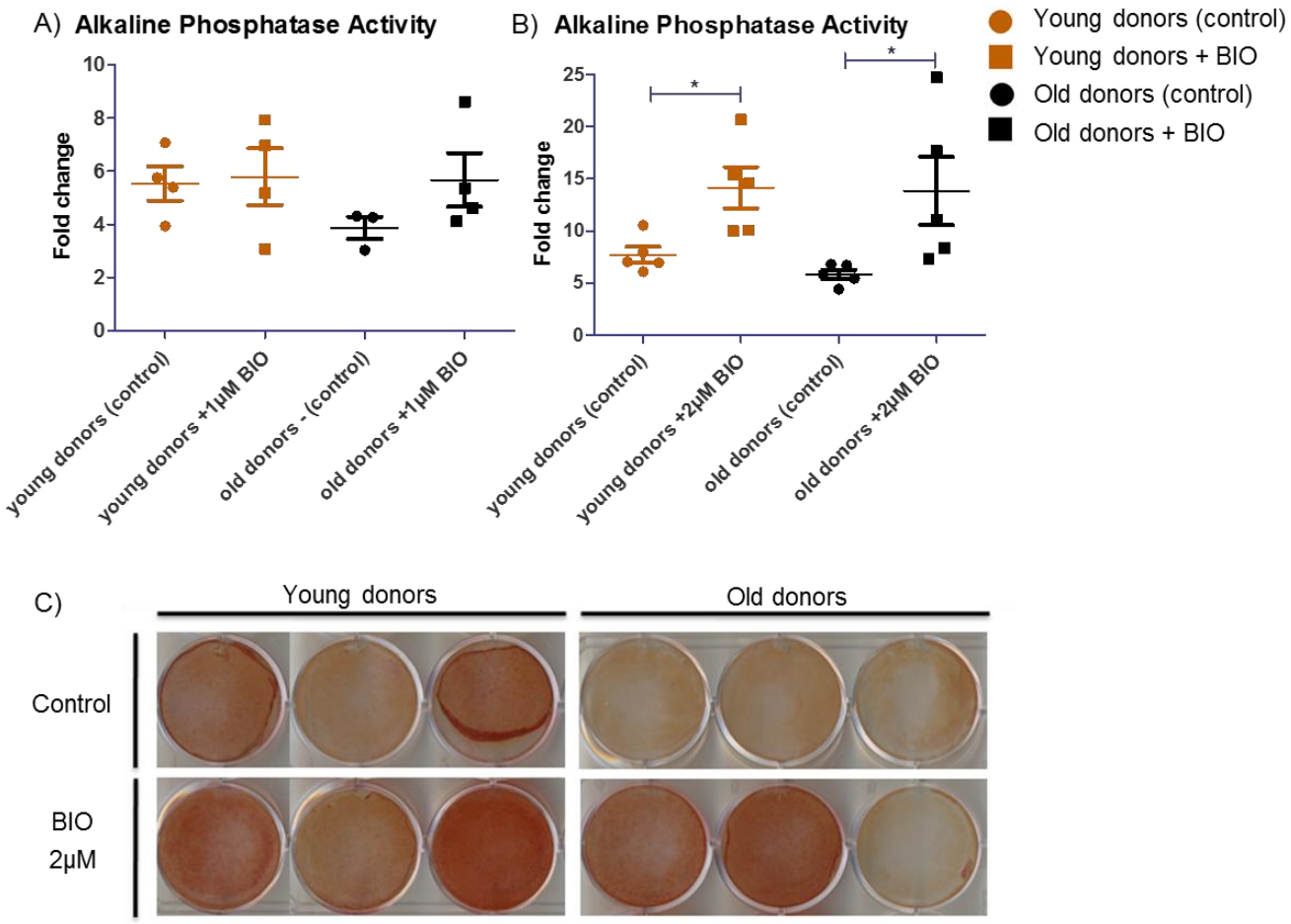
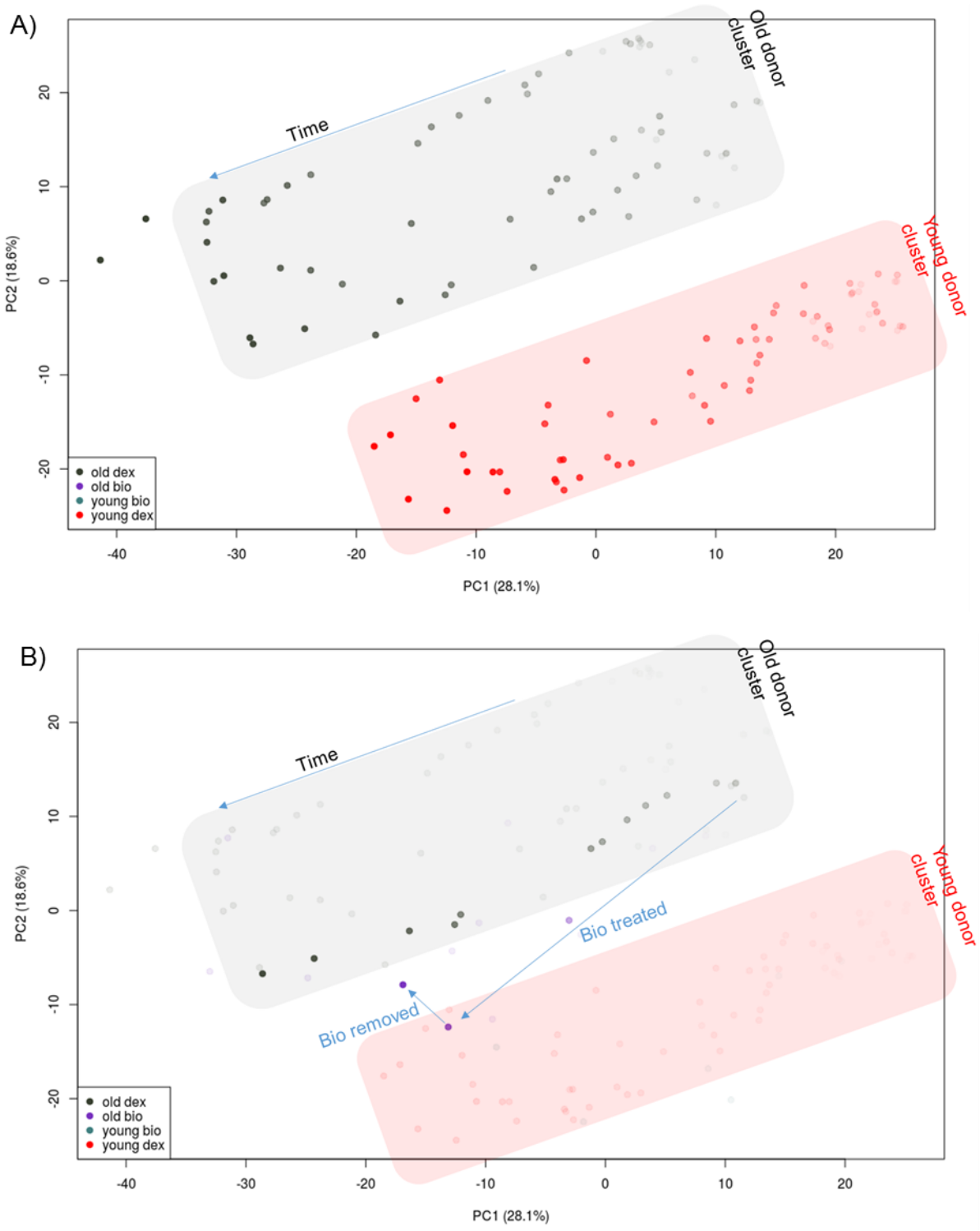
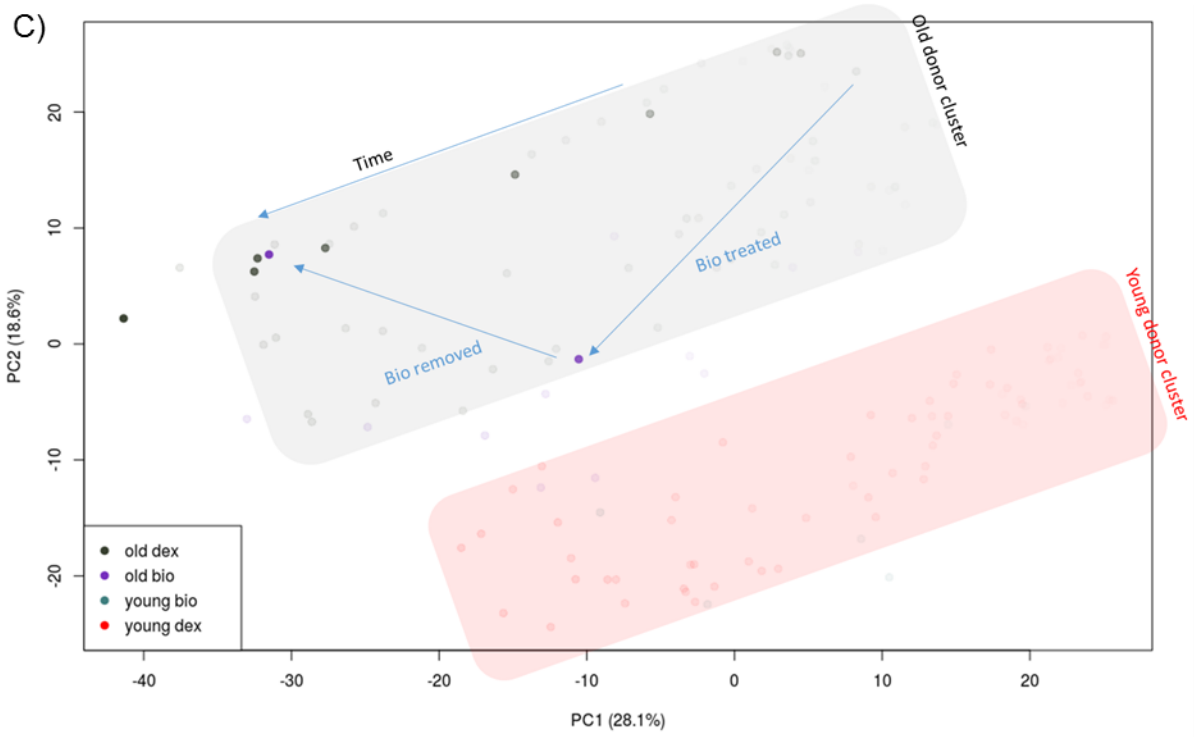


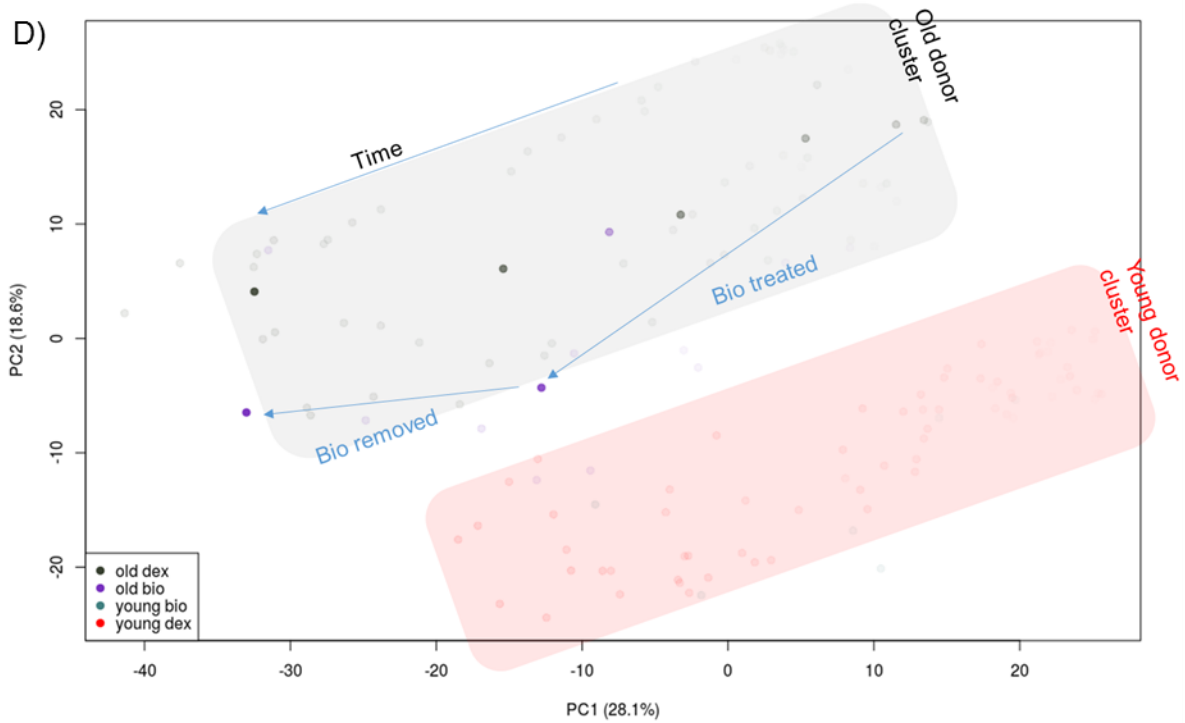
Figure 7-2 ***GSK3B Inhibition rescues osteoblast differentiation in old donors.*** *At day 0, young and old donor MSCs were treated with control or BIO (control = osteogenic media only, BIO = osteogenic media + BIO). In the BIO treated samples, the compound was removed at day 7. ALP assay was carried out at day 10.* ***A)*** *ALP Activity of young and old donor MSCs treated with 1 µM BIO. Young donors (n=4, 20 – 29 years) and old donors (n=4, 62 – 87 years).* ***B)*** *ALP Activity of young and old donor MSCs treated with 2 µM BIO. FC is normalised to MSCs in maintenance media. Young donors (n=5, 20 – 29 years) and old donors (n=5, 62 – 87 years). *Significant at p<0.05.* ***C)*** *Alizarin red staining at day 28. Young and old donors were treated with osteogenic media, with or without 2 µM BIO for the first 7 days. Young donors (n=3, 20 – 29 years) and old donors (n=3, 62 – 87 years).*

7.3.2 Transcriptomic changes after BIO treatment

To gain insight into the mechanisms of WNT activation in restoring the osteogenic potential of old donor MSCs, RNA-seq osteogenesis time-course experiments of the old MSCs treated with BIO (2µM) were carried out (old donors n=4, 62 – 87 years). The RNA-seq time-course consist of 7 time points, where RNA samples were collected at 0, 2, 6, 12, 24, 168 and 504 hrs during osteoblast differentiation. Samples at 0, 168 and 504 hrs were sequenced in all four donors, whereas samples at 2, 6, 12 and 24 hr were only sequenced in a subset of the donors. In a PCA plot, the BIO treated samples were compared to the control RNA-seq data from Chapter 6 (MSCs treated in osteogenic media only). The control young and old donor clusters are highlighted in red and grey, respectively (Figure 7-3-A). In the PCA plots, the individual old donors treated with BIO for 7 days are shown in blue, and the same donors without BIO are shown in black. (Figure 7-3-B,C,D&E). Between day 0 and day 7, all four BIO-treated old donor samples shifted towards the control young donor cluster. This indicates that the BIO treatment reduced the variability in gene expression between the old and young donors. After BIO was removed, the old donor samples shifted back towards the control old donor cluster at day 21. The RNA-seq time-course for a BIO treated young donor was also sequenced, and the samples showed a similar shift in gene expression in the PCA (supplementary figure S8)


A)
Old donor cluster
Young donor cluster
Time
old dex
old bio
young bio
young dex
PC2 (18.6%)
PC1 (28.1%)
B)
Old donor cluster
Young donor cluster
Time
Bio treated
Bio removed
old dex
old bio
young bio
young dex
PC2 (18.6%)
PC1 (28.1%)


C)
Old donor cluster
Young donor cluster
Time
Bio treated
Bio removed
old dex
old bio
young bio
young dex
PC2 (18.6%)
PC1 (28.1%)
20
10
0
-10
-20
-40
-30
-20
-10
0
10
20


D)
Old donor cluster
Young donor cluster
Time
Bio treated
Bio removed
old dex
old bio
young bio
young dex
PC2 (18.6%)
PC1 (28.1%)
20
10
0
-10
-20
-40
-30
-20
-10
0
10
20

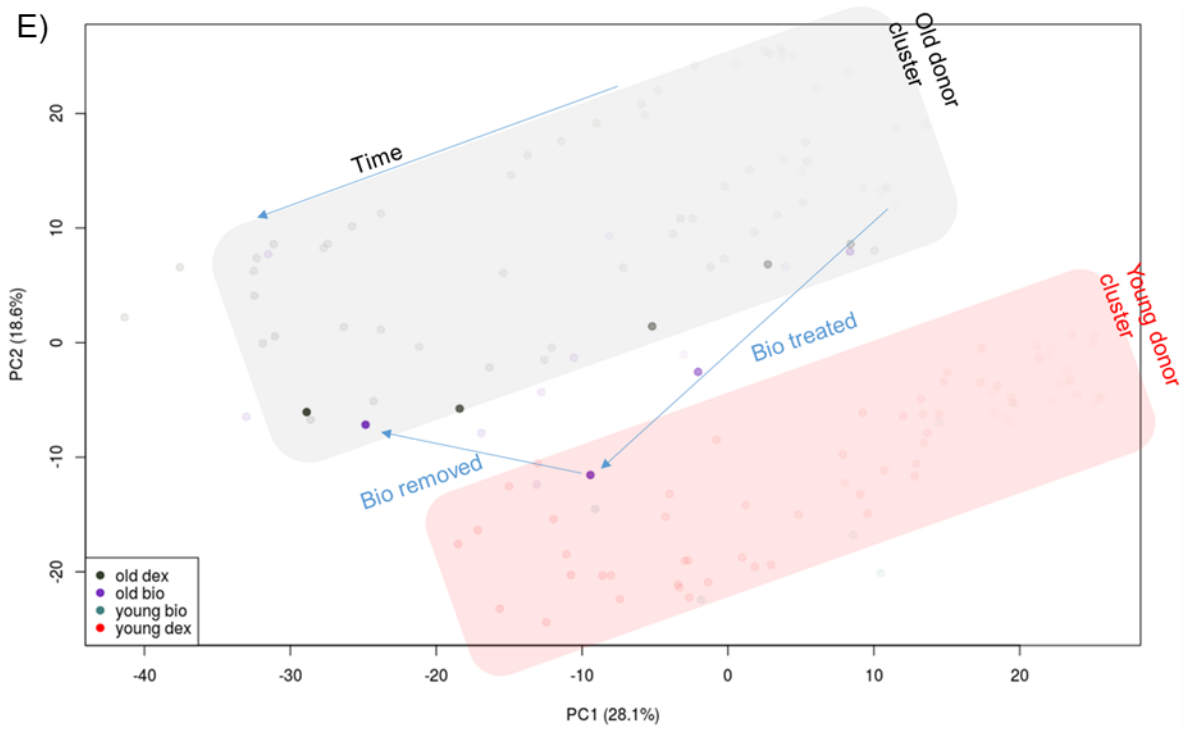


Figure 7-3 ***Transcriptomic changes in old vs young donor MSCs during osteogenesis with BIO treatment. A)*** *PCA of RNA-seq time-course data from chapter 6 – MSCs were treated in osteogenic media only. Young donors (n=6, 20 – 29 years) and old donors (n=6, 62 – 87 years). Light to dark symbols indicate early (0 hr) to late (504 hr) time points. Red and black dots indicate young and old donors. Red and grey shades indicate young and old sample clusters.* ***B, C, D & E)*** *showing individual old donors treated with BIO for 7 days (purple dots), and the same donor without BIO (grey dots).*

Chapter 4 demonstrated that the lineage preference of MSCs was altered with age. To examine whether BIO treatment restored the lineage commitment of MSC towards osteogenesis, the expression of markers for osteogenesis, adipogenesis and chondrogenesis were examined. The heatmap shows the fold change (normalised to 0 hr) in gene expression during osteogenesis of the two age groups (Figure 7-4). The ALP expression was elevated at 168 hrs (day 7) in the old donors with BIO treatment compared to the control old donor samples. After BIO was removed, the ALP expression decreased back to a similar level compared to the control (Figure 7-4, Figure 7-5). RUNX2 and SP7 showed an earlier increase in expression around 12 – 24 hrs with BIO treatment. Conversely, *PPARG*, *ADIPOQ*, *FABP4*, and *CEBPA* showed a decline in expression upon BIO treatment. After BIO was removed, the expression these adipogenic genes did not increase to the level of the old donors. Instead, their overall expression profile was similar to that of the control young donors. BIO treatment also altered the expression profile of the chondrogenic master regulator *SOX9*. In the control old donors, *SOX9* expression was initially repressed, then upregulated at 168 – 504 hrs (day 7 – day 21). With BIO treatment, there was less initial repression of *SOX9* expression at 0 – 24 hrs compared to the control old donors, but its expression was more strongly repressed between 168 – 504 hrs (day 7 – day 21).

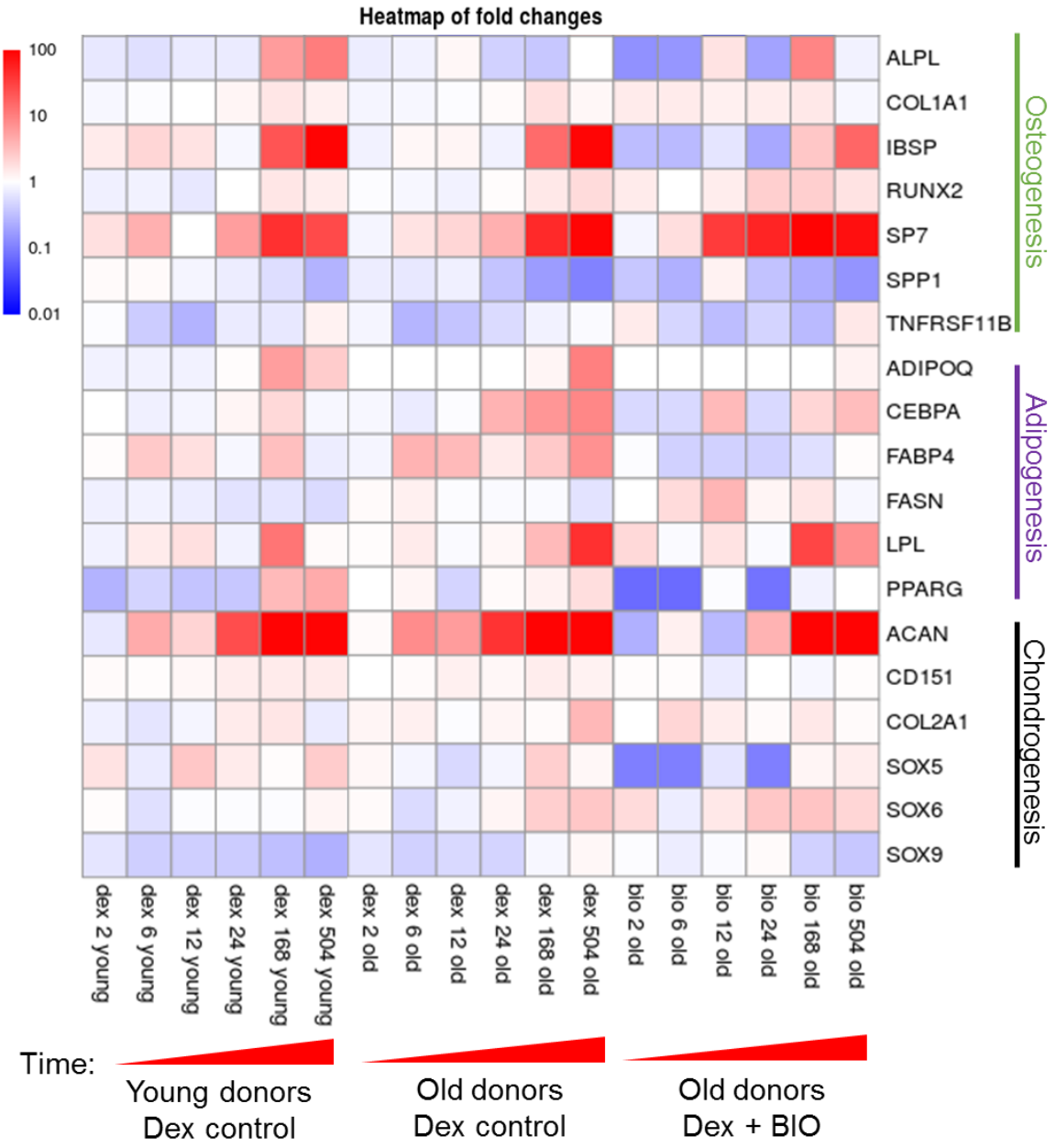


Figure 7-4 ***Lineage commitment of MSCs was altered by BIO treatment.*** *Heatmap of the fold change (normalised to 0 hr) in gene expression of lineage markers of young donor (n=6, 20 – 29 years), young donor with BIO (n=4, 20 – 29 years), old donor (n=4, 62 – 87 years) and old donor with BIO (n=3, 62 – 87 years) MSCs during osteogenesis. Lineage marker panel consists of: osteogenesis (ALPL, COL1A1, IBSP, RUNX2, SPP1, TNFRSF1), adipogenesis (ADIPOQ, CEBPA, FABP4, FASN, LPL, PPARG) and condrogenesis (ACAN, CD151, SOX5, SOX6, SOX9) markers.*

7.3.3 Differentially expressed genes after BIO treatment

To statistically examine the effect of BIO treatment in the old donors, a paired Wald test was carried out to identify the significantly differentially expressed genes at 168 hrs (day 7) and 504 hrs (day 21). 3,451 DEGs were found at day 7, and 209 DEGs were found at day 21 (3451 unique DEGs in total; paired Wald test, sig at padj<0.05, post Benjamini Hochberg correction). At day 7, *RUNX2*, *ALP* and *SP7* were significantly upregulated, and *CD151* was significantly downregulated in the BIO treated old donors (Figure 7-5). At day 21, *SOX9* was significantly downregulated in the BIO treated old donors. The top 10 enriched GO terms amongst the DEGs include processes involved in the regulation of endochondral ossification, chondrogenesis, and matrix organisation (Figure 7-6-A).

A Venn diagram shows that the 3,451 DEGs from 'BIO vs control' overlapped with 30% of the 3111 DEGs from 'young vs old donors in undifferentiated MSCs' (results from chapter 6), and overlapped with 47% of the 91 DEGs from 'young vs old donors during osteogenesis' (results from chapter 6) (Figure 7-6-B). The 43 overlapped DEGs between 'BIO vs control' and 'young vs old donors during osteogenesis' are shown on a heatmap, with the 20 DEGs overlapped in all three datasets marked by "+" (Figure 7-6-C).

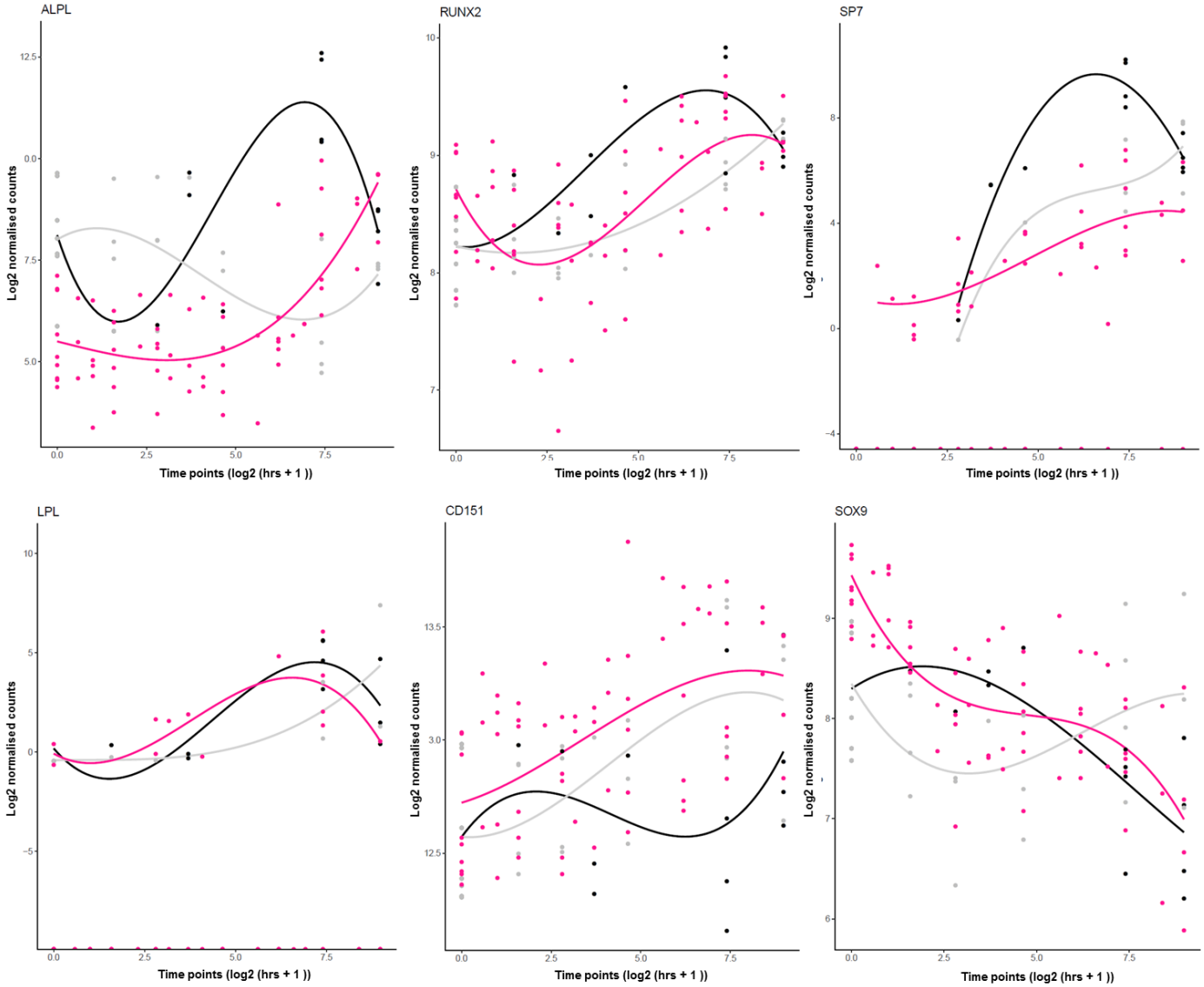
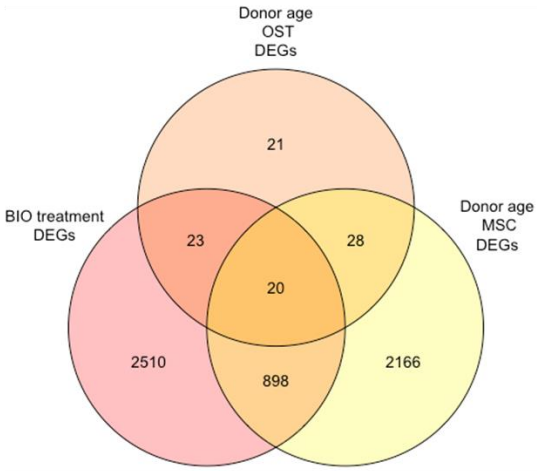


Figure 7-5 ***Differentially expressed lineage panel genes.*** *Scatter plot of gene expression (log2 normalised counts) over time (log2 hr(+1)). Trend line was fitted with non-linear regression. Grey = old donor in control osteogenic media. Black = old donor in Osteogenic media + BIO. Pink = Young donors in control osteogenic media.*

A)

GO Biological process	FDR
Endochondral ossification	1.29E-04
Positive regulation of cell migration involved in sprouting angiogenesis	5.43E-03
Positive regulation of chondrocyte differentiation	5.44E-03
Negative regulation of chondrocyte differentiation	7.23E-03
Regulation of extracellular matrix disassembly	7.96E-03
Kinetochore assembly	2.15E-02
Protein localization to chromosome, centromeric region	2.70E-02
Glomerulus morphogenesis	2.81E-02
UDP-N-acetylglucosamine biosynthetic process	2.95E-02
Negative regulation of extracellular matrix organization	2.96E-02

B)



C)

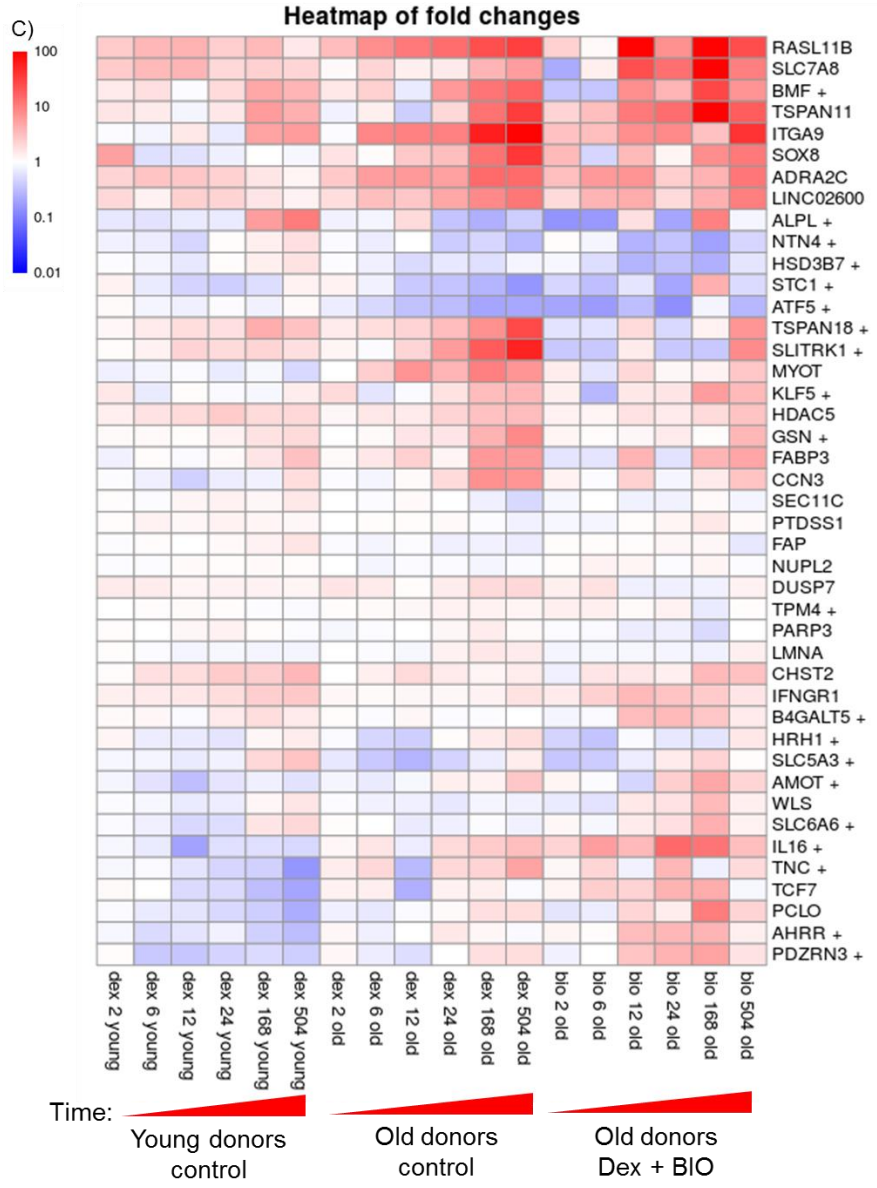


Figure 7-6 ***Overlapped differentially expressed genes in response to osteogenic conditions (+/- BIO) with age. A)*** *The top 10 enriched biological processes amongst the 3451 DEGs.* ***B)*** *Venn diagram shows the 3451 DEGs from BIO vs control overlapped with the 3111 DEGs from young vs old donor undifferentiated MSCs (data from chapter 4), and the 91 DEGs from young vs old donors during osteogenesis (data from chapter 6).* ***C)*** *Heatmap shows the 43 overlapped DEGs between BIO vs control and young vs old donors during osteogenesis, with the DEGs overlapped in all three datasets marked with "+".*

7.4 Discussion

Previous literature has shown that canonical WNT pathway agonists could restore the osteogenic potential and prevent bone loss in old mice [365-370], but its effect on human MSCs remained uncharacterised. Here, the ALP assay and AZR staining showed that the osteogenic potential of the old donor MSCs was elevated after BIO treatment. This was supported by the RNA-seq data showing that the gene expression of the BIO treated old donor MSCs shifted towards the control young donor cluster. This evidence suggests that, in humans, the age driven loss of MSC osteogenic potential could also be rescued by WNT activation.

Mechanistically, BIO treatment significantly increased *ALP*, *RUNX2* and *SP7* expression, while it significantly decreased *SOX9* and *CD151* expression, suggesting that WNT signalling activation promoted osteoblast differentiation while repressing chondrocyte differentiation. Adipogenic regulators *PPARG*, *ADIPOQ*, *FABP4* and *CEBPA* showed a greater than 2 fold decrease in expression at 21 days after BIO treatment. However, the changes in the expression of these adipogenic genes were not significant, primarily due to their low expression values (normalised counts). Further studies using a more sensitive transcriptional quantification method such as qPCR, using more donors to increase statistical power, or carrying out *in vitro* assays to examine adipocyte formation may confirm whether BIO treatment inhibits adipogenesis. Overall, the results suggest that WNT activation shifted the lineage preference of old donor MSCs towards osteogenesis.

The RNA-seq data also showed that canonical WNT signalling activation significantly altered the expression of a large number of genes (3351 DEGs), amongst which, there may be novel regulators and pathways that mediate the pro-osteogenic effect of WNT activation. The heatmap of the DEGs presents several clusters of genes that altered their expression profiles from old donors towards the young donors after BIO treatment. For example, *CCN3* is amongst a cluster of genes that were significantly upregulated in 'old vs young donors' during osteogenesis and was significantly downregulated after BIO treatment. *CCN3* was also amongst the top enriched gene network clusters of the DEGs (old vs young donor during osteogenesis) in chapter 6. CCN3 - Cellular Communication Network Factor 3, also known as Nephroblastoma Overexpressed Gene (*NOV*), is a secreted protein in the CCN family of regulatory proteins. Not surprisingly, *WISP*/*CCN* family gene expression was previously reported to be regulated by the canonical WNT pathway [368, 369]. Other members of *CCN* family genes, in particular, *CCN4/5/6* (*WISP1/2/3*), are regulators of bone turnover [371-373] and *CCN3* has also recently emerged as an important regulator of bone regeneration. One study reported that the overexpression of *CCN3*/*NOV* in osteoblasts antagonises both BMP and WNT signalling, and results in osteopenia [371, 374]. *CCN3*$^{-/-}$ mice showed enlarged vertebrae, elongated long bones and increased bone mineralisation [375]. In contrast, *CCN3* was shown to positively regulate chondrogenesis and was implicated with promoting the progression of chondrosarcoma [376]. Interestingly, *CCN3*$^{-/-}$ mice also showed cardiomyopathy and muscle atrophy, which was also found in patients treated with an inhibitor of SOST - romosozumab. This indicates that *CCN3* may have a similar biological role as *SOST*. This chapter demonstrated that canonical WNT pathway activation rescued the loss of the osteogenic potential of aged MSCs, and repressed *CCN3* expression, indicating that the regulation of osteogenesis by the canonical WNT pathway may be partially mediated through the repression

of *CCN3*. Therefore, it would interesting to examine whether moderate inhibition of *CCN3* could improve osteoblast differentiation in aged MSCs.

8 Discussion

Ageing is associated with a decline in the proliferative and osteogenic potential of MSCs, which results in a decreased bone mass and bone strength, leading to an increased risk of age-related fragility fractures. Restoring MSC function to replenish osteoblast numbers and bone mass remains an important challenge within this field. However, a better understanding of the mechanism of MSC ageing is required. The aim of this thesis was to characterise the transcriptional and epigenetic changes during MSC ageing, and identify candidates that could restore the proliferative and osteogenic potential of aged MSCs.

Chapter 4 provided a systematic characterisation of DNA methylation, chromatin accessibility and transcriptional changes during MSC ageing. No global shifts in DNA methylation or gene expression profiles were observed with ageing, which is consistent with previous literature. Interestingly, a global increase in chromatin accessibility was observed with age. The age-related changes in genome-wide chromatin accessibility of human bone marrow MSCs were reported for the first time in this study, and further investigation is needed to understand the mechanisms and implications of this change. As histone modifications are key regulators of chromatin accessibility, the increase in chromatin accessibility is likely associated with changes in histone marks. ChIP-seq for activating and repressive marks may provide mechanistic insight towards the chromatin changes in MSCs with age. The chromatin changes with age likely contribute towards the decline in MSC osteogenic potential, as there was a significant decline in the chromatin accessibility of genes involved in skeletal system development. In the RNA-seq data, 141 (5% of the DEGs) epigenetic regulators were differentially expressed with age. Targeting these epigenetic regulators may restore the chromatin profiles of the aged MSCs and improve proliferative and osteogenic potential.

Chapter 5 demonstrated a novel approach in using shRNA-seq to systematically screen for epigenetic regulators of proliferation in late passage MSCs. *PYGO1* was identified as a potential candidate for improving the proliferation of aged MSCs. The mechanism of *PYGO1* is unclear but is implicated in regulating the expression of β-catenin target genes. RNA-seq experiments to examine gene expression change after *PYGO1* knockdown may provide insight towards the mechanism of PYGO1. A surprising finding was that simultaneous knockdown of a combination of epigenetic regulators (*PRMT8, TCF20, SND1, PYGO1, EZH1, MTF2, SPIN1, HDAC2)* produced a greater increase in proliferation than knocking down each epigenetic regulator individually. This concept of synergy has previously been demonstrated, where a combination of reprogramming factors was required to restore the pluripotent epigenetic state of cells [16]. Identifying the best combination of the 22 potential candidates to improve the proliferative potential of the aged MSCs will require extensive optimisation. Mechanistically, it is possible that knocking down an individual or a combination of epigenetic regulators was able to restore the epigenetic state of late passage MSCs towards a more youthful state, resulting in the increased proliferative potential observed. If a youthful epigenetic state was achieved, these treated MSCs may also show an increased osteogenic potential, which can be examined using ALP assays and AZR staining.

It is interesting that the lineage fate preference of young and old donor MSCs was already evident in undifferentiated MSCs. The RNA-seq data in chapter 4 showed that the skeletal system morphogenesis related genes were enriched amongst the top 100 genes that separated the young and old donors. Most strikingly, a significant increase in *PPARG* expression and a decline in *RUNX2* expression were observed in the old donor MSCs. This is at least in part due to a less permissible epigenetic state for osteogenesis in the old donor MSCs, as there was a significant increase in DNA methylation of genes containing RUNX2 binding motifs and a significant decrease in chromatin accessibility of genes involved in skeletal system

development. In chapter 6, the expression profiles of the tri-lineage differentiation markers indicated that the old donor MSCs were unable to fully commit towards osteoblast differentiation upon osteogenic induction and were diverted towards an adipogenic fate. This was confirmed by the presence of adipocytes in the old donor MSCs under osteogenic condition. Taken together, the results in chapter 4 and 6 suggests that the transcriptional and epigenetic state of old donor MSCs pre-determined their lineage fate, which was not completely overridden by an osteogenic stimulus. This change in lineage preference in MSCs may contribute towards the increased bone marrow adiposity with age [43]. It would be interesting to examine whether ageing MSCs uniformly increase their tendency to differentiate toward adipocytes, or whether there is a subpopulation of MSCs that become significantly more adipogenic. Recent developments in single cell (sc) RNA-seq [377], scATAC-seq [378] and scDNA methylation-seq [379] technologies could be adapted to examine the changes in the heterogeneity of MSCs in their lineage fate decisions with age.

Comparing the RNA-seq data from Chapter 4 and 5 demonstrated that the majority of the DEGs between donor ageing and passaging in MSCs were different. This is potentially due to the confounding factors present in each of the ageing models, such as inter-donor variability and cell culture changes. However, there was also a significant overlap between the DEGs from the two ageing models, which provides a robust list of 196 concordant DEGs that may underlie the true biological differences in MSCs with age. Interesting targets for future follow up includes *SFRP4*, *FGF2*/*FGFR2*, *GLI3* and *DLX5* which are important regulates of WNT, FGF, HH and HOX pathways, respectively.

Chapter 6 provided the first high-resolution RNA-seq time-course data comparing osteogenesis between young and old donor MSCs. Osteogenesis appears to be a fascinatingly large transcriptomic event with more than 7000 differentially expressed genes between 0 to 21 days. There appear to be two major phases of gene expression during osteogenesis between 0 – 24

hrs and 48 – 504 hrs. The first 24 hrs of osteogenesis likely play a significant role in determining lineage commitment, but these very early timepoints during osteogenesis are generally overlooked in studies [315]. Indeed, significant differences in the gene expression profiles of young and old donor MSCs during osteogenesis started as early as 2 – 24 hrs, including a transient upregulation of AREG, SLC7A8, RASL11B, ADRA2C and LINC02600 in the young donor MSCs, but a delayed or a lack of upregulation of these genes in the old donor MSCs. Further studies could examine whether a transient overexpression of these genes in the old donor MSCs increases osteogenic potential.

The canonical WNT pathway was consistently identified in chapters 4, 5 and 6. In chapter 4, amongst the top 10 enriched processes combining the three –omics datasets, the canonical WNT pathway was the most implicated pathway. In chapter 5, *SFRP4* was amongst the 18 concordant bone development-related genes altered between the two ageing models (donor age and cell culture). In chapter 6, *GSK3B* was misregulated between 8 – 24 hrs during osteogenesis in the old donors, and *CTNNB1* expression was consistently lower in the old donor throughout the time-course. Together, these results strongly suggest that the canonical WNT pathway could be a promising target in restoring the osteogenic potential of old donor MSCs. This led to the experiments in chapter 7, which demonstrated for the first time that BIO treatment can restore the osteogenic potential of old donor MSCs via the activation of the canonical WNT pathway. BIO was used for WNT activation because it is a well characterised GSK3 inhibitor with high specificity [380]. Other WNT activators targeting β-catenin [381], GSK3 [382], DKK1 [355] and SRFP [383] could be used to further validate that the canonical WNT pathway activation can restore the osteogenic potential of aged MSCs. More excitingly, WNT activation shifted the transcriptomic profiles of old donors towards the young donors, suggesting that canonical WNT signalling activation rescued both the phenotype and the gene expression of the old donor MSCs. The data generated provides the opportunity to investigate novel targets

such as *NOV1*, which appears to be associated with the effect of canonical WNT signalling activation in promoting osteogenesis in old donor MSCs.

Overall, the results in this thesis suggest that the canonical WNT pathway plays an important role in MSC ageing, and restoring the canonical WNT signalling activity in aged MSCs may improve their osteogenic potential. More importantly, this study demonstrated the validity of the concept that a multi-omics approach can be used to gain insight towards the mechanisms of MSC ageing and identify promising candidates to restore MSC functions in the elderly. Thus, there is a wealth of information within the data generated in this project that needs to be further investigated, which may enable a better understanding of MSC ageing and lead to additional therapeutic candidates for replenishing MSC and osteoblast numbers in individuals with age-related bone loss.

References

1. Gasser J.A., K.M., *Bone Physiology and Biology.* Bone Toxicology. Molecular and Integrative Toxicology. Springer, Cham, 2017.
2. Long, F., *Building strong bones: molecular regulation of the osteoblast lineage.* Nat Rev Mol Cell Biol, 2011. **13**(1): p. 27-38.
3. Ferretti, C. and M. Mattioli-Belmonte, *Periosteum derived stem cells for regenerative medicine proposals: Boosting current knowledge.* World J Stem Cells, 2014. **6**(3): p. 266-77.
4. Uccelli, A., L. Moretta, and V. Pistoia, *Mesenchymal stem cells in health and disease.* Nat Rev Immunol, 2008. **8**(9): p. 726-36.
5. Augustin, G., A. Antabak, and S. Davila, *The periosteum. Part 1: Anatomy, histology and molecular biology.* Injury, 2007. **38**(10): p. 1115-30.
6. Gibon, E., et al., *Inflammation, ageing, and bone regeneration.* J Orthop Translat, 2017. **10**: p. 28-35.
7. Jaul, E. and J. Barron, *Age-Related Diseases and Clinical and Public Health Implications for the 85 Years Old and Over Population.* Front Public Health, 2017. **5**: p. 335.
8. NICE, *Osteoporosis: assessing the risk of fragility fracture.* https://www.nice.org.uk/guidance/cg146/documents/osteoporosis-final-scope2, 2012.
9. NICE, *Osteoporosis: assessing the risk of fragility fracture*. 2012: https://www.nice.org.uk/guidance/cg146/chapter/Introduction.
10. Demontiero, O., C. Vidal, and G. Duque, *Aging and bone loss: new insights for the clinician.* Ther Adv Musculoskelet Dis, 2012. **4**(2): p. 61-76.
11. Seymour, H.E., et al., *Anti-TNF agents for rheumatoid arthritis.* Br J Clin Pharmacol, 2001. **51**(3): p. 201-8.
12. Stolzing, A., et al., *Age-related changes in human bone marrow-derived mesenchymal stem cells: consequences for cell therapies.* Mech Ageing Dev, 2008. **129**(3): p. 163-73.
13. Ramalho-Santos, M. and H. Willenbring, *On the origin of the term "stem cell".* Cell Stem Cell, 2007. **1**(1): p. 35-8.

14. Chagastelles, P.C. and N.B. Nardi, *Biology of stem cells: an overview.* Kidney Int Suppl (2011), 2011. **1**(3): p. 63-67.

15. Wu, G., L. Lei, and H.R. Scholer, *Totipotency in the mouse.* J Mol Med (Berl), 2017. **95**(7): p. 687-694.

16. Takahashi, K. and S. Yamanaka, *Induction of pluripotent stem cells from mouse embryonic and adult fibroblast cultures by defined factors.* Cell, 2006. **126**(4): p. 663-76.

17. Gurdon, J.B., T.R. Elsdale, and M. Fischberg, *Sexually mature individuals of Xenopus laevis from the transplantation of single somatic nuclei.* Nature, 1958. **182**(4627): p. 64-5.

18. Omole, A.E. and A.O.J. Fakoya, *Ten years of progress and promise of induced pluripotent stem cells: historical origins, characteristics, mechanisms, limitations, and potential applications.* PeerJ, 2018. **6**: p. e4370.

19. Sobhani, A., et al., *Multipotent Stem Cell and Current Application.* Acta Med Iran, 2017. **55**(1): p. 6-23.

20. Monti, M., et al., *Stem cells: sources and therapies.* Biol Res, 2012. **45**(3): p. 207-14.

21. Yoshihara, M., Y. Hayashizaki, and Y. Murakawa, *Genomic Instability of iPSCs: Challenges Towards Their Clinical Applications.* Stem Cell Rev Rep, 2017. **13**(1): p. 7-16.

22. Choumerianou, D.M., H. Dimitriou, and M. Kalmanti, *Stem cells: promises versus limitations.* Tissue Eng Part B Rev, 2008. **14**(1): p. 53-60.

23. Friedenstein, A.J., R.K. Chailakhyan, and U.V. Gerasimov, *Bone marrow osteogenic stem cells: in vitro cultivation and transplantation in diffusion chambers.* Cell Tissue Kinet, 1987. **20**(3): p. 263-72.

24. Caplan, A.I., *Mesenchymal stem cells.* J Orthop Res, 1991. **9**(5): p. 641-50.

25. Dominici, M., et al., *Minimal criteria for defining multipotent mesenchymal stromal cells. The International Society for Cellular Therapy position statement.* Cytotherapy, 2006. **8**(4): p. 315-7.

26. Fitzsimmons, R.E.B., et al., *Mesenchymal Stromal/Stem Cells in Regenerative Medicine and Tissue Engineering.* Stem Cells Int, 2018. **2018**: p. 8031718.

27. Al-Nbaheen, M., et al., *Human stromal (mesenchymal) stem cells from bone marrow, adipose tissue and skin exhibit differences in molecular phenotype and differentiation potential.* Stem Cell Rev Rep, 2013. **9**(1): p. 32-43.

28. Nancarrow-Lei, R., et al., *A Systemic Review of Adult Mesenchymal Stem Cell Sources and their Multilineage Differentiation Potential Relevant to Musculoskeletal Tissue Repair and Regeneration.* Curr Stem Cell Res Ther, 2017. **12**(8): p. 601-610.

29. Langenbach, F. and J. Handschel, *Effects of dexamethasone, ascorbic acid and beta-glycerophosphate on the osteogenic differentiation of stem cells in vitro.* Stem Cell Res Ther, 2013. **4**(5): p. 117.

30. Zou, F., et al., *Effects of oncostatin M on cell proliferation and osteogenic differentiation in C3H10T1/2.* J Musculoskelet Neuronal Interact, 2016. **16**(4): p. 377-385.

31. Kim, I.S., et al., *In vitro response of primary human bone marrow stromal cells to recombinant human bone morphogenic protein-2 in the early and late stages of osteoblast differentiation.* Dev Growth Differ, 2008. **50**(7): p. 553-64.

32. Posa, F., et al., *Vitamin D Effects on Osteoblastic Differentiation of Mesenchymal Stem Cells from Dental Tissues.* Stem Cells Int, 2016. **2016**: p. 9150819.

33. Wittkowske, C., et al., *In Vitro Bone Cell Models: Impact of Fluid Shear Stress on Bone Formation.* Front Bioeng Biotechnol, 2016. **4**: p. 87.

34. Phinney, D.G. and D.J. Prockop, *Concise review: mesenchymal stem/multipotent stromal cells: the state of transdifferentiation and modes of tissue repair--current views.* Stem Cells, 2007. **25**(11): p. 2896-902.

35. Wislet-Gendebien, S., et al., *Plasticity of cultured mesenchymal stem cells: switch from nestin-positive to excitable neuron-like phenotype.* Stem Cells, 2005. **23**(3): p. 392-402.

36. Squillaro, T., G. Peluso, and U. Galderisi, *Clinical Trials With Mesenchymal Stem Cells: An Update.* Cell Transplant, 2016. **25**(5): p. 829-48.

37. Horwitz, E.M., et al., *Isolated allogeneic bone marrow-derived mesenchymal cells engraft and stimulate growth in children with osteogenesis imperfecta: Implications for cell therapy of bone.* Proc Natl Acad Sci U S A, 2002. **99**(13): p. 8932-7.

38. Roberts, S.J. and H.Z. Ke, *Anabolic Strategies to Augment Bone Fracture Healing.* Curr Osteoporos Rep, 2018. **16**(3): p. 289-298.

39. Kanazawa, I., *Osteocalcin as a hormone regulating glucose metabolism.* World J Diabetes, 2015. **6**(18): p. 1345-54.

40. Ferretti, C., et al., *Human periosteum-derived stem cells for tissue engineering applications: the role of VEGF.* Stem Cell Rev Rep, 2012. **8**(3): p. 882-90.

41. Mori, R., et al., *Comparative histology of the laminar bone between young calves and foals.* Cells Tissues Organs, 2003. **175**(1): p. 43-50.

42. Zhao, M. and L. Li, *Dissecting the bone marrow HSC niches.* Cell Res, 2016. **26**(9): p. 975-6.

43. Justesen, J., et al., *Adipocyte tissue volume in bone marrow is increased with aging and in patients with osteoporosis.* Biogerontology, 2001. **2**(3): p. 165-71.

44. Florencio-Silva, R., et al., *Biology of Bone Tissue: Structure, Function, and Factors That Influence Bone Cells.* Biomed Res Int, 2015. **2015**: p. 421746.

45. Kim, S.W., et al., *Intermittent parathyroid hormone administration converts quiescent lining cells to active osteoblasts.* J Bone Miner Res, 2012. **27**(10): p. 2075-84.

46. Dobnig, H. and R.T. Turner, *Evidence that intermittent treatment with parathyroid hormone increases bone formation in adult rats by activation of bone lining cells.* Endocrinology, 1995. **136**(8): p. 3632-8.

47. Goswami, R., *Primer on the metabolic bone diseases and disorders of mineral metabolism.* The Indian Journal of Medical Research, 2016. **144**(3): p. 489-490.

48. Schaffler, M.B., et al., *Osteocytes: master orchestrators of bone.* Calcif Tissue Int, 2014. **94**(1): p. 5-24.

49. Verborgt, O., et al., *Spatial distribution of Bax and Bcl-2 in osteocytes after bone fatigue: complementary roles in bone remodeling regulation?* J Bone Miner Res, 2002. **17**(5): p. 907-14.

50. Pixley, F.J. and E.R. Stanley, *CSF-1 regulation of the wandering macrophage: complexity in action.* Trends Cell Biol, 2004. **14**(11): p. 628-38.

51. Suda, T., et al., *Modulation of osteoclast differentiation and function by the new members of the tumor necrosis factor receptor and ligand families.* Endocr Rev, 1999. **20**(3): p. 345-57.

52. Atkins, G.J., et al., *Osteoprotegerin inhibits osteoclast formation and bone resorbing activity in giant cell tumors of bone.* Bone, 2001. **28**(4): p. 370-7.

53. Yang, Y., *Skeletal morphogenesis during embryonic development.* Crit Rev Eukaryot Gene Expr, 2009. **19**(3): p. 197-218.

54. Thompson, E.M., et al., *Recapitulating endochondral ossification: a promising route to in vivo bone regeneration.* J Tissue Eng Regen Med, 2015. **9**(8): p. 889-902.

55. Boyan, B.D., Z. Schwartz, and L.D. Swain, *In vitro studies on the regulation of endochondral ossification by vitamin D.* Crit Rev Oral Biol Med, 1992. **3**(1-2): p. 15-30.

56. Rucci, N., *Molecular biology of bone remodelling.* Clin Cases Miner Bone Metab, 2008. **5**(1): p. 49-56.

57. Sims, N.A. and T.J. Martin, *Coupling the activities of bone formation and resorption: a multitude of signals within the basic multicellular unit.* Bonekey Rep, 2014. **3**: p. 481.

58. Lips, P., P. Courpron, and P.J. Meunier, *Mean wall thickness of trabecular bone packets in the human iliac crest: changes with age.* Calcif Tissue Res, 1978. **26**(1): p. 13-7.

59. Recker, R., et al., *Bone remodeling increases substantially in the years after menopause and remains increased in older osteoporosis patients.* J Bone Miner Res, 2004. **19**(10): p. 1628-33.

60. MacDonald, B.T., K. Tamai, and X. He, *Wnt/beta-catenin signaling: components, mechanisms, and diseases.* Dev Cell, 2009. **17**(1): p. 9-26.

61. Gaur, T., et al., *Canonical WNT signaling promotes osteogenesis by directly stimulating Runx2 gene expression.* J Biol Chem, 2005. **280**(39): p. 33132-40.

62. Park, B., et al., *Wnt3a disrupts GR-TEAD4-PPARgamma2 positive circuits and cytoskeletal rearrangement in a beta-catenin-dependent manner during early adipogenesis.* Cell Death Dis, 2019. **10**(1): p. 16.

63. Takahashi, N., et al., *Regulatory mechanism of osteoclastogenesis by RANKL and Wnt signals.* Front Biosci (Landmark Ed), 2011. **16**: p. 21-30.

64. Glass, D.A., 2nd, et al., *Canonical Wnt signaling in differentiated osteoblasts controls osteoclast differentiation.* Dev Cell, 2005. **8**(5): p. 751-64.

65. Galea, G.L., et al., *Planar cell polarity aligns osteoblast division in response to substrate strain.* J Bone Miner Res, 2015. **30**(3): p. 423-35.

66. Arnsdorf, E.J., et al., *Mechanically induced osteogenic differentiation--the role of RhoA, ROCKII and cytoskeletal dynamics.* J Cell Sci, 2009. **122**(Pt 4): p. 546-53.

67. McBeath, R., et al., *Cell shape, cytoskeletal tension, and RhoA regulate stem cell lineage commitment.* Dev Cell, 2004. **6**(4): p. 483-95.

68. Crabtree, G.R. and S.L. Schreiber, *SnapShot: Ca2+-calcineurin-NFAT signaling.* Cell, 2009. **138**(1): p. 210, 210 e1.

69. Sun, L., et al., *Calcineurin regulates bone formation by the osteoblast.* Proc Natl Acad Sci U S A, 2005. **102**(47): p. 17130-5.

70. Marina Bolzoni, P.S., Daniela Guasco, Mirca Lazzaretti, Eugenia Martella, Cristina Mancini, Luca Agnelli, Sabrina Bonomini, Antonino Neri, Gaetano Donofrio and Nicola Giuliani, *The Activation of Wnt5a-Mediated Non Canonical Wnt Signaling in Human Bone Marrow Osteoprogenitor Cells Increases Osteoblastogenesis and Counterbalances the Inhibitory Effect of Myeloma Cells on Ror2/FZD5 Expression.* Blood, 2011.

71. Maeda, K., et al., *Wnt5a-Ror2 signaling between osteoblast-lineage cells and osteoclast precursors enhances osteoclastogenesis.* Nat Med, 2012. **18**(3): p. 405-12.

72. James, A.W., *Review of Signaling Pathways Governing MSC Osteogenic and Adipogenic Differentiation.* Scientifica (Cairo), 2013. **2013**: p. 684736.

73. Tsuji, K., et al., *BMP2 activity, although dispensable for bone formation, is required for the initiation of fracture healing.* Nat Genet, 2006. **38**(12): p. 1424-9.

74. Osyczka, A.M., et al., *Different effects of BMP-2 on marrow stromal cells from human and rat bone.* Cells Tissues Organs, 2004. **176**(1-3): p. 109-19.

75. Mishina, Y., et al., *Bone morphogenetic protein type IA receptor signaling regulates postnatal osteoblast function and bone remodeling.* J Biol Chem, 2004. **279**(26): p. 27560-6.

76. Chen, D., et al., *Differential roles for bone morphogenetic protein (BMP) receptor type IB and IA in differentiation and specification of mesenchymal precursor cells to osteoblast and adipocyte lineages.* J Cell Biol, 1998. **142**(1): p. 295-305.

77. Muruganandan, S., A.A. Roman, and C.J. Sinal, *Adipocyte differentiation of bone marrow-derived mesenchymal stem cells: cross talk with the osteoblastogenic program.* Cell Mol Life Sci, 2009. **66**(2): p. 236-53.

78. Pan, A., et al., *A review of hedgehog signaling in cranial bone development.* Front Physiol, 2013. **4**: p. 61.

79. Tu, X., K.S. Joeng, and F. Long, *Indian hedgehog requires additional effectors besides Runx2 to induce osteoblast differentiation.* Dev Biol, 2012. **362**(1): p. 76-82.

80. Zhao, M., et al., *The zinc finger transcription factor Gli2 mediates bone morphogenetic protein 2 expression in osteoblasts in response to hedgehog signaling.* Mol Cell Biol, 2006. **26**(16): p. 6197-208.

81. Zehentner, B.K., U. Leser, and H. Burtscher, *BMP-2 and sonic hedgehog have contrary effects on adipocyte-like differentiation of C3H10T1/2 cells.* DNA Cell Biol, 2000. **19**(5): p. 275-81.

82. Sinha, S. and J.K. Chen, *Purmorphamine activates the Hedgehog pathway by targeting Smoothened.* Nat Chem Biol, 2006. **2**(1): p. 29-30.

83. Wu, M., G. Chen, and Y.P. Li, *TGF-beta and BMP signaling in osteoblast, skeletal development, and bone formation, homeostasis and disease.* Bone Res, 2016. **4**: p. 16009.

84. Tang, Y., et al., *TGF-beta1-induced migration of bone mesenchymal stem cells couples bone resorption with formation.* Nat Med, 2009. **15**(7): p. 757-65.

85. Janssens, K., et al., *Camurati-Engelmann disease: review of the clinical, radiological, and molecular data of 24 families and implications for diagnosis and treatment.* J Med Genet, 2006. **43**(1): p. 1-11.

86. Karst, M., et al., *Roles of stromal cell RANKL, OPG, and M-CSF expression in biphasic TGF-beta regulation of osteoclast differentiation.* J Cell Physiol, 2004. **200**(1): p. 99-106.

87. Crane, J.L., L. Xian, and X. Cao, *Role of TGF-beta Signaling in Coupling Bone Remodeling.* Methods Mol Biol, 2016. **1344**: p. 287-300.

88. Hilton, M.J., et al., *Notch signaling maintains bone marrow mesenchymal progenitors by suppressing osteoblast differentiation.* Nat Med, 2008. **14**(3): p. 306-14.

89. de Jong, D.S., et al., *Regulation of Notch signaling genes during BMP2-induced differentiation of osteoblast precursor cells.* Biochem Biophys Res Commun, 2004. **320**(1): p. 100-7.

90. Su, N., M. Jin, and L. Chen, *Role of FGF/FGFR signaling in skeletal development and homeostasis: learning from mouse models.* Bone Res, 2014. **2**: p. 14003.

91. Lai, W.T., V. Krishnappa, and D.G. Phinney, *Fibroblast growth factor 2 (Fgf2) inhibits differentiation of mesenchymal stem cells by inducing Twist2 and Spry4, blocking extracellular regulated kinase activation, and altering Fgf receptor expression levels.* Stem Cells, 2011. **29**(7): p. 1102-11.

92. Yu, K., et al., *Conditional inactivation of FGF receptor 2 reveals an essential role for FGF signaling in the regulation of osteoblast function and bone growth.* Development, 2003. **130**(13): p. 3063-74.

93. Fei, Y., et al., *Fibroblast growth factor 2 stimulation of osteoblast differentiation and bone formation is mediated by modulation of the Wnt signaling pathway.* J Biol Chem, 2011. **286**(47): p. 40575-83.

94. Farhadi, J., et al., *Differentiation-dependent up-regulation of BMP-2, TGF-beta1, and VEGF expression by FGF-2 in human bone marrow stromal cells.* Plast Reconstr Surg, 2005. **116**(5): p. 1379-86.

95. Li, J., *JAK-STAT and bone metabolism.* JAKSTAT, 2013. **2**(3): p. e23930.

96. Levy, O., et al., *Highly efficient osteogenic differentiation of human mesenchymal stem cells by eradication of STAT3 signaling.* Int J Biochem Cell Biol, 2010. **42**(11): p. 1823-30.

97. Ting, K., et al., *Human NELL-1 expressed in unilateral coronal synostosis.* J Bone Miner Res, 1999. **14**(1): p. 80-9.

98. Pakvasa, M., et al., *Neural EGF-like protein 1 (NELL-1): Signaling crosstalk in mesenchymal stem cells and applications in regenerative medicine.* Genes Dis, 2017. **4**(3): p. 127-137.

99. Chen, F., et al., *NELL-1-dependent mineralisation of Saos-2 human osteosarcoma cells is mediated via c-Jun N-terminal kinase pathway activation.* Int Orthop, 2012. **36**(10): p. 2181-7.

100. Guntur, A.R. and C.J. Rosen, *IGF-1 regulation of key signaling pathways in bone.* Bonekey Rep, 2013. **2**: p. 437.

101. Wabitsch, M., et al., *The role of growth hormone/insulin-like growth factors in adipocyte differentiation.* Metabolism, 1995. **44**(10 Suppl 4): p. 45-9.

102. Xian, L., et al., *Matrix IGF-1 maintains bone mass by activation of mTOR in mesenchymal stem cells.* Nat Med, 2012. **18**(7): p. 1095-101.

103. Parfitt, A.M., *Misconceptions (2): turnover is always higher in cancellous than in cortical bone.* Bone, 2002. **30**(6): p. 807-9.

104. Parfitt, A.M., *Age-related structural changes in trabecular and cortical bone: cellular mechanisms and biomechanical consequences.* Calcif Tissue Int, 1984. **36 Suppl 1**: p. S123-8.

105. Zebaze, R.M., et al., *Intracortical remodelling and porosity in the distal radius and post-mortem femurs of women: a cross-sectional study.* Lancet, 2010. **375**(9727): p. 1729-36.

106. Becerikli, M., et al., *Age-dependent alterations in osteoblast and osteoclast activity in human cancellous bone.* J Cell Mol Med, 2017. **21**(11): p. 2773-2781.

107. Lai, P., et al., *Loss of Rictor with aging in osteoblasts promotes age-related bone loss.* Cell Death Dis, 2016. **7**(10): p. e2408.

108. Udagawa, N., et al., *Osteoblasts/stromal cells stimulate osteoclast activation through expression of osteoclast differentiation factor/RANKL but not macrophage colony-stimulating factor: receptor activator of NF-kappa B ligand.* Bone, 1999. **25**(5): p. 517-23.

109. Walker, R.E., et al., *Myeloma bone disease: pathogenesis, current treatments and future targets.* Br Med Bull, 2014. **111**(1): p. 117-38.

110. Kodric, K., et al., *P4 medicine and osteoporosis: a systematic review.* Wien Klin Wochenschr, 2016. **128**(Suppl 7): p. 480-491.

111. Almeida, M., et al., *Estrogen receptor-alpha signaling in osteoblast progenitors stimulates cortical bone accrual.* J Clin Invest, 2013. **123**(1): p. 394-404.

112. Gao, Y., et al., *Crosstalk between Wnt/beta-catenin and estrogen receptor signaling synergistically promotes osteogenic differentiation of mesenchymal progenitor cells.* PLoS One, 2013. **8**(12): p. e82436.

113. Ardawi, M.S., et al., *High serum sclerostin predicts the occurrence of osteoporotic fractures in postmenopausal women: the Center of Excellence for Osteoporosis Research Study.* J Bone Miner Res, 2012. **27**(12): p. 2592-602.

114. Gibofsky, A., *Overview of epidemiology, pathophysiology, and diagnosis of rheumatoid arthritis.* Am J Manag Care, 2012. **18**(13 Suppl): p. S295-302.

115. Kitaura, H., et al., *Immunological reaction in TNF-alpha-mediated osteoclast formation and bone resorption in vitro and in vivo.* Clin Dev Immunol, 2013. **2013**: p. 181849.

116. Wu, Q., et al., *IL-6 Enhances Osteocyte-Mediated Osteoclastogenesis by Promoting JAK2 and RANKL Activity In Vitro.* Cell Physiol Biochem, 2017. **41**(4): p. 1360-1369.

117. Yoshitake, F., et al., *Interleukin-6 directly inhibits osteoclast differentiation by suppressing receptor activator of NF-kappaB signaling pathways.* J Biol Chem, 2008. **283**(17): p. 11535-40.

118. Scott, L.J., *Tocilizumab: A Review in Rheumatoid Arthritis.* Drugs, 2017. **77**(17): p. 1865-1879.

119. Feldmann, M. and R.N. Maini, *Anti-TNF alpha therapy of rheumatoid arthritis: what have we learned?* Annu Rev Immunol, 2001. **19**: p. 163-96.

120. Lopez-Otin, C., et al., *The hallmarks of aging.* Cell, 2013. **153**(6): p. 1194-217.

121. Almeida, M., *Aging mechanisms in bone.* Bonekey Rep, 2012. **1**.

122. Vidak, S. and R. Foisner, *Molecular insights into the premature aging disease progeria.* Histochem Cell Biol, 2016.

123. Zhang, J., et al., *A human iPSC model of Hutchinson Gilford Progeria reveals vascular smooth muscle and mesenchymal stem cell defects.* Cell Stem Cell, 2011. **8**(1): p. 31-45.

124. Liu, Y., et al., *Prelamin A accelerates vascular calcification via activation of the DNA damage response and senescence-associated secretory phenotype in vascular smooth muscle cells.* Circ Res, 2013. **112**(10): p. e99-109.

125. Olovnikov, A.M., *Telomeres, telomerase, and aging: origin of the theory.* Exp Gerontol, 1996. **31**(4): p. 443-8.

126. Armanios, M., et al., *Short telomeres are sufficient to cause the degenerative defects associated with aging.* Am J Hum Genet, 2009. **85**(6): p. 823-32.

127. Pignolo, R.J., et al., *Defects in telomere maintenance molecules impair osteoblast differentiation and promote osteoporosis.* Aging Cell, 2008. **7**(1): p. 23-31.

128. Roura, S., et al., *Effect of aging on the pluripotential capacity of human CD105+ mesenchymal stem cells.* Eur J Heart Fail, 2006. **8**(6): p. 555-63.

129. Lund, T.C., et al., *Mesenchymal stromal cells from donors varying widely in age are of equal cellular fitness after in vitro expansion under hypoxic conditions.* Cytotherapy, 2010. **12**(8): p. 971-81.

130. Fernandez, A.F., et al., *H3K4me1 marks DNA regions hypomethylated during aging in human stem and differentiated cells.* Genome Res, 2015. **25**(1): p. 27-40.

131. Peffers, M.J., et al., *Age-related changes in mesenchymal stem cells identified using a multi-omics approach.* Eur Cell Mater, 2016. **31**: p. 136-59.

132. Schellenberg, A., et al., *Proof of principle: quality control of therapeutic cell preparations using senescence-associated DNA-methylation changes.* BMC Res Notes, 2014. **7**: p. 254.

133. Bork, S., et al., *DNA methylation pattern changes upon long-term culture and aging of human mesenchymal stromal cells.* Aging Cell, 2010. **9**(1): p. 54-63.

134. Horvath, S., *DNA methylation age of human tissues and cell types.* Genome Biol, 2013. **14**(10): p. R115.

135. Gersch, R.P., et al., *Reactivation of Hox gene expression during bone regeneration.* J Orthop Res, 2005. **23**(4): p. 882-90.

136. Wagner, W., et al., *Aging and replicative senescence have related effects on human stem and progenitor cells.* PLoS One, 2009. **4**(6): p. e5846.

137. Leucht, P., et al., *Embryonic origin and Hox status determine progenitor cell fate during adult bone regeneration.* Development, 2008. **135**(17): p. 2845-54.

138. Candini, O., et al., *Mesenchymal progenitors aging highlights a miR-196 switch targeting HOXB7 as master regulator of proliferation and osteogenesis.* Stem Cells, 2015. **33**(3): p. 939-50.

139. Gonzalez-Martin, M.C., M. Mallo, and M.A. Ros, *Long bone development requires a threshold of Hox function.* Dev Biol, 2014. **392**(2): p. 454-65.

140. Li, Z., et al., *Epigenetic dysregulation in mesenchymal stem cell aging and spontaneous differentiation.* PLoS One, 2011. **6**(6): p. e20526.

141. Viswanathan, M. and H.A. Tissenbaum, *C. elegans sirtuins.* Methods Mol Biol, 2013. **1077**: p. 39-56.

142. Sun, W., et al., *Overexpression of Sirt1 in mesenchymal stem cells protects against bone loss in mice by FOXO3a deacetylation and oxidative stress inhibition.* Metabolism, 2018. **88**: p. 61-71.

143. Herranz, D., et al., *Sirt1 improves healthy ageing and protects from metabolic syndrome-associated cancer.* Nat Commun, 2010. **1**: p. 3.

144. Solomon, J.M., et al., *Inhibition of SIRT1 catalytic activity increases p53 acetylation but does not alter cell survival following DNA damage.* Mol Cell Biol, 2006. **26**(1): p. 28-38.

145. Simic, P., et al., *SIRT1 regulates differentiation of mesenchymal stem cells by deacetylating beta-catenin.* EMBO Mol Med, 2013. **5**(3): p. 430-40.

146. Lemieux, M.E., et al., *The Sirt1 deacetylase modulates the insulin-like growth factor signaling pathway in mammals.* Mech Ageing Dev, 2005. **126**(10): p. 1097-105.

147. Cohen-Kfir, E., et al., *Sirt1 is a regulator of bone mass and a repressor of Sost encoding for sclerostin, a bone formation inhibitor.* Endocrinology, 2011. **152**(12): p. 4514-24.

148. Almeida, M. and R.M. Porter, *Sirtuins and FoxOs in osteoporosis and osteoarthritis.* Bone, 2019. **121**: p. 284-292.

149. Yu, K.R., et al., *MicroRNA-141-3p plays a role in human mesenchymal stem cell aging by directly targeting ZMPSTE24.* J Cell Sci, 2013. **126**(Pt 23): p. 5422-31.

150. Pasumarthy, K.K., et al., *Methylome Analysis of Human Bone Marrow MSCs Reveals Extensive Age- and Culture-Induced Changes at Distal Regulatory Elements.* Stem Cell Reports, 2017. **9**(3): p. 999-1015.

151. Li, C.J., et al., *MicroRNA-188 regulates age-related switch between osteoblast and adipocyte differentiation.* J Clin Invest, 2015. **125**(4): p. 1509-22.

152. Ma, Y., et al., *Autophagy controls mesenchymal stem cell properties and senescence during bone aging.* Aging Cell, 2018. **17**(1).

153. Martin, S.K., et al., *Brief report: the differential roles of mTORC1 and mTORC2 in mesenchymal stem cell differentiation.* Stem Cells, 2015. **33**(4): p. 1359-65.

154. Qi, M., et al., *Autophagy Maintains the Function of Bone Marrow Mesenchymal Stem Cells to Prevent Estrogen Deficiency-Induced Osteoporosis.* Theranostics, 2017. **7**(18): p. 4498-4516.

155. Infante, A. and C.I. Rodriguez, *Osteogenesis and aging: lessons from mesenchymal stem cells.* Stem Cell Res Ther, 2018. **9**(1): p. 244.

156. Fitter, S., et al., *mTORC1 Plays an Important Role in Skeletal Development by Controlling Preosteoblast Differentiation.* Mol Cell Biol, 2017. **37**(7).

157. Morley, J.F. and R.I. Morimoto, *Regulation of longevity in Caenorhabditis elegans by heat shock factor and molecular chaperones.* Mol Biol Cell, 2004. **15**(2): p. 657-64.

158. Tatar, M., A.A. Khazaeli, and J.W. Curtsinger, *Chaperoning extended life.* Nature, 1997. **390**(6655): p. 30.

159. Li, C., et al., *Downregulation of Heat Shock Protein 70 Impairs Osteogenic and Chondrogenic Differentiation in Human Mesenchymal Stem Cells.* Sci Rep, 2018. **8**(1): p. 553.

160. Fontana, L., L. Partridge, and V.D. Longo, *Extending healthy life span--from yeast to humans.* Science, 2010. **328**(5976): p. 321-6.

161. Evdokimova, V., et al., *IGFBP7 binds to the IGF-1 receptor and blocks its activation by insulin-like growth factors.* Sci Signal, 2012. **5**(255): p. ra92.

162. Zhang, W., et al., *IGFBP7 regulates the osteogenic differentiation of bone marrow-derived mesenchymal stem cells via Wnt/beta-catenin signaling pathway.* FASEB J, 2018. **32**(4): p. 2280-2291.

163. Schlupf, J. and H. Steinbeisser, *IGF antagonizes the Wnt/beta-Catenin pathway and promotes differentiation of extra-embryonic endoderm.* Differentiation, 2014. **87**(5): p. 209-19.

164. Johnson, S.C., P.S. Rabinovitch, and M. Kaeberlein, *mTOR is a key modulator of ageing and age-related disease.* Nature, 2013. **493**(7432): p. 338-45.

165. Cho, H.J., et al., *Regulation of adipocyte differentiation and insulin action with rapamycin.* Biochem Biophys Res Commun, 2004. **321**(4): p. 942-8.

166. Redza-Dutordoir, M. and D.A. Averill-Bates, *Activation of apoptosis signalling pathways by reactive oxygen species.* Biochim Biophys Acta, 2016. **1863**(12): p. 2977-2992.

167. Hekimi, S., J. Lapointe, and Y. Wen, *Taking a "good" look at free radicals in the aging process.* Trends Cell Biol, 2011. **21**(10): p. 569-76.

168. Lee, B.Y., et al., *Senescence-associated beta-galactosidase is lysosomal beta-galactosidase.* Aging Cell, 2006. **5**(2): p. 187-95.

169. Collado, M. and M. Serrano, *Senescence in tumours: evidence from mice and humans.* Nat Rev Cancer, 2010. **10**(1): p. 51-7.

170. Ozcan, S., et al., *Unbiased analysis of senescence associated secretory phenotype (SASP) to identify common components following different genotoxic stresses.* Aging (Albany NY), 2016. **8**(7): p. 1316-29.

171. Conboy, I.M. and T.A. Rando, *Heterochronic parabiosis for the study of the effects of aging on stem cells and their niches.* Cell Cycle, 2012. **11**(12): p. 2260-7.

172. Gruber, R., et al., *Fracture healing in the elderly patient.* Exp Gerontol, 2006. **41**(11): p. 1080-93.

173. Molofsky, A.V., et al., *Increasing p16INK4a expression decreases forebrain progenitors and neurogenesis during ageing.* Nature, 2006. **443**(7110): p. 448-52.

174. Shaw, A.C., et al., *Aging of the innate immune system.* Curr Opin Immunol, 2010. **22**(4): p. 507-13.

175. Shen, J., et al., *Transplantation of mesenchymal stem cells from young donors delays aging in mice.* Sci Rep, 2011. **1**: p. 67.

176. Lavasani, M., et al., *Muscle-derived stem/progenitor cell dysfunction limits healthspan and lifespan in a murine progeria model.* Nat Commun, 2012. **3**: p. 608.

177. Takai, D. and P.A. Jones, *Comprehensive analysis of CpG islands in human chromosomes 21 and 22.* Proc Natl Acad Sci U S A, 2002. **99**(6): p. 3740-5.

178. Marini, F., L. Cianferotti, and M.L. Brandi, *Epigenetic Mechanisms in Bone Biology and Osteoporosis: Can They Drive Therapeutic Choices?* Int J Mol Sci, 2016. **17**(8).

179. Clapier, C.R. and B.R. Cairns, *The biology of chromatin remodeling complexes.* Annu Rev Biochem, 2009. **78**: p. 273-304.

180. Mortimer, S.A., M.A. Kidwell, and J.A. Doudna, *Insights into RNA structure and function from genome-wide studies.* Nat Rev Genet, 2014. **15**(7): p. 469-79.

181. Mills, J.D., Y. Kawahara, and M. Janitz, *Strand-Specific RNA-Seq Provides Greater Resolution of Transcriptome Profiling.* Curr Genomics, 2013. **14**(3): p. 173-81.

182. Buenrostro, J.D., et al., *Transposition of native chromatin for fast and sensitive epigenomic profiling of open chromatin, DNA-binding proteins and nucleosome position.* Nat Methods, 2013. **10**(12): p. 1213-8.

183. Corces, M.R., et al., *The chromatin accessibility landscape of primary human cancers.* Science, 2018. **362**(6413).

184. Lara-Astiaso, D., et al., *Immunogenetics. Chromatin state dynamics during blood formation.* Science, 2014. **345**(6199): p. 943-9.

185. Dedeurwaerder, S., et al., *A comprehensive overview of Infinium HumanMethylation450 data processing.* Brief Bioinform, 2014. **15**(6): p. 929-41.

186. Bibikova, M., et al., *High density DNA methylation array with single CpG site resolution.* Genomics, 2011. **98**(4): p. 288-95.

187. Moran, S., C. Arribas, and M. Esteller, *Validation of a DNA methylation microarray for 850,000 CpG sites of the human genome enriched in enhancer sequences.* Epigenomics, 2016. **8**(3): p. 389-99.

188. Heyn, H., et al., *DNA methylation contributes to natural human variation.* Genome Res, 2013. **23**(9): p. 1363-72.

189. Heyn, H., et al., *Distinct DNA methylomes of newborns and centenarians.* Proc Natl Acad Sci U S A, 2012. **109**(26): p. 10522-7.

190. Villanueva, A., et al., *DNA methylation-based prognosis and epidrivers in hepatocellular carcinoma.* Hepatology, 2015. **61**(6): p. 1945-56.

191. Weisenberger, D.J., *Characterizing DNA methylation alterations from The Cancer Genome Atlas.* J Clin Invest, 2014. **124**(1): p. 17-23.

192. Sandoval, J., et al., *A prognostic DNA methylation signature for stage I non-small-cell lung cancer.* J Clin Oncol, 2013. **31**(32): p. 4140-7.

193. Pidsley, R., et al., *Critical evaluation of the Illumina MethylationEPIC BeadChip microarray for whole-genome DNA methylation profiling.* Genome Biol, 2016. **17**(1): p. 208.

194. Bendall, S.C., et al., *Single-cell mass cytometry of differential immune and drug responses across a human hematopoietic continuum.* Science, 2011. **332**(6030): p. 687-96.

195. Duckworth, A.D., et al., *Multiplexed profiling of RNA and protein expression signatures in individual cells using flow or mass cytometry.* Nat Protoc, 2019. **14**(3): p. 901-920.

196. Spitzer, M.H. and G.P. Nolan, *Mass Cytometry: Single Cells, Many Features.* Cell, 2016. **165**(4): p. 780-91.

197. Li, J., et al., *Normalization, testing, and false discovery rate estimation for RNA-sequencing data.* Biostatistics, 2012. **13**(3): p. 523-38.

198. Conesa, A., et al., *A survey of best practices for RNA-seq data analysis.* Genome Biol, 2016. **17**: p. 13.

199. Anders, S. and W. Huber, *Differential expression analysis for sequence count data.* Genome Biol, 2010. **11**(10): p. R106.

200. Gagnon-Bartsch, J.A. and T.P. Speed, *Using control genes to correct for unwanted variation in microarray data.* Biostatistics, 2012. **13**(3): p. 539-52.

201. Leek, J.T. and J.D. Storey, *Capturing heterogeneity in gene expression studies by surrogate variable analysis.* PLoS Genet, 2007. **3**(9): p. 1724-35.

202. Oberg, A.L., et al., *Technical and biological variance structure in mRNA-Seq data: life in the real world.* BMC Genomics, 2012. **13**: p. 304.

203. Seyednasrollah, F., A. Laiho, and L.L. Elo, *Comparison of software packages for detecting differential expression in RNA-seq studies.* Brief Bioinform, 2015. **16**(1): p. 59-70.

204. Chen, Y.A., et al., *Discovery of cross-reactive probes and polymorphic CpGs in the Illumina Infinium HumanMethylation450 microarray.* Epigenetics, 2013. **8**(2): p. 203-9.

205. Fluidigm, *Maxpar® Nuclear Antigen Staining with Fresh Fix.* https://www.fluidigm.com/binaries/content/documents/fluidigm/marketing/maxpar-nuclear-

antigen-staining-400277-pr/maxpar-nuclear-antigen-staining-400277-pr/fluidigm%3Afile, Last accessed 14/09/2019.

206. Lai, L., J.G. Yeo, and S. Albani, *Singlet gating in mass cytometry.* Cytometry A, 2017. **91**(2): p. 170-172.

207. Sims, D., et al., *High-throughput RNA interference screening using pooled shRNA libraries and next generation sequencing.* Genome Biol, 2011. **12**(10): p. R104.

208. Dai, Z., et al., *edgeR: a versatile tool for the analysis of shRNA-seq and CRISPR-Cas9 genetic screens.* F1000Res, 2014. **3**: p. 95.

209. Khan, H., et al., *The effects of ageing on differentiation and characterisation of human mesenchymal stem cells.* Curr Stem Cell Res Ther, 2016.

210. Stenderup, K., et al., *Aging is associated with decreased maximal life span and accelerated senescence of bone marrow stromal cells.* Bone, 2003. **33**(6): p. 919-26.

211. Khan, H., et al., *The Effects of Ageing on Differentiation and Characterisation of Human Mesenchymal Stem Cells.* Curr Stem Cell Res Ther, 2018. **13**(5): p. 378-383.

212. Aksoy, C., et al., *Structural investigation of donor age effect on human bone marrow mesenchymal stem cells: FTIR spectroscopy and imaging.* Age (Dordr), 2014. **36**(4): p. 9691.

213. D'Ippolito, G., et al., *Age-related osteogenic potential of mesenchymal stromal stem cells from human vertebral bone marrow.* J Bone Miner Res, 1999. **14**(7): p. 1115-22.

214. Zaim, M., et al., *Donor age and long-term culture affect differentiation and proliferation of human bone marrow mesenchymal stem cells.* Ann Hematol, 2012. **91**(8): p. 1175-86.

215. Siegel, G., et al., *Phenotype, donor age and gender affect function of human bone marrow-derived mesenchymal stromal cells.* BMC Med, 2013. **11**: p. 146.

216. Moerman, E.J., et al., *Aging activates adipogenic and suppresses osteogenic programs in mesenchymal marrow stroma/stem cells: the role of PPAR-gamma2 transcription factor and TGF-beta/BMP signaling pathways.* Aging Cell, 2004. **3**(6): p. 379-89.

217. Astudillo, P., et al., *Increased adipogenesis of osteoporotic human-mesenchymal stem cells (MSCs) characterizes by impaired leptin action.* J Cell Biochem, 2008. **103**(4): p. 1054-65.

218. Coipeau, P., et al., *Impaired differentiation potential of human trabecular bone mesenchymal stromal cells from elderly patients.* Cytotherapy, 2009. **11**(5): p. 584-94.

219. Mueller, S.M. and J. Glowacki, *Age-related decline in the osteogenic potential of human bone marrow cells cultured in three-dimensional collagen sponges.* J Cell Biochem, 2001. **82**(4): p. 583-90.

220. Yang, Y.K., et al., *Changes in phenotype and differentiation potential of human mesenchymal stem cells aging in vitro.* Stem Cell Res Ther, 2018. **9**(1): p. 131.

221. Bonab, M.M., et al., *Aging of mesenchymal stem cell in vitro.* BMC Cell Biol, 2006. **7**: p. 14.

222. Bertolo, A., et al., *An in vitro expansion score for tissue-engineering applications with human bone marrow-derived mesenchymal stem cells.* J Tissue Eng Regen Med, 2016. **10**(2): p. 149-61.

223. Xue, W., et al., *Senescence and tumour clearance is triggered by p53 restoration in murine liver carcinomas.* Nature, 2007. **445**(7128): p. 656-60.

224. Kang, T.W., et al., *Senescence surveillance of pre-malignant hepatocytes limits liver cancer development.* Nature, 2011. **479**(7374): p. 547-51.

225. Schellenberg, A., et al., *Matrix elasticity, replicative senescence and DNA methylation patterns of mesenchymal stem cells.* Biomaterials, 2014. **35**(24): p. 6351-8.

226. Hanzelmann, S., et al., *Replicative senescence is associated with nuclear reorganization and with DNA methylation at specific transcription factor binding sites.* Clin Epigenetics, 2015. **7**(1): p. 19.

227. Soshnikova, N. and D. Duboule, *Epigenetic regulation of vertebrate Hox genes: a dynamic equilibrium.* Epigenetics, 2009. **4**(8): p. 537-40.

228. Zhu, Y., et al., *Alteration of histone acetylation pattern during long-term serum-free culture conditions of human fetal placental mesenchymal stem cells.* PLoS One, 2015. **10**(2): p. e0117068.

229. Noer, A., L.C. Lindeman, and P. Collas, *Histone H3 modifications associated with differentiation and long-term culture of mesenchymal adipose stem cells.* Stem Cells Dev, 2009. **18**(5): p. 725-36.

230. Lynch, P.J., et al., *Chromatin Changes at the PPAR-gamma2 Promoter During Bone Marrow-Derived Multipotent Stromal Cell Culture Correlate With Loss of Gene Activation Potential.* Stem Cells, 2015. **33**(7): p. 2169-81.

231. Mindaye, S.T., et al., *Global proteomic signature of undifferentiated human bone marrow stromal cells: evidence for donor-to-donor proteome heterogeneity.* Stem Cell Res, 2013. **11**(2): p. 793-805.

232. Day, T.F., et al., *Wnt/beta-catenin signaling in mesenchymal progenitors controls osteoblast and chondrocyte differentiation during vertebrate skeletogenesis.* Dev Cell, 2005. **8**(5): p. 739-50.

233. Tacutu, R., et al., *Human Ageing Genomic Resources: integrated databases and tools for the biology and genetics of ageing.* Nucleic Acids Res, 2013. **41**(Database issue): p. D1027-33.

234. Vaquerizas, J.M., et al., *A census of human transcription factors: function, expression and evolution.* Nat Rev Genet, 2009. **10**(4): p. 252-63.

235. Medvedeva, Y.A., et al., *EpiFactors: a comprehensive database of human epigenetic factors and complexes.* Database (Oxford), 2015. **2015**: p. bav067.

236. Ling, L., V. Nurcombe, and S.M. Cool, *Wnt signaling controls the fate of mesenchymal stem cells.* Gene, 2009. **433**(1-2): p. 1-7.

237. Long, H., et al., *miR-139-5p Represses BMSC Osteogenesis via Targeting Wnt/beta-Catenin Signaling Pathway.* DNA Cell Biol, 2017. **36**(8): p. 715-724.

238. Boyden, L.M., et al., *High bone density due to a mutation in LDL-receptor-related protein 5.* N Engl J Med, 2002. **346**(20): p. 1513-21.

239. Lories, R.J., et al., *Articular cartilage and biomechanical properties of the long bones in Frzb-knockout mice.* Arthritis Rheum, 2007. **56**(12): p. 4095-103.

240. Little, R.D., et al., *A mutation in the LDL receptor-related protein 5 gene results in the autosomal dominant high-bone-mass trait.* Am J Hum Genet, 2002. **70**(1): p. 11-9.

241. Christodoulides, C., et al., *The Wnt antagonist Dickkopf-1 and its receptors are coordinately regulated during early human adipogenesis.* J Cell Sci, 2006. **119**(Pt 12): p. 2613-2620.

242. Kim, J.A., et al., *Regulation of mesenchymal stromal cells through fine tuning of canonical Wnt signaling.* Stem Cell Res, 2015. **14**(3): p. 356-68.

243. Liu, J. and S.R. Farmer, *Regulating the balance between peroxisome proliferator-activated receptor gamma and beta-catenin signaling during adipogenesis. A glycogen synthase kinase 3beta phosphorylation-defective mutant of beta-catenin inhibits expression of a subset of adipogenic genes.* J Biol Chem, 2004. **279**(43): p. 45020-7.

244. Ross, S.E., et al., *Inhibition of adipogenesis by Wnt signaling.* Science, 2000. **289**(5481): p. 950-3.

245. Liu, J., et al., *Functional interaction between peroxisome proliferator-activated receptor gamma and beta-catenin.* Mol Cell Biol, 2006. **26**(15): p. 5827-37.

246. Gong, Y., et al., *LDL receptor-related protein 5 (LRP5) affects bone accrual and eye development.* Cell, 2001. **107**(4): p. 513-23.

247. Lazarenko, O.P., et al., *Netoglitazone is a PPAR-gamma ligand with selective effects on bone and fat.* Bone, 2006. **38**(1): p. 74-84.

248. Boyce, B.F. and L. Xing, *The RANKL/RANK/OPG pathway.* Curr Osteoporos Rep, 2007. **5**(3): p. 98-104.

249. Mori, K., et al., *Diabetic osteopenia by decreased beta-catenin signaling is partly induced by epigenetic derepression of sFRP-4 gene.* PLoS One, 2014. **9**(7): p. e102797.

250. Harmer, D., C. Falank, and M.R. Reagan, *Interleukin-6 Interweaves the Bone Marrow Microenvironment, Bone Loss, and Multiple Myeloma.* Front Endocrinol (Lausanne), 2018. **9**: p. 788.

251. Dai, J., et al., *Chronic alcohol ingestion induces osteoclastogenesis and bone loss through IL-6 in mice.* J Clin Invest, 2000. **106**(7): p. 887-95.

252. Cakouros, D. and S. Gronthos, *Epigenetic Regulation of Bone Marrow Stem Cell Aging: Revealing Epigenetic Signatures associated with Hematopoietic and Mesenchymal Stem Cell Aging.* Aging Dis, 2019. **10**(1): p. 174-189.

253. Ma, Y., K. Kanakousaki, and L. Buttitta, *How the cell cycle impacts chromatin architecture and influences cell fate.* Front Genet, 2015. **6**: p. 19.

254. Hauer, M.H. and S.M. Gasser, *Chromatin and nucleosome dynamics in DNA damage and repair*. Genes Dev, 2017. **31**(22): p. 2204-2221.

255. Gnani, D., et al., *An early-senescence state in aged mesenchymal stromal cells contributes to hematopoietic stem and progenitor cell clonogenic impairment through the activation of a pro-inflammatory program.* Aging Cell, 2019. **18**(3): p. e12933.

256. Alves, H., et al., *A mesenchymal stromal cell gene signature for donor age.* PLoS One, 2012. **7**(8): p. e42908.

257. Mirabella, A.C., B.M. Foster, and T. Bartke, *Chromatin deregulation in disease.* Chromosoma, 2016. **125**(1): p. 75-93.

258. Wu, H., et al., *Genomic occupancy of Runx2 with global expression profiling identifies a novel dimension to control of osteoblastogenesis.* Genome Biol, 2014. **15**(3): p. R52.

259. Del Real, A., et al., *Differential analysis of genome-wide methylation and gene expression in mesenchymal stem cells of patients with fractures and osteoarthritis.* Epigenetics, 2017. **12**(2): p. 113-122.

260. Sanyal, A., et al., *The long-range interaction landscape of gene promoters.* Nature, 2012. **489**(7414): p. 109-13.

261. Jimenez, M.A., et al., *Critical role for Ebf1 and Ebf2 in the adipogenic transcriptional cascade.* Mol Cell Biol, 2007. **27**(2): p. 743-57.

262. Kang, S., et al., *Regulation of early adipose commitment by Zfp521.* PLoS Biol, 2012. **10**(11): p. e1001433.

263. Wilson, R.C. and J.A. Doudna, *Molecular mechanisms of RNA interference.* Annu Rev Biophys, 2013. **42**: p. 217-39.

264. Zufferey, R., et al., *Self-inactivating lentivirus vector for safe and efficient in vivo gene delivery.* J Virol, 1998. **72**(12): p. 9873-80.

265. Bokhoven, M., et al., *Insertional gene activation by lentiviral and gammaretroviral vectors.* J Virol, 2009. **83**(1): p. 283-94.

266. Li, C., et al., *Donor Age and Cell Passage Affect Osteogenic Ability of Rat Bone Marrow Mesenchymal Stem Cells.* Cell Biochem Biophys, 2015. **72**(2): p. 543-9.

267. Kretlow, J.D., et al., *Donor age and cell passage affects differentiation potential of murine bone marrow-derived stem cells.* BMC Cell Biol, 2008. **9**: p. 60.

268. Geissler, S., et al., *Functional comparison of chronological and in vitro aging: differential role of the cytoskeleton and mitochondria in mesenchymal stromal cells.* PLoS One, 2012. **7**(12): p. e52700.

269. Robledo, R.F., et al., *The Dlx5 and Dlx6 homeobox genes are essential for craniofacial, axial, and appendicular skeletal development.* Genes Dev, 2002. **16**(9): p. 1089-101.

270. Pawar, N.M. and P. Rao, *Secreted frizzled related protein 4 (sFRP4) update: A brief review.* Cell Signal, 2018. **45**: p. 63-70.

271. Horvath, S. and K. Raj, *DNA methylation-based biomarkers and the epigenetic clock theory of ageing.* Nat Rev Genet, 2018. **19**(6): p. 371-384.

272. Kessler, R., G. Hausmann, and K. Basler, *The PHD domain is required to link Drosophila Pygopus to Legless/beta-catenin and not to histone H3.* Mech Dev, 2009. **126**(8-9): p. 752-9.

273. Hu, C.J., et al., *The N-terminal transactivation domain confers target gene specificity of hypoxia-inducible factors HIF-1alpha and HIF-2alpha.* Mol Biol Cell, 2007. **18**(11): p. 4528-42.

274. Thompson, B., et al., *A new nuclear component of the Wnt signalling pathway.* Nat Cell Biol, 2002. **4**(5): p. 367-73.

275. Belenkaya, T.Y., et al., *pygopus Encodes a nuclear protein essential for wingless/Wnt signaling.* Development, 2002. **129**(17): p. 4089-101.

276. Schwab, K.R., et al., *Pygo1 and Pygo2 roles in Wnt signaling in mammalian kidney development.* BMC Biol, 2007. **5**: p. 15.

277. Cluse, L.A., et al., *A Comprehensive Protocol Resource for Performing Pooled shRNA and CRISPR Screens.* Methods Mol Biol, 2018. **1725**: p. 201-227.

278. Ranzani, M., et al., *Lentiviral vector-based insertional mutagenesis identifies genes associated with liver cancer.* Nat Methods, 2013. **10**(2): p. 155-61.

279. Piovesan, A., et al., *GeneBase 1.1: a tool to summarize data from NCBI gene datasets and its application to an update of human gene statistics.* Database (Oxford), 2016. **2016**.

280. Zhang, Z., et al., *PRC2 complexes with JARID2, MTF2, and esPRC2p48 in ES cells to modulate ES cell pluripotency and somatic cell reprogramming.* Stem Cells, 2011. **29**(2): p. 229-40.

281. Tong, Z.T., et al., *EZH2 supports nasopharyngeal carcinoma cell aggressiveness by forming a co-repressor complex with HDAC1/HDAC2 and Snail to inhibit E-cadherin.* Oncogene, 2012. **31**(5): p. 583-94.

282. Walker, E., et al., *Polycomb-like 2 associates with PRC2 and regulates transcriptional networks during mouse embryonic stem cell self-renewal and differentiation.* Cell Stem Cell, 2010. **6**(2): p. 153-66.

283. Kuzmichev, A., et al., *Role of the Sin3-histone deacetylase complex in growth regulation by the candidate tumor suppressor p33(ING1).* Mol Cell Biol, 2002. **22**(3): p. 835-48.

284. Knopp, Y., et al., *Transient Retrovirus-Based CRISPR/Cas9 All-in-One Particles for Efficient, Targeted Gene Knockout.* Mol Ther Nucleic Acids, 2018. **13**: p. 256-274.

285. Nakashima, K. and B. de Crombrugghe, *Transcriptional mechanisms in osteoblast differentiation and bone formation.* Trends Genet, 2003. **19**(8): p. 458-66.

286. Komori, T., *Runx2, an inducer of osteoblast and chondrocyte differentiation.* Histochem Cell Biol, 2018. **149**(4): p. 313-323.

287. Lian, J.B. and G.S. Stein, *Runx2/Cbfa1: a multifunctional regulator of bone formation.* Curr Pharm Des, 2003. **9**(32): p. 2677-85.

288. Ito, Y., *Molecular basis of tissue-specific gene expression mediated by the runt domain transcription factor PEBP2/CBF.* Genes Cells, 1999. **4**(12): p. 685-96.

289. Li, Q.L., et al., *Causal relationship between the loss of RUNX3 expression and gastric cancer.* Cell, 2002. **109**(1): p. 113-24.

290. Okuda, T., et al., *AML1, the target of multiple chromosomal translocations in human leukemia, is essential for normal fetal liver hematopoiesis.* Cell, 1996. **84**(2): p. 321-30.

291. Soung do, Y., et al., *Runx3/AML2/Cbfa3 regulates early and late chondrocyte differentiation.* J Bone Miner Res, 2007. **22**(8): p. 1260-70.

292. Schroeder, T.M., et al., *Histone deacetylase 3 interacts with runx2 to repress the osteocalcin promoter and regulate osteoblast differentiation.* J Biol Chem, 2004. **279**(40): p. 41998-2007.

293. D'Alonzo, R.C., et al., *Physical interaction of the activator protein-1 factors c-Fos and c-Jun with Cbfa1 for collagenase-3 promoter activation.* J Biol Chem, 2002. **277**(1): p. 816-22.

294. Baniwal, S.K., et al., *Repression of Runx2 by androgen receptor (AR) in osteoblasts and prostate cancer cells: AR binds Runx2 and abrogates its recruitment to DNA.* Mol Endocrinol, 2009. **23**(8): p. 1203-14.

295. Hanai, J., et al., *Interaction and functional cooperation of PEBP2/CBF with Smads. Synergistic induction of the immunoglobulin germline Calpha promoter*. J Biol Chem, 1999. **274**(44): p. 31577-82.

296. Zhang, Y.W., et al., *A RUNX2/PEBP2alpha A/CBFA1 mutation displaying impaired transactivation and Smad interaction in cleidocranial dysplasia.* Proc Natl Acad Sci U S A, 2000. **97**(19): p. 10549-54.

297. Komori, T., et al., *Targeted disruption of Cbfa1 results in a complete lack of bone formation owing to maturational arrest of osteoblasts.* Cell, 1997. **89**(5): p. 755-64.

298. Mundlos, S., et al., *Mutations involving the transcription factor CBFA1 cause cleidocranial dysplasia.* Cell, 1997. **89**(5): p. 773-9.

299. Miller, J., et al., *The core-binding factor beta subunit is required for bone formation and hematopoietic maturation.* Nat Genet, 2002. **32**(4): p. 645-9.

300. Kundu, M., et al., *Cbfbeta interacts with Runx2 and has a critical role in bone development.* Nat Genet, 2002. **32**(4): p. 639-44.

301. Kawane, T., et al., *Dlx5 and mef2 regulate a novel runx2 enhancer for osteoblast-specific expression.* J Bone Miner Res, 2014. **29**(9): p. 1960-9.

302. Komori, T., *Roles of Runx2 in Skeletal Development.* Adv Exp Med Biol, 2017. **962**: p. 83-93.

303. Hu, H., et al., *Sequential roles of Hedgehog and Wnt signaling in osteoblast development.* Development, 2005. **132**(1): p. 49-60.

304. St-Jacques, B., M. Hammerschmidt, and A.P. McMahon, *Indian hedgehog signaling regulates proliferation and differentiation of chondrocytes and is essential for bone formation.* Genes Dev, 1999. **13**(16): p. 2072-86.

305. Rodda, S.J. and A.P. McMahon, *Distinct roles for Hedgehog and canonical Wnt signaling in specification, differentiation and maintenance of osteoblast progenitors.* Development, 2006. **133**(16): p. 3231-44.

306. Hill, T.P., et al., *Canonical Wnt/beta-catenin signaling prevents osteoblasts from differentiating into chondrocytes.* Dev Cell, 2005. **8**(5): p. 727-38.

307. Bruderer, M., et al., *Role and regulation of RUNX2 in osteogenesis.* Eur Cell Mater, 2014. **28**: p. 269-86.

308. Nakashima, K., et al., *The novel zinc finger-containing transcription factor osterix is required for osteoblast differentiation and bone formation.* Cell, 2002. **108**(1): p. 17-29.

309. Grzesik, W.J., et al., *Age-related changes in human bone proteoglycan structure. Impact of osteogenesis imperfecta.* J Biol Chem, 2002. **277**(46): p. 43638-47.

310. Le Blanc, K., et al., *Fetal mesenchymal stem-cell engraftment in bone after in utero transplantation in a patient with severe osteogenesis imperfecta.* Transplantation, 2005. **79**(11): p. 1607-14.

311. Gioia, R., et al., *Impaired osteoblastogenesis in a murine model of dominant osteogenesis imperfecta: a new target for osteogenesis imperfecta pharmacological therapy.* Stem Cells, 2012. **30**(7): p. 1465-76.

312. Bodziony, J., et al., *[Alkaline phosphatase and its isoenzyme activity of the blood in osteogenesis imperfecta before and during treatment with calcitonin].* Padiatr Grenzgeb, 1988. **27**(4): p. 259-67.

313. Hunter, G.K. and H.A. Goldberg, *Nucleation of hydroxyapatite by bone sialoprotein.* Proc Natl Acad Sci U S A, 1993. **90**(18): p. 8562-5.

314. Hunter, G.K., C.L. Kyle, and H.A. Goldberg, *Modulation of crystal formation by bone phosphoproteins: structural specificity of the osteopontin-mediated inhibition of hydroxyapatite formation.* Biochem J, 1994. **300 (Pt 3)**: p. 723-8.

315. Rutkovskiy, A., K.O. Stenslokken, and I.J. Vaage, *Osteoblast Differentiation at a Glance.* Med Sci Monit Basic Res, 2016. **22**: p. 95-106.

316. Hino, K., et al., *Master regulator for chondrogenesis, Sox9, regulates transcriptional activation of the endoplasmic reticulum stress transducer BBF2H7/CREB3L2 in chondrocytes.* J Biol Chem, 2014. **289**(20): p. 13810-20.

317. Kwok, C., et al., *Mutations in SOX9, the gene responsible for Campomelic dysplasia and autosomal sex reversal.* Am J Hum Genet, 1995. **57**(5): p. 1028-36.

318. Akiyama, H., et al., *The transcription factor Sox9 has essential roles in successive steps of the chondrocyte differentiation pathway and is required for expression of Sox5 and Sox6.* Genes Dev, 2002. **16**(21): p. 2813-28.

319. Smits, P., et al., *Sox5 and Sox6 are needed to develop and maintain source, columnar, and hypertrophic chondrocytes in the cartilage growth plate.* J Cell Biol, 2004. **164**(5): p. 747-58.

320. Takigawa, Y., et al., *The transcription factor Znf219 regulates chondrocyte differentiation by assembling a transcription factory with Sox9.* J Cell Sci, 2010. **123**(Pt 21): p. 3780-8.

321. Topol, L., et al., *Sox9 inhibits Wnt signaling by promoting beta-catenin phosphorylation in the nucleus.* J Biol Chem, 2009. **284**(5): p. 3323-33.

322. Yoshida, C.A., et al., *Runx2 and Runx3 are essential for chondrocyte maturation, and Runx2 regulates limb growth through induction of Indian hedgehog.* Genes Dev, 2004. **18**(8): p. 952-63.

323. Cheng, A. and P.G. Genever, *SOX9 determines RUNX2 transactivity by directing intracellular degradation.* J Bone Miner Res, 2010. **25**(12): p. 2680-9.

324. Inada, M., et al., *Maturational disturbance of chondrocytes in Cbfa1-deficient mice.* Dev Dyn, 1999. **214**(4): p. 279-90.

325. Zhou, G., et al., *Dominance of SOX9 function over RUNX2 during skeletogenesis.* Proc Natl Acad Sci U S A, 2006. **103**(50): p. 19004-9.

326. Lefterova, M.I., et al., *PPARgamma and the global map of adipogenesis and beyond.* Trends Endocrinol Metab, 2014. **25**(6): p. 293-302.

327. Tontonoz, P. and B.M. Spiegelman, *Fat and beyond: the diverse biology of PPARgamma.* Annu Rev Biochem, 2008. **77**: p. 289-312.

328. Lefterova, M.I., et al., *PPARgamma and C/EBP factors orchestrate adipocyte biology via adjacent binding on a genome-wide scale.* Genes Dev, 2008. **22**(21): p. 2941-52.

329. Cariou, B., B. Charbonnel, and B. Staels, *Thiazolidinediones and PPARgamma agonists: time for a reassessment.* Trends Endocrinol Metab, 2012. **23**(5): p. 205-15.

330. Almuraikhy, S., et al., *Interleukin-6 induces impairment in human subcutaneous adipogenesis in obesity-associated insulin resistance.* Diabetologia, 2016. **59**(11): p. 2406-2416.

331. Gervois, P., et al., *Regulation of lipid and lipoprotein metabolism by PPAR activators.* Clin Chem Lab Med, 2000. **38**(1): p. 3-11.

332. Damcott, C.M., et al., *Genetic variation in fatty acid-binding protein-4 and peroxisome proliferator-activated receptor gamma interactively influence insulin sensitivity and body composition in males.* Metabolism, 2004. **53**(3): p. 303-9.

333. Garin-Shkolnik, T., et al., *FABP4 attenuates PPARgamma and adipogenesis and is inversely correlated with PPARgamma in adipose tissues.* Diabetes, 2014. **63**(3): p. 900-11.

334. Ge, C., et al., *Reciprocal Control of Osteogenic and Adipogenic Differentiation by ERK/MAP Kinase Phosphorylation of Runx2 and PPARgamma Transcription Factors.* J Cell Physiol, 2016. **231**(3): p. 587-96.

335. Herlofsen, S.R., et al., *Brief report: importance of SOX8 for in vitro chondrogenic differentiation of human mesenchymal stromal cells.* Stem Cells, 2014. **32**(6): p. 1629-35.

336. Park, O.J., et al., *FGF2-activated ERK mitogen-activated protein kinase enhances Runx2 acetylation and stabilization.* J Biol Chem, 2010. **285**(6): p. 3568-74.

337. Vaidya, M., et al., *Osteoblast-specific overexpression of amphiregulin leads to transient increase in femoral cancellous bone mass in mice.* Bone, 2015. **81**: p. 36-46.

338. Qin, L., et al., *Amphiregulin is a novel growth factor involved in normal bone development and in the cellular response to parathyroid hormone stimulation.* J Biol Chem, 2005. **280**(5): p. 3974-81.

339. Schneider, M.R. and E. Wolf, *The epidermal growth factor receptor ligands at a glance.* J Cell Physiol, 2009. **218**(3): p. 460-6.

340. Capelo, L.P., et al., *The monocarboxylate transporter 8 and L-type amino acid transporters 1 and 2 are expressed in mouse skeletons and in osteoblastic MC3T3-E1 cells.* Thyroid, 2009. **19**(2): p. 171-80.

341. Lee, W.C., et al., *Energy Metabolism of the Osteoblast: Implications for Osteoporosis.* Endocr Rev, 2017. **38**(3): p. 255-266.

342. Stolle, K., et al., *Cloning, genomic organization, and tissue-specific expression of the RASL11B gene.* Biochim Biophys Acta, 2007. **1769**(7-8): p. 514-24.

343. Bombara, C. and R.A. Ignotz, *TGF-beta inhibits proliferation of and promotes differentiation of human promonocytic leukemia cells.* J Cell Physiol, 1992. **153**(1): p. 30-7.

344. Noordermeer, J., et al., *dishevelled and armadillo act in the wingless signalling pathway in Drosophila.* Nature, 1994. **367**(6458): p. 80-3.

345. Komiya, Y. and R. Habas, *Wnt signal transduction pathways.* Organogenesis, 2008. **4**(2): p. 68-75.

346. Rheinbay, E., et al., *An aberrant transcription factor network essential for Wnt signaling and stem cell maintenance in glioblastoma.* Cell Rep, 2013. **3**(5): p. 1567-79.

347. Hiyama, A., et al., *Enhancement of intervertebral disc cell senescence by WNT/beta-catenin signaling-induced matrix metalloproteinase expression.* Arthritis Rheum, 2010. **62**(10): p. 3036-47.

348. Fodde, R. and T. Brabletz, *Wnt/beta-catenin signaling in cancer stemness and malignant behavior.* Curr Opin Cell Biol, 2007. **19**(2): p. 150-8.

349. DeBruine, Z.J., H.E. Xu, and K. Melcher, *Assembly and architecture of the Wnt/beta-catenin signalosome at the membrane.* Br J Pharmacol, 2017. **174**(24): p. 4564-4574.

350. Nusse, R. and H. Clevers, *Wnt/beta-Catenin Signaling, Disease, and Emerging Therapeutic Modalities.* Cell, 2017. **169**(6): p. 985-999.

351. Strakova, K., et al., *Dishevelled enables casein kinase 1-mediated phosphorylation of Frizzled 6 required for cell membrane localization.* J Biol Chem, 2018. **293**(48): p. 18477-18493.

352. Griffin, J.N., et al., *RAPGEF5 Regulates Nuclear Translocation of beta-Catenin.* Dev Cell, 2018. **44**(2): p. 248-260 e4.

353. Shi, J., et al., *Emerging Role and Therapeutic Implication of Wnt Signaling Pathways in Autoimmune Diseases.* J Immunol Res, 2016. **2016**: p. 9392132.

354. Gatti, D., et al., *Sclerostin and DKK1 in postmenopausal osteoporosis treated with denosumab.* J Bone Miner Res, 2012. **27**(11): p. 2259-63.

355. Jin, H., et al., *Anti-DKK1 antibody promotes bone fracture healing through activation of beta-catenin signaling.* Bone, 2015. **71**: p. 63-75.

356. Li, X., et al., *Sclerostin binds to LRP5/6 and antagonizes canonical Wnt signaling.* J Biol Chem, 2005. **280**(20): p. 19883-7.

357. van Lierop, A.H., N.M. Appelman-Dijkstra, and S.E. Papapoulos, *Sclerostin deficiency in humans.* Bone, 2017. **96**: p. 51-62.

358. McClung, M.R., *Sclerostin antibodies in osteoporosis: latest evidence and therapeutic potential.* Ther Adv Musculoskelet Dis, 2017. **9**(10): p. 263-270.

359. Itoh, S., et al., *GSK-3alpha and GSK-3beta proteins are involved in early stages of chondrocyte differentiation with functional redundancy through RelA protein phosphorylation.* J Biol Chem, 2012. **287**(35): p. 29227-36.

360. Zaragosi, L.E., et al., *Effects of GSK3 inhibitors on in vitro expansion and differentiation of human adipose-derived stem cells into adipocytes.* BMC Cell Biol, 2008. **9**: p. 11.

361. Kaidanovich-Beilin, O. and J.R. Woodgett, *GSK-3: Functional Insights from Cell Biology and Animal Models.* Front Mol Neurosci, 2011. **4**: p. 40.

362. Wang, F.S., et al., *Inhibition of glycogen synthase kinase-3beta attenuates glucocorticoid-induced bone loss.* Life Sci, 2009. **85**(19-20): p. 685-92.

363. Meijer, L., M. Flajolet, and P. Greengard, *Pharmacological inhibitors of glycogen synthase kinase 3.* Trends Pharmacol Sci, 2004. **25**(9): p. 471-80.

364. Florio, M., et al., *A bispecific antibody targeting sclerostin and DKK-1 promotes bone mass accrual and fracture repair.* Nat Commun, 2016. **7**: p. 11505.

365. Chen, T., et al., *A WNT protein therapeutic improves the bone-forming capacity of autografts from aged animals.* Sci Rep, 2018. **8**(1): p. 119.

366. Salmon, B., et al., *WNT-activated bone grafts repair osteonecrotic lesions in aged animals.* Sci Rep, 2017. **7**(1): p. 14254.

367. Leucht, P., et al., *Wnt3a reestablishes osteogenic capacity to bone grafts from aged animals.* J Bone Joint Surg Am, 2013. **95**(14): p. 1278-88.

368. Saidak, Z., et al., *Low-dose PTH increases osteoblast activity via decreased Mef2c/Sost in senescent osteopenic mice.* J Endocrinol, 2014. **223**(1): p. 25-33.

369. Guo, J., et al., *Suppression of Wnt signaling by Dkk1 attenuates PTH-mediated stromal cell response and new bone formation.* Cell Metab, 2010. **11**(2): p. 161-71.

370. Yu, B., et al., *Wnt4 signaling prevents skeletal aging and inflammation by inhibiting nuclear factor-kappaB.* Nat Med, 2014. **20**(9): p. 1009-17.

371. Roddy, K.A. and C.A. Boulter, *Targeted mutation of NOV/CCN3 in mice disrupts joint homeostasis and causes osteoarthritis-like disease.* Osteoarthritis Cartilage, 2015. **23**(4): p. 607-15.

372. Hurvitz, J.R., et al., *Mutations in the CCN gene family member WISP3 cause progressive pseudorheumatoid dysplasia.* Nat Genet, 1999. **23**(1): p. 94-8.

373. Blom, A.B., et al., *Involvement of the Wnt signaling pathway in experimental and human osteoarthritis: prominent role of Wnt-induced signaling protein 1.* Arthritis Rheum, 2009. **60**(2): p. 501-12.

374. Canalis, E., et al., *Nephroblastoma overexpressed (Nov) inactivation sensitizes osteoblasts to bone morphogenetic protein-2, but nov is dispensable for skeletal homeostasis.* Endocrinology, 2010. **151**(1): p. 221-33.

375. Heath, E., et al., *Abnormal skeletal and cardiac development, cardiomyopathy, muscle atrophy and cataracts in mice with a targeted disruption of the Nov (Ccn3) gene.* BMC Dev Biol, 2008. **8**: p. 18.

376. Ouellet, V. and P.M. Siegel, *CCN3 modulates bone turnover and is a novel regulator of skeletal metastasis.* J Cell Commun Signal, 2012. **6**(2): p. 73-85.

377. Macosko, E.Z., et al., *Highly Parallel Genome-wide Expression Profiling of Individual Cells Using Nanoliter Droplets.* Cell, 2015. **161**(5): p. 1202-1214.

378. Cusanovich, D.A., et al., *Multiplex single cell profiling of chromatin accessibility by combinatorial cellular indexing.* Science, 2015. **348**(6237): p. 910-4.

379. Lee, H.J. and S.A. Smallwood, *Genome-Wide Analysis of DNA Methylation in Single Cells Using a Post-bisulfite Adapter Tagging Approach.* Methods Mol Biol, 2018. **1712**: p. 87-95.

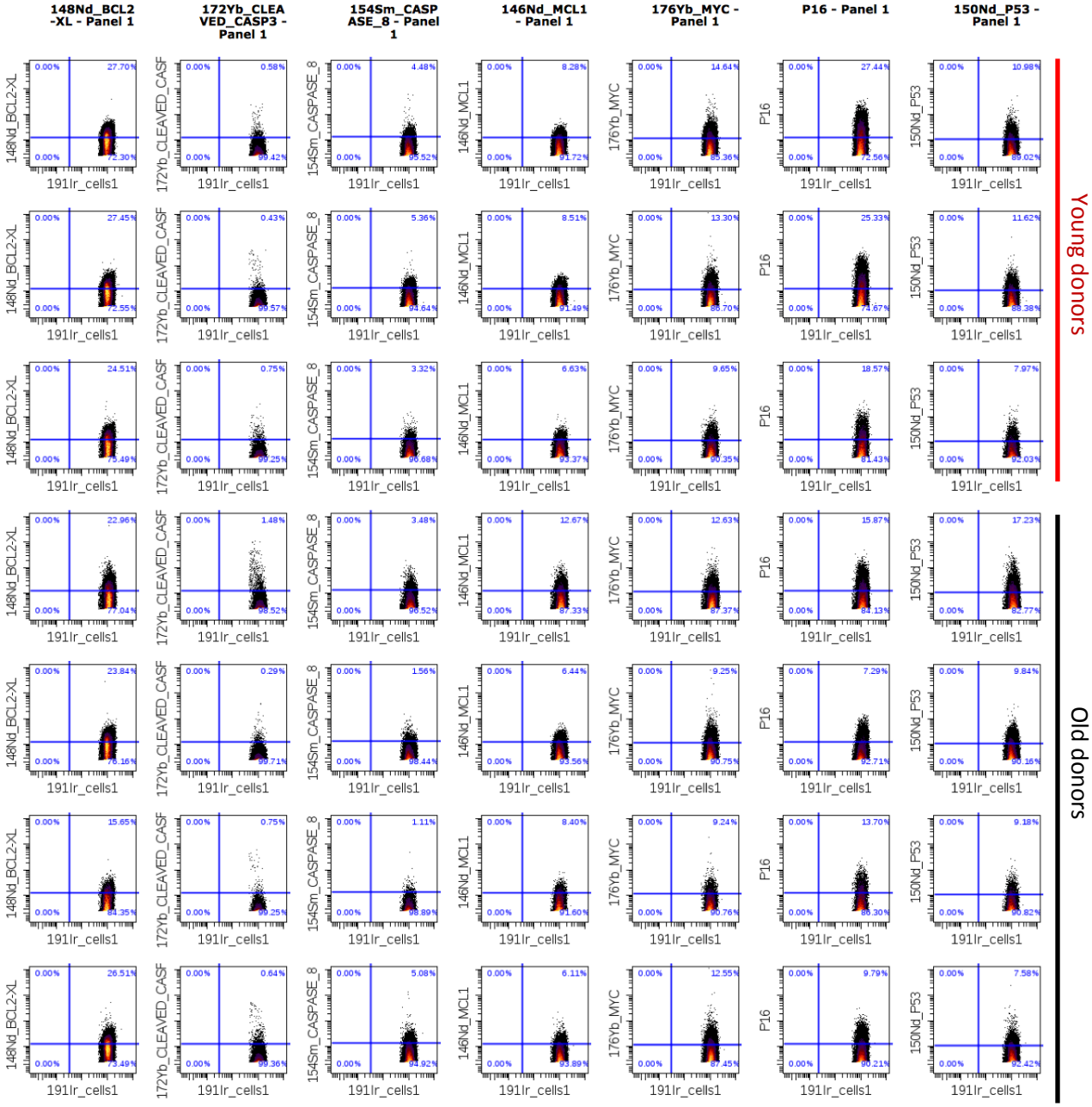
380. Krause, U., et al., *Pharmaceutical modulation of canonical Wnt signaling in multipotent stromal cells for improved osteoinductive therapy.* Proc Natl Acad Sci U S A, 2010. **107**(9): p. 4147-52.

381. Pai, R., A.S. Tarnawski, and T. Tran, *Deoxycholic acid activates beta-catenin signaling pathway and increases colon cell cancer growth and invasiveness.* Mol Biol Cell, 2004. **15**(5): p. 2156-63.

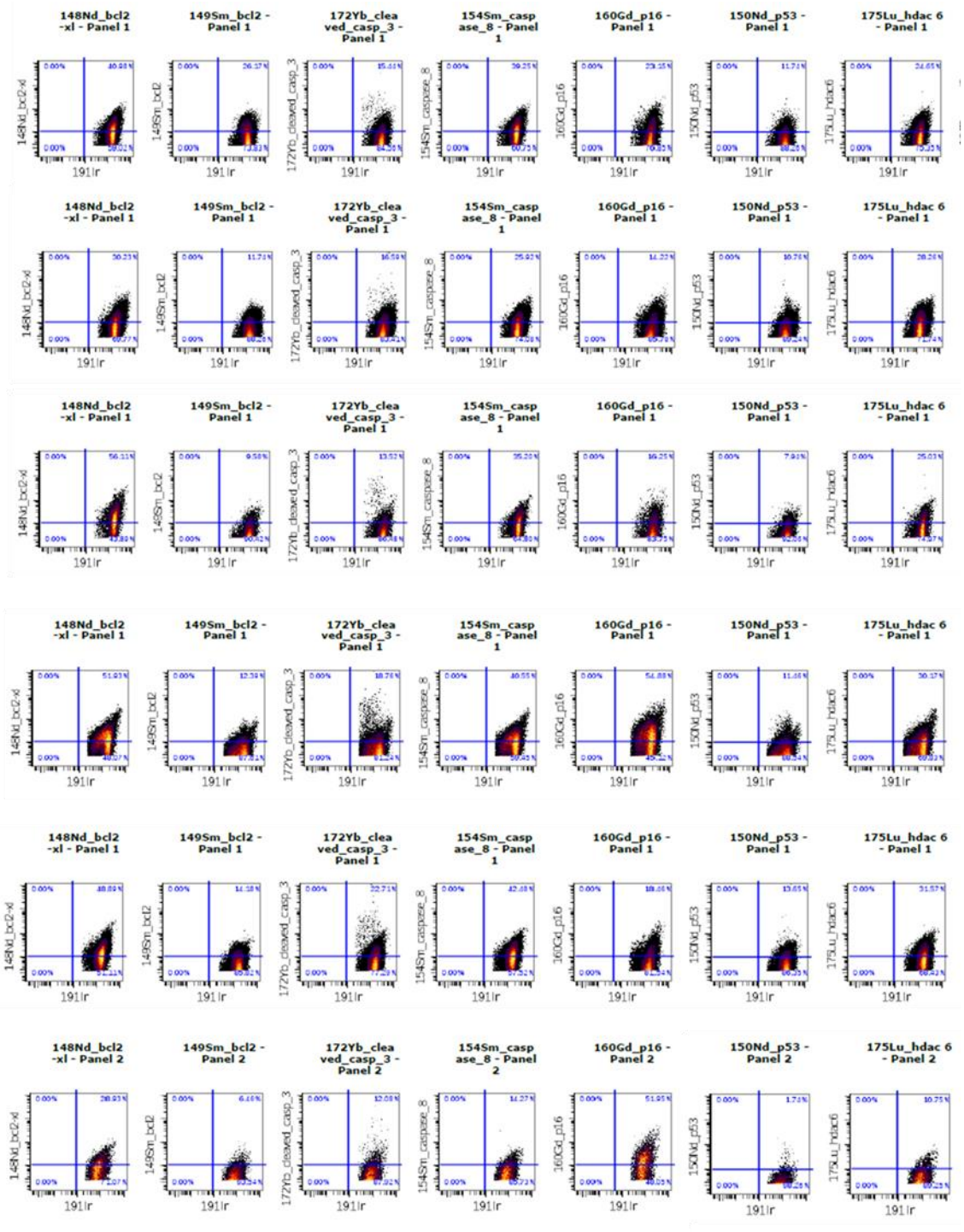
382. Coghlan, M.P., et al., *Selective small molecule inhibitors of glycogen synthase kinase-3 modulate glycogen metabolism and gene transcription.* Chem Biol, 2000. **7**(10): p. 793-803.

383. Bodine, P.V., et al., *A small molecule inhibitor of the Wnt antagonist secreted frizzled-related protein-1 stimulates bone formation.* Bone, 2009. **44**(6): p. 1063-8.

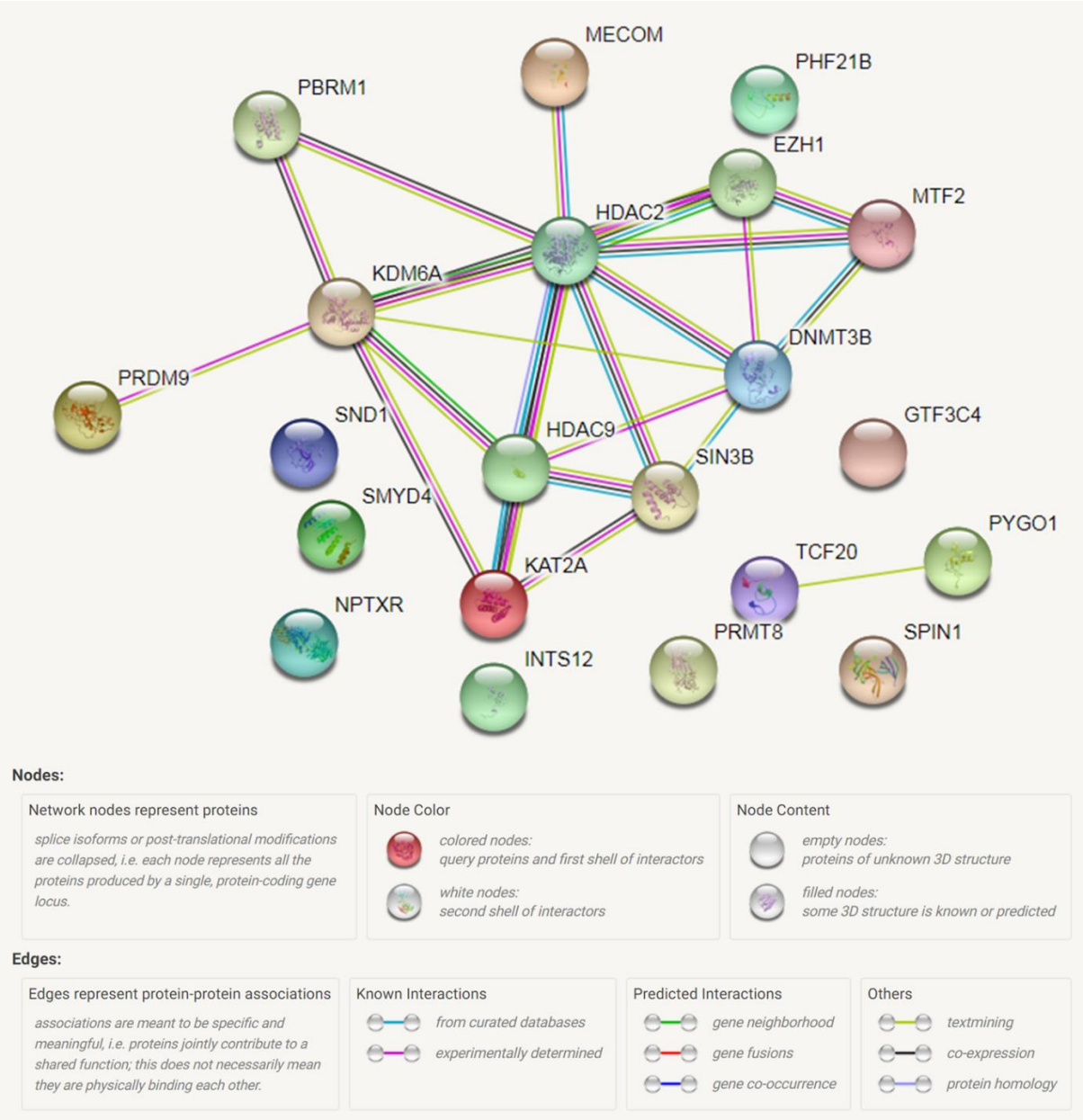
Appendix



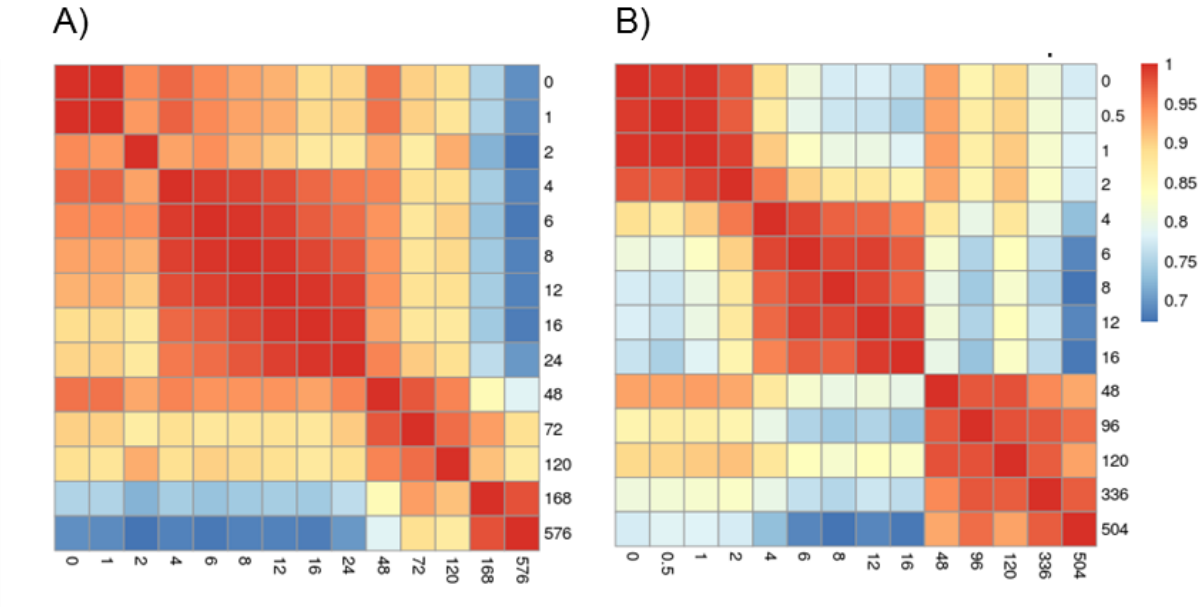
Supplementary Figure S1. ***CyTOF analysis of the expression of senescence and apoptosis regulators in young and old donor MSCs.*** *Gating and dot plots of the expression for senescence regulators: P16, P53 and MYC, and apoptosis regulators: BCL2-XL, CASP-3, CASP-8 and MCL-1. Young donors n=3, age 20 – 29 years; old donors n=4, age 62 – 87 years.*



Supplementary Figure S2. ***CyTOF analysis of the expression of senescence and apoptosis regulators in early and late passage MSCs.*** *Gating and dot plots of the expression for senescence (P16, P53 and HDAC6) and apoptosis (BCL2-XL, BCL2, CASP-3 and CASP-8) markers. Early passage = P5 – P9, Late passage = P7 – P14. Donors n = 3, age 20 – 29 years.*

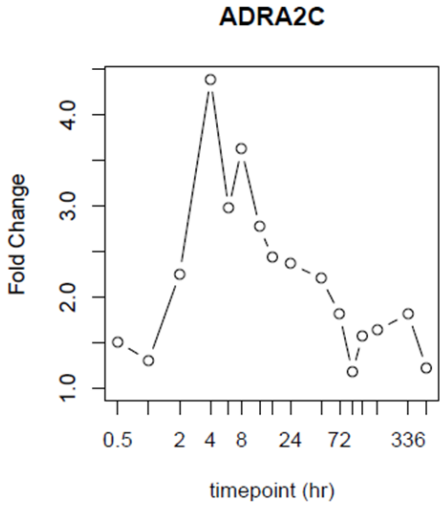


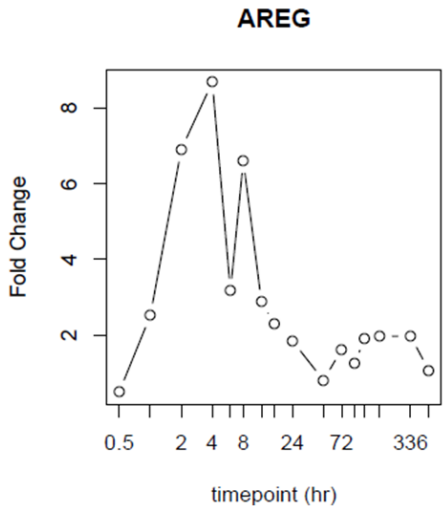
Supplementary Figure S3. ***STRING protein interaction network of the 22 candidate genes from shRNA-seq screening.***

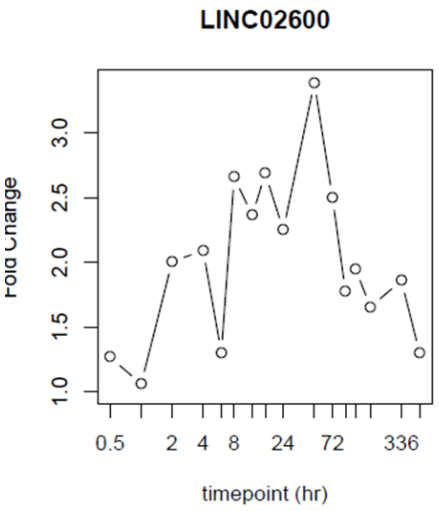


Supplementary Figure S4. ***Phases of change in gene expression during osteogenesis at an individual donor level.*** *Heatmaps of the correlation of gene expression (normalised counts) between different time points during osteogenesis,* ***A)*** *in a representative young donor (24 years, male) and* ***B)*** *in a representative old donor (62 years, male).*

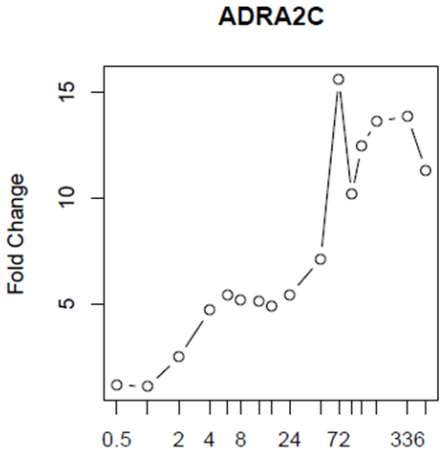
A)

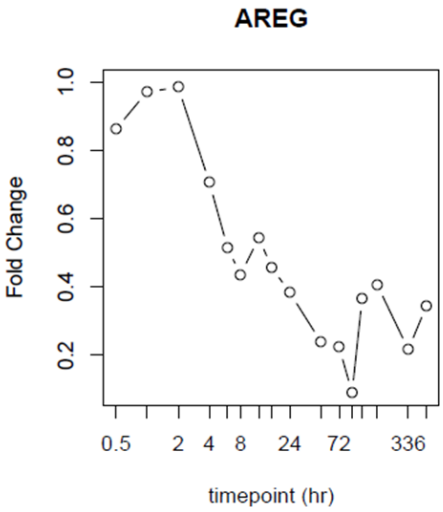

ADRA2C
Fold Change
1.0
2.0
3.0
4.0
0.5
2
4
8
24
72
336
timepoint (hr)

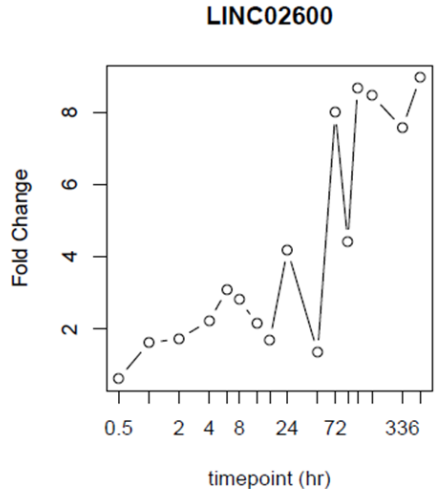

AREG
Fold Change
2
4
6
8
0.5
2
4
8
24
72
336
timepoint (hr)

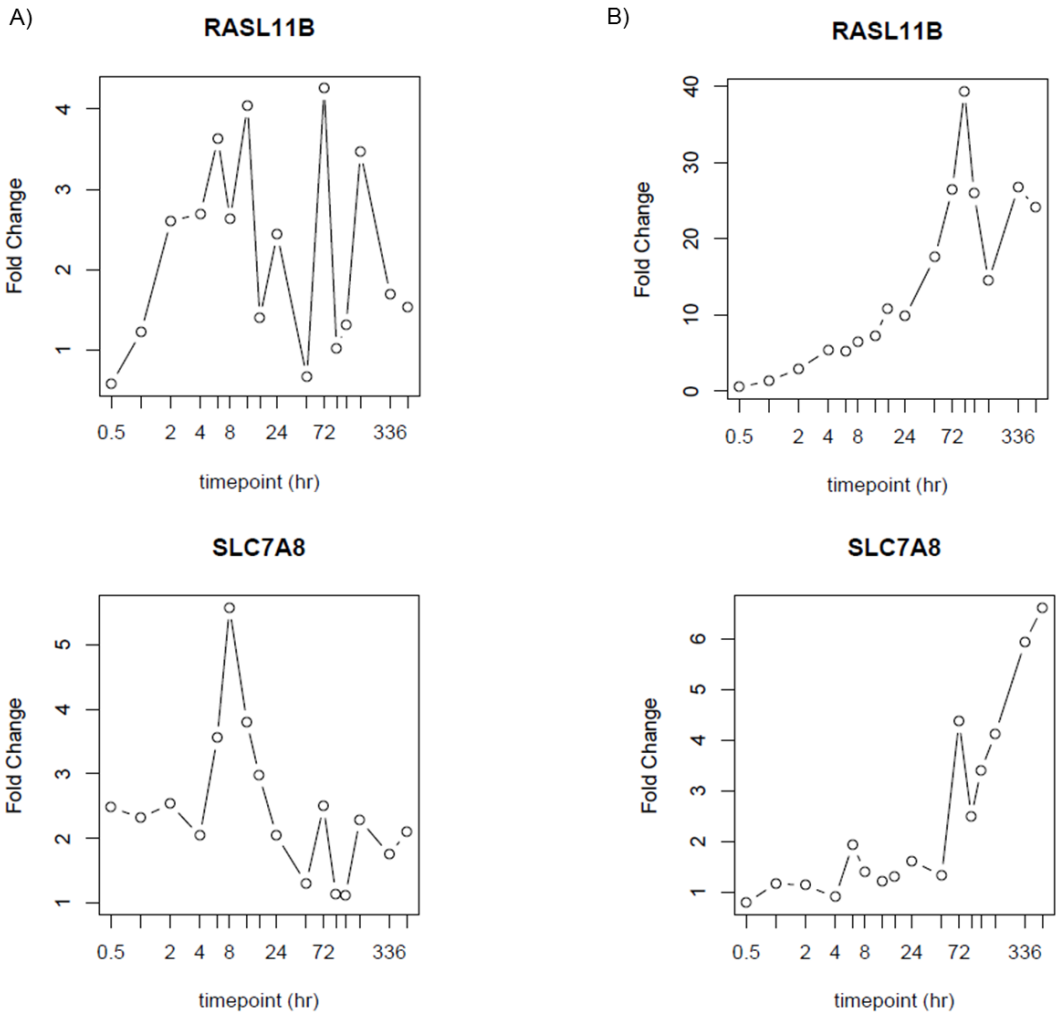

LINC02600
Fold Change
1.0
1.5
2.0
2.5
3.0
0.5
2
4
8
24
72
336
timepoint (hr)

B)

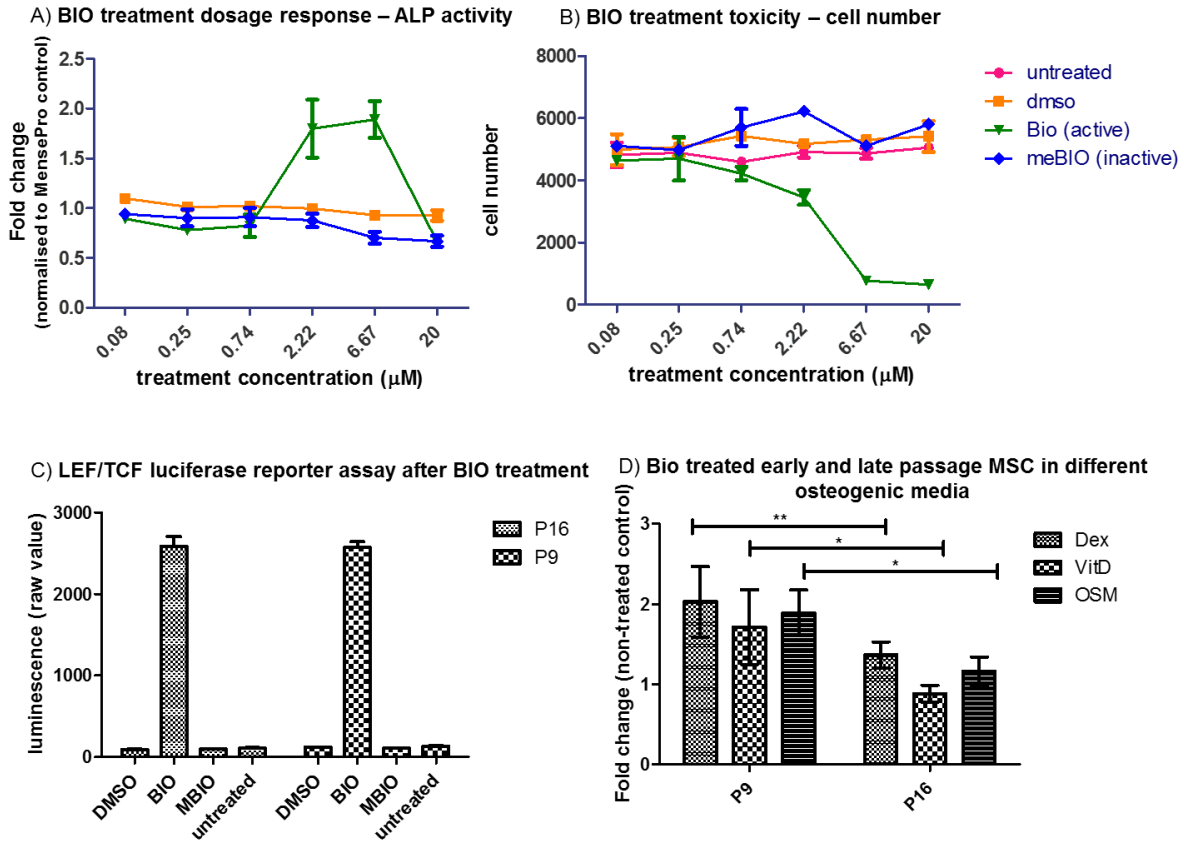

ADRA2C
Fold Change
5
10
15
0.5
2
4
8
24
72
336


AREG
Fold Change
0.2
0.4
0.6
0.8
1.0
0.5
2
4
8
24
72
336
timepoint (hr)

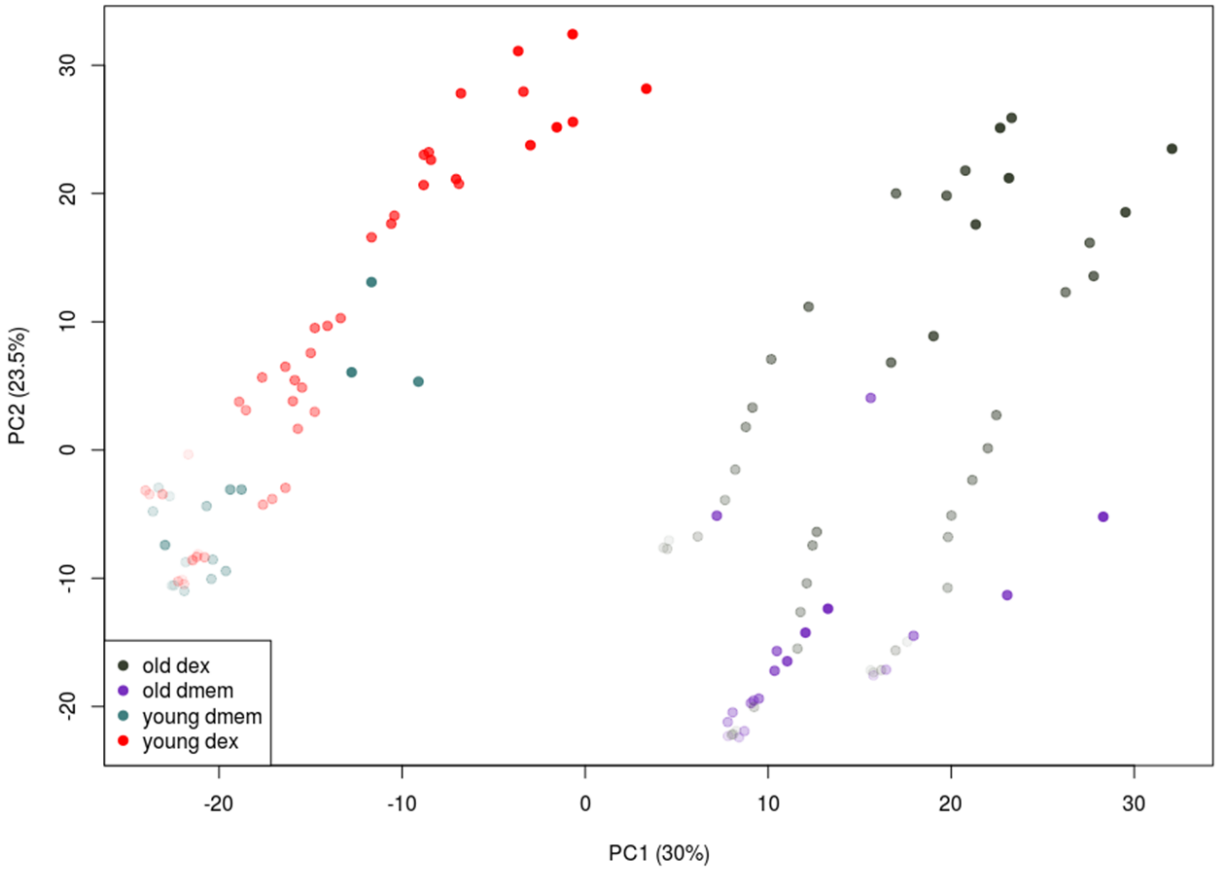

LINC02600
Fold Change
2
4
6
8
0.5
2
4
8
24
72
336
timepoint (hr)



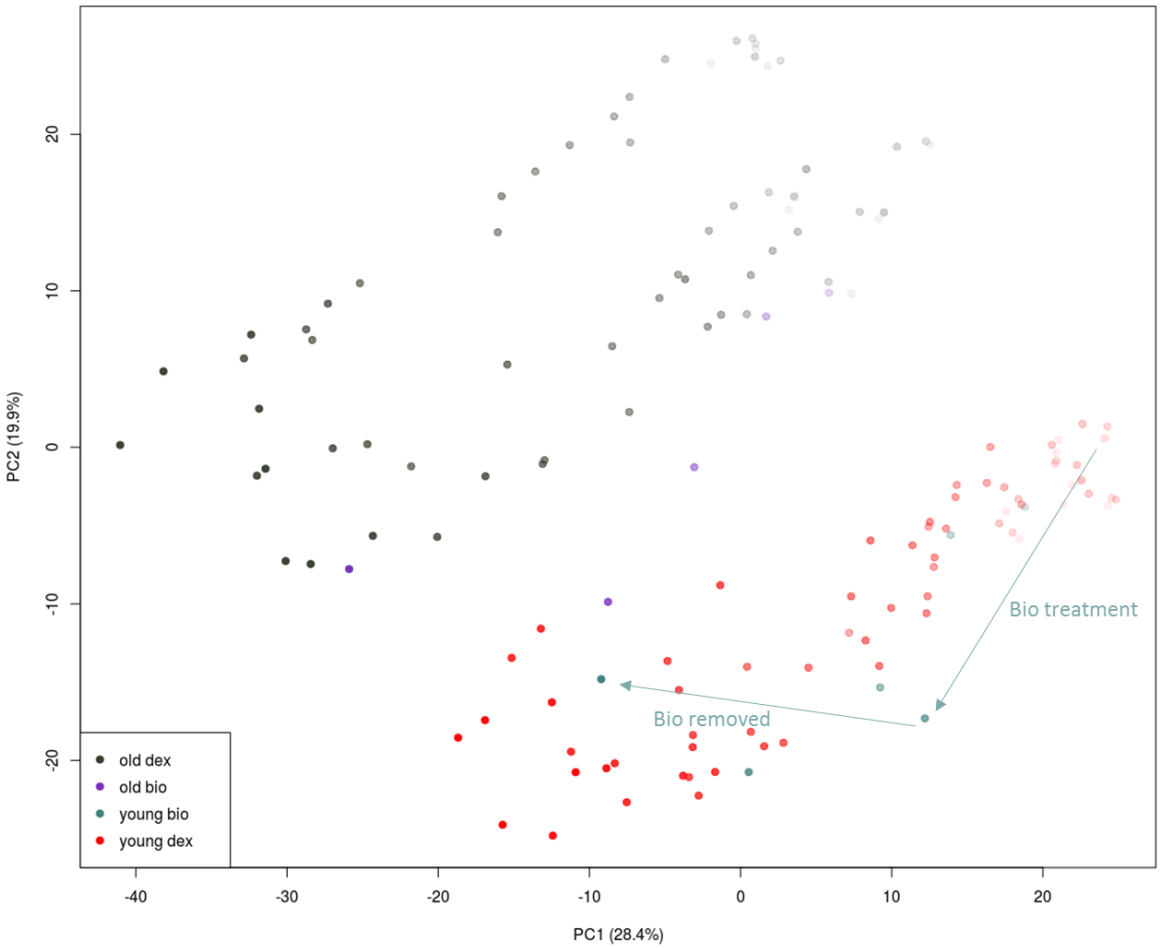
Supplementary Figure S5. ***Transiently upregulated DEGs between 1 – 24 hrs during osteogenesis.*** *Individual expression profiles of the five cluster 1 DEGs in* ***A)*** *young donors and* ***B)*** *old donors.*



Supplementary Figure S6. ***BIO treatment dosage response and validations. A)*** *ALP assay showing the dose response of BIO.* ***B)*** *Cell counting showing the cellular toxicity of BIO at 7 days after treatment.* ***C)*** *LEF/TCF reporter assay 3 days after the addition of BIO.* ***D)*** *1 µM BIO treatment in early and late passage MSCs. BIO was tested in three differentiation media: Dex, VitD and OSM. meBIO = inactive control analog for BIO, untreated = media only control.*



Supplementary Figure S7. ***Transcriptomic changes in old vs young donor MSCs during osteogenesis and in DMEM control. A)*** *PCA of RNA-seq time-course data, showing the variability in gene expression between samples. Young donors (n = 6, 20 – 29 years) and old donors (n = 6, 62 – 87 years). Light to dark shading indicates early (0 hr) to late (504 hr) time points.*



Supplementary Figure S8. ***Transcriptomic changes in old vs young donor MSCs during osteogenesis with BIO treatment.*** PCA of *a representative young donor treated with BIO for 7 days (green dots and line), young donors without BIO (red dots), a representative old donor treated with BIO for 7 days (blue dots), and old donors without BIO (black dots).*

ID	Age	Gender	Ethnicity	Item number	Source
young1	23	Female	Black	27766	Lonza
young2	25	Female	Caucasian	33606	Lonza
young3	26	Male	Caucasian	SCC034	Milipore
young4	25	Male	Caucasian	28386	Lonza
young5	21	Female	Caucasian	27788	Lonza
young6	29	Male	no data	121217	Karamitros
young7	24	Male	Black	130917	Karamitros
young8	23	Male	Black	31177	Lonza
young9	21	Male	Asian	20817	Karamitros
young10	20	Female	no data	220218	Karamitros
old1	81	Male	Caucasian	091001K1AP	Peffers
old2	67	Male	Caucasian	091002K1AP	Peffers
old3	72	Male	Caucasian	091003K1AP	Peffers
old4	73	Female	Caucasian	427Z010.1	Promocell
old5	62	Male	Caucasian	091004K1AP	Peffers
old6	87	Female	Caucasian	429Z001	Promocell
old7	66	Female	Caucasian	421Z029.3	Promocell

Supplementary table S1. ***Donor details.*** *Showing age group, age, gender, ethnicity and source.*

Gene name	Gene description
AC008736.1	tudor domain containing 12
AC009961.1	bromodomain adjacent to zinc finger domain 2B
AC016586.1	sirtuin 6
AIRE	autoimmune regulator
AKAP1	A-kinase anchoring protein 1
ALG13	ALG13 UDP-N-acetylglucosaminyltransferase subunit
ALKBH1	alkB homolog 1, histone H2A dioxygenase
ALKBH2	alkB homolog 2, alpha-ketoglutarate dependent dioxygenase
ALKBH3	alkB homolog 3, alpha-ketoglutaratedependent dioxygenase
ALKBH4	alkB homolog 4, lysine demethylase
ALKBH5	alkB homolog 5, RNA demethylase
ALKBH6	alkB homolog 6
ALKBH7	alkB homolog 7
ALKBH8	alkB homolog 8, tRNA methyltransferase
ARID1A	AT-rich interaction domain 1A
ARID4A	AT-rich interaction domain 4A
ARID4B	AT-rich interaction domain 4B
ASF1A	anti-silencing function 1A histone chaperone
ASF1B	anti-silencing function 1B histone chaperone
ASH1L	ASH1 like histone lysine methyltransferase
ATAD2	ATPase family AAA domain containing 2
ATAD2B	ATPase family AAA domain containing 2B
ATAT1	alpha tubulin acetyltransferase 1
AURKA	aurora kinase A
AURKB	aurora kinase B
AURKC	aurora kinase C
BAZ1A	bromodomain adjacent to zinc finger domain 1A
BAZ1B	bromodomain adjacent to zinc finger domain 1B
BAZ2A	bromodomain adjacent to zinc finger domain 2A
BAZ2B	bromodomain adjacent to zinc finger domain 2B
BPTF	bromodomain PHD finger transcription factor
BRD1	bromodomain containing 1
BRD2	bromodomain containing 2
BRD3	bromodomain containing 3
BRD4	bromodomain containing 4
BRD7	bromodomain containing 7
BRD8	bromodomain containing 8
BRD9	bromodomain containing 9
BRDT	bromodomain testis associated
BRPF1	bromodomain and PHD finger containing 1
BRPF3	bromodomain and PHD finger containing 3
BRWD1	bromodomain and WD repeat domain containing 1
BRWD3	bromodomain and WD repeat domain containing 3
BTG3	BTG anti-proliferation factor 3
CAPRIN2	caprin family member 2
CARM1	coactivator associated arginine methyltransferase 1
CBX1	chromobox 1
CBX2	chromobox 2
CBX3	chromobox 3
CBX4	chromobox 4
CBX5	chromobox 5
CBX6	chromobox 6
CBX7	chromobox 7
CBX8	chromobox 8
CDYL	chromodomain Y like
CDYL2	chromodomain Y like 2
CHAF1A	chromatin assembly factor 1 subunit A
CHAF1B	chromatin assembly factor 1 subunit B
CHD1	chromodomain helicase DNA binding protein 1
CHD1L	chromodomain helicase DNA binding protein 1 like
CHD2	chromodomain helicase DNA binding protein 2
CHD3	chromodomain helicase DNA binding protein 3
CHD4	chromodomain helicase DNA binding protein 4
CHD5	chromodomain helicase DNA binding protein 5
CHD6	chromodomain helicase DNA binding protein 6
CHD7	chromodomain helicase DNA binding protein 7
CHD8	chromodomain helicase DNA binding protein 8
CHD9	chromodomain helicase DNA binding protein 9
CHMP1B	charged multivesicular body protein 1B
CHMP2A	charged multivesicular body protein 2A
CHMP4B	charged multivesicular body protein 4B
CHMP4C	charged multivesicular body protein 4C
CHRAC1	chromatin accessibility complex subunit 1
CLOCK	clock circadian regulator
CREBBP	CREB binding protein
CXXC1	CXXC finger protein 1
DIDO1	death inducer-obliterator 1
DNMT1	DNA methyltransferase 1
DNMT3A	DNA methyltransferase 3 alpha
DNMT3B	DNA methyltransferase 3 beta
DNMT3L	DNA methyltransferase 3 like
DOT1L	DOT1 like histone lysine methyltransferase
DPF1	double PHD fingers 1
DPF2	double PHD fingers 2
DPF3	double PHD fingers 3
EED	embryonic ectoderm development
EHMT1	euchromatic histone lysine methyltransferase 1
EHMT2	euchromatic histone lysine methyltransferase 2
ELP3	elongator acetyltransferase complex subunit 3
EP300	E1A binding protein p300
EPC1	enhancer of polycomb homolog 1
EPC2	enhancer of polycomb homolog 2
EZH1	enhancer of zeste 1 polycomb repressive complex 2 subunit
EZH2	enhancer of zeste 2 polycomb repressive complex 2 subunit
FBXL19	F-box and leucine rich repeat protein 19
FBXO11	F-box protein 11
FMR1	fragile X mental retardation 1
FTO	FTO alpha-ketoglutarate dependent dioxygenase

Supplementary table S2. ***Lentiviral shRNA library gene targets.*** *Part 1*

Gene name	Gene description
FXR1	FMR1 autosomal homolog 1
FXR2	FMR1 autosomal homolog 2
G2E3	G2/M-phase specific E3 ubiquitin protein ligase
GDAP2	ganglioside induced differentiation associated protein 2
GLYR1	glyoxylate reductase 1 homolog
GTF3C4	general transcription factor IIIC subunit 4
H2AFY	H2A histone family member Y
H2AFY2	H2A histone family member Y2
HAT1	histone acetyltransferase 1
HDAC1	histone deacetylase 1
HDAC10	histone deacetylase 10
HDAC11	histone deacetylase 11
HDAC2	histone deacetylase 2
HDAC3	histone deacetylase 3
HDAC4	histone deacetylase 4
HDAC5	histone deacetylase 5
HDAC6	histone deacetylase 6
HDAC7	histone deacetylase 7
HDAC8	histone deacetylase 8
HDAC9	histone deacetylase 9
HDGF	heparin binding growth factor
HDGFL1	HDGF like 1
HDGFL2	HDGF like 2
HDGFL3	HDGF like 3
HIF1AN	hypoxia inducible factor 1 subunit alpha inhibitor
HIRA	histone cell cycle regulator
HR	HR lysine demethylase and nuclear receptor corepressor
HSPBAP1	HSPB1 associated protein 1
ING1	inhibitor of growth family member 1
ING2	inhibitor of growth family member 2
ING3	inhibitor of growth family member 3
ING4	inhibitor of growth family member 4
ING5	inhibitor of growth family member 5
INTS12	integrator complex subunit 12
JADE1	jade family PHD finger 1
JADE2	jade family PHD finger 2
JADE3	jade family PHD finger 3
JARID2	jumonji and AT-rich interaction domain containing 2
JMJD1C	jumonji domain containing 1C
JMJD4	jumonji domain containing 4
JMJD6	jumonji domain containing 6, arginine demethylase and lysine hydroxylase
JMJD8	jumonji domain containing 8
KAT2A	lysine acetyltransferase 2A
KAT2B	lysine acetyltransferase 2B
KAT5	lysine acetyltransferase 5
KAT6A	lysine acetyltransferase 6A
KAT6B	lysine acetyltransferase 6B
KAT7	lysine acetyltransferase 7
KAT8	lysine acetyltransferase 8
KDM1A	lysine demethylase 1A
KDM1B	lysine demethylase 1B
KDM2A	lysine demethylase 2A
KDM2B	lysine demethylase 2B
KDM3A	lysine demethylase 3A
KDM3B	lysine demethylase 3B
KDM4A	lysine demethylase 4A
KDM4B	lysine demethylase 4B
KDM4C	lysine demethylase 4C
KDM4D	lysine demethylase 4D
KDM4E	lysine demethylase 4E
KDM5A	lysine demethylase 5A
KDM5B	lysine demethylase 5B
KDM5C	lysine demethylase 5C
KDM5D	lysine demethylase 5D
KDM6A	lysine demethylase 6A
KDM6B	lysine demethylase 6B
KDM7A	lysine demethylase 7A
KDM8	lysine demethylase 8
KMT2A	lysine methyltransferase 2A
KMT2B	lysine methyltransferase 2B
KMT2C	lysine methyltransferase 2C
KMT2D	lysine methyltransferase 2D
KMT2E	lysine methyltransferase 2E
KMT5A	lysine methyltransferase 5A
KMT5B	lysine methyltransferase 5B
KMT5C	lysine methyltransferase 5C
L3MBTL1	L3MBTL histone methyl-lysine binding protein 1
L3MBTL2	L3MBTL histone methyl-lysine binding protein 2
L3MBTL3	L3MBTL histone methyl-lysine binding protein 3
L3MBTL4	L3MBTL histone methyl-lysine binding protein 4
LBR	lamin B receptor
MACROD1	mono-ADP ribosylhydrolase 1
MACROD2	mono-ADP ribosylhydrolase 2
MBD1	methyl-CpG binding domain protein 1
MBD2	methyl-CpG binding domain protein 2
MBD3	methyl-CpG binding domain protein 3
MBD4	methyl-CpG binding domain 4, DNA glycosylase
MBD5	methyl-CpG binding domain protein 5
MBD6	methyl-CpG binding domain protein 6
MBTD1	mbt domain containing 1
MECOM	MDS1 and EVI1 complex locus
MECP2	methyl-CpG binding protein 2
MLLT10	MLLT10 histone lysine methyltransferase DOT1L cofactor
MLLT6	MLLT6, PHD finger containing
MORF4L1	mortality factor 4 like 1
MPHOSPH8	M-phase phosphoprotein 8
FTO	FTO alpha-ketoglutarate dependent dioxygenase

Supplementary table S2. ***Lentiviral shRNA library gene targets.*** *Part 2*

Gene name	Gene description
MSH6	mutS homolog 6
MSL3	MSL complex subunit 3
MTA1	metastasis associated 1
MTA2	metastasis associated 1 family member 2
MTA3	metastasis associated 1 family member 3
MTF2	metal response element binding transcription factor 2
NAP1L1	nucleosome assembly protein 1 like 1
NAP1L2	nucleosome assembly protein 1 like 2
NAP1L3	nucleosome assembly protein 1 like 3
NAP1L4	nucleosome assembly protein 1 like 4
NAP1L5	nucleosome assembly protein 1 like 5
NCOA1	nuclear receptor coactivator 1
NCOA3	nuclear receptor coactivator 3
NPTXR	neuronal pentraxin receptor
NSD1	nuclear receptor binding SET domain protein 1
NSD2	nuclear receptor binding SET domain protein 2
NSD3	nuclear receptor binding SET domain protein 3
OARD1	O-acyl-ADP-ribose deacylase 1
PADI4	peptidyl arginine deiminase 4
PARP1	poly(ADP-ribose) polymerase 1
PARP10	poly(ADP-ribose) polymerase family member 10
PARP11	poly(ADP-ribose) polymerase family member 11
PARP12	poly(ADP-ribose) polymerase family member 12
PARP14	poly(ADP-ribose) polymerase family member 14
PARP15	poly(ADP-ribose) polymerase family member 15
PARP16	poly(ADP-ribose) polymerase family member 16
PARP2	poly(ADP-ribose) polymerase 2
PARP3	poly(ADP-ribose) polymerase family member 3
PARP4	poly(ADP-ribose) polymerase family member 4
PARP6	poly(ADP-ribose) polymerase family member 6
PARP8	poly(ADP-ribose) polymerase family member 8
PARP9	poly(ADP-ribose) polymerase family member 9
PBRM1	polybromo 1
PHC2	polyhomeotic homolog 2
PHC3	polyhomeotic homolog 3
PHF1	PHD finger protein 1
PHF10	PHD finger protein 10
PHF11	PHD finger protein 11
PHF12	PHD finger protein 12
PHF13	PHD finger protein 13
PHF14	PHD finger protein 14
PHF19	PHD finger protein 19
PHF2	PHD finger protein 2
PHF20	PHD finger protein 20
PHF20L1	PHD finger protein 20 like 1
PHF21A	PHD finger protein 21A
PHF21B	PHD finger protein 21B
PHF23	PHD finger protein 23

Gene name	Gene description
PHF3	PHD finger protein 3
PHF5A	PHD finger protein 5A
PHF6	PHD finger protein 6
PHF7	PHD finger protein 7
PHF8	PHD finger protein 8
PHIP	pleckstrin homology domain interacting protein
PHRF1	PHD and ring finger domains 1
PRDM1	PR/SET domain 1
PRDM10	PR/SET domain 10
PRDM11	PR/SET domain 11
PRDM12	PR/SET domain 12
PRDM13	PR/SET domain 13
PRDM14	PR/SET domain 14
PRDM15	PR/SET domain 15
PRDM16	PR/SET domain 16
PRDM2	PR/SET domain 2
PRDM4	PR/SET domain 4
PRDM5	PR/SET domain 5
PRDM6	PR/SET domain 6
PRDM7	PR/SET domain 7
PRDM8	PR/SET domain 8
PRDM9	PR/SET domain 9
PRMT1	protein arginine methyltransferase 1
PRMT2	protein arginine methyltransferase 2
PRMT3	protein arginine methyltransferase 3
PRMT5	protein arginine methyltransferase 5
PRMT6	protein arginine methyltransferase 6
PRMT7	protein arginine methyltransferase 7
PRMT8	protein arginine methyltransferase 8
PSIP1	PC4 and SFRS1 interacting protein 1
PWWP2B	PWWP domain containing 2B
PWWP3A	PWWP domain containing 3A, DNA repair factor
PYGO1	pygopus family PHD finger 1
PYGO2	pygopus family PHD finger 2
RAG2	recombination activating 2
RAI1	retinoic acid induced 1
RIOX1	ribosomal oxygenase 1
RIOX2	ribosomal oxygenase 2
RNF17	ring finger protein 17
RPH3A	rabphilin 3A
RSF1	remodeling and spacing factor 1
SCMH1	Scm polycomb group protein homolog 1
SCML2	Scm polycomb group protein like 2
SET	SET nuclear proto-oncogene
SETD1A	SET domain containing 1A, histone lysine methyltransferase
SETD1B	SET domain containing 1B, histone lysine methyltransferase
SETD2	SET domain containing 2, histone lysine methyltransferase
SETD3	SET domain containing 3, actin histidine methyltransferase
SETD4	SET domain containing 4

Supplementary table S2. ***Lentiviral shRNA library gene targets.*** *Part 3*

Gene name	
SETD5	SET domain containing 5
SETD6	SET domain containing 6, protein lysine methyltransferase
SETD7	SET domain containing 7, histone lysine methyltransferase
SETDB1	SET domain bifurcated histone lysine methyltransferase 1
SETDB2	SET domain bifurcated histone lysine methyltransferase 2
SETMAR	SET domain and mariner transposase fusion gene
SFMBT1	Scm like with four mbt domains 1
SFMBT2	Scm like with four mbt domains 2
SGF29	SAGA complex associated factor 29
SHPRH	SNF2 histone linker PHD RING helicase
SIN3A	SIN3 transcription regulator family member A
SIN3B	SIN3 transcription regulator family member B
SIRT1	sirtuin 1
SIRT2	sirtuin 2
SIRT3	sirtuin 3
SIRT4	sirtuin 4
SIRT5	sirtuin 5
SIRT7	sirtuin 7
SMARCA1	SWI/SNF related, matrix associated, actin dependent regulator of chromatin, subfamily a, member 1
SMARCA2	SWI/SNF related, matrix associated, actin dependent regulator of chromatin, subfamily a, member 2
SMARCA4	SWI/SNF related, matrix associated, actin dependent regulator of chromatin, subfamily a, member 4
SMARCA5	SWI/SNF related, matrix associated, actin dependent regulator of chromatin, subfamily a, member 5
SMARCAD1	SWI/SNF-related, matrix-associated actin-dependent regulator of chromatin, subfamily a, containing DEAD/H box 1
SMARCB1	SWI/SNF related, matrix associated, actin dependent regulator of chromatin, subfamily b, member 1
SMARCC1	SWI/SNF related, matrix associated, actin dependent regulator of chromatin subfamily c member 1
SMARCC2	SWI/SNF related, matrix associated, actin dependent regulator of chromatin subfamily c member 2
SMARCD1	SWI/SNF related, matrix associated, actin dependent regulator of chromatin, subfamily d, member 1
SMARCD2	SWI/SNF related, matrix associated, actin dependent regulator of chromatin, subfamily d, member 2
SMARCD3	SWI/SNF related, matrix associated, actin dependent regulator of chromatin, subfamily d, member 3
SMC1A	structural maintenance of chromosomes 1A
SMC1B	structural maintenance of chromosomes 1B
SMC2	structural maintenance of chromosomes 2
SMC3	structural maintenance of chromosomes 3
SMC4	structural maintenance of chromosomes 4
SMN1	survival of motor neuron 1, telomeric
SMN2	survival of motor neuron 1, telomeric
SMN2	survival of motor neuron 2, centromeric
SMNDC1	survival motor neuron domain containing 1
SMYD1	SET and MYND domain containing 1
SMYD2	SET and MYND domain containing 2
SMYD3	SET and MYND domain containing 3
SMYD4	SET and MYND domain containing 4
SMYD5	SMYD family member 5
SND1	staphylococcal nuclease and tudor domain containing 1
SP100	SP100 nuclear antigen
SP110	SP110 nuclear body protein
SP140	SP140 nuclear body protein
SP140L	SP140 nuclear body protein like

Gene name	
SPIN1	spindlin 1
SPIN2A	spindlin family member 2A
SPIN2B	spindlin family member 2B
SPIN3	spindlin family member 3
SPIN4	spindlin family member 4
STK31	serine/threonine kinase 31
SUDS3	SDS3 homolog, SIN3A corepressor complex component
SUPT7L	SPT7 like, STAGA complex gamma subunit
SUV39H1	suppressor of variegation 3-9 homolog 1
SUV39H2	suppressor of variegation 3-9 homolog 2
TAF1	TATA-box binding protein associated factor 1
TAF1L	TATA-box binding protein associated factor 1 like
TAF3	TATA-box binding protein associated factor 3
TAF8	TATA-box binding protein associated factor 8
TCF19	transcription factor 19
TCF20	transcription factor 20
TDRD1	tudor domain containing 1
TDRD10	tudor domain containing 10
TDRD3	tudor domain containing 3
TDRD5	tudor domain containing 5
TDRD6	tudor domain containing 6
TDRD7	tudor domain containing 7
TDRD9	tudor domain containing 9
TDRKH	tudor and KH domain containing
TET1	tet methylcytosine dioxygenase 1
TET2	tet methylcytosine dioxygenase 2
TET3	tet methylcytosine dioxygenase 3
TIPARP	TCDD inducible poly(ADP-ribose) polymerase
TNKS	tankyrase
TNKS2	tankyrase 2
TP53BP1	tumor protein p53 binding protein 1
TRAF7	TNF receptor associated factor 7
TRDMT1	tRNA aspartic acid methyltransferase 1
TRIM24	tripartite motif containing 24
TRIM28	tripartite motif containing 28
TRIM33	tripartite motif containing 33
TRIM66	tripartite motif containing 66
TYW5	tRNA-yW synthesizing protein 5
UBE2A	ubiquitin conjugating enzyme E2 A
UBE2B	ubiquitin conjugating enzyme E2 B
UBE2I	ubiquitin conjugating enzyme E2 I
UBE2V1	ubiquitin conjugating enzyme E2 V1
UBR7	ubiquitin protein ligase E3 component n-recognin 7 (putative)
UHRF1	ubiquitin like with PHD and ring finger domains 1
UHRF2	ubiquitin like with PHD and ring finger domains 2
UTY	ubiquitously transcribed tetratricopeptide repeat containing, Y-linked
WDR5	WD repeat domain 5

Supplementary table S2. ***Lentiviral shRNA library gene targets.*** *Part 4*

ZC3HAV1	zinc finger CCCH-type containing, antiviral 1
ZCWPW1	zinc finger CW-type and PWWP domain containing 1
ZCWPW2	zinc finger CW-type and PWWP domain containing 2
ZGPAT	zinc finger CCCH-type and G-patch domain containing
ZMYND11	zinc finger MYND-type containing 11
ZMYND8	zinc finger MYND-type containing 8

Supplementary table S2. ***Lentiviral shRNA library gene targets.*** *Part 5*

shRNA-seq primers	Sequence
P5	AATGATACGGCGACCACCGAGATCTACACTCTTTCCCTACACGACGCTCTTCCGATCTTGCTCCTAAAGTAGCCCCTTGAAT
P7	CAAGCAGAAGACGGCATACGAGATAAAGGAATGTGACTGGAGTTCAGACGTGTGCTCTTCCGATCGTTAACCCAACAGAAGGCTCG

Binding to flow cell
Index
Necessary for sequencing primers
Recognition of shRNA

Supplementary table S3. ***shRNA-seq library prep custom primers.*** *The "P5" primer is constant for all sample preparations. The "P7" primer varies for each sample as this includes the index sequence. The index sequences used were identical to the RNA-seq library indexes from the NEBNext Multiplex Oligos for Illumina (NEB, USA)*